UNDERSTANDING CAMPYLOBACTER JEJUNI CYTOLETHAL DISTENDING TOXIN INTRACELLULAR TRAFFICKING, STRUCTURE FUNCTION RELATIONSHIPS, AND HOST CELL INTERACTION

BY

HENRY CHEN

DISSERTATION

Submitted in partial fulfillment of the requirements
for the degree of Doctor of Philosophy in Microbiology
in the Graduate College of the
University of Illinois Urbana-Champaign, 2024

Urbana, Illinois

Doctoral Committee:

Professor Steven R. Blanke, Chair
Professor Brenda A. Wilson
Professor William M. Brieher
Professor Peter A. Orlean

ABSTRACT

Cytolethal distending toxins (CDTs) are intracellular-acting bacterial genotoxins produced by a diverse group of mucocutaneous human pathogens, including *Campylobacter jejuni*, a major cause of foodborne illnesses in the United States. While CDTs, specifically those generated by *C. jejuni* (*Cj*-CDT), are known to play a crucial role in bacterial infection, understanding their mechanisms of action and contribution to pathogenesis remains limited. This thesis aims to elucidate the functions of different subunits within the multimeric *Cj*-CDT during cellular intoxication. Specifically, our focus is on assessing how these subunits facilitate toxin delivery to the host cell nucleus and the significance of subunit interactions and assembly in toxin functionality. In investigating the intracellular trafficking of *Cj*-CDT subunits, our research confirms the involvement of the endosome, Golgi apparatus, and endoplasmic reticulum in toxin activity. However, our efforts to delineate the roles and organelle trafficking patterns of individual *Cj*-Cdt subunits during cellular intoxication have yielded inconclusive results. To further explore the importance of subunit interaction and assembly in *Cj*-CDT function, we conducted concentration-dependent analyses of subunit interactions and toxin cellular activity using various experimental techniques. Our findings suggest that at minimal toxin concentrations necessary for cell cycle arrest, mixtures of *Cj*-CdtA, *Cj*-CdtB, and *Cj*-CdtC predominantly exist as non-interacting subunit monomers. This discrepancy between toxin structure and cellular activity challenges the prevailing notion that CDTs primarily intoxicate host cells through preassembled

heterotrimeric structures, warranting a reassessment of this model. Finally, we present preliminary and future investigations to understand host cellular relationships, an important gap in knowledge that needs to be addressed in order to advance our understanding of *Cj*-CDT pathogenesis.

I dedicate this work to my family for their unwavering love and support throughout my PhD journey. Their unconditional encouragement and support have shaped me into the person I am today and provided the strength to overcome the myriad challenges encountered along this path.

ACKNOWLEDGEMENTS

I would like to express my deepest gratitude to my advisor, Dr. Steven R. Blanke, for his unwavering support, guidance, and mentorship throughout this journey. His expertise, encouragement, and constructive feedback have been invaluable in shaping the work in this dissertation. I am also immensely grateful to my committee members, Dr. Brenda A. Wilson, Dr. William M. Brieher, and Dr. Peter A. Orlean, for their insightful comments, suggestions, and dedication to excellence. Their collective expertise has enriched this work and contributed significantly to its quality. I extend heartfelt appreciation to my many lab mates Molly K. Crowder, Ami Y. Seeger, Megan D. Ringling, and Zachary P. Shaefer for their insightful comments and support at various stages of this research. As well as my past undergraduate students Claire J. Ang and Ria R. Ravi for their hard work and experimental contributions to this research. Lastly, I am indebted to my family for their unwavering love, support, and understanding throughout this endeavor. Their sacrifices, encouragement, and unwavering belief in my abilities have been a constant source of strength and motivation. This dissertation would not have been possible without these individuals, and for that, I am profoundly grateful.

TABLE OF CONTENTS

CHAPTER 1: INTRODUCTION

1.1 INTRODUCTION

Microbes are the most prevalent and adaptable organisms on Earth, thriving across diverse environments, even coexisting within other life forms. Remarkably, the human body houses trillions of these microorganisms and the significance of microbes in human health is undeniable owing to their pervasive presence within us. However, while numerous microbes coexist symbiotically, certain bacterial entities, referred to as pathogens, can incite diseases when they grow within human hosts. Understanding the intricate relationships between bacterial pathogens and their human hosts has played a pivotal role in the progress of human health and medical interventions. Moreover, comprehending how pathogens successfully colonize and cause diseases in hosts has been instrumental in deciphering various host cellular processes.

For a pathogen to colonize a host effectively, it must navigate a series of challenges that impede its survival. Hostile factors such as temperature fluctuations, atmospheric conditions, limited nutrients, and host defense mechanisms act as obstacles. To surmount these barriers, pathogens employ virulence factors—complex cellular apparatus aiding in colonization and disease progression. These factors encompass diverse mechanisms, including adherence factors, motility factors, capsules/spores/membranes, and protein toxins. This dissertation, however, delves into bacterial protein toxins, centering on the cytolethal distending toxin (CDT). Bacterial protein toxins are synthesized

by pathogens and are capable of eliciting a broad spectrum of responses and effects within the host. Their mechanisms are diverse, disrupting host cell membranes, inhibiting crucial cellular processes, and manipulating immune responses. Despite their significance, the pathogenesis of cytolethal distending toxins (CDT) remains largely uncharted territory. Hence, this thesis focuses on comprehending various facets of CDT pathogenesis, particularly the interactions between its subunits and their correlation with toxin function, as well as elucidating how host cells recognize the toxin. Unraveling the intricacies of CDT pathogenesis holds importance due to the distinctive mechanisms wielded by this toxin, offering potential insights into novel therapeutic interventions.

1.2 AB-TYPE TOXINS AND THEIR ROLE IN PATHOGENESIS

Bacterial protein toxins exhibit a remarkable diversity, presenting a multitude of mechanisms through which pathogens ensure their survival. These toxins stand as some of the most potent poisons for humans, both in terms of their efficacy and lethal dosages. Not only do these toxins differ vastly in their functions, but they also vary in size, shape, and composition. Broadly categorized into four major groups, bacterial toxins showcase distinct modes of action: 1) Toxins acting directly on host cell plasma membrane receptors: These toxins function as agonists or antagonists of host receptors, influencing vital host signal transduction pathways. 2) Toxins disrupting membrane integrity: They achieve this by either forming pores within the membrane or possessing phospholipase activity, leading to the destabilization of the membrane lipid

bilayer. 3) Toxins with enzymatic components internalized into host cells: These toxins gain entry into host cells through receptor-mediated endocytosis, carrying enzymatic components that exert their effects internally. 4) Toxins directly injected into host cells via specialized secretion systems: Some bacteria possess injection systems akin to needles, enabling direct delivery of toxins into host cells.

Despite their diverse origins, structures, and enzymatic activities, the most potent bacterial toxins identified thus far target conserved key cellular factors and pathways. Notable among these are actin, small RHO GTPases, ubiquitin, translocation and snare machineries, DNA, ER stress responses, and cAMP (85). Here are some examples of bacterial protein toxins and the host processes that they target (Figure 1.1). Understanding the impact of bacterial protein toxins on host cellular processes has been pivotal in scientific research. For instance, researchers have investigated receptor endocytosis and vesicular trafficking, exemplified by the retrograde transport of Shiga toxin (Stx) from the cell surface to the endoplasmic reticulum, elucidating the translocation of their enzymatic domains across intracellular membranes, and exploring the regulation and function of their cellular targets.

Exploiting the diverse functions of bacterial toxins has led to numerous therapeutic applications. Common toxins used in therapeutic contexts include botulinum neurotoxin, lethal toxin, pertussis toxin, and cytotoxic necrotizing factor 1. Additionally, bacterial toxins serve as adjuvants or drug delivery agents, exemplified by cholera toxin, zonula occludens toxin, and pertussis toxin (51).

Notably, the unique features of cytolethal distending toxin (CDT) pathogenesis offer intriguing subjects for study, serving as the focal point of investigation within this thesis.

1.2.1 AB-type Toxins

AB-type toxins belong to the third group of toxins, which harbor enzymatic components internalized into host cells through receptor-mediated endocytosis. These toxins are characterized by a two-component structure consisting of an enzymatic A component coupled with one or more B components. The B component(s) play a pivotal role in facilitating entry into host cells, while the A component typically harbors varying enzymatic activities, exerting specific effects on the host depending on the toxin's function. The entry of AB-type toxins into host cells occurs through receptor-mediated endocytosis. This mechanism allows the pathogenic bacteria to specifically target and affect host cells, evading the host's defenses while causing various detrimental effects. Understanding the intricate mechanisms behind these toxins holds paramount significance in the study of bacterial virulence, unraveling how pathogenic bacteria manipulate host cells to establish infections.

Among the myriad of bacterial protein toxins, AB-type toxins represent a subset with distinct and impactful examples. These include cholera toxin, heat labile enterotoxin (LT), Shiga toxin, pertussis toxin, anthrax toxin, ricin toxin, and cytolethal distending toxin. The study of these toxins not only elucidates their individual mechanisms of action but also unveils commonalities and unique

features among them. Furthermore, it sheds light on the different strategies used by bacteria on their host organisms, showcasing the constant adaptation and competition within the realm of infectious diseases. Understanding the intricate relationship between the A and B components of AB-toxins is crucial for their functionality. Unsurprisingly, there exists a diversity in structure as well as how the components of AB toxins interact, elucidating the complexity behind their biological functions. Included is a table summarizing the structure and function of some extensively studied AB-type toxins: cholera toxin (CT), heat labile enterotoxin (LT), Shiga toxin (ST), pertussis toxin (PT), anthrax toxin, and ricin toxin. (Table 1.1). In addition, a figure that summarizes the structural and amino acid sequence homology among these AB toxins (Figure 1.2). To further examine their diversity and functionalities, a brief review of these AB-type toxins will be presented, including the lesser understood cytolethal distending toxins. Exploring the architecture of toxins stands as a pivotal focus of this dissertation work, with a particular emphasis on dissecting toxin subunit interactions and their functional significance.

1.2.2 Cholera Toxin

Cholera enterotoxin (CT) is a complex multimeric protein exotoxin produced by the Gram-negative bacterium *Vibrio cholerae*, and it plays a central role in the development of severe secretory diarrhea during infection. This secretory diarrhea primarily occurs in the upper part of the small intestine. The architecture of CT follows an AB5 format, consisting of a single large A subunit

(CTA) with an approximate molecular weight of 27 kDa and a pentameric B subunit (CTB) composed of monomers weighing around 10.6 kDa each (92) (Figure 1.3). However, this seemingly straightforward structure has additional intricacies.

The CTA subunit is further divided into CTA1 and CTA2 subunits linked by a disulfide bond, with CTA1 being the key player in toxicity (138). CTA1 exhibits ADP-ribosylating activity, while the CTA2 fragment, which has a helical structure, serves to anchor CTA1 within the center of the circular-shaped CTB pentameric oligomer.(146) In addition, the CTB subunit is stabilized by hydrogen bonds and salt bridges (100). Cholera toxin shares a significant structural resemblance with another diarrhea-causing AB-type bacterial toxin, the heat-labile enterotoxin (LT), boasting an approximate 80% amino acid sequence homology and highly similar three-dimensional molecular structures (146).

The CT toxin is thought to be secreted as an assembled complex, although it has not been definitively established. Following this, the toxin binds with high affinity to GM1 ganglioside located in lipid rafts on the epidermal cell surface of the small intestine's lumen. GM1 binding facilitates toxin endocytosis through both caveolin-coated and clathrin-coated vesicles (129). Some conflicting reports even suggest the internalization of CT may or may not require an Arf6-dependent pathway and is independent from Dynamin-dependent endocytic pathways (93).

The toxin's journey further continues as it is transported to the trans-Golgi network, where the toxin is then transported to the endoplasmic reticulum (ER) via Golgi retrograde transport mechanisms (137). This ER targeting is facilitated by an endoplasmic reticulum retention motif (KDEL) located near the C-terminus of the CTA chain, which interacts with the KDEL receptor, allowing the recycling of ER components from the trans-Golgi network back to the ER (25). From the ER, CTA escapes to the cytosol where it can act. In the cytosol, CTA1 induces adenylate cyclase activity by stimulating the ADP ribosylation of the adenylate cyclase Gsa subunit (110). This leads to an increase in cyclic AMP (cAMP) levels, resulting in an electrolyte influx imbalance, ultimately causing substantial water and electrolyte loss from the intestinal epithelium.

1.2.3 Heat Labile Toxins

Another type of AB toxins are the heat labile toxins. There are two types of heat labile toxins, Type I and Type II, both of which are structurally and functionally similar to cholera toxin. In fact, these toxins exhibit extensive amino acid sequence similarity to cholera toxin. (146). Produced by enterotoxigenic strains of *E. coli*, both types of heat-labile toxins consist of a catalytic A subunit (LTA) and a pentamer of B subunits (LTB), forming the characteristic AB5 architecture akin to cholera toxin (Figure 1.4). Remarkably, heat-labile toxin was among the first AB toxins with a solved crystal structure (148).

The A subunit, analogous to cholera toxin, comprises two subunits linked by a disulfide bridge: A1, the catalytically active region, and A2, a linker peptide connecting A1 to the LTB pentamer (7). Interaction with host cells involves the assembled hexameric complex of cholera toxin. Toxin delivery into host cells hinges on the robust binding of the LTB subunit to the ganglioside receptor GM1, a process mirroring that of cholera toxin (139). The N-terminus of the B subunits serves a dual role in protein stabilization, protecting against proteolytic degradation, and housing the GM1 binding site for the holotoxin complex (7). Additionally, LTB interacts with paraglobosides, GM2, polyglycoceramides, and glycoproteins containing polylactosamine (with lower affinity), expanding its binding profile (31, 77, 115). The binding characteristics of LT-IIa and LT-IIb variants remain less understood.

Uptake of the LT toxin necessitates the simultaneous binding of pentameric LTB to five GM1 ganglioside receptors. For functional activation, LT undergoes endocytosis and translocation to the cytoplasm, with localization to lipid rafts being crucial for complex uptake (147). Although LT endocytosis is believed to involve various pathways, including clathrin-dependent and caveolar-dependent pathways, other unidentified intracellular transport mechanisms may also play a role. The toxin undergoes retrograde trafficking in a manner similar to CT, eventually reaching the endoplasmic reticulum (ER) (25). The catalytic A1 subunit of LT acts as an ADP-ribosyltransferase, activating the G protein Gsα. This activated G protein induces cytotoxicity through adenylate cyclase, leading

to an elevation in intracellular cAMP levels (149). The heightened levels of cAMP contribute to the characteristic "rice water" diarrhea associated with LT toxicity.

1.2.4 Shiga and Shiga-like Toxins

Shiga toxin (Stx) was first identified in *Shigella dysenteriae*, and it belongs to a toxin family that includes Shiga toxin as well as other closely related Shiga like toxins: Shiga-like toxin-1 (Stx1) and Shiga-like toxin-1 (Stx2) which are produced by Enterohemorrhagic *Escherichia coli* and Shiga toxin producing *E. coli* (74, 131, 157). These pathogens are gram-negative, rod-shaped, anaerobic, and non-sporulating. Shiga toxin is considered a hexameric protein with a molecular weight of 70.5 kDa. These toxins are composed of an enzymatic subunit StxA monomer and a receptor-binding StxB homopentamer (116) (Figure 1.5).

The StxA subunit of the Shiga toxin has two fragments covalently associated by a disulfide bridge, these two fragments A1 and A2 are approximately 28 kDa and 4 kDa in size, respectively. The A2 subunit associates with the B subunit homopentamer, with the Leu282, Gly283, Ala284, Ile285, Leu286, and Met287 residues in the C-terminus being important for holding together the complex (55). The A1 subunit also bears significant amino acid sequence homology to the plant enterotoxin, ricin, A subunit (136). Both Shiga and ricin A subunits depurinate adenosine in the 28S ribosomal RNA of the 60S ribosomal subunit. This modification makes tRNAs that are unable to associate with the ribosomal complex, which ultimately leads to the inhibition of protein

synthesis in target cells (136). The StxB subunit of the Shiga toxin consists of five identical B subunits that form a symmetric homopentameric ring-like complex. This StxB complex associates with the StxA complex asymmetrically by having only three of its B subunits interacting with the C-terminus of the A2 fragment, which results in StxA bending to the side opposite from the three B subunits (Figure 1.5) (55). The StxB subunit preferentially binds to globotriaosylceramide (Gb3) and facilitates the internalization of the StxA into the target cells (74).

The Shiga toxin enters host cells via the retrograde transport pathway. The first step involves Stx binding to Gb3 ganglioside that are located on lipid rafts of target host membranes. The toxin is internalized via clathrin-mediated endocytosis (135), where Stx is then carried into the trans-Golgi network via the endocytic recycling compartment (134). Stx then is retro-trafficked from the trans-Golgi network to the ER in coat protein complex I (COPI)-coated vesicles in a KDEL-independent manner (133). From the ER lumen, Stx links with a pre-associated large multi-chaperone complex of HEDJ, BiP, and a 94 kDa glucose-regulated protein (GRP94) in order to partially unfold the Stx toxin so that it can escape using host ERAD pathways (170). Stx avoids proteosome degradation by evading ubiquitination, through the absence of lysine residues in its structure, which is required to target the protein for degradation. The StxA subunit of the toxin is activated via proteolytic cleavage by the enzyme furin at Cys242-Cys261 within vesicles of the Golgi apparatus (74).

1.2.5 Pertussis Toxin

The pertussis toxin is an AB type toxin that's produced by the gram-negative bacterium *Bordetella pertussis*. The pathogen *B. pertussis* is a human specific pathogen that's best known for causing Whooping Cough and was first identified in 1906. The pertussis toxin has a six membered oligometric structure (152). The A component of pertussis toxin (PTA) consist of a single subunit (S1) that contains enzymatic activity that transfers the ADP-rose from nicotinamide adenine dinucleotide (NAD) to the cysteine residue of trimeric guanine nucleotide-binding proteins (G-proteins), leading to a decoupling of the G-protein a-subunit from its receptor. This results in the inhibition of adenylate cyclase activity which results in an increase in intracellular cAMP (9).

The B component of pertussis toxin (PTB) consist of 5 subunits that, unlike cholera and heat-labile toxin, are not similar: the S2 (23 kDa), S3 (22 kDa), two S4's (11.7 kDa each), and an S5 (9.3 kDa) that come together to form an asymmetrical heteropentameric ring structure (Figure 1.6) (152). The PTB binds preferentially to receptor glycoproteins and glycolipids, such as ganglioside GD1a, which is located on lipid rafts on the host plasma membrane (67). Once bound the toxin complex is internalized and retro- trafficked through the trans-Golgi Network to the endoplasmic reticulum (42, 151). Travel through these organelles results in activation of the PTA, establishing its ADP-ribosylating activities. Once at the endoplasmic reticulum, the partially unfolded PTA is recognized by the ER as a misfolded protein and is secreted into the cytosol for endoplasmic reticulum associated protein degradation (151). Similar to Shiga

toxin, PTA lacks lysine residues which allow it to evade degradation and conduct its enzymatic functions (168).

1.2.6 Anthrax Toxin

The anthrax toxin is produced by the gram-positive bacteria *Bacillus anthracis.* This toxin consist of a tripartite structure that is composed of three independent polypeptide chains, the edema factor (EF), lethal factor (LF), and protective antigen (PA). Unlike the previously mentioned toxins (cholera, heat-liable, Shiga, and pertussis) which consists of 6 subunit components. In the case of the anthrax toxin, the EF and LF are considered the active A components, and the PA to the binding B component (Figure 1.7).

The PA plays a role in delivering the EF and LF into host cells. PA is an 83 kDa polypeptide that binds to two identified anthrax receptors, tumor endothelial marker 8 or capillary morphogenesis 2 (161). Once bound to its receptor, PA is processed by furin into a 63 kDa polypeptide, leading to activation of the PA triggering self-association into a heptameric pre-pore structure (124). Formation of the heptameric complex induces the seven bound receptors to cluster in lipid rafts or detergent-resistant membrane microdomains that results in the endocytosis of the complex (3). This heptameric complex is able to competitively bind up to three LF and /or EF subunits (104), this binding triggers activation of src-like kinases that is required to initiate a conformational change in the PA heptamer that facilitates uptake and ultimately the translocation of the LF or EF into the cytoplasm (2). Receptor activation results in the endocytosis of the

anthrax complex via ubiquitin, actin, and clatherin dependent mechanisms and fusion with an endosome (1). Once in the endosome, the PA forms a pore in the endosome bilayer in a pH dependent manner. More specifically, this change in pH disrupts a salt bridge that results in the decreased stability of PA and its receptor interactions which results in detachment of the PA domain II which forms the pore (60). The pore acts as a proton/protein symporter that drives translocation of LF and EF into the cell cytoplasm, where these subunits can exert its effects (11). So, unlike the previously mentioned toxins, anthrax as B component that is able to oligomerize with itself to form a 7 membered binding complex that is able to aid in the internalization of either the LF and/or EF subunits, with a maximum capacity of three subunits.

One in the host cell cytoplasm, LF is able to target and cleave mitogen-activated protein kinase kinases (MAPKKs) within the N-terminal proline-rich regions that precedes the kinase domain. This inactivation of MAPKKs results in disruption of many signal transduction pathways and the decrease in transcription/protein synthesis (41, 162). The other subunit, EF, acts as a calcium independent calmodulin-dependent adenylate cyclase that results in the increase of intracellular cAMP (86). The effects of both LF and EF results in a variety of cytotoxin effects such as disruption of intracellular signaling pathways along with sever altered water homeostasis.

1.2.7 Ricin Toxin

Ricin Toxin is the only toxin non-bacterial protein toxin mentioned in this dissertation, produced by the castor oil plant, *Ricinus communis*. Ricin is an enterotoxin that exists in several isoforms including ricin D and ricin E. The ricin holotoxin contains a catalytically active A chain (RTA) that is 32 kDa and possesses ribosome-inactivating activities similar to Shiga toxin. The RTA chain is linked by several disulfide bonds to the 34 kDA B subunit (RTB), which is a galactose-binding lectin (Figure 1.8) (106). Unlike the other AB toxins mentioned, the ricin toxin consists only of two protein polypeptide subunits. The ricin toxin is synthesized as a single polypeptide that is cleaved into the A and B subunits. The RTA subunit acts as an N-glycosidase that depurinates specific adenine residues in 28S rRNA (rats) and 23S rRNA (*E. coli*). This results in the inactivation of ribosomal activities which is detrimental to the cell (47).

The RTB subunit is responsible for binding the toxin to both glycoprotein and glycolipids on the cell surface (150). While there is no specific receptor identified for ricin, the lectin nature of ricin allows it to bind to a wide range of galactosidases and glycoproteins (46). Ricin is thought to involve several cholesterol dependent endocytosis mechanisms, including clathrin and caveolae mediated endocytosis (137). Once endocytoses, ricin is thought to traffic from late endosomes to the Golgi apparatus in a Rab9 independent manner and instead involving Rab5 dependent vesicles (105). Ricin is thought to follow a similar retro-trafficking route as cholera and Shiga toxin, however in a KDEL independent manner. Alternatively, ricin is thought to interact with calreticulin,

which has a KDEL retention motif, in the Golgi network which may be involved in its delivery from Golgi to the endoplasmic reticulum (36). For most bacterial toxins that require proteolytic cleavage, the A and B subunits of the toxins enter the endoplasmic reticulum linked by disulfide bonds. For ricin, the B subunit hinders the A subunit's catalytic activity, and the two subunits are dissociated by the ER chaperone protein disulfide isomerase (14).

1.3 CYTOLETHAL DISTENDING TOXINS: OVERVIEW

Cytolethal distending toxins are protein toxins produced by a wide range of gamma and epsilon proteobacteria and are the group of toxins that will of primary focus in this thesis. Remarkably, CDTs are the first and only bacterial genotoxins to be identified, with the CDT genotoxin being first reported in E. coli in 1987 (75). Out of the wide range of bacteria producing CDT, some of the clinically relevant mucosal pathogens that produce CDT *are Aggregatibacter actinomycetemcomitans* (Aa-Cdt), *Campylobacter jejuni* (*Cj*-CDT), *Escherichia coli* (Ec-CDT), and *Haemophilus ducreyi* (Hd-CDT) (75, 123, 154). In addition, CDTs have been shown to play an important role in the pathogenesis of many of these pathogens (54, 121). Since these are common mucosal pathogens that contribute to a wide range of clinical diseases, studying the toxin is an attractive target for the development of pharmaceuticals. What categorizes CDT as a genotoxin is that it has the ability to cause DNA damage on cells affected by the toxin. This DNA damage leads to a wide range of outcomes such as G_2/M cell

cycle arrest, cellular senescence, dysregulation of the immune response, dysregulation of autophagy, and even cell death.

One major point in the CDT field that I would like to comment on and emphasize is that many aspects of CDT pathogenesis are poorly understood. The major limitation to the overall understanding of CDT pathogenesis is the incomplete and diverse work done in the field of CDT. There are several factors that make our understanding of CDT pathogenesis very challenging. For one, CDTs from different species have been shown to behave differently from one another, making it hard to generalize the overall consequences of CDT activity for the entire family of toxins. In addition, DNA damage elicits a wide range of host responses that are different depending on the cell types affected and mostly involve crosstalk between multiple systems, thus requiring the use of a more comprehensive model/tissue level model in order to truly understand toxin pathogenesis and more unity in the host systems used to study consequences of CDT intoxication. Finally, a lot of the limited work done in the field of CDT has a lot of variances in experimental conditions such as toxin concentration and duration of toxin exposure, which we are becoming increasingly aware can have profound effects on phenotypes. Despite these differences, this section of the thesis will review several key aspects of CDT pathogenesis that are important to the understanding of gaps in knowledge in the CDT field that will be covered in this thesis.

The CDTs are encoded by three genes (*cdtA, cdtB,* and *cdtC*) which are arranged on what is thought to be a single operon. Unlike the previously

mentioned examples of AB-type toxins, the three CDT genes in code for three distinct polypeptides named CdtA, CdtB, and CdtC whose molecular masses vary depending on the species of toxin but are thought to interact to form a heterotrimeric complex. This is very different from the previously discussed AB toxins, which often have multimers of their B component that allow for host cell recognition (Table 1). The difference in architecture between CDTs and other AB type toxins begs the question of how CDTs are capable of delivering their cargo? One major gap in knowledge in the field is the relationship between CDT toxin structure and the function of the toxin.

Following the AB toxin paradigm, the CdtB subunit is thought to perform like the A component, possessing DNase-like activities, while the CdtA and CdtC are thought to perform like the B component, by playing a role in delivering the CdtB component to the nucleus. One of the most unique features of all CDTs is the ability of the active CdtB subunit to retro traffic to the nucleus where it causes DNA damage. Both delivery to the nucleus and DNA damage activities has not been demonstrated for any other protein toxin. To achieve successful localization of the CdtB subunit and host cell DNA damage, the toxin requires the presence of all three CdtA, CdtB, and CdtC subunits (81, 87, 127). This delivery pathway of the CdtB subunit is poorly understood, but it is thought to follow a rather unconventional/backward trafficking pathway within host cells, supposedly utilizing existing host machinery (65). This reverse transport pathway is thought to be similar to those utilized by many different AB type toxins, as previously mentioned. For all AB toxins, the first step in this transport pathway requires the

association of the toxin complex to its host cell receptor. Once bound to the host cell, the toxin is then taken up in the cell. Typically, proteins are trafficked post synthesis through the endoplasmic reticulum to the Golgi apparatus, where they are then shipped to various destinations within the cells. While it's known that eukaryotic cells can retrograde traffic important molecules in the cell, the mechanisms with which host cells achieve this is poorly understood. Thus, better understanding the mechanism with which CDT traffics to the nucleus may provide novel insights to the players of intracellular retrograde trafficking. Understanding the mechanism behind CDT nuclear transport remains a major gap in knowledge in the field and is a topic that will be briefly addressed and investigated in this thesis.

To achieve successful localization of the CdtB subunit and host cell DNA damage, the toxin requires the presence of all three CdtA, CdtB, and CdtC. This is because the CdtA and CdtC subunits are thought to play an important yet poorly understood role in the delivery of the CdtB subunit to the nucleus. A major gap in knowledge in the CDT field is the relationship between quaternary structure of the CDT toxin and activity. The goal of my dissertation is to deeply investigate the relationship between *Cj*-CDT holotoxin formation and biological activity, focusing on understanding how the *Cj*-CDT subunits are involved with toxin pathogenesis.

1.4 CELLULAR CONSEQUENCES OF CDT INTOXICATION

The consequences of CDT intoxication have been fairly well studied, however there are still many things we have yet to understand. Since being able to evaluate biological activity of CDT is so important to our studies, this section will provide a brief overview of the major consequences to CDT intoxication, focusing primarily on DNA damage and host DNA damage response. As previously mentioned, one of the many consequences of cellular intoxication with all three CDT subunits is host cell cycle arrest at the G_2/M phase. This is one of the first phenotypes associated with CDTs (13, 29, 118, 122, 165) and is commonly used to measure CDT activity. Cell cycle arrest activities of CDT are a result of CDT directly dealing DNA damage on host cells. DNA damage is due to the delivery of the catalytically active CdtB subunit to the nucleus. The CdtB subunit from all species of CDTs are fairly conserved and belong to the DNase I Mg^{+2}-dependent phosphodiesterase family. A protein-specific iterated BLAST (PSI-BLAST) analysis of the *E. coli* CDT-II polypeptide revealed striking homologies between the CdtB subunit to mammalian type I DNases. Furthermore, purified CdtB subunit was shown to have DNase like activity, and was able to degrade supercoiled plasmid DNA in vitro (45) as well as having the ability to induce nuclear fragmentation and marked chromatin disruption in treated cells (82, 88). To further confirm that it was the CdtB subunits DNAse like activity that causes DNA damage and to better understand how CdtB causes DNA damage in host cells, mutations in conserved residues that play an important role in mammalian DNase I activity such as those that were important

for catalysis or magnesium binding were generated in Ec-CDT, as a results these mutations abolished both the DNase as well as cytosolic activities of the CdtB subunit (45). More notably, it's been shown that the Cdt's have much weaker activities (almost 100 fold lower) compared to mammalian DNase I (purified bovine) (44, 88). This weak DNA damage activity of the CDT toxins has been a major question in the field, specifically, why would a weakly acting bacterial genotoxin be maintained and shared by so many species of bacteria. If the goal of the toxin was to induce DNA damage, then shouldn't the toxin be more potent? Several studies have been done to better understand the type of DNA damage done by CDTs. However, one of the major challenges in understanding the consequences of CDT treatment lies in the variance between experimental conditions.

Detailed studies using *E. coli* CDT (Ec-CDT) revealed that the toxin induces early DNA damage in the form of single-strand DNA breaks within 3 hrs of low concentration (50 pg/mL) exposure to the toxin (53) and that this activity required the histidine at position 153, as the EcCDT^{H153A} mutant had no activity. At higher toxin concentrations (>75 ng/mL) and longer intoxication periods, intoxication results in double strand breaks in host DNA (53). This is thought to be a result of accumulation of juxtaposing single strand breaks on opposite strands. In addition, this accumulation of damage that leads to double strand breaks is thought to be independent of the cell cycle phase but are thought to require progression through the S phase of the cell cycle. From the pathogen's perspective, what makes DNA damage an attractive target is the wide range of

cellular response with which it affects. In order to protect itself from the DNA damage caused by CDTs, the cell activates a series of complex mechanisms referred to as DNA damage responses (DDRs) that act to repair the genome and minimize the probability of more permanent damage (72). These damage responses are thought to be trigger by a wide range of DNA damage, such as from reactive oxygen species, ionizing radiation, as well as other genotoxin drugs. In addition, CDTs from different bacteria have been shown to induce similar DNA damage responses on target cells (120). Host DNA damage response can be broken into three stages: the recognition of DNA damage by sensor proteins (MRN and Ku complexes, RPA) which activate phosphatidylinositol 3-kinase-related protein kinases (ATM, ATR, and DNA-PK), the signal amplification of these sensors by transducing proteins (p53, CDC25, etc.), and finally the activation of DNA repair pathways (72). There are two key signaling pathways that are activated in response to DNA damage, which are the ATM-CHK2 and the ATR-CHK1 pathways. The ATM-CHK2 pathway is activated in response to DNA damage that occurs in the form of double strand breaks (DSB). When a DSB is formed, the MRN complex, which consists of the proteins MRE11, RAD50, and NBS1, recruits the ATM kinase to the site of the breaks (83). Once the MRN complex is localized to the site of the DSB, ATM is activated by autophosphorylation, leading to the phosphorylation of many different substrates, the most well known of them being CHK2 and p53. In addition, ATM phosphorylates the H2AX histone around the site of DSBs which allows for further signal amplification of sensors to DNA damage (125). The activated

CHK2 and p53 leads to a wide range of response including host cell repair mechanisms for the DSB damage. Alternatively, the ATM-CHK1 pathway is activated in response to DNA damage that occurs due to the accumulation of single-stranded DNA (ssDNA). This typically occurs during the stalling of the replication fork, for instance, when replication is blocked by DNA lesions (whether it be from SSB, DSB, inter-strand and intra-strand crosslinks, base modifications or adducts) the DNA polymerase is uncoupled from the replicative helicase which results in the generation of ssDNA. ssDNA is recognized by the RPA protein complex, which protects and stabilizes the ssDNA, and leads to the recruitment of the ATR/ATRIP complex (174). ATR then phosphorylates the CHK1 transducing protein leading to a wide range of response and repair mechanisms to remedy the damage (163, 171). These two response pathways are summarized in Figure 1.9. In addition, there is a lot of cross talk between these two pathways, but ultimately, depending on the type of DNA damage, the ATM and ATR pathways can be specifically or sequentially activated, resulting in cell cycle arrest, the activation of DNA repair machinery, and if need be, cell death (94).

In the case of CDT there is a fair amount of research investigating the cellular effects of toxin damage. We know intoxication leads to cell cycle arrests at the G2/M interphase, which suggests that CDT induces the activation of the DSB-related pathway, and therefore prompted an investigation of the recruitment of the different DDR proteins that are involved in CDT mediated damage. First, I will go over what is known about the DNA damage response to CDT intoxication.

Upon CDT mediated DNA damage resulting in DSB, the cell recruits the MRN complex at the site of the damage (88), followed by the activation of ATM. In addition to activation of ATM and the phosphorylation of H2AX has been measured in response to CDT from various species (16, 18, 52, 53, 66, 88, 91). The phosphorylation of histone 2AX (gH2AX) is one of the standards in measuring/detecting bacterial genotoxin-induced DNA damage. To further support the idea that CDT induces DSB, another DSB marker, 53BP1, has been shown to form foci after CDT treatment (18, 52, 53). ATM activation in response to CDT leads to CHK2 phosphorylation, which in turn phosphorylates different effectors, including two important cell cycle regulators of the phosphatase family, CDC25A and CDC25C, as well as the activation and stabilization of p53, which enhances the transcription of another cell cycle regulator p21 (15). In addition, CDT treatment has also been associated with activation of the ATR-CHK1 pathway (52). As you can imagine, there is a lot of cross talk between cell cycle regulators and transcription factors in order to maintain homeostasis and a proper repair response.

One of the common responses to the DNA damage response is the regulation of the cell cycle, which is regulated by sequential activation and nuclear re-localization of CDK/Cyclin complexes (69). To briefly outline the involvement of CDK/Cyclin complexes chronologically, we begin with the regulation of G1-phase progression and entry into the S-phase, which is controlled by CDK4/Cycin D and CDK2/Cycin E complexes respectively. S-phase progression is regulated by the CDK2/Cyclin A complex. Completion of the S-

phase and transition into the G2-phase is coordinated by the activation of CDK1/Cyclin A complex. Finally, G2-phase transition to mitosis is dependent on the activation and nuclear localization of the CDK1/Cyclin B complex. All these CDK/Cyclin complexes are activated by CDC25-dependent dephosphorylation and can be inhibited by different regulators such p16, p21, p27, and Wee1 (80).

In the case of CDT mediated DNA damage, CHK2 activation results in the sequestration of CDC25C phosphatase in the cytoplasm, which prevents its ability to activate the CDK1/Cyclin B complex in the nucleus (6). This results in the hyperphosphorylation and inactivation of the CDK1/Cyclin B complex, which prevents the cells from transitioning out of the G2-phase (27). CDC25C was shown to play a major role in this process as overexpression of CDC25C is able to prevent CDT mediated G2/M cell cycle arrest (48). As mentioned before, other factors that play an important role in cell cycle regulation are p53 and its downstream target p21 (56). One of the most confusing aspects of understanding the consequences of CDT mediated DNA damage is that different cell types have different responses to CDT intoxication at the cellular level, this includes variation of p53 status. Without getting too complicated, the general interpretation is that CDT intoxication leads to activation of p53 as well as p21, which ultimately leads to cell cycle arrest at the G2/M interphase (Figure 1.10) (56, 66). By measuring G2/M arrest activity of cells treated with CDT, we can evaluate whether we have biologically active toxin.

1.5 ROLE OF CDTS IN PATHOGENESIS

Understanding the intricate role of protein toxins in the pathogenesis of microbial infections poses a significant challenge. Pathogenesis, being a complex interplay of factors, encompasses not only the cellular activities of toxins but also various elements contributing to a pathogen's ability to induce disease. To unravel the role of toxins in pathogenesis, it becomes imperative to decipher the intricate crosstalk between toxin-induced damage, the goals of the pathogen, and the host responses to the infectious agent. This task is particularly formidable, given that a comprehensive understanding of all processes during pathogenesis is necessary. While there has been considerable research on CDT-mediated DNA damage and the subsequent activation of host DNA damage response pathways, the beneficial aspects of CDT-induced DNA damage for pathogens remain relatively unexplored. Despite the incomplete comprehension of CDT's role in pathogenesis, this section will delve into current models proposing how CDT might contribute to the intricate processes underlying disease development. Notably, limited literature exists on the contributions of CDT to pathogenesis, with investigations focusing on specific CDT-producing pathogens such as *A. actinomycetemcomitans* and *C. jejuni.*

Given the diversity in pathogens, each colonizing distinct host niches, utilizing different virulence factors, and causing varied diseases, the role played by CDTs in pathogenesis is inherently pathogen dependent. The complexity is compounded by the intricate crosstalk between DNA damage and the DNA damage response in different host systems, making it challenging to discern the

connections between specific host cell responses and the role of CDTs in the pathogenesis of diverse pathogens. This section will spotlight the investigations into the contributions of CDT to pathogenesis, with a particular focus on *A. actinomycetemcomitans* and *C. jejuni*. However, it is essential to acknowledge that the presented models are inherently incomplete. The scarcity of research on CDTs, spread across various CDT-producing species, coupled with the variability introduced by the use of different cell lines, tissue samples, and toxin treatment conditions, limits the depth of our understanding. Ultimately, the potential roles of CDTs during pathogenesis are rooted in the DNA damage response induced by CDT-mediated damage and the diverse effects of this damage on host cells.

1.5.1 Involvement of CDTs in the immune response

First and foremost, there is a widely held belief that CDT plays a crucial role in the pathogenesis of numerous pathogens carrying the CDT genes. The significance of this belief is underscored by the understanding that DNA damage, induced by CDT, not only poses a threat to host cells but also has the potential to disrupt their proper functioning. Moreover, DNA damage becomes an attractive target for pathogens due to its capacity to elicit a diverse array of cellular responses. Delving into this complexity, CDTs impact a broad spectrum of cells during pathogenesis, particularly those constituting the various niches where different CDT-containing pathogens establish colonization.

Among the myriad of cells affected by CDTs during pathogenesis, immune cells emerge as a particularly attractive target for the genotoxic activities of CDT.

Immune cells play a pivotal role in the pathogenesis of all three discussed species of CDT-containing pathogens. Notably, CDT's DNA-damaging actions have been implicated in the modulation of the immune response (IR). The immune response, akin to the DNA damage response (DDR), constitutes a complex system crucial for detecting and eliminating threats, essential for maintaining organismal homeostasis. However, unlike the DDR, which operates at the single-cell level, the IR is characterized by a higher level of complexity, involving multiple cells and eliciting responses at the whole tissue level.

The immune response (IR) to host threats is extensive, and much of its intricacies fall beyond the scope of this thesis. Nonetheless, a concise exploration of how the DNA damage response (DDR) influences immunity is important when thinking about role of CDT toward pathogenesis. The immune response, tailored to the nature of threats and their effects, can be categorized into three types: 1) response to intracellular threats, 2) response to large extracellular threats, and 3) response against extracellular microorganisms. Successful threat elimination relies on the coordinated efforts of innate and adaptive immune cells. In addition, the nature of the response activated in the face of an insult is not solely determined by the type of threat but is also influenced by the specific tissue affected. This adaptive feature enables the host to deploy optimal mechanisms for threat elimination while mitigating unnecessary damage that could compromise tissue or organ function. Given that both the DDR and IR are conserved systems dedicated to maintaining organismal homeostasis, the intriguing possibility of crosstalk between these two systems

emerges as an important rationale behind pathogens acquiring bacterial genotoxin effectors. This section will only briefly delve into the consequences of CDT mediated DNA damage and the modulation of the host immune response. Understanding how CDTs influence the intricate dynamics of the immune response is thus significant to comprehending the multifaceted role these toxins play in the broader landscape of pathogenesis.

A significant immune phenotype that has garnered attention in research is the proinflammatory impact of CDTs, as these inflammatory signals play a crucial role in orchestrating an appropriate immune response. Notably, exposure to AaCDTs has been associated with heightened secretion of IL-1B, IL-6, IFN-g, and IL-8 in peripheral blood mononuclear cells, displaying a dose-dependent pattern (5). Furthermore, induction of IL1B, IL6, and TNFa has been observed in TPA-differentiated human THP-1 cells and monocyte-derived macrophages (145). Importantly, the induction of pro-inflammatory mediators is not confined to immune cells but has also been noted in cells of epithelial and mesenchymal origin. For instance, Aa-CDT has been shown to stimulate the secretion of IL-6 from resident fibroblasts [110], while *Cj*-CDT and *Hh*-CDT induce IL-8 secretion or mRNA production in human embryo intestinal INT407 cells, as well as various colorectal-derived cell lines (T84, CaCo-2, HCA-7) 72 hours post-treatment (68, 117, 172). Despite the clear association between CDT treatment and the production of proinflammatory signals, the precise role of proinflammatory signaling in CDT-mediated pathogenesis remains inadequately characterized. Regrettably, there is limited published work on the in vivo effects of CDT during

pathogenesis. Given the complexity of the immune response, which involves diverse cell types coordinating at a tissue level or even higher, the understanding of CDT's impact necessitates exploration beyond isolated cellular studies. Tissue explants and animal models serve as valuable tools to assess the immune response to pathogens, offering insights into the overall process, albeit in a snapshot fashion. To unravel the intricate dynamics of CDT-mediated pathogenesis, future research should strive to bridge the existing gaps in knowledge by employing more comprehensive in vivo models and investigating the long-term effects of CDT exposure on host immune responses.

Beyond its proinflammatory effects, CDT is believed to exert immunosuppressive effects on the host microenvironment. This is primarily attributed to CDT's capacity to induce apoptosis, inhibit cell proliferation, and diminish IFN-g secretion by activated human CD8+ and CD4+ T lymphocytes (112, 113, 142, 143). Additionally, CDT impacts the viability of monocytes and immature monocyte-derived dendritic cells (DCs), compromising the stimulatory activities of activated DCs (63, 155, 167). These cellular responses are integral to the orchestration of an appropriate immune response. It is crucial to note that a majority of these immunosuppressive effects have been demonstrated in in vitro models, and there is limited data regarding the immunosuppressive effects of CDTs within the context of in vivo natural infection models in immunocompetent hosts. Despite this limitation, the accumulating evidence suggests that CDTs may play a role in modulating the host immune

microenvironment to create a conducive niche for the pathogen to replicate and spread.

Considering these findings, it becomes evident that CDTs may contribute to the intricate balance of inflammatory and anti-inflammatory responses, thereby shaping the host immune microenvironment. The potential outcome of these responses is complex and is likely influenced by various factors, including the pathogen's characteristics and tissue tropism. As research progresses, gaining a comprehensive understanding of how CDTs impact the host immune system, both in vitro and in vivo, will be crucial for unraveling the nuanced role of these toxins in pathogenesis. Future investigations employing immunocompetent hosts and more physiologically relevant infection models will be instrumental in elucidating the full spectrum of CDT-mediated effects on the host immune response.

1.5.2 Importance/Potential Role of different species of CDTs on pathogenesis

In the examination of the potential contributions of Aa-CDT and *Cj*-CDTs to the pathogenesis of their respective pathogens, it is crucial to underscore the limited extent of in vivo investigations on CDTs, especially the lack of studies on the roles of other species of CDT toward pathogenesis. Despite this dearth of direct studies, a handful of work suggest the potential role of these toxins in the intricate landscape of pathogenesis. As previously mentioned, unraveling the multifaceted role of CDT in pathogenesis is inherently challenging, given its involvement in diverse biological systems. In light of this, this section aims to

briefly evaluate select studies that shed light on the repercussions of CDT exposure, that could provide clues to understanding the potential role of CDT for pathogenesis.

The first pathogen extensively investigated in the context of CDTs is *A. actinomycetemcomitans*, a gram-negative coccobacillus implicated in various human diseases, including endocarditis, meningitis, osteomyelitis, subcutaneous abscesses, and periodontal disease. The discovery of Aa-CDTs dates back to 1998 (154) and their strong association with the development of aggressive periodontitis (95). has since fueled extensive research endeavors. Much of the focus on Aa-CDTs has been directed toward understanding their impact on periodontal health, particularly their effects on cells within the oral epithelia. Similar to CDTs found in other bacterial species, Aa-CDT has been shown to induce cell distention and arrest in diverse cell lines, such as HeLa and Hep-2 (5). Human lymphocytes, in particular, exhibit heightened sensitivity to Aa-CDTs, leading to apoptosis in response to treatment (141, 142). In contrast, Aa-CDTs exhibit a different effect on human monocytes and macrophages, triggering the release of pro-inflammatory cytokines rather than inducing cell death (8, 144). This differential sensitivity and cytokine release in response to CDT suggest a potential immunomodulatory role for Aa-CDT in the context of *A. actinomycetemcomitans* pathogenesis. One major role attributed to Aa-CDT involves its potential contribution to the pathogenesis of periodontitis. Aa-CDT-mediated DNA damage has been shown to induce the expression of receptor activator of NF-kB ligand (RANKL) in human gingival fibroblasts and periodontal

ligament cells (12). Significantly, RANKL expression is linked to osteoclast differentiation and contributes to bone resorption, suggesting that CDT-induced RANKL expression may play a role in the pathogenesis of periodontitis. Further exploration using an in vivo rat model demonstrated that the application of CDT resulted in junctional epithelial tissue abrasion, neutrophil infiltration, and overall gingival epithelial damage (32, 34, 114). Notably, despite the presence of CDT during infection, it did not influence the colonization or invasion of the pathogen (140). From these studies, it is evident that the presence of Aa-CDT influences the damage and severity of periodontal disease caused by A. actinomycetemcomitans. However, despite these insights, the precise role of the toxin during pathogenesis remains incompletely understood.

Campylobacter jejuni, a gram-negative bacterium, is recognized as a major causative agent of food-borne infections in humans and is notably a producer of CDT. Despite its prevalence and clinical significance, there has been limited exploration to elucidate the precise role of the toxin in *C. jejuni* pathogenesis. Existing research, however, provides valuable insights into the potential contributions of *Cj*-CDT to the virulence of *C. jejuni*. Studies have demonstrated that *Cj*-CDT is implicated in damaging the colons of SCID mice, pointing towards its potential role in the pathogenesis of this bacterium. Additionally, *Cj*-CDT has been shown to facilitate colonization in mice, suggesting a direct link between the toxin and the ability of *C. jejuni* to establish and persist within the host (96, 122). Notably, further investigations have revealed that the presence of *Cj*-CDT results in more aggressive gastritis and

proximal duodenitis in mice, indicating a potential impact on the severity of the infection (54, 73). Collectively, these studies imply that CDT plays a significant role in the colonization, persistence, and virulence of *C. jejuni*. Despite these findings, the intricate mechanisms by which *Cj*-CDT contributes to the pathogenesis of *C. jejuni* warrant more in-depth exploration.

1.6 TOXIN ASSEMBLY, SECRETION, AND TRAFFICKING

1.6.1 Assembly and secretion of CDTs

The induction of DNA damage by CDTs hinges upon the successful transportation of the catalytic CdtB subunit into the nucleus. The initial phase of CDT pathogenesis involves the synthesis and excretion of the protein toxin. Similar to many AB toxins, CDTs are presumed to be secreted into the extracellular environment. However, our knowledge regarding the secretion mechanisms of the CDT toxin remains limited, with only two studies delving into CDT assembly and secretion. In a study focusing on Aa-CDT, researchers proposed a model where CDT subunits assemble into a holotoxin complex within the bacteria's periplasm, subsequently being secreted as a complex into the extracellular milieu (158, 159). According to this model, the CdtA, CdtB, and CdtC subunits are translocated from the bacterial cytoplasm across the inner membrane to the periplasm in a manner reliant on the Sec-dependent pathway. The assembly of the holotoxin occurs in stages, commencing with the interaction between the CdtA and CdtC subunits at the outer membrane. Once the CdtA-CdtC complex is formed, the dimer is liberated from the outer membrane,

facilitating interaction with CdtB to form a tripartite CDT holotoxin complex (159). Subsequently, this tripartite CDT complex is purportedly secreted from the bacteria using yet-to-be-understood mechanisms. However, for other CDT species, the mechanisms governing holotoxin assembly and bacterial secretion remain unknown.

Alternatively, CDTs have been discovered within outer membrane vesicles (OMVs), though the exact role of OMVs in bacterial pathogenesis remains poorly understood. These vesicles are believed to harbor several potential roles in pathogenesis, including the delivery of virulence factors to the host. Both *A. actinomycetemcomitans* and *C. jejuni* OMVs have been found to contain CDTs (43, 126). Furthermore, studies have demonstrated that these OMVs containing Aa-CDTs induce a cytolethal distending effect on HeLa and HGF cells, indicating their capacity to deliver biologically active CDTs (126). The intriguing aspect of CDT secretion via OMVs lies in the potential impact on interactions with the plasma membrane and potential receptors requiring toxin binding and internalization. Despite the presence of CDTs in OMVs, the extent to which OMVs contribute to CDT pathogenesis remains unclear. The precise role of OMVs in the context of CDT pathogenesis warrants further investigation to understand their significance in the overall mechanism of CDT-mediated toxicity.

1.6.2 Intracellular trafficking of CDTs

After protein toxins are released into the extracellular milieu, their next crucial step involves identifying and binding to specific host cells to initiate their

pathogenic effects. CDTs operate under a similar paradigm, relying on binding to a particular host receptor as a prelude to infiltrating host cells. A critical knowledge gap within the CDT research domain pertains to the elusive identity of the host receptor that facilitates CDT binding—a pivotal yet poorly facet of CDT biology. Addressing this gap stands as one of the objectives in this thesis, emphasizing the delineation of the receptor associated with *Cj*-CDT internalization. Addressing this gap in knowledge constitutes a focal point of the concluding section of the thesis, and it will provide invaluable insights into understanding the mechanism by which CDTs invade host cells, a crucial step in comprehending their pathogenic effects.

Once bound to the host receptor, CDT's are thought to be internalized via a dynamin-dependent and Clathrin-dependent mechanism of endocytosis, as shown for Hd-CDTs on HeLa cells (30). Subsequently, CDTs are thought to travel through the endosomal compartments, specifically from the early endosomes to the late endosomes. This was elucidated from experiments where treatment of cells with drugs that block early-late endosomal maturation, such as NH_4Cl, bafilomycin A1 and monensin, as well as using a dominant negative mutant of the small GTPase Rab7, lead to an inhibition of CDT mediated DNA damage (62, 65). Microscopy evidence also supports the endosomal localization of Ec-CDTs (40). From the early to late endosomes, CDTs are believed to journey to the trans-Golgi network—a phenomenon akin to other AB toxins like Shiga toxin and cholera toxin (132, 164). However, the mechanism orchestrating CDT delivery to the Golgi remains elusive. Several key findings substantiate the

importance of Golgi trafficking in CDT activity. Disruption of the Golgi apparatus with the drug Brefeldin A nullified Hd-CDT activity (62, 65). In addition, Hd-CDT was shown to be sulphated during CDT intoxication of HeLa cells. Protein sulphation is a post-translational modification that occurs exclusively in the trans-Golgi and using a mutant Hd-CdtB containing a sulphation site (65). Transport through the Golgi apparatus was also shown to be required for Ec-CDT (62). Subsequently, CDTs are speculated to travel from the Golgi to the endoplasmic reticulum (ER). This transition has been demonstrated via microscopy for both Hd-CDT and Ec-CDT (62). Furthermore, biochemical assays utilizing a mutant Hd-CdtB subunit containing a specific glycosylation site, an ER-specific post-translational modification, corroborated this transit (65). However, understanding the precise localization within the endoplasmic reticulum for Aa-CDT remains elusive, as it has been inconclusively shown to localize in discrete foci, possibly representing the trans-Golgi network or ER compartments via immuno-fluorescence microscopy (4, 33).

The subsequent step in CDT pathogenesis involves its presumed exit from the endoplasmic reticulum and subsequent translocation to the nucleus. This process remains poorly understood and poses conflicting data. The ER-associated degradation pathway has been shown to be crucial for the ER-cytosol translocation for several other AB toxins mentioned previously, such as cholera, Shiga, pertussis, and ricin toxins. One study by the Guerra group proposed that Hd-CDT does not employ the classical ER-associated degradation pathway to transition from the ER to the cytosol (65). Conversely, Eshraghi et al., identified

three components of the ERAD pathway, namely Derlin-2, Hrd1, and ATPase 97, as essential for the biological activities of *Aa*, *Cj*, *Ec*, and *Hd*-CDTs (49). Although efforts using confocal microscopy analysis and biochemical assays failed to detect Hd and Ec-CDT in the cytosol of intoxicated cells (62, 65), suggesting the possibility of a direct translocation from the ER to the nucleus, Aa-CDTs have been readily detected in the cytosol of CHO cells using fluorescent microscopy (33).

Once in the cytosol, the prevailing hypothesis suggests that CDTs translocate to the nucleus via a nuclear localization signal (NLS) found within the amino-terminal region of CdtB (109). For Ec-CdtB, two NLS sequences (NLS1 and NLS2) have been identified in the carboxy-terminal region. Deleting these regions prevented cell cycle arrest activities and nuclear localization without affecting DNase activity (97). However, such NLS sequences remain unidentified for Aa, *Cj* or Hd-CDTs. An overview of the potential retrograde transport pathway taken by CDT is represented in Figure 1.11. The overall retro-transport mechanism utilized by *Cj*-CDTs and less-studied CDTs from the cell surface to the nucleus stands as a significant gap in knowledge, warranting further investigation to unravel the intricate molecular pathways governing *Cj*-CDT retro-trafficking, a crucial step in understanding its pathogenic mechanisms.

A poorly addressed and crucial gap in knowledge in CDT research lies in comprehending the roles undertaken by the CdtA and CdtC subunits in orchestrating the intracellular trafficking of the CdtB subunit. There exists a compelling belief that these accessory subunits might significantly influence

distinct routes of endosomal trafficking, as evidenced by observations made with Hd and Ec-CDTs (40). Intriguingly, insights into the trafficking of Aa-CDT subunits suggest potential differences from the other CDTs. Notably, it is hypothesized that while the Aa-CdtA subunit might not undergo internalization, the Aa-CdtC subunit likely traffics alongside the Aa-CdtB subunit, albeit not to the nucleus (33). These observations align with unpublished data indicating that only the Hd-CdtC subunit translates to the Golgi apparatus, distinct from the Hd-CdtA subunit. This collective data implicates the necessity of the CdtA and CdtC subunits in the proper internalization of CDT. However, it raises intriguing speculations that the intracellular trafficking of the CdtB subunit might depend on one or both of these accessory subunits. Furthermore, the notion emerges that different species of CDTs might employ disparate trafficking mechanisms to facilitate the nuclear localization of the CdtB subunit. A clearer comprehension of the functions executed by the CdtA and CdtC subunits could potentially illuminate the strategies employed by CDTs to reach the nucleus. This understanding is important in unraveling the intricate interplay and roles undertaken by individual CDT subunits in dictating the complex trafficking routes and cellular destinations of the toxin. By delineating the functions of these accessory subunits, researchers could gain crucial insights into the mechanisms by which CDT orchestrates its intracellular journey and ultimately achieves its pivotal role in inducing cellular damage.

1.7 STRUCTURAL INSIGHTS INTO CDTS

The three CDT genes in code for three distinct polypeptides named CdtA, CdtB, and CdtC whose molecular masses vary depending on the species of toxin, ranging from 20-30 kDa per subunit. Among the studied CDT variants, Aa and Hd-CDT showcase the highest sequence similarity, with the CdtB subunit emerging as the most conserved among all species (95, 120). These three CDT subunits are thought to interact non-covalently in a 1:1:1 ratio, with points of contact between all three subunits, to form a heterotrimeric complex. This is very different from the previously discussed AB toxins, which often have multimers of their B component (binding component) that allow for host cell recognition. For these AB toxins, one common theme is that the multimeric B components form a platform that enables the toxin to recognize their host receptor. We speculate that having multiple binding subunits is required for these toxins in order to interact with their receptors. An essential gap in current understanding, which forms a pivotal focus in this dissertation, pertains to the relationship between the CDT holotoxin complex and its biological activity. Presently, there exists no conclusive evidence for the in vivo formation of a CDT holotoxin complex. Detecting the CDT holotoxin complex in vivo poses a substantial challenge due to the limited amounts of toxin secreted by pathogens during growth or infection. The only CDT where the toxin subunits have been detected, using westernblot analysis, from their native pathogen is Hd-CDT (153), suggesting that CDTs are typically expressed in low concentrations from their native pathogens. Given the

low expression of CDTs, most research laboratories utilize recombinantly expressed CDTs for their investigative studies.

The prevailing belief that CDT subunits assemble into a heterotrimeric complex is strongly influenced by the elucidation of crystal structures for Hd and Aa-CDTs (Figure 1.12) (107, 169). High-resolution structural data for Aa-CDT and Hd-CDT at toxin concentrations surpassing 100 uM indicated the formation of a triangular tripartite structure where the three toxin subunits intricately interface with one another. Notably, mutations designed based on these structural insights, aimed at potentially disrupting subunit interactions, were reported to attenuate the cellular activity of Aa-CDT (22, 169). However, despite these crystallographic revelations, the structurally defined biologically active form of the toxin binding to sensitive host cell surfaces remains inadequately understood. The structural data from crystallography strongly suggests the potential of Aa and Hd-CDT subunits to form a complex in solution. However, these experiments were conducted at toxin concentrations far exceeding what is believed to be physiologically relevant during infections. In vitro studies with recombinant CDTs, including those from our laboratory and others, have demonstrated toxin biological activity at much lower nanomolar concentrations. Unlike other AB toxins that typically interact covalently, CDTs are believed to interact with each other in a non-covalent manner. Whether the CDTs are secreted as an assembled complex or exist as an assembled complex in solution remains an area of uncertainty.

It's notable that while Aa and Hd-CDTs exhibit significant sequence homology (>90%), other species of CDTs differ substantially from each other. For instance, *Cj*-CdtA shares only 25% amino acid sequence similarity with Hd-CdtA, *Cj*-CdtB shares only 50% similarity with Hd-CdtB, and *Cj*-CdtC shares a mere 24% similarity with Hd-CdtC (120). This raises questions regarding how and whether other species of CDTs interact to form a heterotrimeric complex, akin to Aa and Hd-CDTs. Despite the known requirement for all three CDT subunits for maximum cellular activity, it remains uncertain whether assembly into a heterotrimeric complex is a prerequisite for the toxin's cellular activity. One potential scenario posits that toxin activity might be achievable without the subunits interacting, while another proposes that assembly into a holotoxin complex might be necessary for activity but could occur prior to toxin secretion, possibly at the host cell surface. Addressing this gap in understanding constitutes a primary focus of the second chapter of this thesis, aiming to shed light on the dynamics of CDT subunit interactions and their correlation with the toxin's biological activity.

1.8 CDT HOST CELL BINDING AND RECEPTOR RECOGNITION

As previously highlighted, the initial phase of extracellular protein toxin intoxication involves binding to a specific host cell receptor. For AB toxins to gain entry into host cells, they must recognize and bind to these receptors, triggering the endocytosis of the toxin. In the realm of CDT research, a major knowledge gap pertains to the identification of the host cell receptor, and a goal of our work

is to pinpoint potential receptors essential for CDT activity. Although the exact receptor for CDT remains elusive, valuable insights shed light on how CDTs interact with the host plasma membrane. Notably, CDTs have demonstrated a reliance on lipid rafts for association with host cells. Several experiments have evidenced that the depletion of cholesterol significantly diminishes toxin association with the host cell surface, concurrently abrogating biological activity(19, 50, 65, 89). This importance of cholesterol for CDT binding is further supported by bioinformatics and molecular simulation data, indicating the presence of a cholesterol recognition amino acid consensus (CRAC) region within the CdtA and CdtC subunits of Aa, *Cj*, and Hd-Cdts, alongside surface-exposed residues implicated in membrane binding. Mutations in these CRAC sites and surface elements have shown a decrease in CDT binding and biological activities (20, 108). Nevertheless, conflicting reports exist where cholesterol depletion did not impede CDT binding and toxicity (33, 50). These discrepancies likely stem from variations in cell lines used across different studies, coupled with limitations in the use of compounds like methyl β-cyclodextrin to explore toxin internalization. Chemical agents may induce varying alterations in cellular pathways and functions, yielding different outcomes based on cell type. Moreover, factors such as toxin concentration and experimental design may influence observed results.

Apart from cholesterol, Aa-CDT has exhibited co-localization with ganglioside GM1, a recognized lipid raft marker, observed through immuno-fluorescence microscopy (19). Sphingomyelin is also believed to play a crucial

role in CDT receptor recognition. The inactivation of the SGMS1 gene, responsible for encoding sphingomyelin synthase 1, an enzyme pivotal in sphingomyelin biogenesis, markedly reduced the biological activity of Aa, *Cj*, Ec, and Hd-CDTs (23).

Despite efforts, identifying the specific receptor for CDTs remains a challenge in the field, although the ideal receptor recognized by CDTs on the cell surface is believed to be widely expressed, considering the sensitivity of diverse cell types to CDT activity (64). Glycoproteins and glycolipids stand out as potential candidates for CDT receptors. Several studies have explored potential cell surface receptors for CDTs, yielding diverse findings. For instance, investigations with Ec-CDT indicated the toxin's binding to fucose and fucose-containing glycoproteins in vitro. Researchers demonstrated this through competition experiments using fucose-specific lectins and by removing N-linked surface sugar moieties, effectively blocking CDT intoxication of HeLa cells (98). Similarly, a study involving Aa-CDT suggested that Aa-CdtA might interact with fucosylated thyroglobulin, with a single point mutation in the Aa-CdtA subunit disrupting this interaction (22). On the other hand, contrasting reports from our lab have demonstrated that N- or O- linked glycosylation as well as fucose biosynthesis was not required for the intoxication by Aa, *Cj*, Ec, and Hd-Cdts (50). Intriguingly, our findings revealed diverse behaviors among different CDTs. For example, inhibiting N-glycosylation using tunicamycin either prevented or significantly reduced CHO cell intoxication by Aa, Ec, and Hd-CDTs, while notably enhancing *Cj*-CDT activity. Tunicamycin has been demonstrated to affect

receptor folding and export to the cell surface, suggesting that while receptors for CDTs might be glycosylated proteins, glycosylation could also be pivotal for the proper presentation of the receptor on the cell surface. Moreover, research on Aa-CDT highlighted its binding to surface glycosphingolipids. Inhibitors of glycosphingolipid synthesis or pre-incubation of Aa-CDT with GM3-containing liposomes effectively hindered the intoxication of human monocytic U937 cells. Additionally, they revealed strong binding of Aa-CDT to GM1, GM2, GM3, and Gb4, with Aa-CdtC exhibiting a preference for GM1 and GM2, determined through thin-layer chromatography analysis (103).

Collectively, these findings depict significant discrepancies regarding CDT receptor identification. A plausible explanation for these disparities might lie in different CDT members binding to distinct receptors. This notion is not unfounded, given the lower conservation degree of the binding subunits, CdtA and CdtC, among various toxin family members. Additionally, factors like experimental design and cell type could substantially influence these outcomes. The forthcoming third chapter of this thesis endeavors to evaluate the receptor dynamics concerning *Cj*-CDTs, aiming to contribute valuable insights into understanding the complex interplay between CDTs and their potential receptors across different cellular contexts.

1.9 OVERALL CONCLUSIONS

Our studies support the idea that the *Cj*-CdtA and *Cj*-CdtC subunits play an important role in the delivery of the catalytically active *Cj*-CdtB subunit into the

nucleus. The retro-transport of the *Cj*-CdtB subunit relies on intact Golgi apparatus and endoplasmic reticulum, although the exact role of these organelles as well as the roles of *Cj*-CdtA and *Cj*-CdtC subunits in the delivery of the *Cj*-CdtB subunit to these organelles remains unclear. While the 3 *Cj*-CDT subunits are thought to interact to form a heterotrimer complex that is required for biological activity, our experimental results suggest solution mixtures of *Cj*-CDT, at the lowest concentrations at which the toxin is biologically active, are comprised primarily of non-interacting subunit monomers. These results suggest that the existing paradigm that *Cj*-CdtA, *Cj*-CdtB, and *Cj*-CdtC functionally interact with host cells as a preassembled, heterotrimeric complex should be revisited. We propose alternative models, backed by preliminary work, to address the disparity between heterotrimeric formation before host cell interaction and toxin activity. Our proposed models include: 1) the *Cj*-CDT subunits assemble into a functional heterotrimeric complex but at the host cell surface. 2) The *Cj*-CDT subunits do in fact interact with cells as an assembled heterotrimeric complex, albeit at very low concentrations that are undetectable by experimental approaches used in this study, implying that assembled *Cj*-CDT possesses a much higher specific activity than has been previously experimentally determined. In addition, the weak toxin affinity might be a strategy to allow the pathogen to limit toxin activity on host cells. Overall, these studies challenge our understanding of the structure function relationships of *Campylobacter jejuni* cytolethal distending toxin and bring new and important insights to the behavior of CDTs and even other multimeric AB-type toxins.

1.10 FIGURES AND TABLE

Figure 1.1

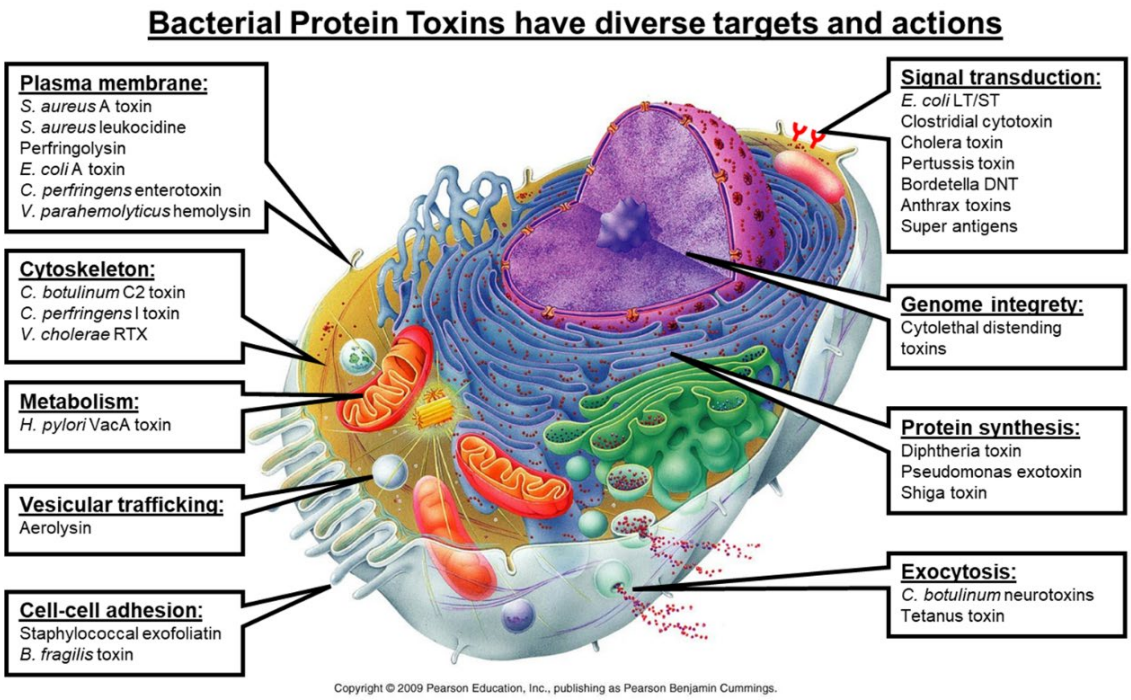

Figure 1.1: Diversity of bacterial protein toxins. Bacterial toxins have a diverse range of targets and functions. Here is a list of several examples of different bacterial protein toxins and the cellular processes that they target. (Chen, unpublished 2024)

Table 1.1

Table 1. Summary of Plant and Bacterial AB Toxin Structure and Function.

	A Subunit(s)	B Subunit(s)	Enzymatic Activity	Target	Receptor(s)
Cholera toxin	A1: 22 kDa A2: 5 kDa	(×5) 10.6 kDa	ADP-ribosyl transferase	Adenylate cyclase *G*-protein ($G_{s\alpha}$)	GM1 ganglioside
***E. coli* (LT)**	A1: 22 kDa A2: 5 kDa	(×5) 11.6 kDa	ADP-ribosyl transferase	*G*-protein ($G_{s\alpha}$)	GM1 ganglioside Asialoganglioside
Shiga toxin	A1: 28 kDa A2: 4 kDa	(×5) 7.7 kDa	*N*-glycosylase (Cleaves adenine 4324)	rRNA (28S)	Gb3 glycolipid
Pertussis toxin	S1: 28 kDa	S2: 23 kDa S3: 22 kDa S4: (×2) 11.7 kDa S5: 9.3 kDa	ADP-ribosyl transferase	*G*-protein ($G_{s\alpha}$)	GD1a ganglioside
Anthrax	(LF): 90 kDa (EF): 89 kDa	(PA): (×7) 83 kDa	Zn metalloprotease Adenylate cyclase	MAPKK Protein kinases	ANTXR 1 ANTXR 2
Ricin	30 kDa	29 kDa	*N*-glycosylase (Cleaves adenine 4324)	rRNA (28S)	Glycoprotein Glycolipid

Table 1.1: Comparison of AB toxin Structure and Function. Summary of the six well studied AB toxins, highlighting the different compositions of their A subunits and B subunits, enzymatic activity of their A subunits and their targets, and the receptor with which the B subunits recognize (111).

Figure 1.2

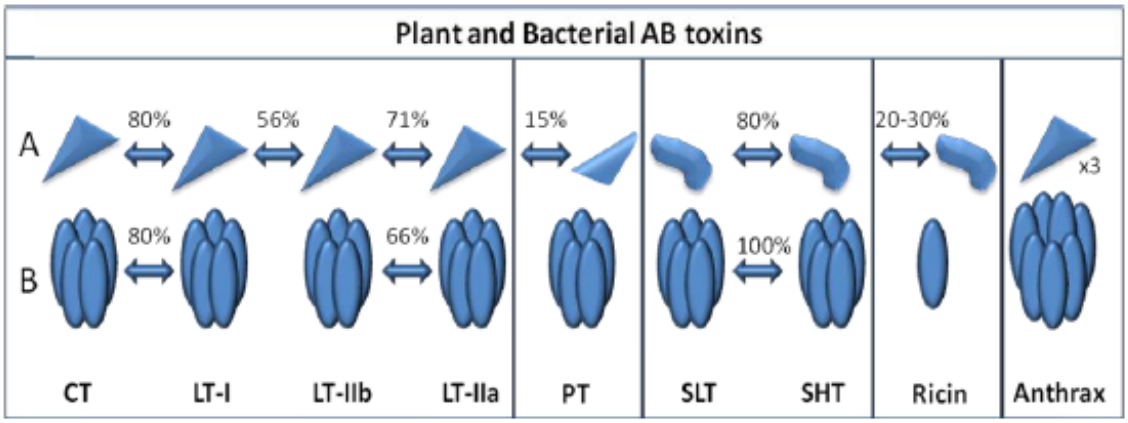

Figure 1.2: Diagram representation of the structural and amino acid sequence homologies among bacterial and plant AB toxins. (A) The top panel represents the catalytic A subunit proteins. **(B)** The bottom panel represents the membrane binding B subunit proteins. The approximate values for amino acid sequence homologies observed among these AB subunits depicted from different enterotoxins are provided as percentages. Enterotoxin subunits with no arrows between them share little or no amino acid or structural homologies (99).

Figure 1.3

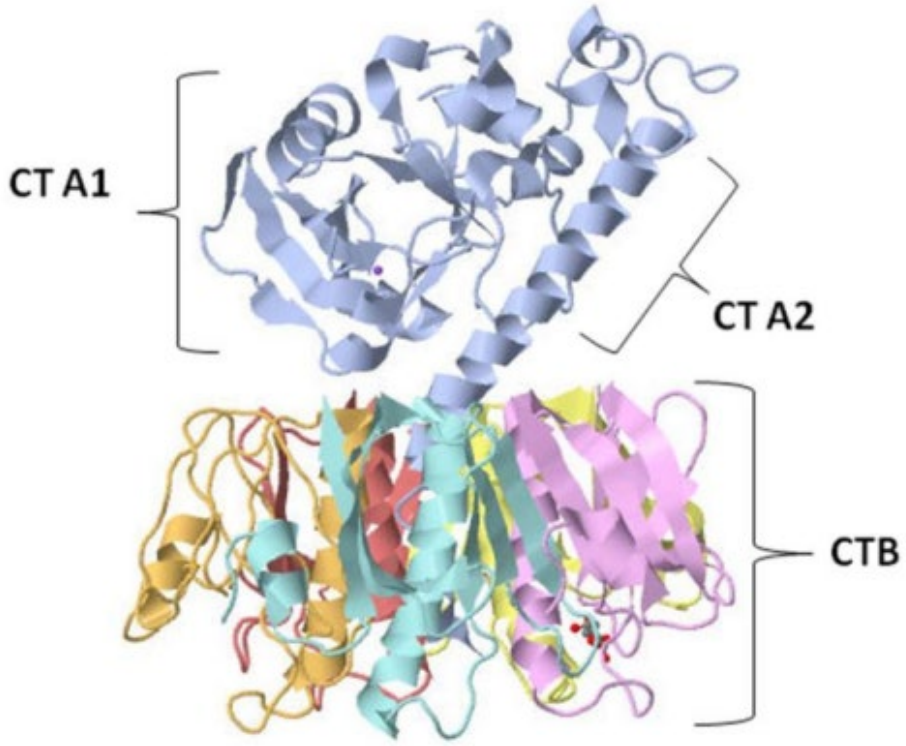

Figure 1.3: Cholera toxin. Crystal structure of cholera toxin. Cholera toxin A subunit (CTA), in blue, is a heterodimeric protein composed of two polypeptide chains, CTA1 (22 kDa) and CTA2 (5 kDa), linked by a single disulfide bond. The CTA2 subunit links the active CTA1 subunit to the pentameric cholera toxin B subunits (CTB). The CTB (10.6 kDa) is composed of five identical polypeptide subunits (yellow, purple, red, orange, and turquoise), each with membrane receptor GM1 ganglioside binding capacity (111).

Figure 1.4

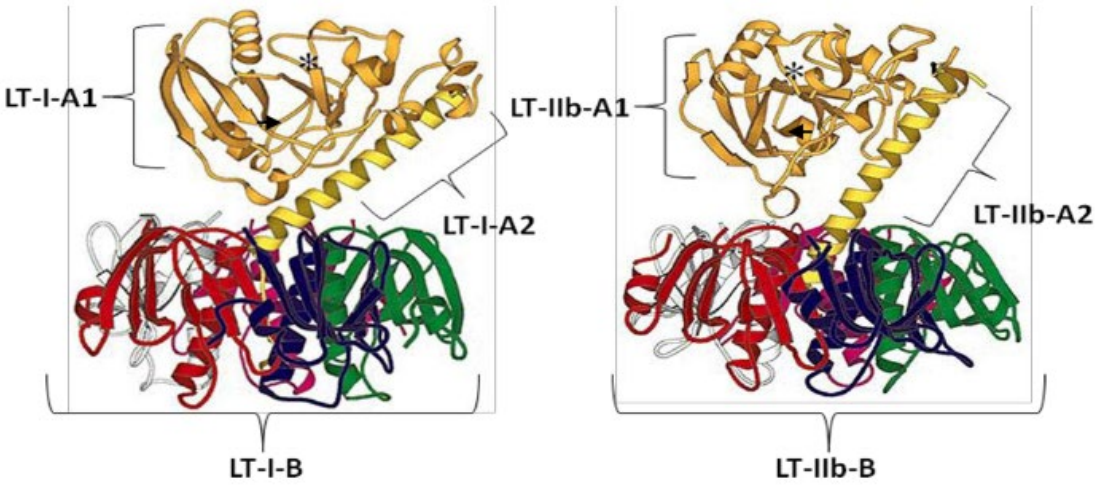

Figure 1.4: Heat labile toxin. Crystal structure of Heat Labile LT-1 (Left) and LT-IIb (Right). The A1 subunits are in gold (upper left) and the A2 subunits are in yellow (upper right). The B subunits are identical and are displayed as red, white, pink, green, and blue ribbon structures. The asterisks highlight the active site, while the black arrows highlight the disfulfide bonds that link the two A subunits together (160).

Figure 1.5

Figure 1.5: Shiga Toxin. Crystal structure of the Shiga toxin. The A subunit (StxA) is depicted in yellow, is composed of two subunits A1 (28 kDa) and A2 (4 kDa) and sits upon the pentameric B subunits (StxB) depicted in blue, purple, green, magenta, and red (each identical and 7.7 kDa). The A subunit amino and carboxy terminus are labelled N and C respectively. C242 and C261 mark the two cysteines of the disulfide bridge linking A1 and A2. All 5 B subunits are linked together via disulfide bridges. StxB associates with StxA by having only three of the B subunits interacting with the C-terminus of the A2 fragment, thus making StxA bend to the side opposite from the B subunit (55).

Figure 1.6

A) **B)**

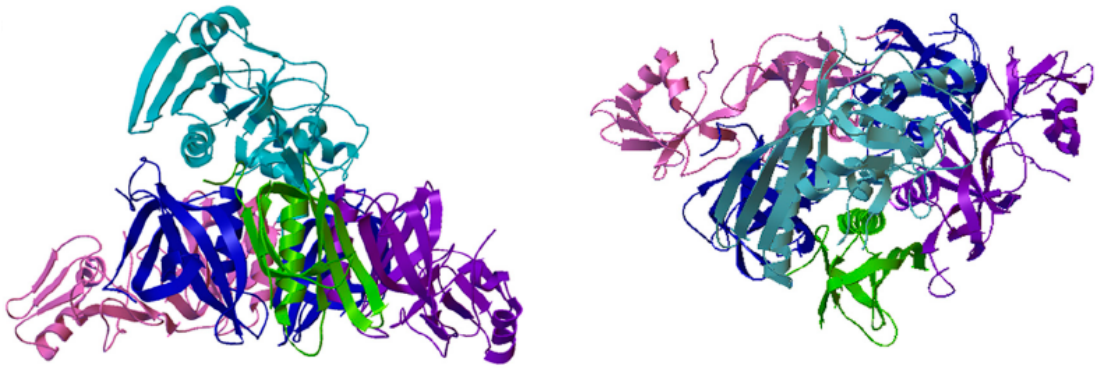

Figure 1.6: Pertussis toxin. Pertussis crystal structure with side **(A)** and top-down **(B)** views of the pertussis toxin (PT). The A subunit (PTS1, light blue) sits above and within the central cavity of the B pentamer which is composed of an S2 subunit (purple), an S3 subunit (pink), two copies of the S4 subunit (blue), and an S5 subunit (green) (156).

Figure 1.7

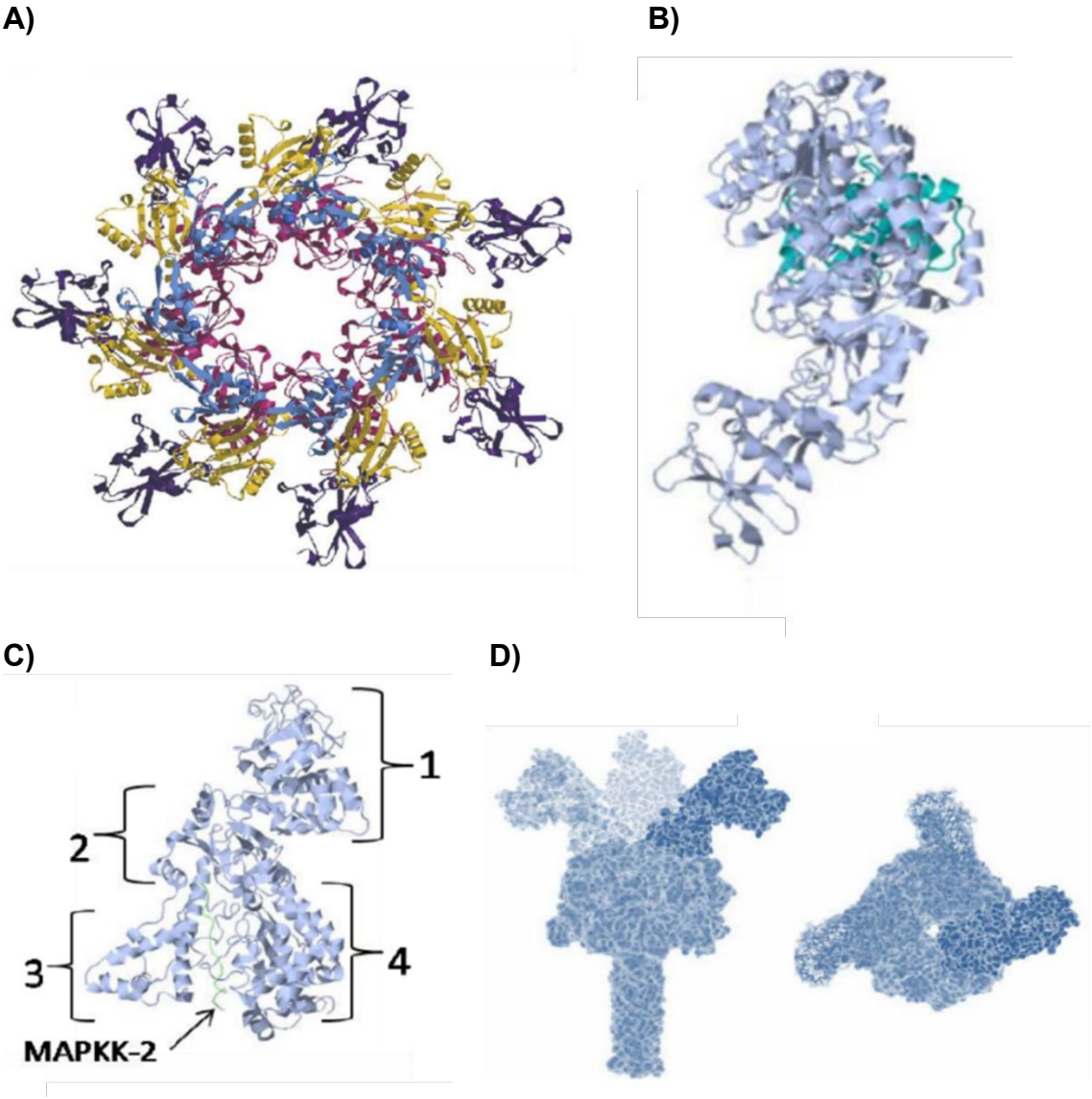

Figure 1.7: Anthrax Toxin. (A) Computer modeled top-down view of anthrax toxins protective antigen (63 kDa) that forms a heptamer. Each individual PA monomer is comprised of four domains. A hydrophobic region that binds LF and EF (blue), a heptamerization domain that plays a role in membrane insertion (red), a functional domain (yellow), and a receptor binding domain (purple). **(B)** Model of the anthrax edema factor (light blue) protein bound to calmodulin (turquoise). **(C)** The anthrax lethal factor (LF), with domains 1-4 labeled respectively. **(D)** Computational prediction of anthrax holotoxin structure (26, 111).

Figure 1.8

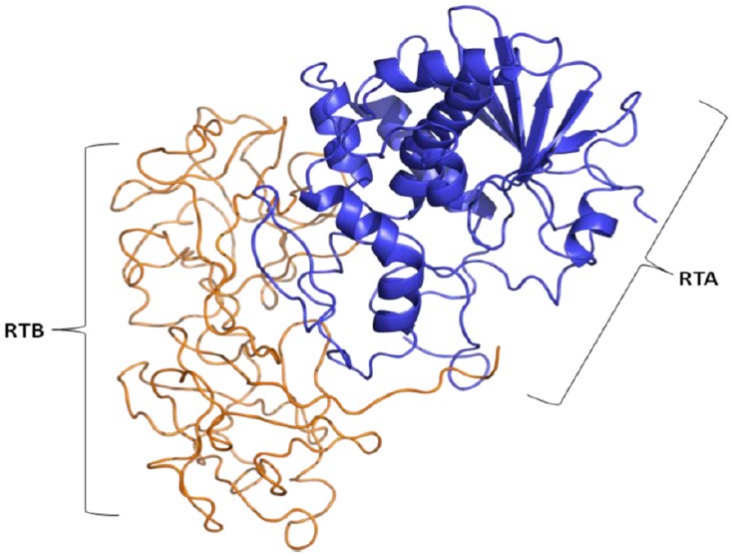

Figure 1.8: Ricin Toxin. Computer generated crystal structure of ricin with the A subunit (blue) and the B subunit (gold). Ricin contains a catalytically active ribosome-inactivating (32 kDa) A chain (RTA) linked by disulfide bonds to a galactose-binding lectin B subunit (34 kDa) (RTB) (58).

Figure 1.9

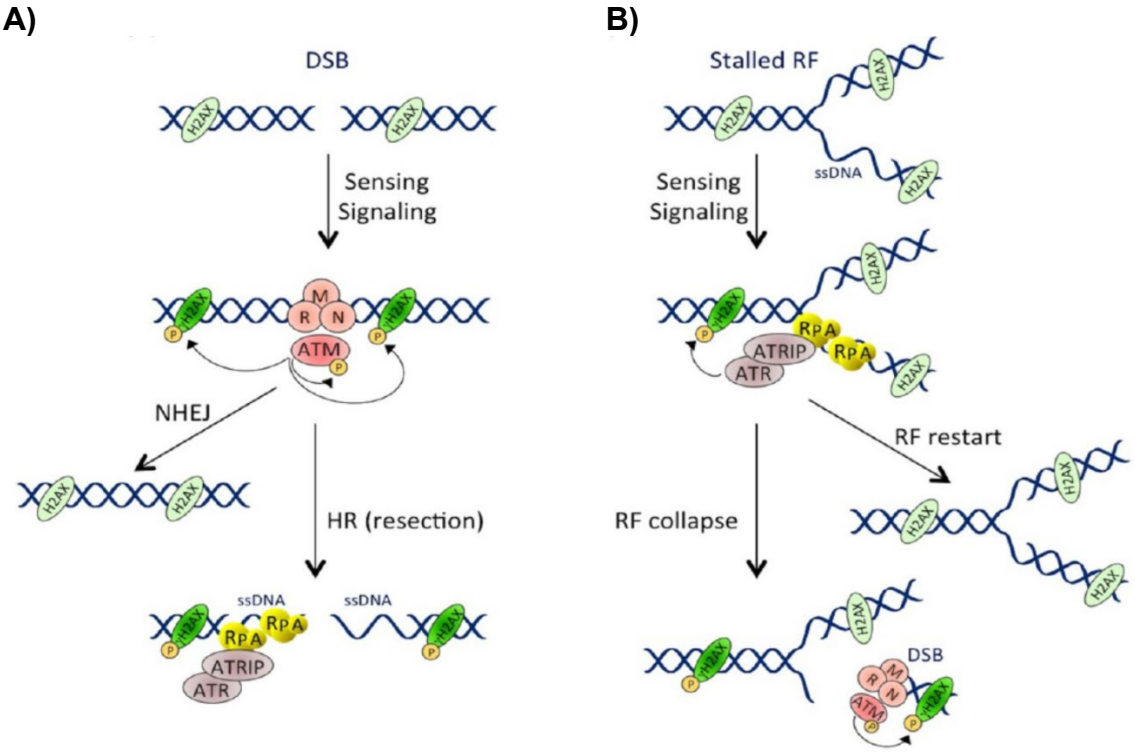

Figure 1.9: Activation and cross talk between ATM and ATR pathways. (A) Pathway in response to double-stranded DNA breaks (DSB). The formation of DSBs results in the recruitment of the MRN complex in an ATM-dependent manner. ATM also phosphorylates numerous substrates, including itself and H2AX near the site of the DSB. The repair of the DSB occurs through non-homologous end joining (NHEJ) or homologous recombination (HR) mechanisms. During HR repair, DSB usually results in stretches of ssDNA that are recognized and coated by RPA, leading to ATRIP-dependent ATR recruitment and activation. **(B)** Pathway in response to ssDNA, which is usually produced as a result of replication fork (RF) stalling. ssDNA is recognized and coated by RPA. Accumulation of RPA is recognized by ATRIP, which recruits and activates ATR. ATR then phosphorylates other substrates, including H2AX. At this point the RF can restart or collapse, which in this cause induces DSB formation and the previously mentioned ATM-dependent repair response (15).

Figure 1.10

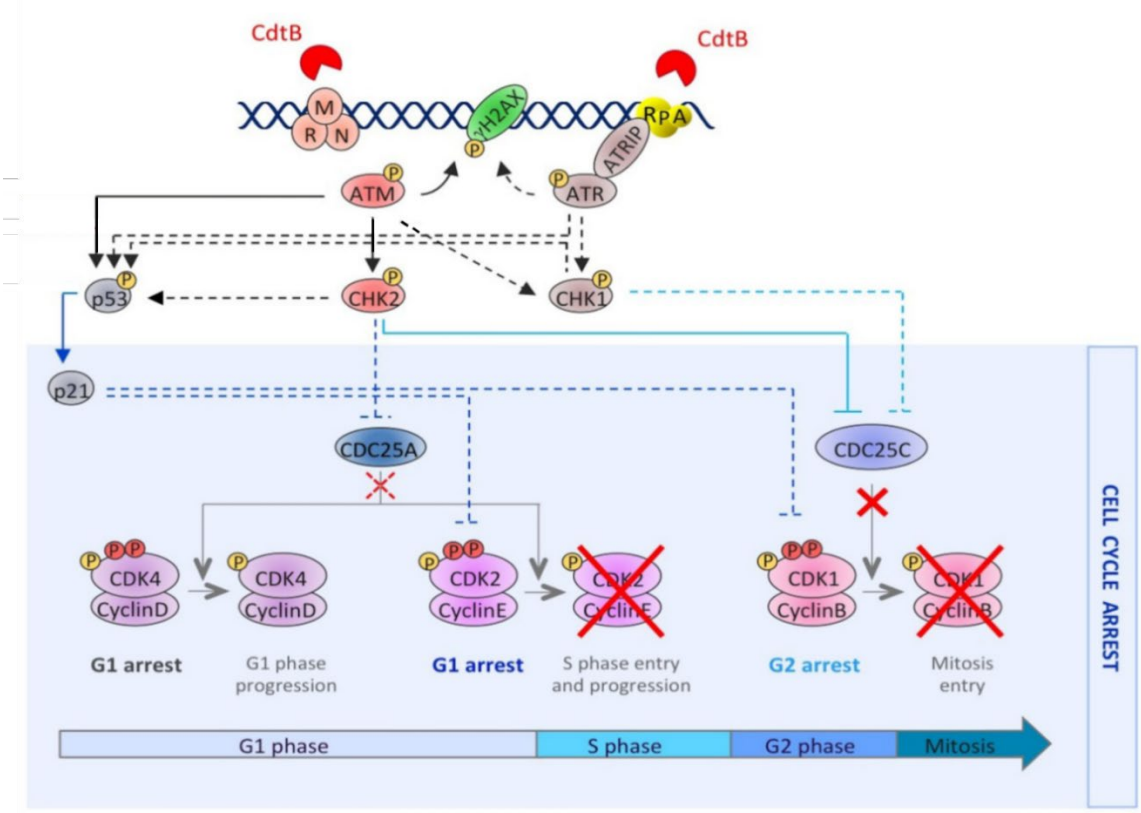

Figure 1.10: Consequence of CDT mediated DNA damage on the host cell cycle. This model depicts the molecular events of the DDR response to CDT mediated DNA damage and the consequences on host cell cycle progression. The dotted lines signify known events occurring during the DDR but have not yet been demonstrated for CDT exposure. CdtB induces DNA lesions that are detected by cellular sensors such as the MRN coplex and RPA, resulting in the recruitment and the activation of the PI3K related kinases, ATM and ATR. ATM and ATR then phosphorylate many different substrates, including H2AX, CHK1, CHK2 and p53 (black arrows). This signaling cascade results in the regulation of cell cycle modulators (blue lines), through the inhibition of CDC25C phosphatase by CHK2 and CHK1. Phosphorylated CDC25C is inactivated and unable to activate the cyclin B/CDK1 complex (red crosses), which results in G_2/M phase arrest. In addition, p53 can lead to an accumulation of p21, which can result in cellular arrest in the G_1 phase by inhibiting the CDK2/cyclin E complex (15).

Figure 1.11

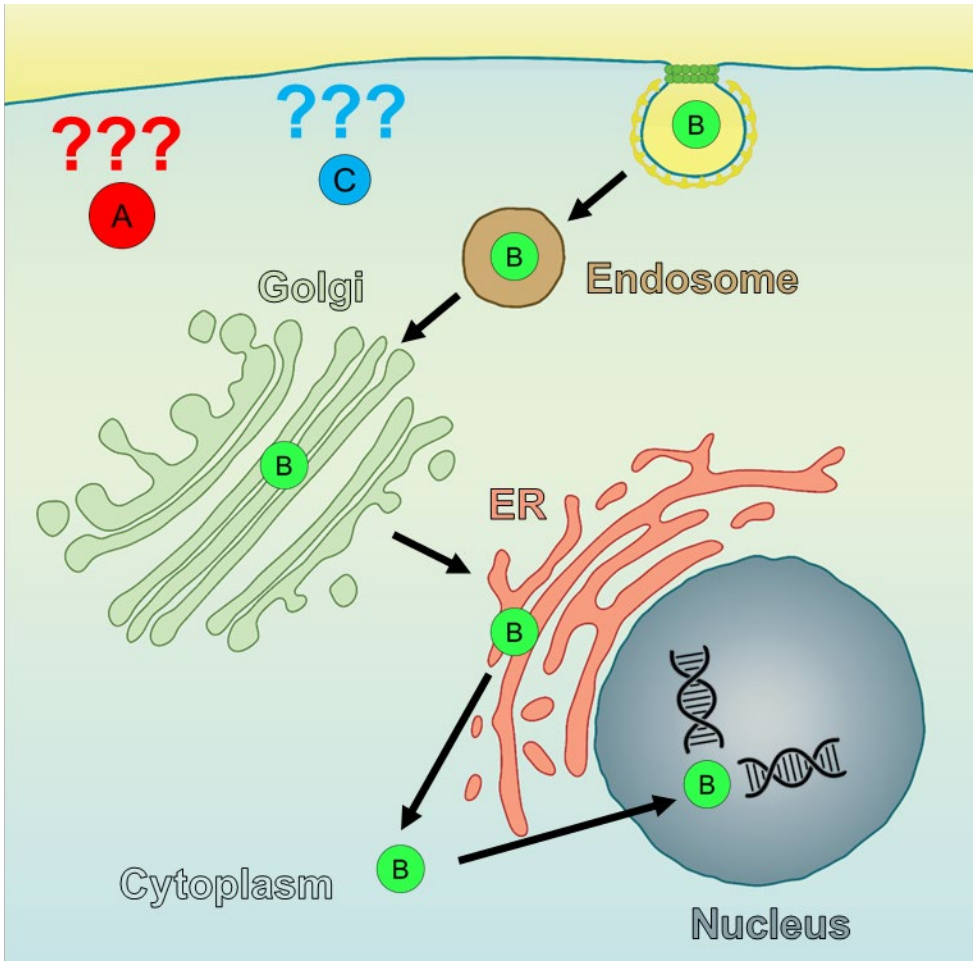

Figure 1.11: Intracellular Trafficking of CDT. The CdtB subunit is believed to undergo retro-trafficking from the host cell surface to the nucleus. Initially, the CdtB subunit binds to an unidentified host cell receptor, leading to internalization into endosomes. The CdtB subunit is then hypothesized to traverse from early to late endosomes. From the late endosomes, the CdtB subunit is then believed to traffic to the Golgi apparatus, where it engages with retro-trafficking machinery to reach the endoplasmic reticulum. From the endoplasmic reticulum, the CdtB subunit is thought to escape to the host cell cytoplasm using the endoplasmic reticulum associated degradation pathway. Once in the cytoplasm, the CdtB subunit is then believed to localize to the nucleus, using a non-canonical nuclear localization signal. The roles of the CdtA and CdtC subunits in the retro-trafficking of the CdtB subunit remain poorly understood (Chen, unpublished 2024).

Figure 1.12

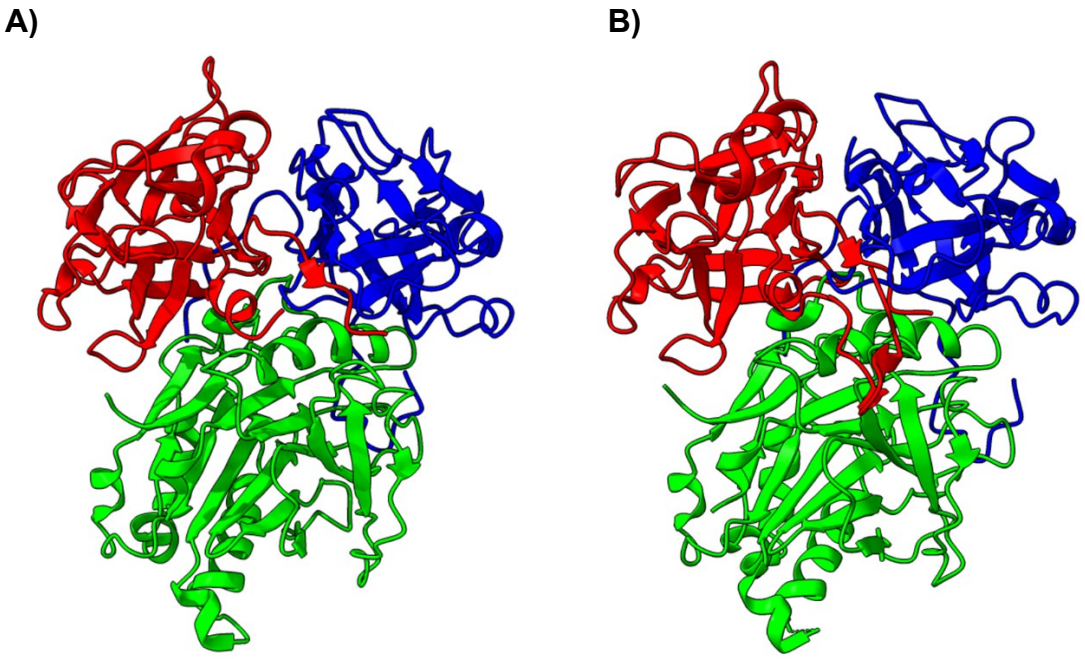

Figure 1.12: Cytolethal distending toxin. (A) Crystal structure of Aa-CDT with the A subunit (Red), CdtB subunit (Green), and CdtC subunit (Blue). Each subunit (~24.5 kDa, ~28 kDa, and ~18 kDa, respectively) has domains that contact one another form a heterotrimeric complex (107). **(B)** Crystal structure of Hd-CDT with the A subunit (Red), CdtB subunit (Green), and CdtC subunit (Blue). Each subunit (~24.5 kDa, ~31.5 kDa, and ~20.6 kDa, respectively) has domains that contact one another form a heterotrimeric complex (169).

CHAPTER 2: THE INTRACELLULAR TRAFFICKING OF THE CJ-CDT SUBUNITS

2.1 INTRODUCTION

The cytolethal distending toxins (CDT) belong to the AB-type toxin family, characterized by their genotoxic properties, and are produced by a diverse array of clinically relevant gamma and epsilon proteobacteria. Among these bacteria, *Campylobacter jejuni* stands out as a significant contributor to foodborne illnesses in the United States. AB-type toxins exhibit a unique two-component structure enabling the targeted delivery of enzymatic proteins to specific intracellular sites within host cells, thereby manipulating essential cellular processes. To achieve this, these protein toxins typically hijack host cellular processes for site-specific transport. CDTs consist of three polypeptides: CdtA, CdtB, and CdtC, with CdtB being the presumed active subunit possessing DNase-like activities. Meanwhile, CdtA and CdtC are believed to aid in delivering CdtB to the host cell nucleus. Previous studies, including our own, suggest that CdtA and CdtC likely participate in the retrograde transport of CdtB to the nucleus. However, the precise roles of CdtA and CdtC in this transport process remain poorly understood.

After binding to host cell receptors, CDT is believed to undergo sequential transport through various cellular compartments, including the endosome, Golgi apparatus, endoplasmic reticulum, cytosol, and ultimately the nucleus. However, a significant gap in our understanding lies in the role of the CdtA and CdtC

subunits in facilitating this transport across different compartments. Unlike cells, proteins lack inherent mechanisms for physical transport between compartments and thus rely on cellular transport mechanisms to reach their destinations, whether inside or outside the cell. Typically, proteins are synthesized by ribosomes in the cytoplasm before being transported to the endoplasmic reticulum for proper folding, a critical step for their functionality. Once folded correctly, these proteins are sorted and directed to their designated locations within the host cell by the Golgi apparatus. Transport of these proteins often occurs within specialized organelle compartments known as endosomes. AB toxins such as CDTs present a unique challenge as they require transport in the opposite direction of the typical pathway followed by host proteins. To achieve this, they exploit existing host transport mechanisms, a process known as retrograde transport, which remains poorly understood. Specifically concerning CDTs, the mechanism by which the CdtB subunit is transported from the host cell surface to the nucleus remains elusive.

Here, we present investigations into *Campylobacter jejuni* CDT (*Cj*-CDT) aimed at elucidating the involvement of the *Cj*-CdtA and *Cj*-CdtC subunits in the retrograde transport of the *Cj*-CdtB subunit to the nucleus. Previous in vitro studies, both from other labs and our own, have underscored the significance of the CdtA and CdtC subunits for the biological activity of the toxin. In addition, the importance of functional endosomes, Golgi apparatus, and endoplasmic reticulum for toxin activity has been supported in our studies. However, the specific roles and fates of these subunits remain unresolved. We hypothesize

that if the *Cj*-CdtA and *Cj*-CdtC subunits indeed facilitate the delivery of *Cj*-CdtB through various organellar compartments, we would expect to observe co-localization of these subunits with *Cj*-CdtB at the respective organelles involved in the delivery process. Through immunofluorescence microscopy imaging, we attempted to capture the intracellular trafficking of the *Cj*-CdtA and *Cj*-CdtC subunits within host cells. However, our findings proved inconclusive. While these results do not provide definitive answers, they suggest potential explanations. It is plausible that the techniques at our disposal lack the necessary sensitivity to detect the intracellular trafficking of the *Cj*-CdtA and *Cj*-CdtC subunit accurately. Alternatively, these subunits may not contribute significantly to the intracellular transport of the active *Cj*-CdtB subunit. It is important to highlight that this chapter presents unpublished work comprising preliminary data, underscoring the need for further exploration and refinement of our understanding in this area.

2.2 MATERIALS AND METHODS

Cell Culture. HCT116 (Human colon cancer epithelial cell line, male) cells were maintained in McCoy's 5A (modified) medium supplemented with a 10% final concentration of fetal bovine serum (FBS). HeLa (Human adenocarcinoma epithelial cell line) cells were maintained in DMEM supplemented with a 10% final concentration of FBS. Cell lines were tested for mycoplasma contamination using MycoAlert Mycoplasma Detection Kit. All cells were maintained at 37°C in a humidified atmosphere under CO_2 (5%).

Bacterial Strains. Escherichia coli BL21 used for protein expression and purification were grown in Luria broth (LB) supplemented with ampicillin (100 μg/mL final concentration) to select for *E. coli* BL21 containing the desired pET-15b expression plasmid. *Escherichia coli* DH5α used for cloning were grown in LB supplemented with ampicillin (100 μg/mL final concentration to select for *E. coli* DH5 α containing the desired plasmid.

Cj-CDT expression and purification. Recombinant CDT subunits (CdtA, CdtB, and CdtC) derived from *Campylobacter jejuni* (*Cj*-CDT), *Haemophilus ducreyi* (*Hd*-CDT), and *Escherichia coli* (*Ec*-CDT) were expressed and purified separately, as described previously (50). Briefly, the genes encoding the individual CdtA, CdtB, and CdtC subunits (within pET-15b protein expression plasmids, Millipore Sigma, 69661), each expressed with an amino-terminal polyhistidine fusion peptide, were expressed separately in *E. coli* BL21 (DE3) protein expression strains. 1 L of Luria broth (LB) in 6 L flasks were inoculated with 1-3 mL starter cultures of E. coli BL21 (DE3) and were cultivated at 37 °C with rotary agitation. Once cultures reached an optical density at 600 nm (OD600) of 0.4-0.6, cultures were further cultivated with rotary agitation at 37 °C in the presence of 0.2 mM isopropyl1-thio-β-D-galactopyranoside (IPTG) to induce CDT subunit expression. After 3 h, cultures were harvested by centrifugation at 8,000 × g at 4 °C. After 8 min, pellets were resuspended in 10 mL of ice-cold PBS pH 7.4 and disrupted via sonication (Fisher Scientific Model: FB505 (500 Watt), Ampl. 25%, 2 sec ON / 5 sec OFF, Total ON = 3 min) on ice and in the presence of 1 mM phenylmethylsulfonyl fluoride (PMSF). After

sonication, contents were centrifuged at 8,000 × g at 4 °C. After 30 min, the supernatant was discarded and pellets resuspended in 15 mL of 8 M urea solution (8 M urea, 20 mM HEPES, 200 mM NaCl in water, pH 7.5 at 4°C) and agitated on a rotary shaker on ice. After 30 min, contents were disrupted on ice via sonication (Fisher Scientific Model: FB505 (500 Watt), Ampl. 25%, 2 sec ON / 5 sec OFF, Total ON = 3 min). The sonicated cell lysates were centrifuged at 8,000 × g at 4 °C. After 30 min, the supernatant was transferred into clean conical tubes and purified by cobalt metal affinity chromatography using approximately 4-6 mL of cobalt resin slurry (Talon Metal Affinity Resin) within a gravity-flow column. Columns were washed with 1 mM imidazole (1 mM imidazole in 8 M urea solution at pH 7.5) and eluted with 100 mM imidazole (100 mM imidazole in 8 M urea solution at pH 7.5) for the CdtA subunit and approximately 25 mM imidazole (25 mM imidazole in 8 M urea solution at pH 7.5) for the CdtB and CdtC subunits. The concentrations of each of the purified subunits were then determined using a BCA Protein Assay Kit (ThermoFisher, Rockford, IL). For the generation of refolded holotoxin, eluted subunits were then diluted to 100 μg/mL with 8 M urea solution, combined in equimolar amounts of CdtA, CdtB, and CdtC subunits in a final volume of around 200 mL, and then transferred into regenerated cellulose dialysis tubing (6000 – 8000 MWCO). For the generation of individual refolded subunits, eluted subunits were then diluted to 100 μg/mL with 8 M urea solution and then individually transferred into regenerated cellulose dialysis tubing (6000 – 8000 MWCO). The CdtA, CdtB, and CdtC subunits were dialyzed, on a stir plate at 4 °C, against 4 L of HEPES buffer

(20 mM HEPES, 200 mM NaCl, and 5% glycerol in water, pH 7.5). After every 6 h, for the next 12 h, dialysis tubing was transferred into fresh 4 L of HEPES buffer and dialyzed on a stir plate at 4 °C. For refolded holotoxin, after 18 h of dialysis in HEPES buffer, dialysis tubing containing CDT was transferred into 4 L of phosphate buffer (PB buffer, 0.456g NaH_2PO_4, 4.343g $Na_2HPO_4 \cdot 7H_2O$, 5% glycerol in 1 L H_2O, pH 7.5) and dialyzed on a stir plate at 4 °C. After 6 h, dialysis tubing was transferred into fresh 4 L of PB buffer and incubated on a stir plate at 4 °C. After 12 h of dialysis in PB buffer, for *Cj*-CDT holotoxin, contents of the dialysis tubing, around 200 mL, were concentrated by binding the diluted CDT holotoxin from the dialysis tubing onto a gravity flow anion exchange column (DEAE SephaceI) containing 3 mL of slurry, and then eluted with 10 mL of PBS. Approximately, 500 μL fractions were collected and analyzed for the presence of all three subunits (refolded holotoxin) or individual subunits, as well as increased protein band intensity using SDS-PAGE and Coomassie Brilliant Blue staining. For individually refolded *Cj*-CDT subunits, the toxin was dialyzed in 4 L of PBS, 3 times similar to refolded holotoxin. After the final dialysis, the individually refolded toxin subunits were then concentrated using Amicon Ultra – 15, 10,000 NMWL centrifugal filter tubes (Millipore, Carrigtwohill, Co), to approximately 100x final volume. For *Ec*- and *Hd*-CDT holotoxins, contents of the dialysis tubing were transferred into centrifugal filters (Amicon Ultra – 15) in order to concentrate the diluted individually refolded subunits post-dialysis. To isolate refolded holotoxin containing equimolar concentrations of CdtA, CdtB, and CdtC subunits, concentrated fractions containing CDT holotoxin were loaded onto a gravity flow

size exclusion column (1 g, P-60 resin) pre-equilibrated with PBS as the mobile phase and 500 μL elution fractions taken. Fractions were then analyzed for stoichiometric equivalency of CdtA, CdtB, and CdtC subunits by assessing for approximately equal band intensities of the CdtA, CdtB, and CdtC subunits using SDS-PAGE and Coomassie Brilliant Blue staining. Fractions found to contain approximately stoichiometrically equivalent amounts of CdtA, CdtB, and CdtC subunits were aliquoted, with each aliquot containing toxin in PBS, and stored at -80 °C. The individually refolded CdtA, CdtB, and CdtC subunits were also aliquoted, with each aliquot containing toxin in PBS, and stored at -80 °C. The concentration of the purified holotoxin or individual CDT subunits was determined using a BCA Protein Assay Kit prior to storage. Activity of purified CDTs was assessed through cell cycle phase assays, as described below.

Generation of mutant Cj-Cdt subunits. *Cj*-CdtA-Myc, *Cj*-CdtB-Myc, *Cj*-CdtB-3xFLAG, *Cj*-CdtB-3xFLAG-Sulfation, *Cj*-CdtB-3xFLAG-Sulfation-Glycosylation, and *Cj*-CdtC-HA tagged subunits were generated through Gibson assembly to enhance immunofluorescence detection of the *Cj*-CDT subunits. Briefly, the *Cj*-CdtA-Myc tagged subunit was generated onto the *Cj*-CdtA gene using a pET-16b protein expression vector containing *Cj*-CdtA as a template, PfuUltra II Fusion HS DNA polymerase, and primers targeting the 6 x histag at the *Cj*-CdtA N-terminus (forward primer: GAA CAA AAA CTC ATC TCA GAA GAG GAT CTG CAT CAT CAT CAT CAT CAC AGC AGC, reverse primer: GCT GCT GCC CAT GGT ATA). The *Cj*-CdtB-Myc tagged subunit was generated onto the *Cj*-CdtB gene using a pET-16b protein expression vector containing *Cj*-

CdtB as a template, PfuUltra II Fusion HS DNA polymerase, and primers targeting the 6 x histag at the *Cj*-CdtB N-terminus (forward primer: GAA CAA AAA CTC ATC TCA GAA GAG GAT CTG CAT CAT CAT CAT CAT CAC AGC AGC, reverse primer: GCT GCT GCC CAT GGT ATA).The *Cj*-CdtB-3xFLAG tagged subunit was generated onto the *Cj*-CdtB gene using a pET-16b protein expression vector containing *Cj*-CdtB as a template, PfuUltra II Fusion HS DNA polymerase, and primers targeting the 6 x histag at the *Cj*-CdtB N-terminus (forward primer: CAT GAC ATC GAT TAC AAG GAT GAC GAT GAC AAG CAT CAT CAT CAT CAT CAC AGC AGC, reverse primer: ATC TTT ATA ATC ACC GTC ATG GTC TTT GTA GTC GCT GCT GCC CAT GGT ATA). The *Cj*-CdtB-3xFLAG-Sulfation tagged subunit was generated onto the *Cj*-CdtB gene using a pET-16b protein expression vector containing *Cj*-CdtB-3xFLAG tag as a template, PfuUltra II Fusion HS DNA polymerase, and primers targeting the 6 x histag at the *Cj*-CdtB-3xFLAG N-terminus (forward primer: CAT CAC AGC AGC GGC AGC GCA GAA GAC TAC GAA TAC CCA TCT, reverse primer: AGA TGG GTA TTC GTA GTC TTC TGC GCT GCC GCT GCT GTG ATG). The *Cj*-CdtB-3xFLAG-Sulfation-Glycosylation tagged subunit was generated onto the *Cj*-CdtB gene using a pET-16b protein expression vector containing *Cj*-CdtB-3xFLAG-Sulfation tag as a template, PfuUltra II Fusion HS DNA polymerase, and primers targeting the *Cj*-CdtB-3xFLAG N-terminus (forward primer: AAC GGC ACC AAA AAT AAC ACA TCC CAG GGC GGC AGC GAC TAC AAA GAC CAT GAC GG, reverse primer: AGA TGG GTA TTC GTA GTC TTC TGC GCT GCC GCT GCT GTG ATG) The sulfation and glycosylation tagged subunits are reporter

constructs that we wanted to use to monitor Golgi and ER localizaiton. The *Cj*-CdtC-HA tagged subunit was generated onto the *Cj*-CdtC gene using a pET-16b protein expression vector containing *Cj*-CdtC as a template, PfuUltra II Fusion HS DNA polymerase, and primers targeting the 6 x histag at the *Cj*-CdtC N-terminus (forward primer: GTT CCA GAT TAC GCT CAT CAT CAT CAT CAT CAC, reverse primer: ATC GTA TGG GTA GCT GCT GCC CAT GGT ATA). Recombinant *Cj*-CDT subunits containing the specified epitope tags were expressed and purified exactly as described above for the production of recombinant *Cj*-CDT subunits containing the specified epitope tags and biochemical modification.

Removal of polyhistidine fusion peptides. His-tagged recombinant subunits, containing a thrombin cleavage site, were incubated at 21 ˚C with biotinylated thrombin (Novagen, Billerica, MA), at approximately 1 units of biotinylated thrombin per 1.5 mg of CDT toxin. After 20 – 24 h, biotinylated thrombin was removed by incubation at room temperature with streptavidin agarose beads (32 µL/unit of thrombin; (Thermo, Waltham, MA). After 30 min of gentle mixing, the resin was removed using Spin-X centrifuge tube filters (pore size, 0.22 µm; Corning Costar, NY) and centrifuged at 500 *x g* for 5 min. The filtrates, containing thrombin-cleaved *Cj*-CDT subunits, free of biotinylated thrombin, were quantified using the Pierce BCA assay (Thermo, Rockford, IL), then aliquoted and stored at -20 ˚C. Thrombin cleavage was confirmed using SDS-PAGE followed by staining with Coomassie Brilliant Blue. His-tagged recombinant subunits containing a TEV cleavage site, were incubated at 30 ˚C

with TEV protease-7 x histag (NEB, Ipswich, MA), at approximately 1 unit of TEV per 15 ug of CDT toxin. After 1 h, TEV protease- 7 x histag was incubated with 10 uL of cobalt resin slurry (1-3 mg of 7 x histag binding capacity per 1 uL) on ice. After 20 min of gentle mixing, the resin was removed using Spin-X centrifuge tube filters and centrifuged at 500 *x g* for 5 min. The filtrates, containing TEV-cleaved *Cj*-CDT subunits, free of TEV protease, were quantified using the Pierce BCA assay, then aliquoted and stored at -20 ˚C. Thrombin cleavage was confirmed using SDS-PAGE followed by staining with Coomassie Brilliant Blue.

SDS-PAGE Coomassie and Immunoblot detection of CDT subunits. Protein or cellular lysate samples were run in a 12% SDS-PAGE gel for protein analysis. After completion of the SDS-PAGE, gels were either stained with Coomassie brilliant blue or used for western blot analysis. For western blot analysis, following SDS-PAGE, resolved proteins were transferred to PVDF membranes (MilliporeSigma, Burlington, MA) using a wet/tank blotting system (Bio-Rad, Hercules, CA). Membranes were blocked at room temperature with 5% bovine serum albumin (BSA, Sigma-Aldrich, St. Louis, MO) in TBS-T (0.1% Tween-20 in TBS pH 7.4, Fisher, Fair Lawn, NJ). After 5 min, membranes were washed with TBS-T to remove residual blocking buffer and then incubated at 4 °C with the indicated primary antibodies diluted in TBS-T. *Cj*-CdtA-specific antibodies (1:1,000 antibody:buffer ratio) targeting the *Cj*-CdtA-specific sequence 255-CPFTAKPLYRQGEVR-268, *Cj*-CdtB-specific antibodies (1:1,000 antibody:buffer ratio) targeting the *Cj*-CdtB-specific sequence 185-CDFNRDPSTITSTVDRELANR-204, and *Cj*-CdtC-specific antibodies (1:5,000

antibody:buffer ratio) targeting the *Cj*-CdtC-specific sequence 44-CFRDTSKDPIDQNWNIK-59 (YenZme, San Francisco, CA). After overnight incubation, membranes were washed with TBS-T, and further incubated at room temperature with anti-rabbit IgG biotinylated antibodies diluted in TBS-T (Cell Signaling, Danvers, MA). After 1 h, membranes were washed with TBS-T, and the membranes were further incubated at room temperature with anti-biotin HRP-linked antibodies diluted in TBS-T (Cell Signaling, Danvers, MA). After 1 h, membranes were washed with TBS-T, and then incubated with enhanced chemiluminescent substrate for HRP detection (1:5 mixture of SuperSignal West Femto Maximum Sensitivity and Pico Plus Chemiluminescent Substrates (Thermo, Rockford, IL)). Immunoblots were imaged using the ChemiDoc system (XRS+, Bio-Rad, Hercules, CA). Immunoblot densitometry analyses were performed using Image Lab software (Bio-Rad, Version 6.0). For western blot detection of the *Cj*-CdtA-Myc, *Cj*-CdtB-FLAG, *Cj*-CdtB-Myc, and *Cj*-CdtC-HA tagged subunits, membranes were incubated at 4 °C with the indicated primary antibodies diluted in TBS-T. Rabbit monoclonal anti-FLAG or anti-HA antibodies (Cell Signaling Technology, Danvers, MA) at a 1:1000 dilution in PBS, or rabbit monoclonal anti-Myc antibodies (Cell Signaling Technology, Danvers, MA) at a 1:5000 dilution in PBS.

Assessing DNA damage response initiation. The indicated cell lines were seeded (approximately 0.04-0.05 X 10^6 cells per well) on 24-well culture plates and incubated at 37 °C and under 5% CO_2. After 24 – 36 h, the cells were incubated with refolded *Cj*-CDT holotoxin at the concentrations indicated. After

24 h, 24-well plates were placed on ice and cell monolayers were washed twice with cold PBS pH 7.4. After washing the monolayers, 75-150 μL of RIPA buffer (Thermo, Waltham, MA) supplemented with HALT protease and phosphatase inhibitor cocktail (Thermo, Waltham, MA) were added to each well and the plate incubated at 4 °C on a platform rocker with occasional agitation. After 20 min, lysates were transferred to chilled microcentrifuge tubes and Laemmli sample buffer (Thermo, Waltham, MA), supplemented with β-mercaptoethanol, was added to generate a 1 x concentration of Laemmli sample buffer in cell lysate. Lysates, on ice, were then passed through a 25-gauge needle three times to fully homogenize samples and then boiled at 100°C for 10 min. Cellular lysates were fractionated by SDS-PAGE using 12% polyacrylamide gels, transferred to PVDF membranes, and membranes were blocked with 5% non-fat milk in TBS-T. Membranes were then incubated with rabbit monoclonal anti-phospho-histone H2AX (Ser139) (α-H2AX) (Cell Signaling Technology, Danvers, MA) antibodies at a 1:3000 dilution in TBS-T, followed by anti-rabbit IgG, HRP-linked secondary antibodies at a 1:10,000 dilution in TBS-T. HRP-conjugated secondary antibody binding, immunoblot imaging, and immunoblot densitometry analysis were performed as described above.

Cell cycle phase determination. Cj-CDT-dependent arrest of cell cycle progression at the G2/M interface was assessed using flow cytometry (FACSymphony A1, BD Biosciences, Franklin Lakes, NJ) as previously described (50, 62). Briefly, the indicated cell lines were seeded (approximately 0.04-0.05 X 10^6 cells per well) on 24-well culture plates and incubated at 37 °C

and under 5% CO_2. For continuous intoxication conditions, after 24-36 h the cells were incubated at 37 °C and under 5% CO_2 in complete medium containing CDT at the indicated preparations, conditions, combinations, and concentrations, or, were incubated with PBS pH 7.4 in place of CDT, as indicated in the figure legends. All individually refolded *Cj*-CDT subunit combinations were mixed together at a final concentration of 10 μM and incubated on ice for 1 h prior to dilution and subsequent intoxication. After 24 h, cell culture medium containing CDT or PBS, as the carrier control, was removed and cells were washed twice with PBS. Cells were then detached from the cell culture plate by trypsinization at 37 °C. After detachment of cells was observed, 10% final concentration of FBS in PBS was added to inhibit trypsin activity. Cells were then pelleted (500 × g, 5 min) and resuspended by adding ice cold 70% ethanol dropwise with constant vortexing. Cells were incubated at -20 °C in the presence of 70% ethanol. After a minimum of 1 h, cells were pelleted (800 × g, 5 min) and resuspended in PBS. After 30 min at room temperature, cells were pelleted and resuspended in staining solution (300 μL per sample; containing 0.1% Triton X-100, 1 mg/mL RNase A, and 10 μg/mL propidium iodide in PBS pH 7.4). After 1 h at room temperature, cells were analyzed using a BD FACS Canto II flow cytometry analyzer (FACSymphony A1, BD Biosciences, Franklin Lakes, NJ). Flow cytometry data were processed using FCS Express software (De Novo Software) and statistics performed using GraphPad Prism 7 (GraphPad Software). For pulse intoxications, after 24-36 h the cells were incubated on ice and under atmospheric conditions. After 30 mins, media was removed and cells were

incubated with cold PBS containing CDT or in the absence of CDT at the combinations and concentrations as indicated in the figures, on ice under atmospheric conditions. After 1 h, PBS with or without toxin was removed and replaced with complete medium and incubated at 37 °C and under 5% CO_2. After 24, cell culture medium was removed and cells were washed twice with PBS. Cells were then detached from the cell culture plate by trypsinization at 37 °C, harvested, and analyzed in the same manner as the continuous intoxication conditions described above.

Assessing cell cycle arrest in the presence of trafficking inhibitors. Cells were seeded (approximately 0.04-0.05 X 10^6 cells per well) on 24-well culture plates and incubated at 37 °C and under 5% CO_2. After 24-36 h, the cells were incubated at 37 °C and under 5% CO_2 in complete medium, with 125 nM Bafilomycin A (InvivoGen), 0.2 μg/mL Brefeldin A (ThermoFisher), 50 μM Exo-2 (MedchemExpress), and 10 μM Golgicide A (Cayman Chemical) in the presence or absence of 2 nM of refolded *Cj*-CDT holotoxin. After 24 h, cell culture medium containing inhibitors and CDT or PBS pH 7.4 were removed and cells were harvested and evaluated for G_2/M cell cycle arrest as previously described.

DIC/Fluorescence microscopy. 8-well cell culture chamber slides (Lab-Tek II) were stained with the indicated anti-bodies (at a 1:1000 antibody to media ratio) post treatment and analyzed using a DeltaVision RT microscope (GE Life Sciences). Olympus Plan Apo x60 oil objectives were used. Images were acquired using a Photometrics CoolSnap HQ camera (Photometrics). Images were processed using SoftworX Explorer Suite (GE Life Sciences, Version 3.5.1).

For each cell, images were collected from an average of approximately 6 Z-planes using 0.2 µm intervals. Deconvolution was performed using SoftworX constrained iterative deconvolution tool (ratio mode) and analyzed using Imaris (Bitplane, Version 7.4.2).

Cellular localization of Cj-CDT subunits with immunofluorescence microscopy. Cells were seeded, approximately 20,000 cells per well of an 8-well cell culture microscope slide, and incubated at 37 °C and under 5% CO_2. For the visualization of Golgi apparatus, endoplasmic reticulum, and nucleus, after 24 – 36 h, monolayers were washed three times with PBS pH 7.4. The cell monolayers were then fixed with 4% formaldehyde in PBS. After 15 min at room temperature, fixative was removed, and cell monolayers washed three times with PBS. After washing, cells were permeabilized with 0.1% Triton X-100 in PBS at room temperature. After 15 min, cell monolayers were then blocked with blocking buffer (5% final concentration of bovine serum albumin in PBS pH 7.4). After 1 h, cell monolayers were washed three times with PBS. After washing, cell monolayers were incubated at 4 °C with rabbit polyclonal anti-Giantin (Golgi) antibodies (Abcam, Cambridge, United Kingdom) and rabbit polyclonal anti-Calreticulin (405-417) (ER) antibodies (Millipore Sigma, Darmstadt, Germany) at a 1:5000 dilution in PBS. After overnight primary antibody incubation, cell monolayers were washed three times with PBS. Cell monolayers were then incubated in the presence of secondary antibody (goat anti-rabbit IgG (H+L) Alexa Fluor 555 (Giantin) and 647 (Calreticulin) conjugates at a 1:1000 dilution in PBS-T) (Invitrogen, Waltham, MA). After 1 h at room temperature, cell

monolayers were washed three times with PBS. DAPI (500 ng/mL) (ThermoFisher, Waltham, MA) staining solution was then added to the cellular monolayers. After 30 min at room temperature, cell monolayers were washed three times with PBS. Prolong Gold antifade reagent (ThermoFisher, Waltham, MA) was then added to stained monolayers and coverslip applied and sealed with clear nail polish. Cells were then analyzed using a DeltaVision RT microscope. For evaluating cell surface localization of wildtype *Cj*-CDT subunits, after 24 – 36 h, monolayers were incubated on ice under atmospheric conditions. After 30 mins, cells were washed twice with cold PBS and incubated in the presence or absence of *Cj*-Cdt holotoxin (mixed assembled, 10 nM final concentration) on ice under atmospheric conditions. After 30 mins, monolayers were washed twice with cold PBS. The cell monolayers were then fixed with 4% formaldehyde in PBS. After 15 min at room temperature, fixative was removed, and cell monolayers washed three times with PBS. After washing, cells were permeabilized with 0.1% Triton X-100 in PBS at room temperature. After 15 min, cell monolayers were then blocked with blocking buffer (5% final concentration of bovine serum albumin in PBS). After 1 h, cell monolayers were washed three times with PBS. After washing, cell monolayers were incubated at 4 °C with rabbit polyclonal anti-*Cj*-CdtA or anti-*Cj*-CdtB at a 1:1000 dilution in PBS, or anti-*Cj*-CdtC antibodies (YenZme) at a 1:5000 dilution in PBS. After overnight primary antibody incubation, cell monolayers were washed three times with PBS. Cell monolayers were then incubated in the presence of secondary antibody (goat anti-rabbit IgG (H+L) Alexa Fluor 488 conjugate at a 1:1000 dilution in PBS)

(Invitrogen, Waltham, MA). After 1 h at room temperature, cell monolayers were washed three times with PBS. DAPI (500 ng/mL) (ThermoFisher) staining solution was then added to the cellular monolayers. After 30 min at room temperature, cell monolayers were washed three times with PBS. Prolong Gold antifade reagent (ThermoFisher) was then added to stained monolayers and coverslip applied and sealed with clear nail polish. Cells were then analyzed using a DeltaVision RT microscope. For evaluating cell surface localization of epitope tagged *Cj*-CdtA-Myc and *Cj*-CdtB-FLAG subunits, the same procedure was performed as the cell surface localization of the wildtype *Cj*-CDT subunits, with the exception of the intoxication step which was performed with *Cj*-CDT holotoxin assembled with either the *Cj*-CdtA-Myc or *Cj*-CdtB-FLAG subunits, as well as the primary antibody incubation step which was conducted using rabbit monoclonal anti-Myc and anti-FLAG antibodies (Cell Signaling Technology, Danvers, MA). For evaluating intracellular localization of epitope tagged *Cj*-CdtB-FLAG, *Cj*-CdtB-Myc, and *Cj*-CdtC-HA subunits, after 24 – 36 h, monolayers were incubated on ice. After 30 mins, cells were washed twice with cold PBS and incubated in the presence or absence of *Cj*-Cdt holotoxin (mixed assembled, 100 nM final concentration) assembled using either the *Cj*-CdtB-FLAG, *Cj*-CdtB-Myc, or *Cj*-CdtC-HA subunits. After 30 mins, monolayers were washed twice with cold PBS and incubated at 37 °C and under 5% CO_2. After 1 h or 24 h, monolayers were washed three times with PBS. The cell monolayers were then fixed with 4% formaldehyde in PBS. After 15 min at room temperature, fixative was removed, and cell monolayers washed three times with PBS. After washing, cells were

permeabilized with 0.1% Triton X-100 in PBS at room temperature. After 15 min, cell monolayers were then blocked with blocking buffer (5% final concentration of bovine serum albumin in PBS). After 1 h, cell monolayers were washed three times with PBS. After washing, cell monolayers were incubated at 4 °C with rabbit monoclonal anti-FLAG or anti-HA antibodies (Cell Signaling Technology, Danvers, MA) at a 1:1000 dilution in PBS, or rabbit monoclonal anti-Myc antibodies (Cell Signaling Technology, Danvers, MA) at a 1:5000 dilution in PBS. After overnight primary antibody incubation, cell monolayers were washed three times with PBS. Cell monolayers were then incubated in the presence of secondary antibody (goat anti-rabbit IgG (H+L) Alexa Fluor 488 conjugate at a 1:1000 dilution in PBS) (Cell Signaling Technology). After 1 h at room temperature, cell monolayers were washed three times with PBS. DAPI (500 ng/mL) (ThermoFisher) staining solution was then added to the cellular monolayers. After 30 min at room temperature, cell monolayers were washed three times with PBS. Prolong Gold antifade reagent (ThermoFisher) was then added to stained monolayers and coverslip applied and sealed with clear nail polish. Cells were then analyzed using a DeltaVision RT microscope.

Statistical Analyses. Each experiment was performed at least three independent times, signified as n = 3, unless otherwise indicated. Error bars represent standard deviations. Statistical analyses were performed using GraphPad Prism 8.1.2. Dose response curves were fit to a log (agonist) vs response (three parameters) equation. R2 values indicate fit of the data to the regression model. Analysis of statistical differences was performed using one-

way ANOVA followed by the Tukey's post-hoc test. Statistical significance ($P < 0.05$) was determined at $\alpha = 0.05$.

2.3 RESULTS

2.3.1 *Cj*-CDT cellular intoxication leads to a cell cycle arrest under different experimental conditions

Host cell intoxication with CDTs induces DNA damage and leads to cell cycle arrest at the G2/M phase, as previously demonstrated both in our laboratory and others (81, 84). Like most CDTs, *Cj*-CDT comprises three subunits: *Cj*-CdtA, *Cj*-CdtB, and *Cj*-CdtC, with predicted molecular masses of 29.9, 29.4, and 21.4 kDa, respectively (119). We confirm that the molecular masses of the *Cj*-CDT subunits used in this study align with previous findings, and we successfully detect these subunits using Coomassie staining and specific antibodies for each (Figure 2.1 and Figure 2.2). The successful immunoblot detection is crucial for our study, as we intend to employ these antibodies to probe and quantify the trafficking of individual *Cj*-CDT subunits during cellular intoxication, thereby elucidating their roles and mechanisms in trafficking to the nucleus. For the *Cj*-CdtB subunit to localize to the nucleus of intoxicated cells and induce DNA damage, it is believed that all three CDT subunits must interact with each other prior to entering the target cell. This trafficking process of the *Cj*-CdtB subunit likely involves the *Cj*-CdtA and *Cj*-CdtC subunits, a model primarily derived from trafficking studies involving *H. ducreyi* and *E. coli* CDTs (40). To experimentally evaluate this proposed model, we conducted experiments to

assess the trafficking of *Cj*-CdtA, *Cj*-CdtB, and *Cj*-CdtC subunits within host cells. One major limitation from previous CDT studies is the variability in experimental conditions used to assess CDT activity. Therefore, prior to investigating the trafficking of *Cj*-CDT subunits, we conducted extensive studies to evaluate the activity of our *Cj*-CDT toxin under various experimental conditions. These studies were essential to validate the biological activity and proper functioning of the toxin under different experimental conditions employed in subsequent studies.

Consistent with previous studies on *Cj*-CDTs (81, 84), our research demonstrates that *Cj*-CDT-mediated activation of the DNA damage response and subsequent host cell cycle arrest occur in a dose-dependent manner. This dose-dependent response of cells to CDT intoxication is critical for comparing specific activities among different preparations and treatment conditions. To assess the DNA damage response to *Cj*-CDT, we evaluated the dose-dependent phosphorylation of Histone-2AX, a widely recognized marker for assessing the DNA damage response, in HCT116 cells exposed to refolded *Cj*-CDT holotoxin (ranging from 0.1 to 100 nM) continuously for 24 h. Under these conditions, we observed an increase in phosphorylated H2AX at concentrations of 10 and 100 nM of toxin (Figure 2.3). This finding aligns with unpublished data from our laboratory (Crowder, unpublished) and confirms the successful purification of functional *Cj*-CDT holotoxin. Furthermore, it verifies that our toxin preparations exhibit activities consistent with our previous observations.

One of the primary outcomes of CDT-mediated DNA damage in host cells is the arrest of cell cycle progression at the G_2/M stage, a widely reported

phenotype associated with CDT intoxication. To assess *Cj*-CDT's capacity to induce host cell arrest, we examined the dose-dependent progression of cell cycle arrest at the G_2/M interface. In these cell cycle progression studies, we evaluated G_2/M cell cycle progression under various conditions of *Cj*-CDT treatment. This was essential for ensuring comparable toxin biological activities across different treatment conditions used in subsequent experiments, as well as for comparing the effects of different treatment conditions on *Cj*-CDT toxin activities. As outlined in the materials and methods section, we employed two methods for preparing our *Cj*-CDT holotoxin. In one approach, denatured forms of the *Cj*-CdtA, *Cj*-CdtB, and *Cj*-CdtC subunits (in 8M urea) were combined and allowed to refold together simultaneously. Alternatively, we individually refolded the *Cj*-CdtA, *Cj*-CdtB, and *Cj*-CdtC subunits and then mixed them in stoichiometrically equal ratios post-refolding. Subsequently, we exposed HCT116 cells to the toxin in a dose-dependent manner over a continuous 24 h period and determined the concentration of *Cj*-CDT toxin required to induce 50% maximum cell cycle arrest (CCA_{50}) within a monolayer of cells. Our experimental findings revealed CCA_{50} values of approximately 3 nM for the concurrently refolded toxin and 2 nM for our individually refolded toxin (Figure 2.4A). These results indicate that both toxin preparations, whether refolding all three subunits together or individually, resulted in active toxins with comparable biological activities. In the field, the evaluation of G_2/M arrest activities of CDTs is a common readout for CDT activity. However, CCA_{50} values for CDTs are seldom reported despite their significance in determining the specific activities of different CDT toxin

preparations and experimental designs. Given the considerable variability in toxin activity evaluation across studies due to differences in toxin species, cell lines, and treatment conditions, establishing CCA_{50} values for experiments assessing toxin activity should be widely adopted to facilitate comparisons among various studies of CDTs.

In a previous study, we assessed the impact of individually refolded versus concurrently refolded toxin subunits on toxin biological activity. To purify our recombinantly expressed *Cj*-CDT subunits, we employed a 6x polyhistidine tag, a method commonly used for protein purification. While this tag has been suggested to have no significant effect on the biological activity of other CDTs such as *Hd*-CDT and *Ec*-CDT (Eshraghi and Gargi, unpublished), its potential impact on the functionality of other CDT species, particularly *Cj*-CDT, has not been clearly reported. Given that our thesis work focuses on understanding the role of subunits during trafficking, which necessitates subunit interaction, it is critical to establish that the addition of polyhistidine tags does not interfere with toxin function. To evaluate this, we removed the polyhistidine tags from purified and individually refolded Cj-CDT subunits as described in the materials and methods. Subsequently, we mixed the three Cj-CDT subunits together at stoichiometrically equal ratios to form active holotoxin. We then treated HCT116 cells with the individually refolded, polyhistidine tag-deficient toxin in a dose-dependent manner over a continuous 24 h exposure and evaluated the CCA_{50} activity. Comparing it to the polyhistidine-tagged individually refolded *Cj*-CDT toxin, which had a CCA_{50} of 2 nM, the polyhistidine-deficient individually refolded

Cj-CDT toxin exhibited a CCA_{50} of 1 nM. This suggests that the polyhistidine tag had minimal effect on toxin biological activity and function in HCT116 cells under continuous toxin exposure (Figure 2.4A). We were unable to assess the effects of the polyhistidine tag on the concurrently refolded toxin because we couldn't remove the tag under the denaturing conditions necessary to maintain the toxin subunits unfolded. However, since all three preparations of *Cj*-CDT, concurrently refolded, individually refolded, and polyhistidine tag-deficient individually refolded toxin, yielded similar biological activities, it indicates that any of the three toxin preparations functioned comparably. Additionally, we evaluated the CCA_{50} activity of *Cj*-CDT on HeLa cells in a similar manner, by intoxication with individually refolded *Cj*-CDT in a dose-dependent manner over continuous 24-hour exposure (Figure 2.4B). Compared to HCT116 cells, which exhibited a CCA_{50} of about 2 nM, HeLa cells had a CCA_{50} of approximately 4 nM, suggesting similar specific activities of *Cj*-CDT and consistent functionality across different cell lines.

The 24 h continuous exposure of toxin in media, as described earlier, was one of the conditions used to assess toxin function, a commonly adopted method by labs studying CDT. To measure the time-associated trafficking of *Cj*-CDT subunits during cellular intoxication, we employed pulse intoxications. This technique, previously used to study the role of *Hd*-CdtA/B and *Ec*-CdtA/B subunits in the transport of the CdtB subunit (40), allowed us to control the timing and quantity of toxin entry into the cell, a crucial aspect for evaluating the temporal and spatial organellar retro-transport associated with *Cj*-CDT nuclear

localization. By chilling cells on ice, we permitted toxin binding to host cells while limiting internalization (38, 78). Subsequently, we removed any unassociated toxin before transitioning cells to 37 °C to initiate toxin entry, enabling us to monitor the time-dependent trafficking of toxin subunits to various organellar compartments from the moment of toxin internalization. However, given the different variables associated with pulse intoxication compared to continuous intoxication, we sought to assess whether this affected toxin activity on host cells. Initially, we compared the effects of dose-dependent pulse intoxication of individually refolded polyhistidine tagged *Cj*-CDT subunits to those of continuous intoxication on HCT116 cells. Interestingly, under both conditions, we observed a CCA_{50} of approximately 2 nM (Figure 2.5A). Next, we evaluated the effects of pulse and continuous intoxication on HeLa cells. In this case, while continuous intoxication resulted in a CCA_{50} of 4 nM, pulse intoxication led to a slightly higher CCA_{50} of 6 nM (Figure 2.5B). These findings suggest that, for both HCT116 and HeLa cells, pulse versus continuous intoxication did not significantly impact toxin activity.

The experiments outlined above indicate that the different toxin preparations, treatment conditions, and cell lines used to assess toxin activity were comparable to each other. Our next objective was to evaluate the significance of the *Cj*-CdtA and *Cj*-CdtC subunits on toxin cellular activity. Prior studies have demonstrated that maximum toxin cellular activity necessitates the presence of all three *Cj*-CDT subunits (81, 84), as the CdtA and CdtC subunits from all CDT species are believed to share a similar role: facilitating the delivery

of the catalytically active CdtB subunit to the nucleus of intoxicated cells. To confirm that all three *Cj*-CDT subunits are indeed required for maximal cellular activity, we conducted a dose-dependent continuous (Figure 2.6A,B) and pulse intoxication (of host cells with different combinations of individually refolded *Cj*-CDT subunits (*Cj*-CdtA + *Cj*-CdtB, *Cj*-CdtA + *Cj*-CdtC, *Cj*-CdtB + *Cj*-CdtC, and *Cj*-CdtA + *Cj*-CdtB + *Cj*-CdtC). Consistent with previous findings, we observed that maximal cellular activity necessitates the presence of all three *Cj*-Cdt subunits in both HCT116 and HeLa cells. Moreover, in line with earlier research (84), intoxication of HeLa cells with the *Cj*-CdtB + *Cj*-CdtC subunits resulted in toxin activity lower than that observed with all three *Cj*-CDT subunits. These findings strongly suggest that the *Cj*-CdtA and *Cj*-CdtC subunits play crucial roles in cellular intoxication.

2.3.2 The endosome, Golgi apparatus, and endoplasmic reticulum are important for *Cj*-CDT biological activity

As previously mentioned, the current model for the intracellular trafficking of CDTs suggests sequential transport to the endosome, Golgi apparatus, endoplasmic reticulum, cytosol, and finally the nucleus. To evaluate the importance of these organellar compartments for the intracellular trafficking of *Cj*-CDT, we investigated their involvement in the biological activity of *Cj*-CDT. We employed four different drugs to disrupt the function of endosomes, Golgi apparatus, and endoplasmic reticulum and evaluated *Cj*-CDT's ability to confer its biological activity.

First, Bafilomycin, an inhibitor of vacuolar H+-ATPases (V-ATPases), was used to prevent the acidification of endosomes, a process crucial for various endosomal functions including vesicular/protein trafficking, receptor recycling, and endocytosis. We treated HeLa cells in the presence or absence of 125 nM of Bafilomycin A and in the presence or absence of 2 nM *Cj*-CDT. After 24 h of continuous exposure to both the drug and toxin, we observed inhibition of *Cj*-CDT mediated G_2/M arrest in cells, but not cells treated with toxin alone, suggesting that endosome acidification played an important role in *Cj*-CDT mediated cellular activity (Figure 2.7A).

Golgicide A is a specific inhibitor of the Arf1-GEF, GBF1. GBF1, the ArfGEF responsible for Arf1 activation and COPI recruitment to cis-Golgi membranes and plays an important role in coordinating bidirectional transport and maintaining structural integrity of the Golgi. We treated HCT116 cells in the presence or absence of 10 μM of Golgicide A and in the presence or absence of 2 nM *Cj*-CDT. After 24 h of continuous exposure to both the drug and toxin, we observed inhibition of *Cj*-CDT mediated G_2/M arrest in cells that were given Golgicide A, suggesting that protein transport from the Golgi apparatus played an important role in *Cj*-CDT mediated cellular activity (Figure 2.7B).

Brefeldin A disrupts the activity of at least three guanine exchange factors of Arf1 (including BIG1, BIG2, and GBF1) and effects Arf3 and Arf4. Incubation of cells in culture with Brefeldin A leads to blockade of protein transport from the endoplasmic reticulum and leads to the accumulation of proteins in the endoplasmic reticulum. We treated HCT116 cells in the presence or absence of

0.2 μg/mL of Brefeldin A and in the presence or absence of 2 nM *Cj*-CDT. After 24 h, only cells exposed to the drug and toxin had inhibition of *Cj*-CDT mediated G_2/M arrest in cells, suggesting that protein transport from the endoplasmic reticulum played an important role in *Cj*-CDT mediated cellular activity (Figure 2.7C).

Finally, Exo2 is a small-molecule inhibitor of secretion and retrograde trafficking in cells. The exact target of Exo-2 is unknown; however, it is believed to interact with a subset of the Arf-GEF targets of Brefeldin A. Cellular treatment with Exo2 stimulates morphological changes in the Golgi and trans-Golgi network, fusing the endoplasmic reticulum (ER) and Golgi apparatus. These morphological changes have been demonstrated to prevent the release of secretory cargo from the ER and disrupts the Golgi apparatus. We treated HCT116 cells in the presence or absence of 50 μM of Exo-2 and in the presence or absence of 2 nM *Cj*-CDT. After 24 h of continuous exposure to both the drug and toxin, we also observed inhibition of *Cj*-CDT mediated G_2/M arrest in cells that were administered Exo-2, further suggesting that protein transport from the endoplasmic reticulum and functional Golgi played an important role in *Cj*-CDT mediated cellular activity (Figure 2.7D).

These studies demonstrated that disruption of endosome, Golgi apparatus, and endoplasmic reticulum function led to a loss of *Cj*-CDT-mediated G2/M arrest. While these findings do not elucidate the intracellular transport of *Cj*-CDT subunits through these compartments, they suggest that proper function of endosomes, Golgi apparatus, and the endoplasmic reticulum is essential for

transporting *Cj*-CDT to the nucleus, where the toxin can damage host DNA, resulting in cell cycle arrest at the G_2/M stage.

2.3.3 Intracellular trafficking of Cj-CdtA and Cj-CdtC subunits is not observable with current immunofluorescence microscopy conditions use in our lab

The experiments described above underscored the significance of endosomes, Golgi apparatus, and endoplasmic reticulum for the biological activities of *Cj*-CDT. However, they did not address whether the *Cj*-CdtA and *Cj*-CdtC subunits were involved in the transport through these intracellular organelles. To delve deeper into the involvement of the *Cj*-CdtA and *Cj*-CdtC subunits in the intracellular retrograde trafficking of *Cj*-CdtB, we examined the intracellular trafficking of each of the *Cj*-CdtA, *Cj*-CdtB, and *Cj*-CdtC subunits from the cell surface to the Golgi apparatus and endoplasmic reticulum using immunofluorescence microscopy in a time-dependent manner. To order to assess subunit trafficking to these organelles, we stained for the Golgi apparatus using antibodies against Giantin, a protein located at the cis-medial rims of the Golgi apparatus (Figure 2.8A), and for the endoplasmic reticulum using antibodies against Calreticulin, a highly conserved chaperone protein primarily residing in the endoplasmic reticulum (Figure 2.8B).

First, we investigated the association of each individual *Cj*-CDT subunit at the plasma membrane. Cells were treated with equimolar concentrations of all three subunits (10 nM) on ice to allow toxin interaction with host cell receptors while preventing internalization. After 30 mins, unbound toxin was removed, cells

were washed, and then fixed in 4% paraformaldehyde to capture membrane-associated toxin. Using primary antibodies specific for each *Cj*-CDT subunit, we probed for membrane association of the individual subunits. However, from these studies, we encountered challenges in clearly identifying the association of the *Cj*-CdtA or *Cj*-CdtC subunits at the host cell membrane. Immunofluorescence staining from our primary antibody showed similar intensity between intoxicated and unintoxicated cells, indicating the inability to detect the subunits at the cell surface. Additionally, we observed high background immunofluorescence detection due to significant interaction of either the primary or secondary antibody with our CDT-deficient slides (Figure 2.9A,C). Regarding the Cj-CdtB subunit, although we observed an increased signal over background, the signal appeared to be localized to the nucleus. This localization was unexpected since the cells were treated under conditions where the toxin should remain at the plasma membrane and not be internalized (Figure 2.9B). These findings suggested that immunofluorescence staining with our primary antibodies and/or the conditions used for immunofluorescence detection of host cell surface-associated Cj-CDT subunits were insufficient for measuring surface binding of our Cj-CDT subunits and subsequent localization to intracellular compartments.

In addition to the challenges posed by high background and non-specificity of our primary antibodies for individual *Cj*-CDT subunits, another limitation was our inability to perform subunit colocalization studies due to all three primary antibodies being generated from rabbits. To address these limitations and to enhance our ability to study subunit localization and trafficking

during cellular intoxication, we generated *Cj*-CDT subunit mutants with different epitope tags: *Cj*-CdtA-Myc, *Cj*-CdtB-Myc, *Cj*-CdtB-FLAG, and *Cj*-CdtC-HA. These epitope tags were selected to increase sensitivity to detection and enable the use of commercially available primary antibodies specific to each tag, facilitating subunit colocalization studies. We confirmed the purity of our epitope-tagged subunits (Figure 2.10A), demonstrated their detectability using western blot analysis with specific antibodies against the epitope tags (Figure 2.10B), and validated their capacity for toxin activity by measuring their cell cycle arrest activities (Figure 2.11A-E).

In previous studies conducted in our lab, the *Hd*-CdtB and *Ec*-CdtB subunits were observed to localize in the host cell nucleus after 1 h of intoxication (62). To assess whether *Cj*-CdtB could similarly localize to the host cell nucleus, we conducted nuclear localization studies using two epitope-tagged subunits: *Cj*-CdtB-FLAG under continuous intoxication and *Cj*-CdtB-Myc under pulse intoxication, both for 24 hours. For continuous intoxication, cells were treated with equimolar concentrations of all three subunits (*Cj*-CdtA + *Cj*-CdtB-FLAG + *Cj*-CdtC, 100 nM) at 37 °C and under 5% CO_2 for 24 hours. Following treatment, cells were fixed to capture nuclear-localized toxin. In contrast, for pulse intoxication, cells were treated with equimolar concentrations of all three subunits (*Cj*-CdtA + *Cj*-CdtB-Myc + *Cj*-CdtC, 100 nM) on ice for 30 minutes to prevent internalization. After removing unbound toxin, cells were then incubated in media at 37 °C and under 5% CO_2 for 24 h before fixation. Using primary antibodies specific for the FLAG and Myc epitopes, we observed nuclear

localization of both *Cj*-CdtB-FLAG and *Cj*-CdtB-Myc subunits. This observation supports the model that *Cj*-CdtB, akin to other CdtB subunits, can localize to the nucleus post-intoxication of host cells. Notably, in the pulse-intoxicated *Cj*-CdtB-Myc subunit, we observed clear fluorescence puncta in the nucleus after 24 h, suggesting predominant nuclear localization. (Figure 2.12A). However, in the continuously intoxicated *Cj*-CdtB-FLAG subunits, we observed a weaker fluorescence signal, with puncta distributed throughout the cell, indicating ongoing uptake and trafficking to the nucleus over the 24 h period. (Figure 2.12B). An unexpected observation from the experiment was the absence of enlarged cellular nuclei after 24 h, which is a common phenotype of *Cj*-CDT intoxication.

In order to investigate the association of epitope-tagged *Cj*-CdtA-Myc, *Cj*-CdtB-FLAG, and *Cj*-CdtB-Myc subunits at the plasma membrane, we employed the same method as described earlier for the non-epitope tagged subunits. Host cells were treated with holotoxin (100 nM) consisting of each of the three epitope-tagged subunits separately under pulse conditions to assess membrane association. However, we encountered challenges in detecting the *Cj*-CdtB-FLAG subunit at the host cell membrane due to high background immunofluorescence from our primary antibody stain, resulting in indistinguishable signals between intoxicated and unintoxicated cells (Figure 2.13A). In contrast, the Myc epitope-tagged subunits exhibited better signal detection, but with unexpected results. For the *Cj*-CdtA-Myc subunit, we observed signal localized to the nucleus, contrary to our expectation of uniform

distribution throughout the cell membrane (Figure 2.13B). Similarly, the distribution of puncta throughout the cell for the *Cj*-CdtB-Myc subunit was inconsistent with our expectations of membrane association (Figure 2.13C). While nuclear localization of the *Hd* and *Ec*-CdtB subunit has been previously reported in our lab (62), the localization of the three subunits at the host cell surface has not clearly reported. The difficulty in detecting cell surface localization of the CDT subunits suggests challenges similar to those encountered in detecting the cell surface localization of the *Hd* and *Ec*-Cdt subunits.

In order to evaluate intracellular localization, we performed a 1 h pulse intoxication experiment using the epitope-tagged *Cj*-CdtB-FLAG, *Cj*-CdtB-Myc, and *Cj*-CdtC-HA subunits. The goal was to examine whether the *Cj*-CdtC and *Cj*-CdtB subunit could be captured in precursor trafficking organelles such as the Golgi apparatus or endoplasmic reticulum, prior to reaching the host cell nucleus. However, our observations did not yield any clear localization signals for the *Cj*-CdtB-FLAG, *Cj*-CdtB-Myc, or *Cj*-CdtC-HA subunits compared to untreated cells (Figure 2.14A-C), thus making it challenging to draw conclusions regarding intracellular trafficking of these subunits. We also attempted several additional pulse time points, such as 30 and 240 minutes, using the *Cj*-CdtB-Myc epitope-tagged subunit, which showed more sensitivity in immunofluorescence staining (Figure 2.12A and 2.13C). Despite these efforts, we were unable to obtain clear results from various trafficking time points and epitope tag combinations (data not shown), which led us to make the decision that conducting further intracellular

trafficking experiments was not warranted at this stage and should possibly be revisited later.

The results from our experiments collectively indicate the significance of endosomes, Golgi apparatus, and endoplasmic reticulum in the biological activity of *Cj*-CDT. However, the trafficking experiments we conducted to elucidate the intracellular transport of *Cj*-CDT subunits during cellular intoxication yielded inconclusive results. Despite our efforts to investigate the involvement of the *Cj*-CdtA and *Cj*-CdtC subunits in the retrograde trafficking of the *Cj*-CdtB subunit to the nucleus, we encountered challenges in reliably detecting subunit localization at the plasma membrane and subsequent intracellular organelles. The limitations in immunofluorescence detection sensitivity, coupled with the lack of clear subunit association signals, hindered our ability to draw definitive conclusions regarding subunit trafficking. While our findings provide valuable insights into the role of key organelles in *Cj*-CDT activity, further research employing alternative methodologies or improved detection techniques may be necessary to fully elucidate the trafficking mechanisms of *Cj*-CDT subunits during cellular intoxication.

2.4 DISCUSSION

The studies described herein were designed to address one of the most poorly understood aspects of CDT biology, which is the role and mechanism of the *Cj*-CDT subunits for the intracellular trafficking and ultimately nuclear localization of the *Cj*-CdtB subunit. Similar to other AB-type toxins, CDTs are thought to function as two component toxins where the CdtA and CdtC subunits function as the binding/delivery subunits which transports the catalytically active CdtB subunit to the cytoplasm where the CdtB subunit is then able to localize to the nucleus. In addition, the CdtB subunit is widely considered the only active subunit as it possesses structural homology to DNase I (107) as well as is the only subunit that is able to cause DNA damage by itself when microinjected into host cells (82). Before conducting studies aimed at elucidating the trafficking fates of the *Cj*-CDT subunits we demonstrated that host cell intoxication resulted in G2/M cell cycle arrest, consistent with previous work, and that treating cells under different experimental conditions, specifically a pulse intoxication where cells were expose to toxin for a limited duration, had little effect on toxin activity. Furthermore, our activity studies revealed the *Cj*-CDT toxin had CCA_{50} values that were in the low nanomolar range (< 10 nM). A closer look at the structure of the CdtA and CdtC subunit reveals several motifs that may play a role in recognition of the host cell membrane (107), supporting their role as delivery components. Similar to previous work (40, 81, 141), our studies with *Cj*-CDT also demonstrated that all three *Cj*-CDT subunits were required for maximal cellular activity under different experimental conditions, cell lines, and in a dose

dependent manner, supporting the previously established model suggesting that nuclear localization of the *Cj*-CdtB subunit required the *Cj*-CdtA and *Cj*-CdtC subunits.

While compelling evidence suggests that the nuclear trafficking of the CdtB subunit follows a retrograde pathway involving sequential transport from the host surface into endosomes (30, 40, 65), Golgi apparatus (62, 65), endoplasmic reticulum (49, 62, 65), cytosol (33, 49), and finally the nucleus (97, 109), understanding the role and mechanism of the individual subunits during trafficking remains limited. This chapter of the thesis aims to address a significant knowledge gap concerning *Cj*-CDT transport: the intracellular trafficking fates of the individual *Cj*-CDT subunits during cellular intoxication. To assess the involvement of *Cj*-CdtA and *Cj*-CdtC subunits in nuclear delivery, we confirmed the significance of endosomes, Golgi apparatus, and endoplasmic reticulum, implying their importance in the nuclear trafficking of the *Cj*-CdtB subunit. However, we encountered challenges in measuring the time-dependent intracellular transport of the individual *Cj*-CDT subunits during cellular intoxication. Despite employing immunofluorescence microscopy, we were unable to detect the trafficking of *Cj*-CdtA and *Cj*-CdtC, even with epitope-tagged subunit isoforms. Conversely, we did observe nuclear localization of the *Cj*-CdtB subunit, consistent with prior reports. Unfortunately, these negative and incomplete findings do not clarify the involvement of the *Cj*-CdtA and *Cj*-CdtC subunits in intracellular trafficking and, ultimately, the nuclear localization of *Cj*-CdtB. Additionally, we generated sulfation and glycosylation *Cj*-CdtB mutants as

an alternative approach to evaluate Golgi apparatus and endoplasmic reticulum trafficking of the *Cj*-CdtB subunit. However, we were also unable to assess trafficking to these organelles using these *Cj*-CdtB mutants (data not shown).

Outside of these studies, there has been relatively little published work on the trafficking nature of the individual CDT subunits, particularly CdtA and CdtC. Previous immunofluorescence microscopy studies have shown that for *Hd* and *Ec*-CDTs, CdtA and CdtC influence distinct routes of endosomal trafficking, implying their involvement in the intracellular trafficking of the CdtB subunit (40). Specifically, the *Ec*-CdtBC subunit combination has been observed to localize to early and late endosomes in a time-dependent manner, while the *Ec*-CdtAB combination is internalized but does not localize at the endosomal level. However, this study also revealed that both *Hd* and *Ec*-CDT subunits exhibited toxin activity with binary combinations (AB or BC). This is in contrast to other studies that have shown that partial *Hd*-CDT combinations does not have activity (57, 87), same with partial *Aa*-CDT subunit combinations (127), and *Cj*-CDT combinations (81). Nevertheless, since both AB and BC combinations of *Ec*-CDT were shown to be able to enter host cells, it suggests several models. Firstly, for *E. coli* CDTs, both the CdtA and CdtC subunits are capable of binding to a host cell receptor, as the toxins are able to enter host cells, but may play distinct roles in trafficking. For instance, the *Ec*-CdtAB subunit may traffic in a manner that does not involve the endosomes, such as caveolar mediated endocytosis pathway which has not been demonstrated for *Ec*-CDTs. While on the other hand, the *Ec*-CdtBC subunit combination might be trafficking in a manner that

involves endosomes, which is the more widely observed model for CDT entry. In addition, it's important to note that for these studies, different cell lines have different sensitivities to the different combinations of *Ec*-CDT subunits, suggesting that the CdtA and CdtC subunit not only might play a role in trafficking, but also might play a role in targeting different host cell types and have different trafficking properties in different cell lines.

For other CDTs, such as *Aa*-CDTs, it has been shown that while the *Aa*-CdtA subunit may not undergo internalization, the *Aa*-CdtC subunit likely traffics alongside the *Aa*-CdtB subunit, although not reaching the nucleus (33). Utilizing live immunofluorescence microscopy techniques, researchers observed that the *Aa*-CdtC subunit was also present at the host cell surface but primarily trafficked along with the *Aa*-CdtB subunit to the host cell cytoplasm after 18 h of toxin exposure.

These findings leave gaps in understanding the intracellular localization of the CdtA and CdtC subunits between cellular internalization and cytoplasmic localization of the CdtB subunit, as well as their role in the retrograde trafficking of the CdtB subunit. The challenge of measuring the intracellular trafficking of the CdtA and CdtC subunits persists in the CDT field. Efforts to measure toxin subunit intracellular transport have yielded either vague or incomplete results across various laboratories. This suggests several possibilities regarding the role of the CdtA and CdtC subunits in toxin trafficking and our ability to study them. One possibility is that the CdtA and CdtC subunits do not play a major role in the intracellular trafficking of the CdtB subunit and may only be involved in receptor

recognition and internalization, as their intracellular trafficking remains elusive. However, this does not explain the difficulty in detecting toxin at the host cell surface, which may be due to challenges such as epitope masking when toxin subunits are complexed and bound to host receptors or even scarce host cell receptors at the surface which would limit that amount of toxin associated at the membrane. Another possibility is that toxin internalization is much less efficient than previously assumed, with limited toxin entering host cells due to factors such as scarce host cell receptors at the surface or complicated conditions required for productive toxin internalization and trafficking to the cell nucleus. Given these limitations, a better understanding of the relationship between CDT holotoxin complex formation and biological activity is crucial. While the prevailing model suggests that CDT binds to and intoxicates sensitive host cells as an assembled tripartite toxin, the biologically active structure of the toxin that binds to the surface of sensitive host cells remains poorly understood. Addressing this significant knowledge gap has prompted our next series of major studies.

2.5 FIGURES

Figure 2.1

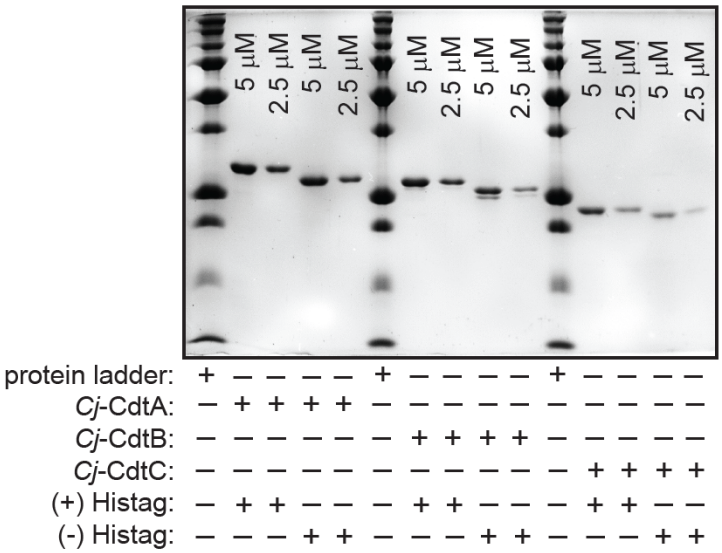

Figure 2.1: Coomassie analysis of purified *Cj*-CDT subunits with and without the polyhistidine tag. Individually purified and refolded *Cj*-CDT subunits (*Cj*-CdtA, *Cj*-CdtB, and *Cj*-CdtC) with and without the polyhistidine tag were diluted to a final concentration of 5 μM and 2.5 μM. Each of the subunits were then loaded separately, as indicated in the figure, ran on a 12% SDS-PAGE gel, and stained with Coomassie brilliant blue. Data shown are representative of 3 independent biological replicates (n = 3).

Figure 2.2

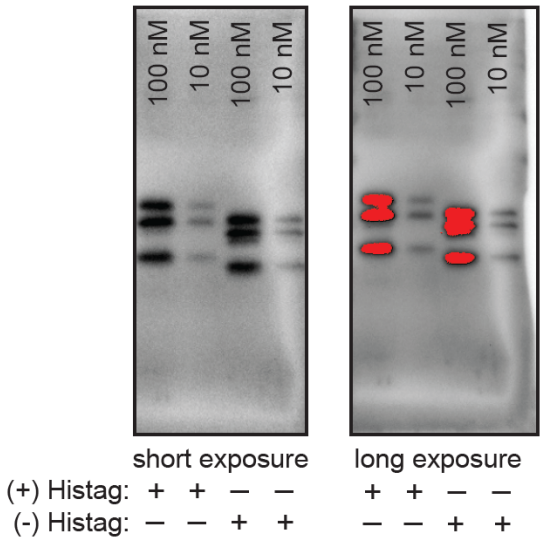

Figure 2.2: Immunoblot analysis of purified *Cj*-CDT subunits with and without the polyhistidine tag. Individually purified and refolded *Cj*-CDT subunits (*Cj*-CdtA, *Cj*-CdtB, and *Cj*-CdtC) with and without the polyhistidine tag were combined at stoichiometrically equivalent ratios, as determined by BCA protein quantification and Coomassie staining, and diluted to a final concentration of 100 nM and 10 nM. Each of the subunit combinations consisting of all three *Cj*-CDT subunits were then loaded separately as indicated in the figure, ran on a 12% SDS-PAGE gel, and immunoblotted with primary antibodies specific to each *Cj*-CDT subunit. Data shown are representative of 3 independent biological replicates (n = 3).

Figure 2.3

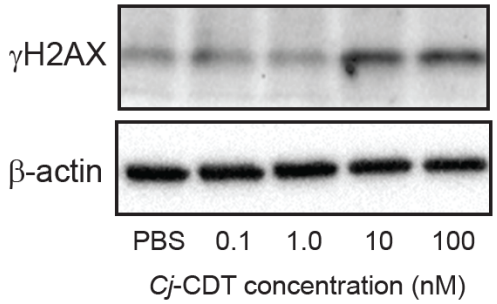

Figure 2.3: H2AX response of HCT116 cells exposed to refolded *Cj*-CDT for a 24 h continuous exposure. HCT116 cells were incubated in McCoy's 5A medium + 10% FBS, at 37 °C, and under 5% CO_2, in the absence or presence of concurrently refolded *Cj*-CDT (100 pM – 100 nM). 24 h after the initial intoxication, cells were harvested and cell lysates were analyzed by immunoblot analysis for γH2AX and β-actin. Data shown are representative of 3 independent biological replicates (n = 3).

Figure 2.4

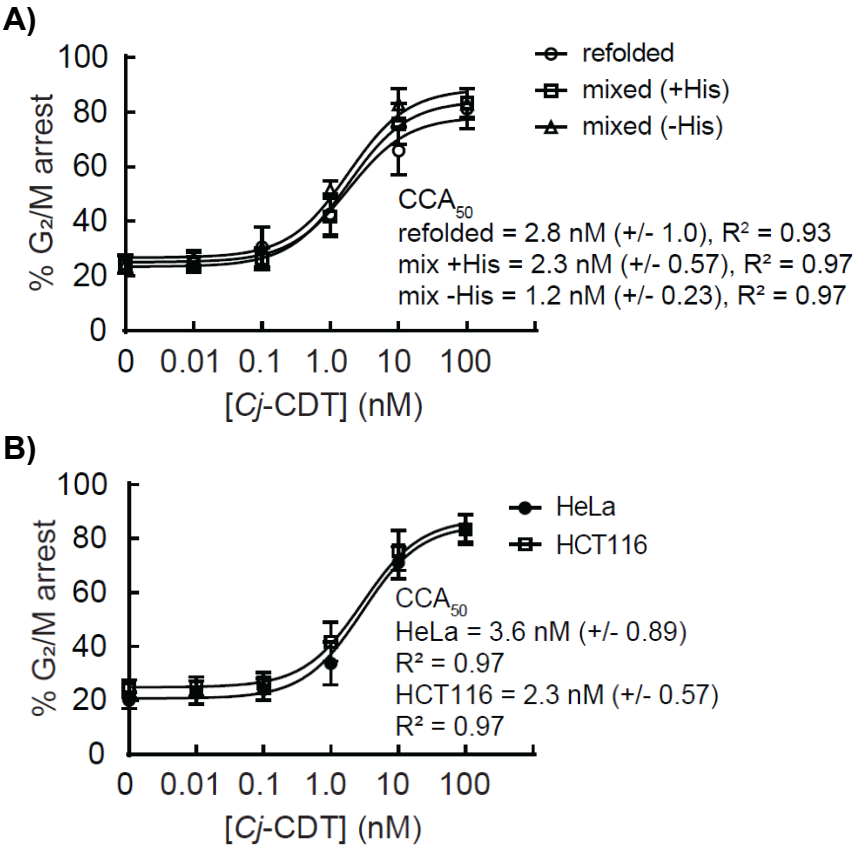

Figure 2.4: Concurrently refolded and individually refolded *Cj*-CDT subunits have similar activities in HCT116 and HeLa cells. (A) HCT116 cells were incubated in McCoy's 5A medium + 10% FBS, at 37 °C, and under 5% CO_2, in the absence or presence of concurrently refolded *Cj*-CDT subunits, or individually refolded *Cj*-CDT subunits with or without the polyhistidine tag (10 pM – 100 nM). 24 h after the initial intoxication, cells were harvested and evaluated for cell cycle arrest progression. **(B)** HCT116 cells and HeLa cells were incubated in cell culture medium + 10% FBS, at 37 °C, and under 5% CO_2, in the absence or presence of individually refolded *Cj*-CDT subunits (10 pM – 100 nM). 24 h after the initial intoxication, cells were harvested and evaluated for cell cycle arrest progression. The data were combined from 3 independent biological replicates (n = 3) and represent the percentage of cells within the monolayer arrested at the G_2/M interface. Error bars represent standard deviations. The data were fit to a log[*Cj*-CDT] vs response equation on GraphPad Prism (version 8.1.2). The CCA_{50} (i.e., EC_{50}) value was determined for each condition. R^2 values indicate fit of the data to the regression model.

Figure 2.5

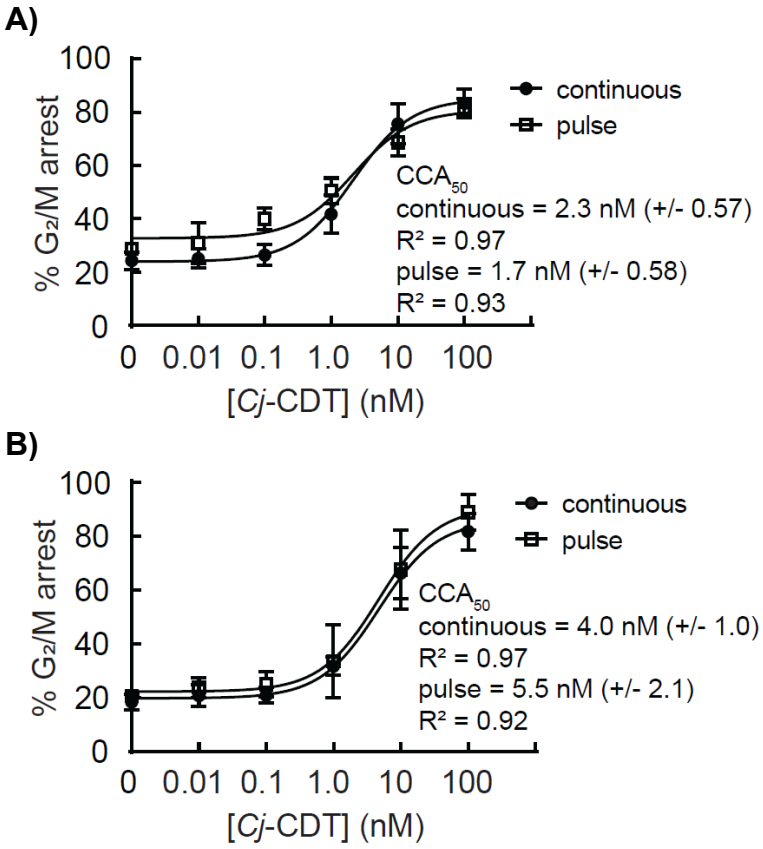

Figure 2.5: Continuous and pulse intoxication of *Cj*-CDTs leads to similar activity. For the continuous intoxication condition, HCT116 cells **(A)** or HeLa cells **(B)** were incubated in culture medium + 10% FBS, at 37 °C, and under 5% CO_2, in the absence or presence of *Cj*-CDT, containing all three individually refolded *Cj*-CdtA, *Cj*-CdtB, and *Cj*-CdtC subunits (10 pM – 100 nM). 24 h after the initial intoxication, cells were harvested and evaluated for cell cycle arrest progression. For the pulse intoxication condition, HCT116 cells **(A)** or HeLa cells **(B)** were chilled on ice. After 30 mins, cells were incubated in PBS, on ice, and under atmospheric conditions in the absence or presence of *Cj*-CDT, containing all three individually refolded *Cj*-CdtA, *Cj*-CdtB, and *Cj*-CdtC subunits (10 pM – 100 nM). After an additional 30 mins, toxin was removed and incubated in culture medium + 10% FBS, at 37 °C, and under 5% CO_2. 24 h after the initial intoxication, cells were harvested and evaluated for cell cycle arrest progression. The data were combined from 3 independent biological replicates (n = 3) and represent the percentage of cells within the monolayer arrested at the G_2/M interface. Error bars represent standard deviations. The data were fit to a log[*Cj*-CDT] vs response equation on GraphPad Prism (version 8.1.2). The CCA_{50} (i.e., EC_{50}) value was determined for each condition. R^2 values indicate fit of the data to the regression model.

Figure 2.6

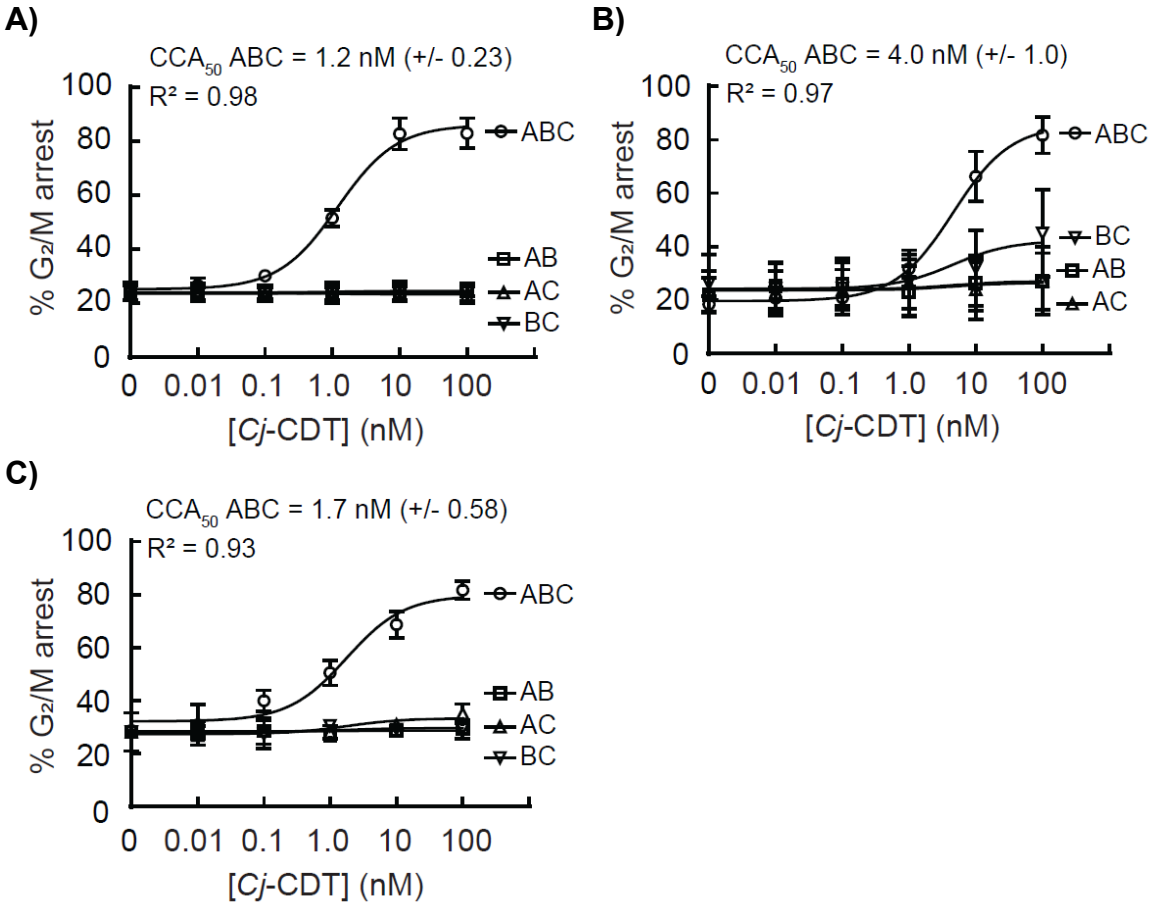

Figure 2.6: Maximal *Cj*-CDT activity requires all three subunits. HCT116 cells **(A)** or HeLa cells **(B)** were incubated in McCoy's 5A medium + 10% FBS, at 37 °C, and under 5% CO_2, in the absence or presence of *Cj*-CDT (ABC), *Cj*-CdtA + *Cj*-CdtB (AB), *Cj*-CdtA + *Cj*-CdtC (AC), or *Cj*-CdtB + *Cj*-CdtC (BC) (10 pM – 100 nM). 24 h after the initial intoxication, cells were harvested and evaluated for cell cycle arrest progression. **(C)** HCT116 cells were chilled on ice. After 30 mins, cells were incubated in PBS, on ice, and under atmospheric conditions, in the absence or presence of *Cj*-CDT (ABC), *Cj*-CdtA + *Cj*-CdtB (AB), *Cj*-CdtA + *Cj*-CdtC (AC), or *Cj*-CdtB + *Cj*-CdtC (BC) (10 pM – 100 nM). After an additional 30 mins, toxin was removed and cells were incubated with culture medium + 10% FBS, at 37 °C, and under 5% CO_2. 24 h after the initial intoxication, cells were harvested and evaluated for cell cycle arrest progression. The data were combined from 3 independent biological replicates (n = 3) and represent the percentage of cells within the monolayer arrested at the G_2/M interface. Error bars represent standard deviations. The data were fit to a log[*Cj*-CDT] vs response equation on GraphPad Prism (version 8.1.2). The CCA_{50} (i.e., EC_{50}) value was determined for *Cj*-CDT (ABC) but not the binary subunit combinations. R^2 values indicate fit of the data to the regression model.

Figure 2.7

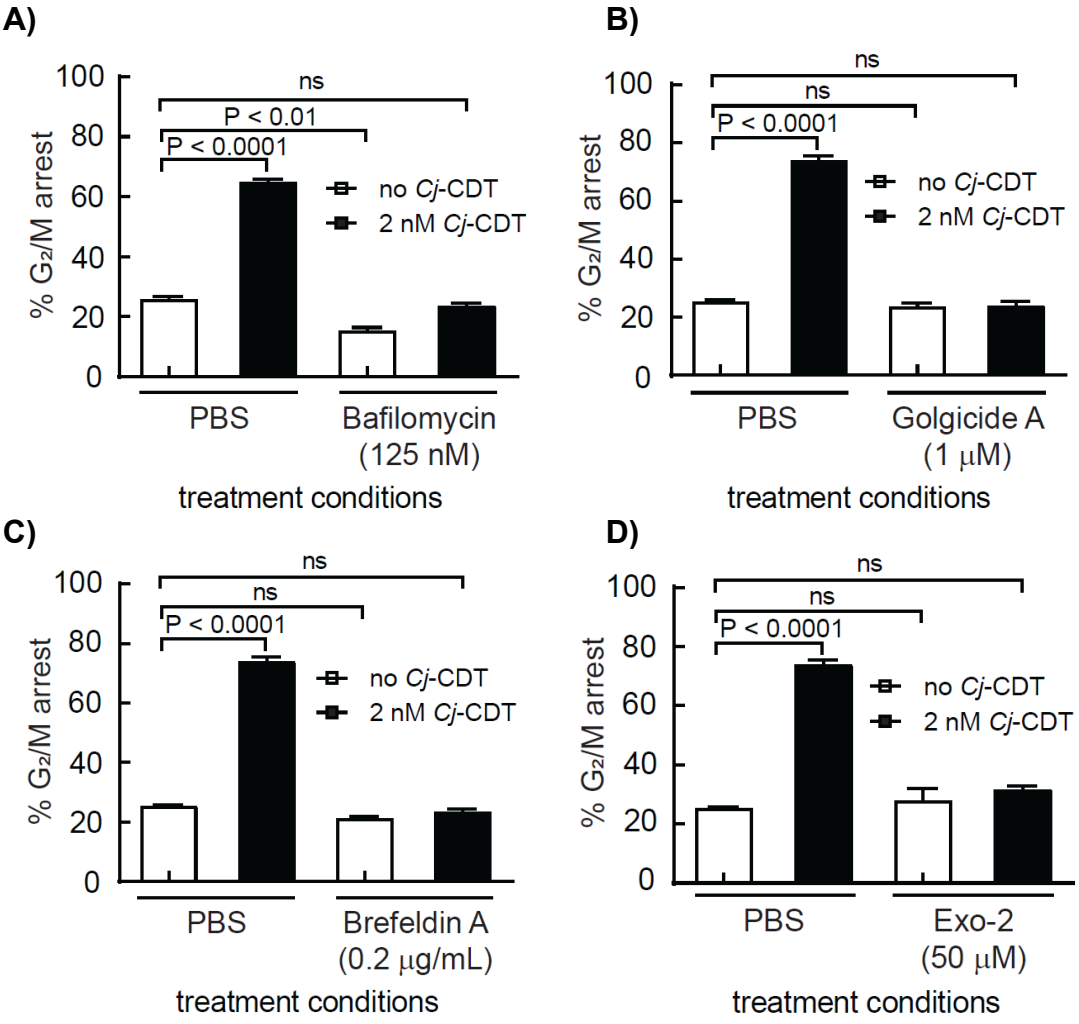

Figure 2.7: Effect of endosome, Golgi apparatus, and endoplasmic reticulum disruption on *Cj*-CDT activity. (A) HeLa cells were incubated in DMEM medium + 10% FBS, at 37 °C, and under 5% CO_2, in the absence or presence of *Cj*-CDT (2 nM), with or without Bafilomycin (125 nM). 24 h after the initial intoxication, cells were harvested and evaluated for cell cycle arrest progression. HCT116 cells were incubated in McCoy's 5A medium + 10% FBS, at 37 °C, and under 5% CO_2, in the absence or presence of *Cj*-CDT (2 nM), with or without **(B)** Golgicide A (1 μM), **(C)** Brefeldin A (0.2 mg/mL), and **(D)** Exo-2 (50 μM). 24 h after the initial intoxication, cells were harvested and evaluated for cell cycle arrest progression. The data were combined from 2 independent biological replicates (n = 2) and represent the percentage of cells within the monolayer arrested at the G_2/M interface. Error bars represent standard deviations. Statistical analyses of the data were conducted using one-way Anova, followed by Tukey's multiple comparisons test. $P < 0.05$ indicates statistical significance ($\alpha = 0.05$). "ns" indicates differences were not statistically significant.

Figure 2.8

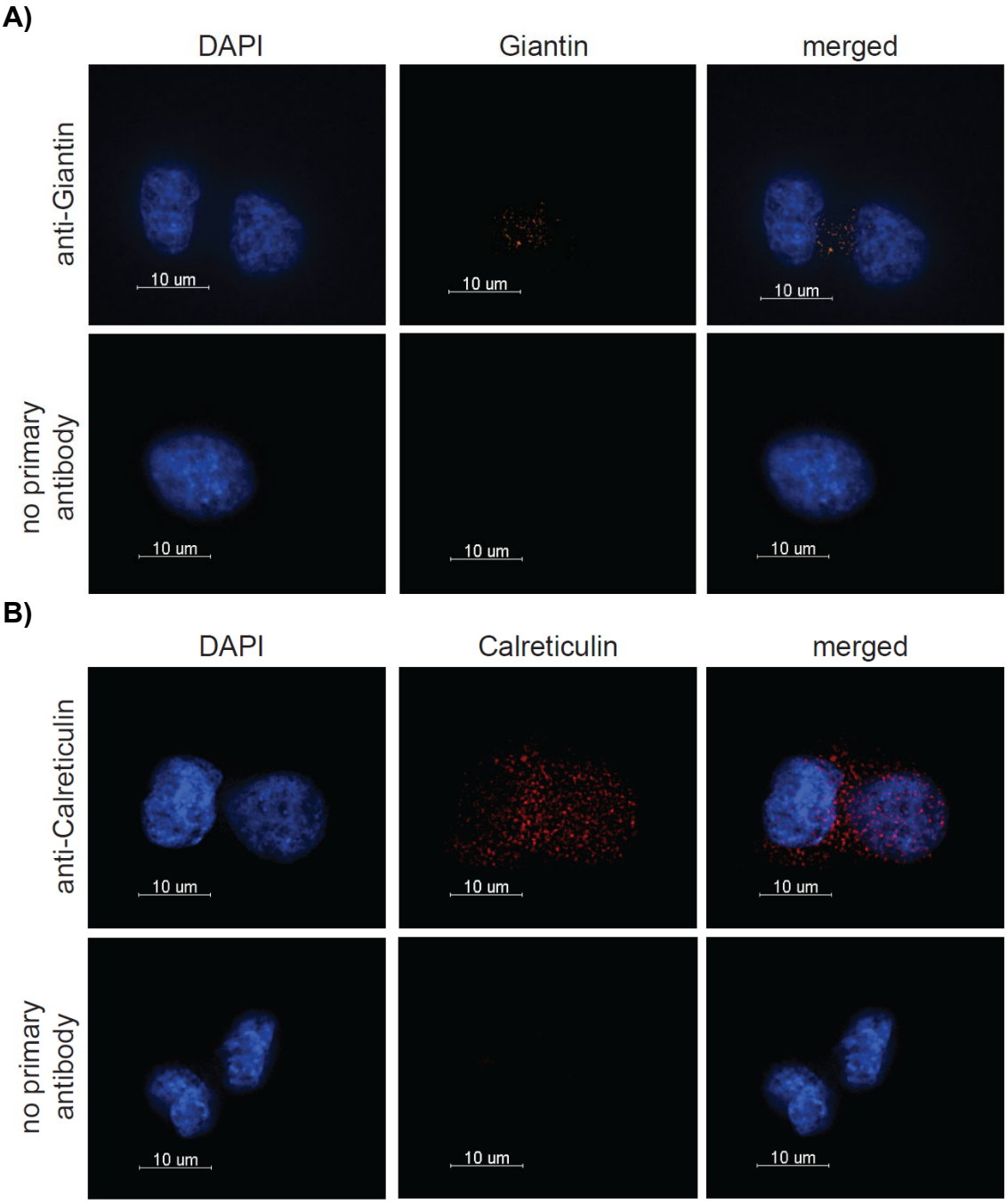

Figure 2.8: HCT116 cells stained with Golgi apparatus and Endoplasmic reticulum markers. HCT116 cells within McCoy's 5A + 10% FBS medium were probed with **(A)** the Golgi apparatus marker Giantin or **(B)** the endoplasmic reticulum marker Calreticulin, then examined using immunofluorescence microscopy. Images are representative of those collected from 2 biologically independent replicates (n = 2) collected at 60X magnification.

Figure 2.9

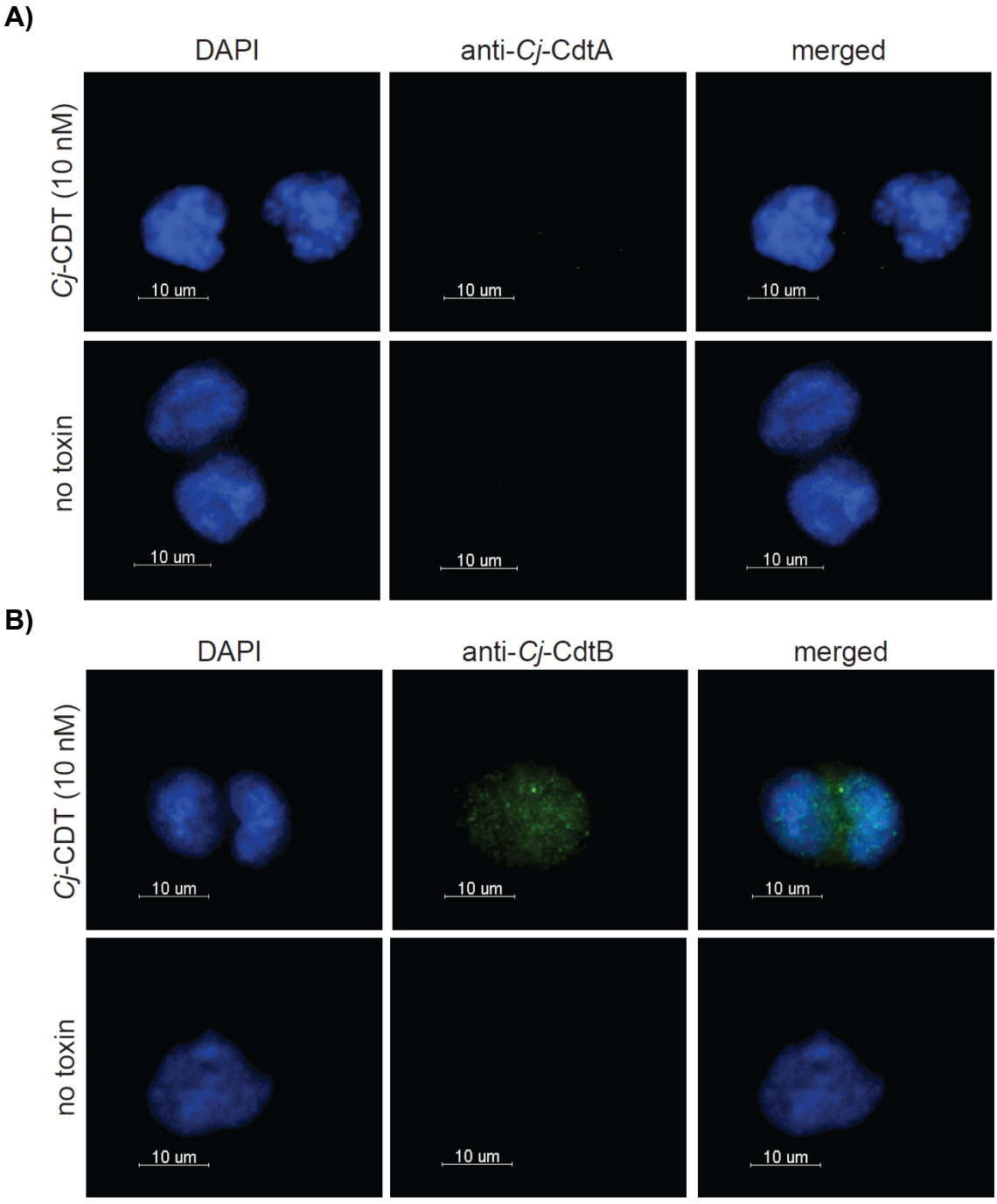
A)
DAPI
anti-Cj-CdtA
merged
Cj-CDT (10 nM)
no toxin
10 um
B)
DAPI
anti-Cj-CdtB
merged
Cj-CDT (10 nM)
no toxin
10 um

Figure 2.9 (cont.)

C)

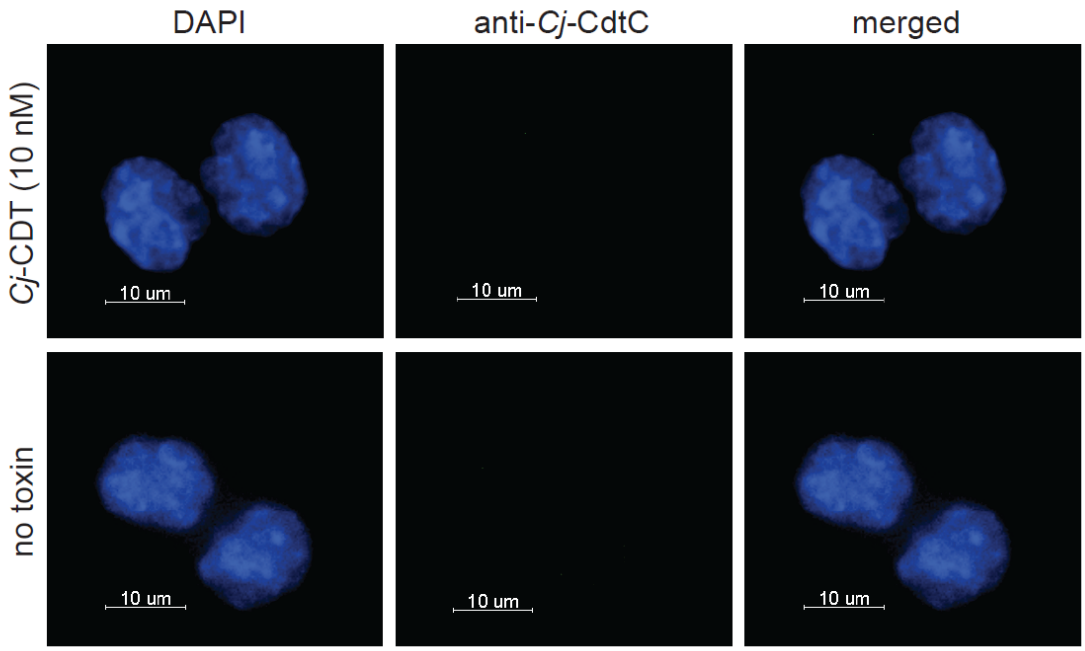

Figure 2.9: Plasma membrane localization of the *Cj*-CDT subunits. HCT116 cells were incubated in McCoy's 5A + 10% FBS medium, on ice, at atmospheric conditions, and in the absence or presence of *Cj*-CDT containing all three subunits (*Cj*-CdtA, *Cj*-CdtB, and *Cj*-CdtC) (10 nM). After 30 mins, unbound toxin was removed and cells were imaged using fluorescence microscopy staining with **(A)** anti-*Cj*-CdtA, **(B)** anti-*Cj*-CdtB, and **(C)** anti-*Cj*-CdtC primary antibodies. Cell nuclei were stained with DAPI. White scale bars from representative images indicate 10 μm. Images are representative of those collected from 2 biologically independent experiments (n = 2) collected at 60X magnification.

Figure 2.10

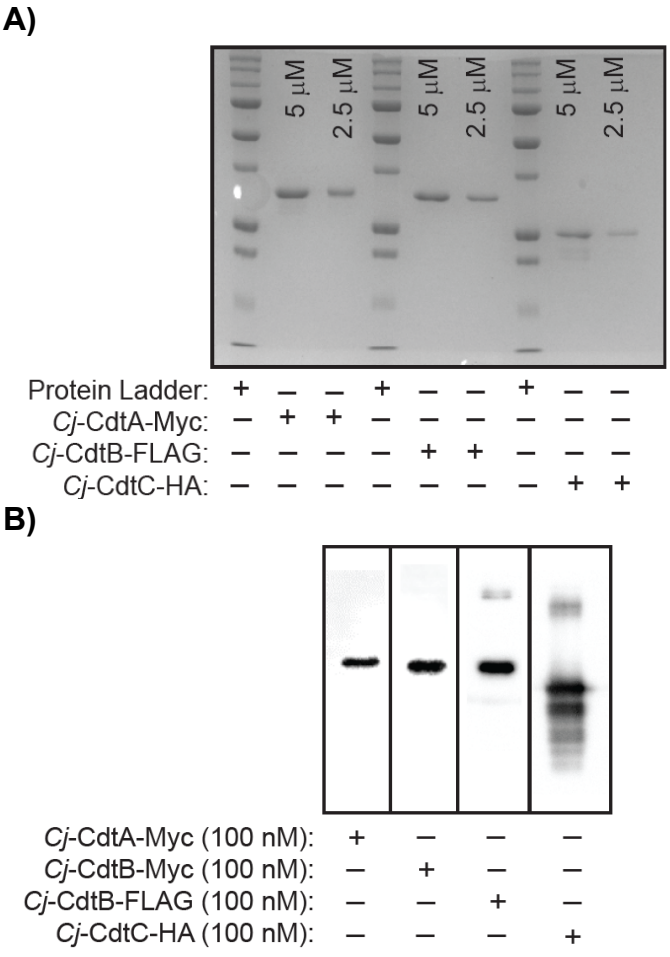

Figure 2.10: Coomassie and immunoblot analysis of purified epitope tagged *Cj*-CDT subunits. Individually purified and refolded epitope tagged *Cj*-CDT subunits (*Cj*-CdtA-Myc, *Cj*-CdtB-FLAG, and *Cj*-CdtC-HA) were diluted to a final concentration of 5 μM, 2.5 μM, and 100 nM. Each of the subunits were then loaded separately as indicated in the figure, ran on a 12% SDS-PAGE gel, and stained with Coomassie brilliant blue or immunoblotted with primary antibodies specific to each epitope. Data shown are representative of 2 independent biological replicates (n = 2).

Figure 2.11

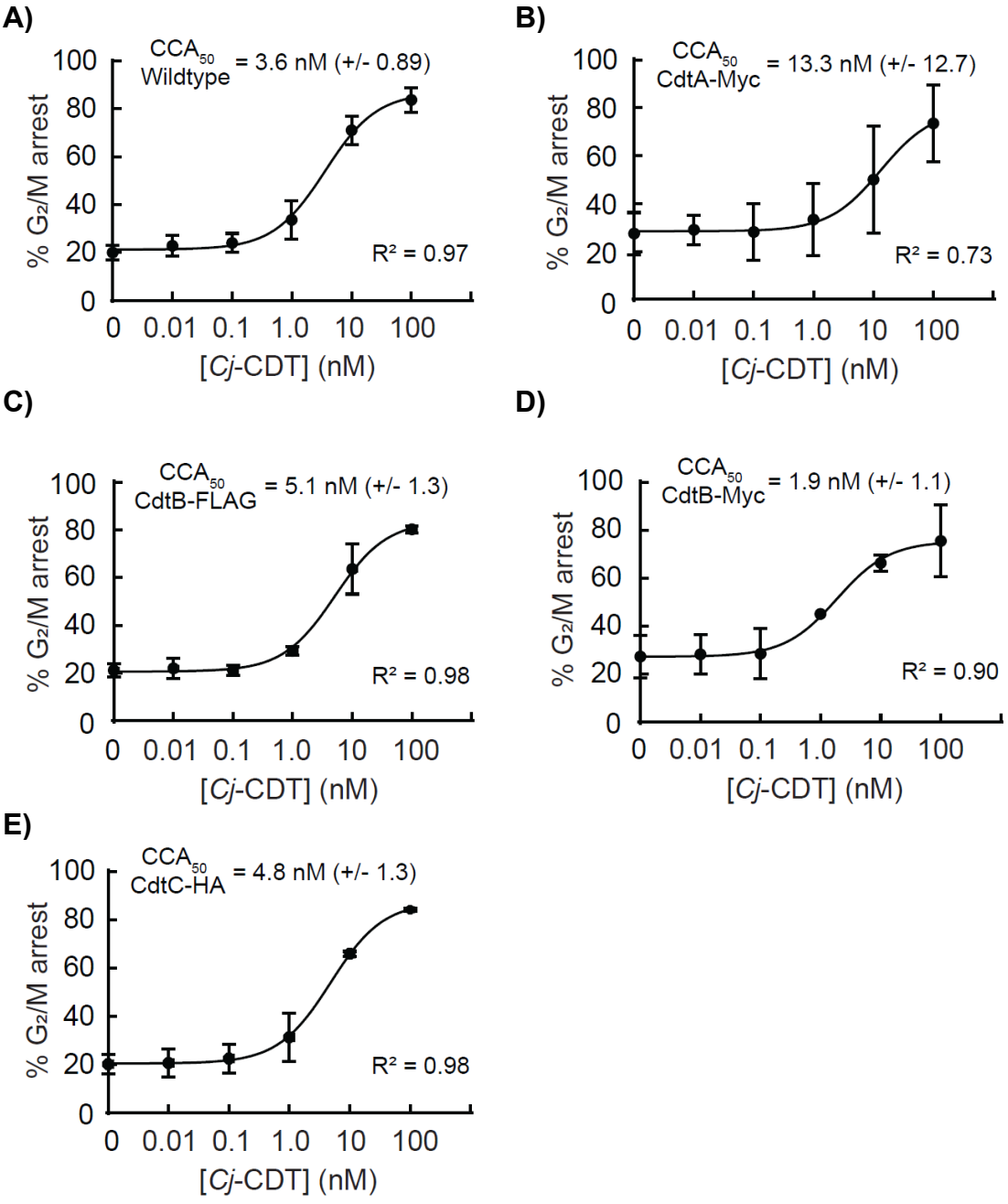
A)
CCA50 Wildtype = 3.6 nM (+/- 0.89)
% G2/M arrest
R² = 0.97
[Cj-CDT] (nM)
B)
CCA50 CdtA-Myc = 13.3 nM (+/- 12.7)
% G2/M arrest
R² = 0.73
[Cj-CDT] (nM)
C)
CCA50 CdtB-FLAG = 5.1 nM (+/- 1.3)
% G2/M arrest
R² = 0.98
[Cj-CDT] (nM)
D)
CCA50 CdtB-Myc = 1.9 nM (+/- 1.1)
% G2/M arrest
R² = 0.90
[Cj-CDT] (nM)
E)
CCA50 CdtC-HA = 4.8 nM (+/- 1.3)
% G2/M arrest
R² = 0.98
[Cj-CDT] (nM)

Figure 2.11 (cont.)

Figure 2.11: Epitope tagged *Cj*-CDT is biologically active. HCT116 cells were incubated in McCoy's 5A medium + 10% FBS, at 37 °C, and under 5% CO_2, in the absence or presence of individually refolded *Cj*-CDT subunits (10 pM – 100 nM) at the following combinations: **(A)** *Cj*-CdtA + *Cj*-CdtB + *Cj*-CdtC, **(B)** *Cj*-CdtA-Myc + *Cj*-CdtB + *Cj*-CdtC, **(C)** *Cj*-CdtA + *Cj*-CdtB-FLAG + *Cj*-CdtC, **(D)** *Cj*-CdtA + *Cj*-CdtB-Myc + *Cj*-CdtC, or **(E)** *Cj*-CdtA + *Cj*-CdtB + *Cj*-CdtC-HA. 24 h after the initial intoxication, cells were harvested and evaluated for cell cycle arrest progression. The data were combined from 2 independent biological replicates (n = 2) and represent the percentage of cells within the monolayer arrested at the G_2/M interface. Error bars represent standard deviations. The data were fit to a log [*Cj*-CDT] vs response equation on GraphPad Prism (version 8.1.2). The CCA_{50} (i.e., EC_{50}) value was determined for each condition. R^2 values indicate fit of the data to the regression model.

Figure 2.12

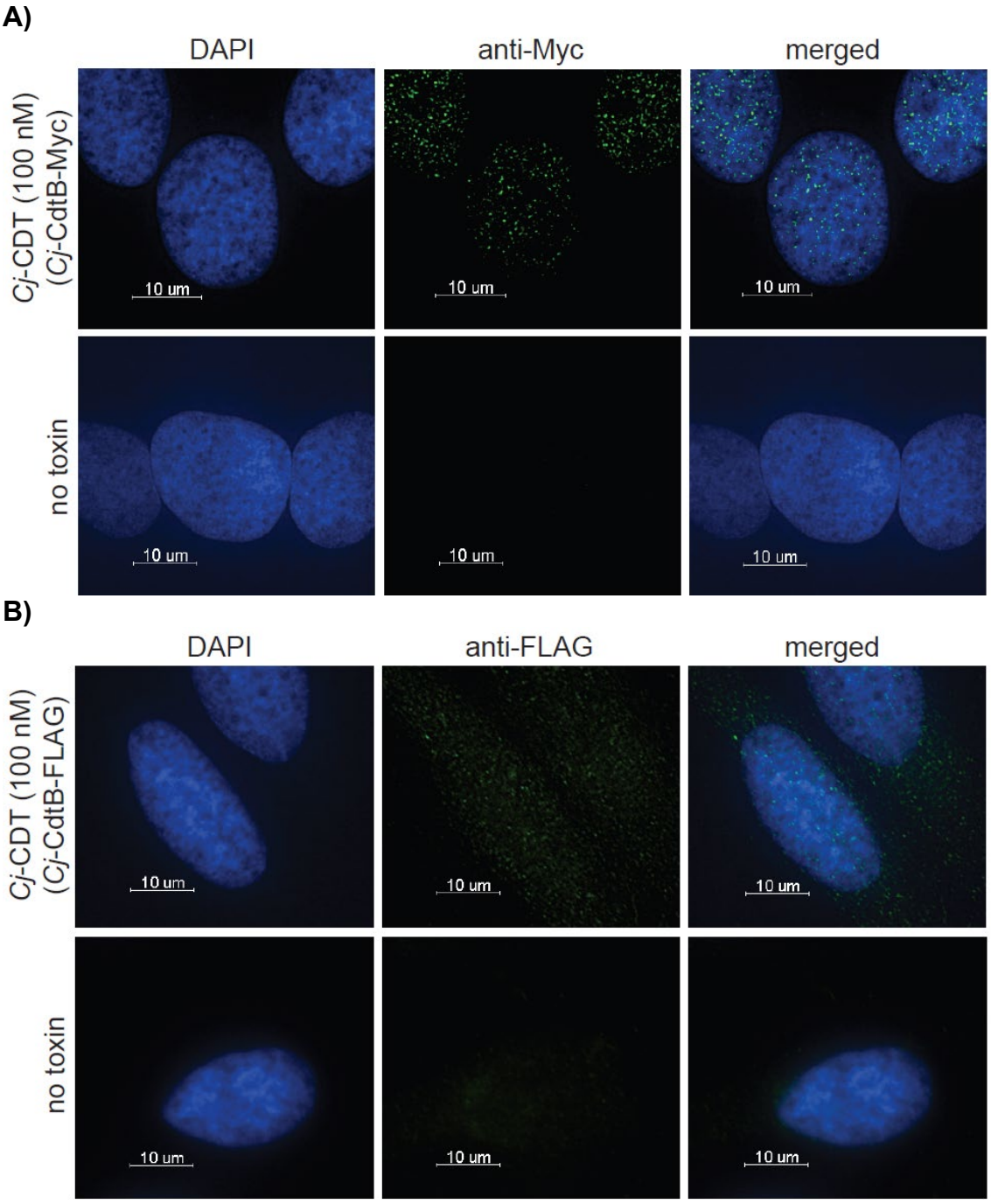
A)
DAPI
anti-Myc
merged
Cj-CDT (100 nM) (Cj-CdtB-Myc)
no toxin
10 um
B)
DAPI
anti-FLAG
merged
Cj-CDT (100 nM) (Cj-CdtB-FLAG)
no toxin
10 um

Figure 2.12 (cont.)

Figure 2.12: 24 h localization of epitope tagged *Cj*-CDT subunits. HeLa cells were incubated in DMEM + 10% FBS medium, on ice, at atmospheric conditions, and in the absence or presence of *Cj*-CDT containing **(A)** *Cj*-CdtA + *Cj*-CdtB-Myc + *Cj*-CdtC (100 nM), or **(B)** *Cj*-CdtA + *Cj*-CdtB-FLAG + *Cj*-CdtC (100 nM). After 30 mins, unbound toxin was removed and cells were incubated in DMEM + 10% FBS medium at 37 °C and under 5% CO_2. After 24 h, cells were fixed and imaged using fluorescence microscopy staining with **(A)** anti-Myc and **(B)** anti-FLAG primary antibodies. Cell nuclei were stained with DAPI. White scale bars from representative images indicate 10 μm. Images are representative of those collected from 2 biologically independent experiments (n = 2) collected at 60X magnification.

Figure 2.13

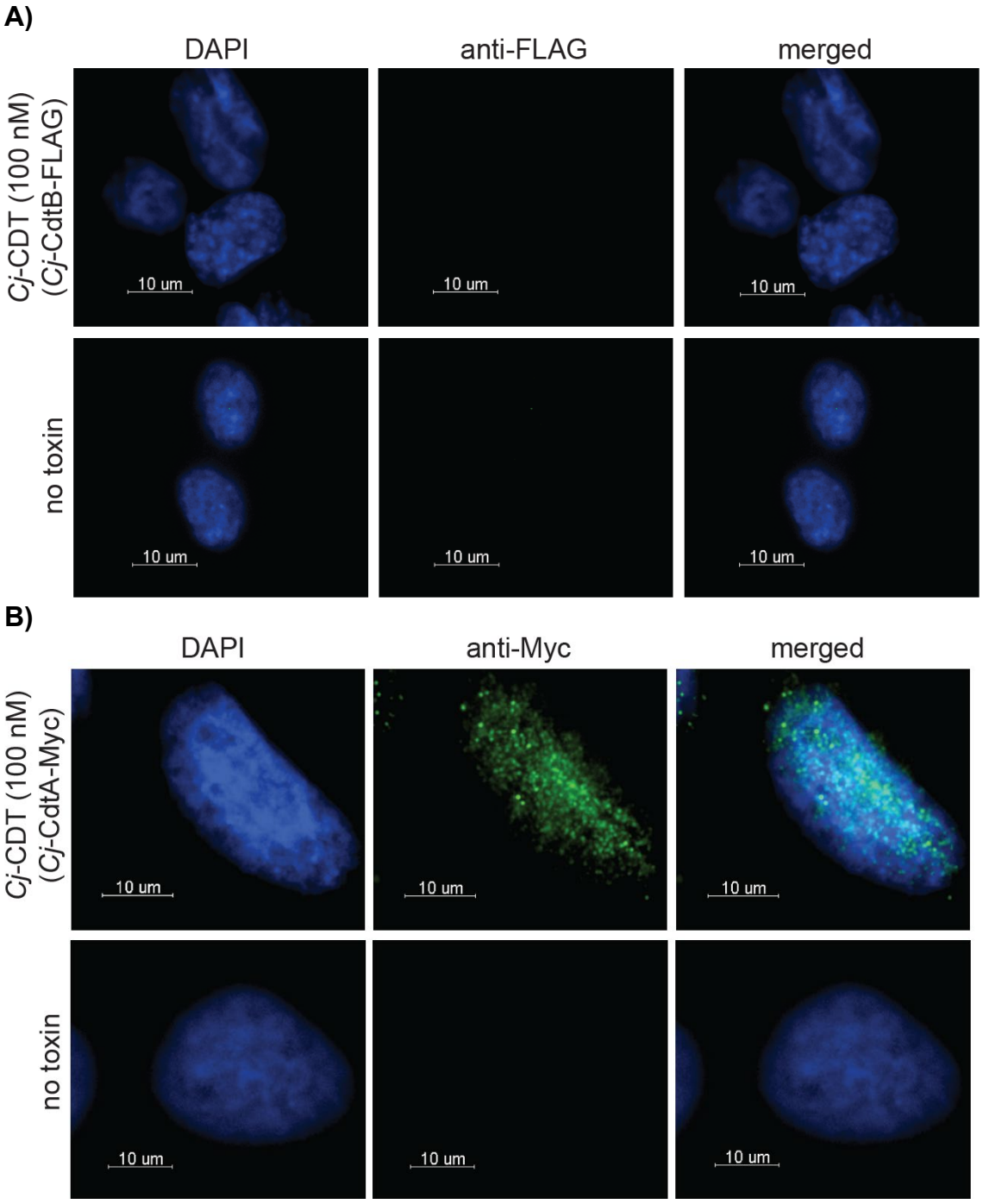
A)
DAPI
anti-FLAG
merged
Cj-CDT (100 nM) (Cj-CdtB-FLAG)
no toxin
10 um
B)
DAPI
anti-Myc
merged
Cj-CDT (100 nM) (Cj-CdtA-Myc)
no toxin
10 um

Figure 2.13 (cont.)

C)

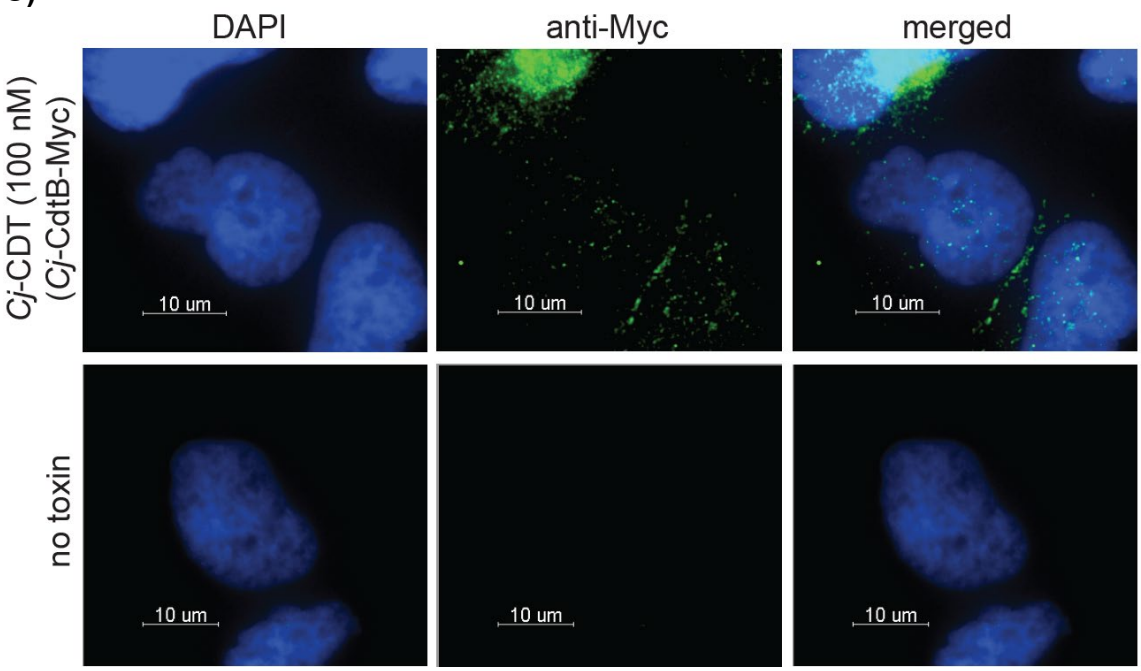

Figure 2.13: Plasma membrane localization of epitope tagged *Cj*-CDT subunits. HeLa cells were incubated in DMEM + 10% FBS medium, on ice, at atmospheric conditions, and in the absence or presence of *Cj*-CDT containing **(A)** *Cj*-CdtA + *Cj*-CdtB-FLAG + *Cj*-CdtC (100 nM), **(B)** *Cj*-CdtA-Myc + *Cj*-CdtB + *Cj*-CdtC (100 nM), or **(C)** *Cj*-CdtA + *Cj*-CdtB-Myc + *Cj*-CdtC (100 nM). After 30 mins, unbound toxin was removed and cells were imaged using fluorescence microscopy staining with **(A)** anti-FLAG and **(B+C)** anti-Myc primary antibodies. Cell nuclei were stained with DAPI. White scale bars from representative images indicate 10 μm. Images are representative of those collected from 2 biologically independent experiments (n = 2) collected at 60X magnification.

Figure 2.14

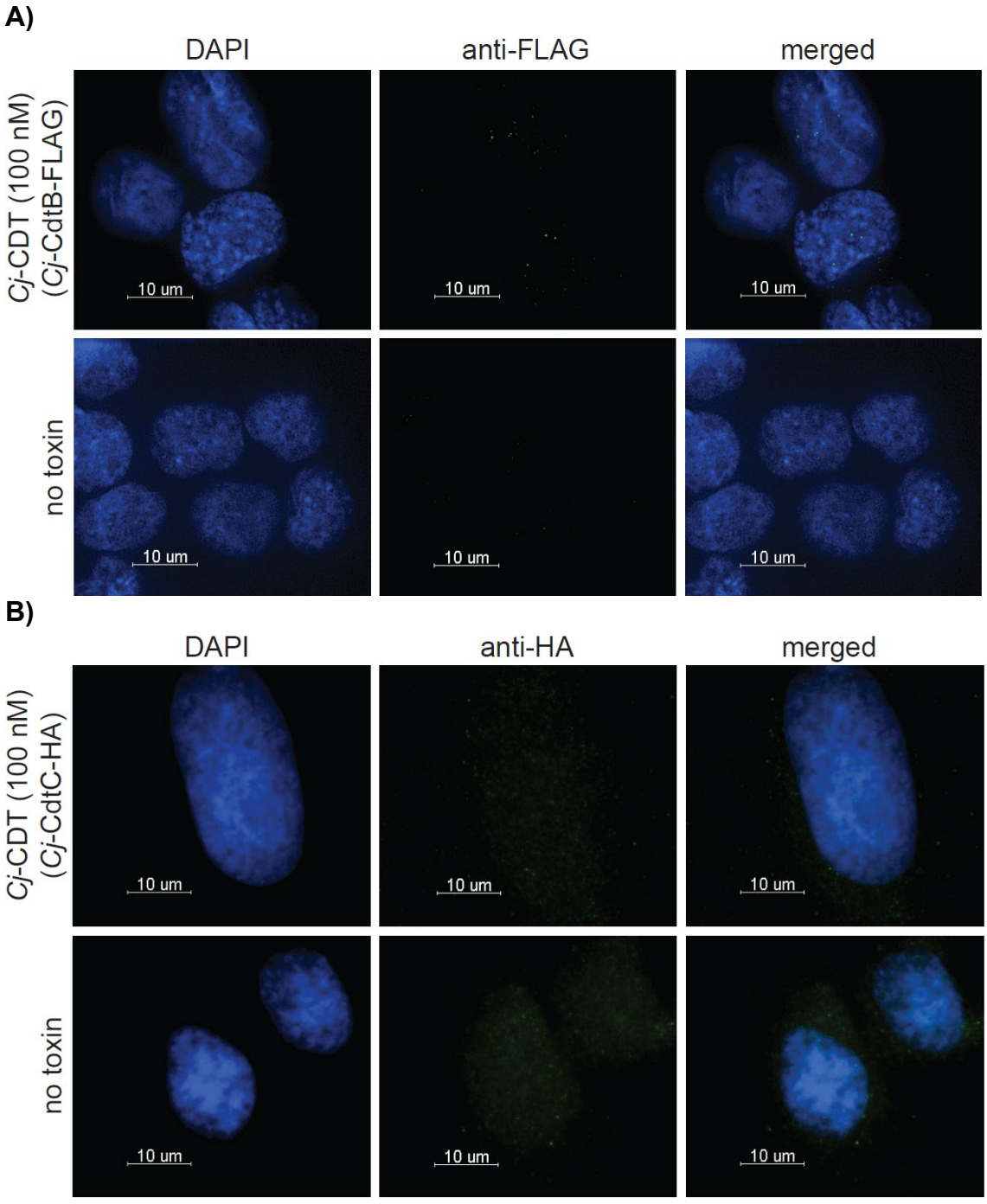
A)
DAPI
anti-FLAG
merged
Cj-CDT (100 nM) (Cj-CdtB-FLAG)
no toxin
10 um
B)
DAPI
anti-HA
merged
Cj-CDT (100 nM) (Cj-CdtC-HA)
no toxin
10 um

Figure 2.14 (cont.)

C)

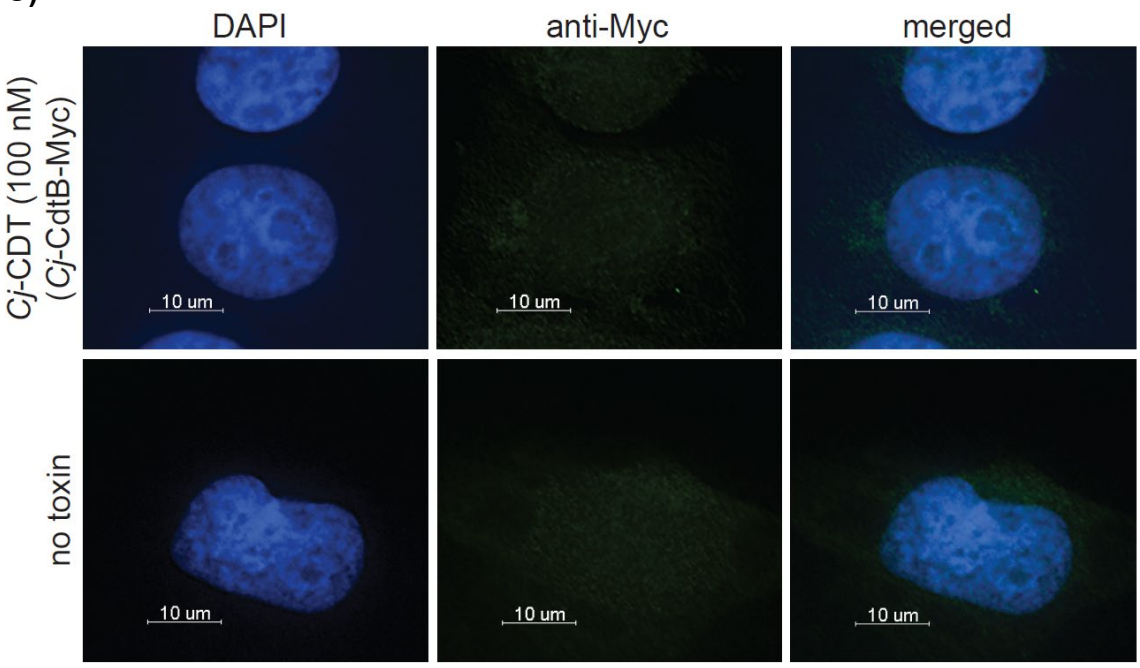

Figure 2.14: 1 h localization of epitope tagged *Cj*-CDT subunits. HeLa cells were incubated in DMEM + 10% FBS medium, on ice, at atmospheric conditions, and in the absence or presence of *Cj*-CDT containing **(A)** *Cj*-CdtA + *Cj*-CdtB-FLAG + *Cj*-CdtC (100 nM), **(B)** *Cj*-CdtA + *Cj*-CdtB + *Cj*-CdtC-HA (100 nM), or **(C)** *Cj*-CdtA + *Cj*-CdtB-Myc + *Cj*-CdtC (100 nM). After 30 mins, unbound toxin was removed and cells were incubated in DMEM + 10% FBS medium at 37 °C and under 5% CO_2. After 1 h, cells were fixed and imaged using fluorescence microscopy staining with **(A)** anti-FLAG and **(B)** anti-Myc primary antibodies. Cell nuclei were stained with DAPI. White scale bars from representative images indicate 10 μm. Images are representative of those collected from 2 biologically independent experiments (n = 2) collected at 60X magnification.

CHAPTER 3: THE RELATIONSHIP BETWEEN CJ-CDT STRUCTURE AND FUNCTION

3.1 INTRODUCTION

The cytolethal distending toxins (CDTs) are a broadly distributed family of intracellular-acting genotoxins produced by mucocutaneous pathogens of the γ- and ε-Proteobacteria (79, 165). CDTs have been isolated and functionally characterized from multiple pathogens, including *Aggregatibacter actinomycetemcomitans* (*Aa*), *Hemophilus ducreyi* (*Hd*), *Escherichia coli* (*Ec*), and *Campylobacter jejuni* (*Cj*) (28, 35, 95, 165). Within the extracellular environment, CDTs bind and are taken up into host cells, ultimately resulting in DNA damage, activation of the DNA damage response, and arrest of cell cycle progression (64). Phosphatidylinositol-3,4,5-triphosphate phosphatase activity has also been associated with *Ec*-CDT, *Cj*-CDT, *Hd*-CDT, and *Aa*-CDT (62, 70, 143). Although increasing evidence implicates individual CDTs as important determinants of virulence (54, 73, 121), the structure-function relationships that underlie toxin interactions with host cells remain incompletely understood.

Most CDTs comprise three distinct subunits, CdtA, CdtB, and CdtC, which are encoded by contiguous genes within a single operon (61). Analogous to most intracellular-acting bacterial protein exotoxins, CDTs are believed to possess classic “A-B” functional architecture, where the CdtA and CdtC subunits together are thought to constitute the “B component”, which facilitates the binding, uptake, and intracellular trafficking of the “catalytically active A component” (17), CdtB,

within host cells (33, 49, 71, 97). High-resolution structural data indicate that, at high concentrations (>100 μM), the CdtA, CdtB, and CdtC subunits of *Hd*-CDT (107) and *Aa*-CDT (169) are assembled into heterotrimeric complexes, leading to a widely accepted model that these three subunits assemble into a functional, oligomeric holotoxin complex. Nonetheless, the importance of an assembled tripartite toxin complex for CDT cellular activity has not been definitively established.

Herein, we describe studies designed to evaluate the importance of the CDT tripartite structure for the cellular activity of the toxin from the human intestinal pathogen *Campylobacter jejuni* (*Cj*-CDT). Human epidemiological data coupled with animal infection studies support a role for Cj-CDT as an important determinant of pathogen colonization and virulence (54, 73). However, the mechanisms by which *Cj*-CDT is assembled and secreted from *C. jejuni* resulting in functional toxin have not been reported. Also, the structure of functional *Cj*-CDT generated and released by the bacterium prior to intoxication of host cells has not been experimentally resolved. Strikingly, the isolation and purification of *Cj*-CDT from *C. jejuni* in culture has never been reported which makes it challenging to effectively carry out studies to delineate toxin structure-function relationships. Using three different experimental approaches, our studies here suggest that at concentrations at which *Cj*-CDT induces the arrest of cell cycle progression in mammalian cells, the three subunits (*Cj*-CdtA, *Cj*-CdtB, and *Cj*-CdtC) exist in solution as predominantly non-assembled monomers. These results suggest that the existing paradigm that *Cj*-CdtA, *Cj*-CdtB, and *Cj*-CdtC

functionally interact with host cells as a preassembled tripartite toxin should be revisited.

3.2 MATERIALS AND METHODS

Cj-CDT expression and purification. Recombinant forms of *Cj*-CdtA, *Cj*-CdtB, *Cj*-CdtC were generated and purified as previously described (50). Subunit purity was evaluated using sodium dodecyl sulfate polyacrylamide gel electrophoresis (SDS-PAGE) (Biorad, Hercules, CA) followed by Coomassie Brilliant Blue staining (Sigma, St. Louis, MO), and quantified using the Pierce BCA protein assay (Thermo, Rockford, IL).

Removal of polyhistidine fusion peptides. His-tagged recombinant subunits were incubated at 21 ˚C with biotinylated thrombin (Novagen, Billerica, MA). After 20–24 h, biotinylated thrombin and cleaved polyhistidine peptides were removed using Pierce streptavidin agarose beads (ThermoFisher, Waltham, MA) and TALON Metal Affinity Resin (TaKaRa, Mountain View, CA), respectively. The beads and resin were removed using Spin-X centrifuge tube filters (pore size, 0.22 μm; Corning Costar, NY). *Cj*-CDT subunits free of polyhistidine fusion peptides, were quantified using the Pierce BCA assay. Polyhistidine removal was confirmed using SDS-PAGE and Coomassie Brilliant Blue staining.

Mammalian cell culture. Human cancer colonic epithelial cells (HCT116, ATCC, Manassas, VA) were maintained in McCoy's 5a Modified Medium (Corning, Manassas, VA) supplemented with 10% fetal bovine serum (Sigma, St.

Louis, MO) and cultivated at 37 °C and under 5% CO_2 within a humidified environment.

Cell cycle phase determination. Cj-CDT-dependent arrest of cell cycle progression at the G_2/M interface was assessed using flow cytometry (FACSymphony A1, BD Biosciences, Franklin Lakes, NJ) as previously described (50, 62).

Dialysis retention assays. Purified *Cj*-CDT subunits were incubated together on ice or 37 °C. After 1 h, the mixtures were dialyzed at 37 °C against PBS pH 7.4 (1:1000 sample to buffer ratio), using Micro Float-A-Lyzer Dialysis Devices with a Molecular weight cutoff (MWCO) of 50 kDa (Spectrum Labs, CA). After 48 h, samples were harvested and evaluated for retention of *Cj*-CdtB using immuno-blot analyses.

Immunoblotting. Following SDS-PAGE, resolved proteins were transferred to PVDF membranes (Millipore Sigma, Burlington, MA) using a wet/tank blotting system (Bio-Rad). Membranes were blocked with 5% bovine serum albumin (Sigma-Aldrich, St. Louis, MO) in TBS-T (0.1% Tween-20 in TBS pH 7.4, Fisher, Fair Lawn, NJ) and incubated with primary antibodies. Primary antibodies specific for each *Cj*-CDT subunit were generated commercially against peptide sequences unique to *Cj*-CdtA, *Cj*-CdtB, and *Cj*-CdtC (YenZme, San Francisco, CA) as follows: antibodies specifically targeting the *Cj*-CdtA-specific sequence 255-CPFTAKPLYRQGEVR-268, the *Cj*-CdtB-specific sequence 185-CDFNRDPSTITSTVDRELANR-204, and the *Cj*-CdtC-specific sequence 44-CFRDTSKDPIDQNWNIK-59. Membranes were then incubated with anti-rabbit

IgG biotinylated antibodies (Cell Signaling, Danvers, MA), and subsequently with anti-biotin HRP-linked antibodies (Cell Signaling, Danvers, MA). Immunoblots were imaged using the ChemiDoc system (XRS+, Bio-Rad, Hercules, CA) following exposure to a 1:5 mixture of SuperSignal West Femto Maximum Sensitivity: Pico Plus Chemiluminescent Substrates (Thermo, Rockford, IL). Immunoblot densitometry analyses were performed using Image Lab software (Bio-Rad, Version 6.0).

Microscale thermophoresis analysis (MST). Polyhistidine-tagged *Cj*-CDT subunits, which had been labeled with NTA – Atto 647 N dye (NanoTemper, München, Germany), were incubated at 37 °C and with non-polyhistidine-tagged, non-labeled, non-cognate subunits. After 1 h, samples were loaded into capillary tubes (Monolith NT .115 Series capillaries, NanoTemper, München, Germany) and placed into the microscale thermophoresis instrument (Monolith NT .115, software version 1.2.1, NanoTemper, München, Germany). Samples were allowed to equilibrate, in the instrument, for an additional 15 min at 37 °C before collecting data. All readings were taken using the MO.Control program (version 1.6.1, NanoTemper, München, Germany) using red excitation (650 nm, 30-100% power), and medium MST power (40%). MST values were determined, at the 3 second temperature jump. Data were normalized to the fraction of complexed molecules (FB) as previously described (173). MST values were fit to a log [*Cj*-CDT subunit] vs response equation to generate binding curves (GraphPad Prism version 8.1.2).

Cj-CDT co-immunoprecipitation. Co-immunoprecipitation was conducted using antibodies bound to protein A magnetic beads (Dynabeads, Invitrogen, Waltham, MA). Purified *Cj*-CDT subunits were incubated on ice. After 1 h, the mixtures were further incubated at 4 °C with the indicated antibodies. Immunoprecipitation (IP) antibodies were generated from sera obtained from rabbits immunized with full length recombinant *Cj*-CDT subunits (Immunological Resource Center, Univ. Illinois, Urbana, IL). After 24 h, the bound proteins were recovered by incubating beads in NuPAGE sample reducing agent plus LDS sample buffer (Invitrogen, Norway). Recovered *Cj*-CDT subunits were analyzed using SDS-PAGE followed by immunoblot analyses.

Statistical Analyses. Each experiment was performed at least three independent times, signified as n=3. Error bars represent standard deviations. Statistical analyses were performed using GraphPad Prism 8.1.2. Dose response curves were fit to a log (agonist) vs response (three parameters) equation. R^2 values indicate fit of the data to the regression model. Analysis of statistical differences was performed using one-way ANOVA followed by the Tukey's post-hoc test. Statistical significance ($P < 0.05$) was determined at $\alpha = 0.05$.

3.3 RESULTS

3.3.1 *Cj*-CdtA, *Cj*-CdtB, and *Cj*-CdtC are required for maximal Cj-CDT cellular activity

The active form of *Cj*-CDT is generally considered to constitute a tripartite complex comprising equimolar *Cj*-CdtA, *Cj*-CdtB, and *Cj*-CdtC (61, 84), which is

a model that has emerged primarily from high resolution structural data obtained for *Aa*-CDT and *Hd*-CDT (107, 169) and previous functional studies of *Cj*-CDT (81). To experimentally evaluate this widely accepted model, we conducted experiments to compare the concentrations at which mixtures of *Cj*-CdtA, *Cj*-CdtB, and *Cj*-CdtC are assembled into a tripartite structure and induce arrest of cell cycle progression at the G_2/M interface within human colonic intestinal epithelial-derived HCT116 cells. Congruent with previous reports (81, 84), our studies revealed that Cj-CDT-dependent arrest of cell cycle progression occurs in a dose-dependent manner (Figure 3.1). Moreover, maximal cellular activity requires all three CDT subunits. The concentration of Cj-CDT subunit mixtures required to arrest approximately 50% of HCT116 cells within a monolayer (i.e., CCA50) was experimentally determined to be approximately 1 nM (Figure 3.1). Notably, this concentration was >10,000-fold lower than the toxin concentration used to generate crystals suitable for collecting high-resolution structural data for *Aa*-CDT and *Hd*-CDT. These results were comparable to those obtained with preassembled recombinant toxin (CCA50 = 2.8 (± 1.0) nM), which is prepared by concurrently refolding together equimolar concentrations of purified and denatured recombinant *Cj*-CdtA, *Cj*-CdtB, and *Cj*-CdtC subunits. Arrest of Cell cycle progression was observed in cells exposed to mixtures of *Cj*-CdtA, *Cj*-CdtB, and *Cj*-CdtC (each at 10 nM) for only 60 min, which was comparable to cells that had been continuously exposed to the toxin for 24 h (Figure 3.2). These results are consistent with previous work (165) showing that within the first hour of exposure to *Cj*-CDT, the toxin had sufficiently bound and been internalized into

host cells, resulting in DNA damage, induction of the DNA damage response, and arrest of cell cycle progression.

Additional studies to assess whether concurrent exposure of HCT116 cells to mixtures of *Cj*-CdtA, *Cj*-CdtB, and *Cj*-CdtC is essential for toxin cellular activity, revealed that prebinding of *Cj*-CdtA and *Cj*-CdtC, followed by removal of unbound subunits, and subsequent addition of *Cj*-CdtB, resulted in detectable arrest of cell cycle progression, albeit to a lesser degree than cells exposed to equimolar mixtures of the three subunits (Figure 3.3). While these studies did not reveal the mechanism of cellular intoxication in the absence of concurrent *Cj*-CDT subunit exposure, the results are consistent with a conclusion that concurrent administration of *Cj*-CdtA, *Cj*-CdtB, and *Cj*-CdtC to cells is not essential for intoxication.

3.3.2 High molecular weight *Cj*-CDT tripartite structures are not captured during dialysis at low concentrations of toxin sufficient to induce arrest of cell cycle progression

To evaluate the importance of the predicted tripartite *Cj*-CDT structure for toxin activity, we next determined the concentrations at which mixtures of *Cj*-CdtA, *Cj*-CdtB, and *Cj*-CdtC are retained within dialysis tubing. Equimolar concentrations of *Cj*-CdtA, *Cj*-CdtB, and *Cj*-CdtC (between 0.01 and 10 μM) were premixed on ice. After 1 h, the subunit mixtures were transferred to dialysis membrane cassettes (50 kDa molecular weight cutoff (MWCO)), which were then incubated in dialysis buffer at a 1:1000 volume ratio of sample to dialysis buffer.

After 48 h, the retentates were collected, and analyzed versus the corresponding input (i.e., non-dialyzed) mixtures of *Cj*-CdtA, *Cj*-CdtB, and *Cj*-CdtC. Based on the molecular mass cutoff of 50 kDa, we predicted that *Cj*-CdtA (29.9 kDa), *Cj*-CdtB (29.4 kDa), and *Cj*-CdtC (21.4 kDa), if assembled into a heterotrimeric complex (with a calculated molecular mass of approximately 80.7 kDa), would be recoverable from the dialysis membrane. In contrast, we predicted that if mixtures of *Cj*-CdtA, *Cj*-CdtB, and *Cj*-CdtC failed to assemble, then the subunits would diffuse out from the dialysis membrane and not be detected within the dialysis retentate. For these studies, we used immunoblot analyses to compare the relative levels of *Cj*-CdtB in both the input mixtures and corresponding recovered retentates of the same concentration, under the premise that *Cj*-CdtB would be recovered within the retentate when in complex with *Cj*-CdtA and *Cj*-CdtC, but not if the subunit was present as a non-associated monomer. To compare the relative recovery of *Cj*-CdtB more easily within individual dialysis retentates, each of the input mixtures and recovered retentate samples were equally diluted to a final theoretical concentration of 0.01 μM, as a point of comparison against the non-dialyzed input *Cj*-CdtB sample at 0.01 μM (Figure 3.4A). As an example, for the 1 μM condition, both the non-dialyzed and dialyzed samples were diluted 100-fold prior to immunoblot analysis. These experiments revealed that *Cj*-CdtB was not detected within the retentates of dialyzed subunit mixtures at concentrations of 0.01, 0.1, or 1.0 μM (Figure 3.4A). However, *Cj*-CdtB was detected within the retentates of Cj-CDT subunit mixtures dialyzed at concentrations of 5 or 10 μM (Figure 3.4A). The same degree of *Cj*-CdtB

retention within the dialysis tubing was observed in studies where the preincubation of equimolar mixtures of *Cj*-CDT subunits was conducted at 37 °C (Figure 3.4B). Similar results were also obtained using preassembled toxin, which is toxin prepared by concurrently refolding purified and denatured recombinant forms of *Cj*-CdtA, Cj-CdtB, and *Cj*-CdtC subunits (Figure 3.4C). These data suggest that, at the lowest concentrations of toxin that are sufficient to induce arrest of cell cycle progression, *Cj*-CdtA, *Cj*-CdtB, and *Cj*-CdtC interact with cell monolayers predominantly as mixtures of non-interacting subunit monomers.

3.3.3 MST reveals low affinity interactions between *Cj*-CDT subunits

Dialysis retention experiments described immediately above (Figure 3.4A) suggested that at low nanomolar concentrations, biologically active *Cj*-CDT exists primarily as mixtures of non-associated monomers of *Cj*-CdtA, *Cj*-CdtB, and *Cj*-CdtC, complicit with the idea that *Cj*-CDT subunits interact with relatively low affinities. To evaluate *Cj*-CDT subunit interactions more quantitatively, we employed microscale thermophoresis (MST) (166). Overall, these studies indicated that *Cj*-CDT subunit interactions (i.e., *Cj*-CdtA and *Cj*-CdtB, *Cj*-CdtA and *Cj*-CdtC, *Cj*-CdtB and *Cj*-CdtC) occur with relatively low affinity (Table 3.1) and were not detectable by MST at concentrations at which the toxin induces arrest of cell cycle progression (i.e., 1-10 nM) (Figure 3.1). Sigmoidal, saturable binding curves were obtained for mixtures of *Cj*-CdtA and *Cj*-CdtC as well as mixtures of *Cj*-CdtB and *Cj*-CdtC, with dissociation constants (KD) of

approximately 0.7 μM and 0.5 μM, respectively (Figure 3.5A and Figure 3.5B). *Cj*-CdtA interactions with *Cj*-CdtB occurred with even lower affinity, as MST measurements yielded an apparent KD of >20 μM (Figure 3.5C). Non-sigmoidal, non-saturable binding curves were obtained from experiments using NTA-565 dye-labeled *Cj*-CdtC, suggesting that labeling of *Cj*-CdtC interfered with interactions between *Cj*-CdtA and *Cj*-CdtB. Our MST data suggest aberrant binding between amino-terminal labeled *Cj*-CdtC and *Cj*-CdtA. The source of these aberrant binding data cannot be readily explained, as high-resolution structural data are not yet available for *Cj*-CDT. However crystal structures of the tripartite structures of *Hd*-CDT and *Aa*-CDT, reveal that the amino-terminus of the CdtC subunit contacts both the CdtA and CdtB subunits at the interdomain surfaces present in the assembled tripartite structures of both these toxins. From these structures, it's reasonable to predict that alterations in the interdomain spanning CdtC amino-terminal peptide might impact the stability of the assembled heterotrimer. Nonetheless, it's not clear whether the relevance of these interdomain interactions of the CdtC subunit carboxyl termini of *Hd*-CDT and *Aa*-CDT extends to *Cj*-CdtC as well. Overall, these data are consistent with those obtained using dialysis retention, where at the lowest concentrations of toxin found to be sufficient to induce arrest of cell cycle progression, mixtures of *Cj*-CdtA, *Cj*-CdtB, and *Cj*-CdtC consist primarily of non-interacting, subunit monomers.

3.3.4 Immunoprecipitation of Cj-CDT tripartite complex

To more directly assess the capacity of *Cj*-CDT subunits in solution to assemble into tripartite complexes, we examined the recovery of *Cj*-CdtA, *Cj*-CdtB, and *Cj*-CdtC from co-immunoprecipitation experiments using antibodies specifically targeting *Cj*-CdtA, *Cj*-CdtB, or *Cj*-CdtC. In experiments using 0.1 μM mixtures of *Cj*-CdtA, *Cj*-CdtB, and *Cj*-CdtC, immunoprecipitation of *Cj*-CdtB resulted in the recovery of *Cj*-CdtB, but neither *Cj*-CdtA nor *Cj*-CdtC, indicating that detectable complex had not formed (Figure 3.6A). In contrast, immunoprecipitation of *Cj*-CdtB from mixtures containing *Cj*-CdtB (at 0.1 μM) with 10-fold higher concentrations of either *Cj*-CdtA, and *Cj*-CdtC (both at 1.0 μM), revealed the detectable recovery of all three subunits (Figure 3.6A), consistent with the idea that *Cj*-CdtA and *Cj*-CdtC were recovered as part of the heterotrimeric complex with *Cj*-CdtB. Likewise, at the higher 1.0 μM subunit concentrations, *Cj*-CdtB and *Cj*-CdtC were recovered from coimmunoprecipitation experiments using an antibody targeting *Cj*-CdtA (Figure 3.6B). Finally, again at 1.0 μM subunit concentrations, *Cj*-CdtA and *Cj*-CdtB were recovered from coimmunoprecipitation experiments using an antibody targeting *Cj*-CdtC (Figure 3.6C). When taken together with the dialysis retention and MST results described above, the findings from our coimmunoprecipitation studies that heterotrimeric complexes were only recovered when using higher subunit concentrations, further support the idea that, at the lowest concentrations of toxin found to be sufficient to induce arrest of cell cycle progression, mixtures of *Cj*-

CdtA, *Cj*-CdtB, and *Cj*-CdtC consist primarily of non-interacting subunit monomers.

3.4 DISCUSSION

The studies described herein were designed to address one of the most poorly understood aspects of CDT biology, which is the relationship between CDT holotoxin structure and toxin cellular activity. Work conducted using CDTs from several mucocutaneous human pathogens have repeatedly demonstrated that all three toxin subunits, CdtA, CdtB, and CdtC, are necessary for maximal toxin cellular activity (40, 81, 141). High resolution structural data for *Aa*-CDT and *Hd*-CDT indicated that, at high toxin concentrations exceeding 100 μM, the three toxin subunits assemble into a triangle-shaped tripartite structure with each CDT subunit in direct contact with the other two subunits (107, 169). Structurally inspired mutations, designed to potentially interfere with subunit-subunit interactions, were reported to attenuate cellular activity for *Aa*-CDT (22, 169). Collectively, these results have contributed to the emergence of a widely-accepted model that CDT binds to and intoxicates sensitive host cells as an assembled tripartite toxin (61). Nonetheless, the biologically active structure of toxin that binds to the surface of sensitive host cells remains poorly understood. Here, we addressed this gap in knowledge by experimentally comparing the concentrations of *Cj*-CDT subunits required for both toxin biological activity, and the assembly of *Cj*-CdtA, *Cj*-CdtB, and *Cj*-CdtC into a heterotrimeric structure. Three independent experimental approaches revealed that solution mixtures of

Cj-CDT, at the lowest concentrations at which the toxin is biologically active, are comprised primarily of non-interacting subunit monomers. These results bring into question the existing model that *Cj*-CDT cellular intoxication is initiated through interactions of an assembled tripartite toxin, as the biologically active form required for cell surface interactions.

The binding of intracellular-acting AB exotoxins to the plasma membrane of sensitive cells is critical for defining the cell and tissue tropism for specific toxins (17). As such, a thorough understanding of the molecular determinants by which CDTs recognize and bind to the cell surface is necessary for the development of strategies to mitigate the consequences of toxin action during infection. The experimental observation that both *Cj*-CdtA and *Cj*-CdtC are required for maximal toxin cellular activity (Figure 3.1A), is consistent with the prevailing model that these two subunits together comprise the B component of *Cj*-CDT, which is responsible for the binding of the catalytically active A component, *Cj*-CdtB, to the surface of sensitive host cells. However, studies to identify the *Cj*-CDT subunits that bind to the plasma membrane of sensitive cells revealed that both *Cj*-CdtA and *Cj*-CdtC, but not *Cj*-CdtB, were able to bind independently and in the absence of the other subunits (84). Similar observations have also been made for *Aa*-CDT (19), *Ec*-CDT (98), and *Hd*-CDT (71). Taken together, these results suggest the possibility that active toxin complexes need not be preassembled to productively interact with host cells, but instead may assemble directly at the surface of host cells in a sequential manner involving initial binding of CdtA and/or CdtC as a requisite step preceding CdtB binding. In

addition, because both CdtA and CdtC are required for maximal cellular activity of all the characterized CDTs, and each subunit can independently bind to the plasma membrane of host cells, we speculate that CdtA and CdtC may contribute in disparate ways to the binding, uptake, and intracellular trafficking of CdtB. This, in fact, has been reported for *Aa*-CDT, *Ec*-CDT and *Hd*-CDT (33, 40).

The exclusive use of recombinant forms of *Cj*-CDT subunits in the work described here and from other groups (81, 84) stems from the notoriously low levels of the toxin recovered from culture supernatants of *C. jejuni*. The successful purification or concentration of secreted *Cj*-CDT from *C. jejuni* has not been reported. In our laboratory, toxin cellular activity within liquid or biphasic cultures (in which bacteria are cultivated within a thin layer of liquid medium overlaying the surface of solid agar plates) is detectable at levels equivalent to recombinant toxin at low or sub-nanomolar levels. Detection of individual subunits by immunoblot analysis is difficult, suggesting that active toxin is present in culture filtrates at subnanomolar levels.

The structure of functional *Cj*-CDT generated and released by the bacterium prior to intoxication of host cells has not been definitively resolved. One model is that the tripartite complex of the toxin is assembled prior to release into the extracellular environment, possibly following translocation of *Cj*-CdtA, *Cj*-CdtB, and *Cj*-CdtC across the inner membrane from the cytosol to the periplasmic space, which promotes protein folding and assembly of multi-component proteins (101). Indeed, cholera and pertussis toxins, both multi-subunit toxins, are believed to be secreted following assembly in the periplasm of

the pathogens that generate these toxins (21, 130). In contrast, the multi-component anthrax toxins (26) and Iota toxin from Clostridium perfringens (128) are secreted as individual subunits, which assemble only after secretion. In the case of the anthrax lethal and edema toxins, the individual components assemble on the surface of host cells. An important gap in knowledge in *Cj*-CDT biology remains the mechanisms by which the individual CDT subunits are folded, assembled, and released into the extracellular environment. Interestingly, genes homologous to those typically found in type II secretion systems, which facilitate secretion of a variety of toxins to the extracellular environment, have not been identified in the genomes of *C. jejuni*, as well as other ε-proteobacteria (59). *Cj*-CDT has been reported to be associated with outer membrane vesicles (OMVs) (90), which are generated and released by many Gram-negative bacteria (76), although the role of OMVs in the *Cj*-CDT intoxication mechanism remains to be delineated. Nonetheless, the robust biological activity of highly purified recombinant CDT subunits indicates that association with OMVs is not essential for the capacity of the toxin to bind and enter host cell in order to exert genotoxic activity.

In summary, the results of the studies described here suggest that the existing paradigm that *Cj*-CdtA, *Cj*-CdtB, and *Cj*-CdtC functionally interact with host cells as a preassembled, heterotrimeric complex should be revisited. Although the mechanism of how mixtures of *Cj*-CDT subunits interact with sensitive host cells has not been definitively established, our data prompt consideration of alternative models. In particular we speculate that individual

subunits assemble into biologically active toxin at the cell surface, probably by a mechanism facilitated by interactions with one or more cell surface receptors. However, because equilibrium binding between subunits occur at very high and perhaps non-physiological concentrations of *Cj*-CdtA, *Cj*-CdtB, and *Cj*-CdtC, we cannot rule out the possibility that the toxin does interact with cells as an assembled heterotrimeric complex, albeit at very low concentrations that are undetectable by experimental approaches used in this study. Notably, such a scenario implies that assembled *Cj*-CDT possess a much higher specific activity than has been previously experimentally determined. Additional work will be required to fully understand how *Cj*-CDT subunits collaborate to carry out cellular intoxication.

3.5 FIGURES AND TABLE

Figure 3.1

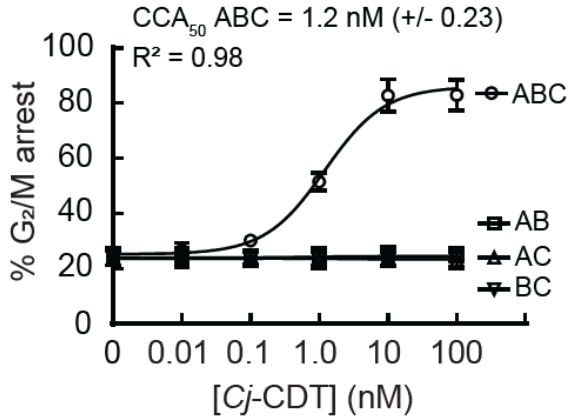

Figure 3.1: Maximal *Cj*-CDT activity requires all three subunits. HCT116 cells were incubated in McCoy's 5A medium + 10% FBS, at 37 °C, and under 5% CO_2, in the absence or presence of *Cj*-CDT (ABC), *Cj*-CdtA + *Cj*-CdtB (AB), *Cj*-CdtA + *Cj*-CdtC (AC), or *Cj*-CdtB + *Cj*-CdtC (BC) (10 pM – 100 nM). 24 h after the initial intoxication, cells were harvested and evaluated for cell cycle arrest progression. The data were combined from 3 independent biological replicates (n = 3) and represent the percentage of cells within the monolayer arrested at the G_2/M interface. Error bars represent standard deviations. The data were fit to a log[*Cj*-CDT] vs response equation on GraphPad Prism (version 8.1.2). The CCA_{50} (i.e., EC_{50}) value was determined for *Cj*-CDT (ABC) but not the binary subunit combinations. R^2 values indicate fit of the data to the regression model.

Figure 3.2

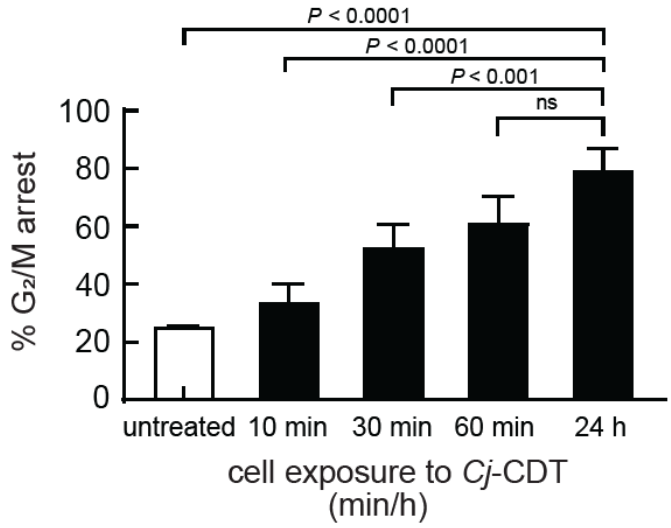

Figure 3.2: *Cj*-CDT activity is time dependent. HCT116 cells were incubated in the absence or presence of *Cj*-Cdt (ABC) (10 nM). After 10, 30, 60 min, or 24 h, cells were washed twice to remove unbound *Cj*-CDT, and further incubated at 37 °C. 24 h after the initial intoxication, cells were harvested and evaluated for cell cycle arrest progression. The data were combined from 3 independent biological replicates (n = 3) and represent the percentage of cells within the monolayer arrested at the G_2/M interface. Error bars represent standard deviations. Statistical analyses of the data were conducted using one-way Anova, followed by Tukey's multiple comparisons test. $P < 0.05$ indicates statistical significance ($\alpha = 0.05$), "ns" indicates differences were not statistically significant.

Figure 3.3

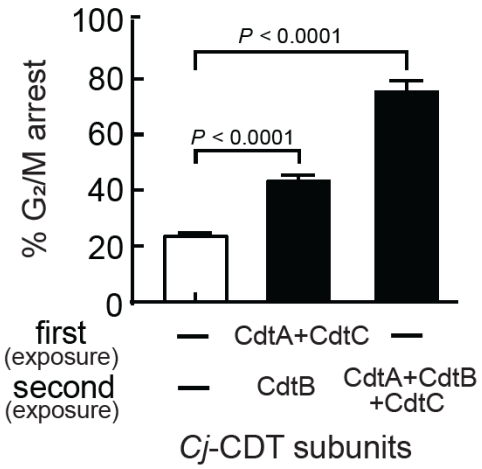

Figure 3.3: Concurrent exposure to all three *Cj*-CDT subunits is not required for toxin activity. Pre-chilled HCT116 cells were incubated on ice in the absence or presence of *Cj*-CdtA and *Cj*-CdtC subunits (100 nM) (first exposure). After 30 mins, cells were washed twice with cold medium and then further incubated at 37 °C, in the absence or presence of *Cj*-CDT or *Cj*-CdtB (second exposure). 24 h after the initial intoxication, cells were harvested and evaluated for cell cycle arrest progression. The data were combined from 3 independent biological replicates (n = 3) and represent the percentage of cells within the monolayer arrested at the G_2/M interface. Error bars represent standard deviations. Statistical analyses of the data were conducted using one-way Anova, followed by Tukey's multiple comparisons test. $P < 0.05$ indicates statistical significance ($\alpha = 0.05$).

Figure 3.4

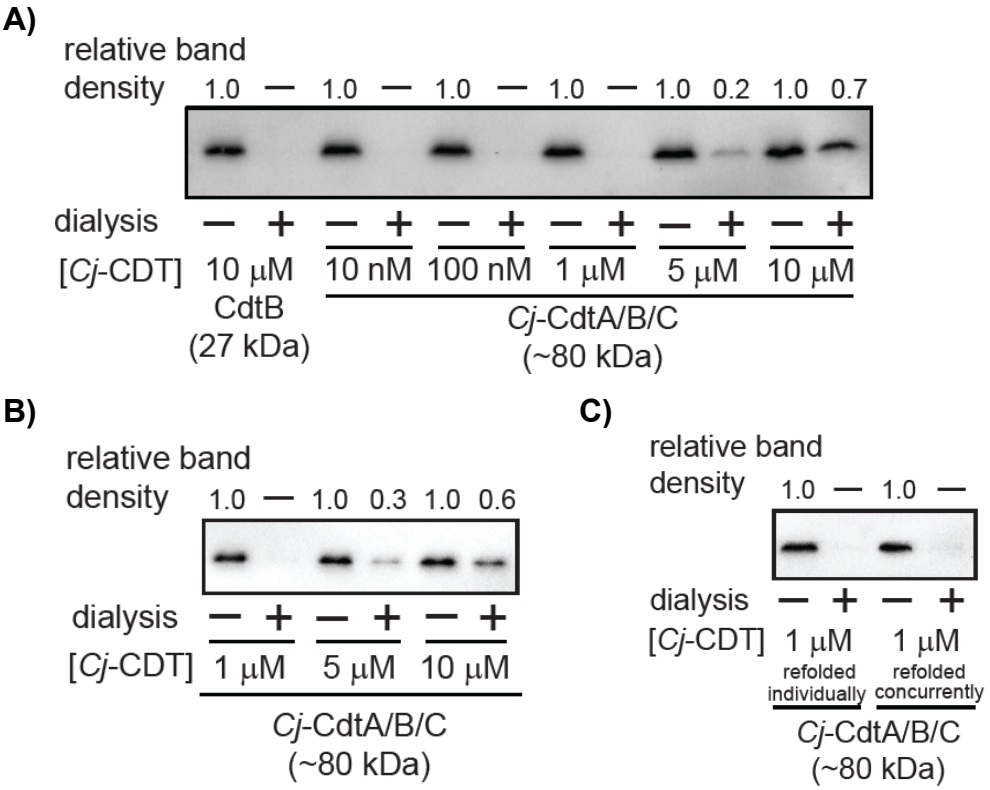

Figure 3.4: High molecular weight *Cj*-CDT tripartite structures are not captured during dialysis of biologically active mixtures of *Cj*-CDT subunits. Equimolar concentrations of *Cj*-CdtA, *Cj*-CdtB, and *Cj*-CdtC (all 10 μM), were incubated together on **(A)** ice or **(B)** at 37 °C. After 1 h, the mixture was diluted in PBS pH 7.4 (to final concentrations of 10 μM, 5 μM, 1 μM, 100 nM, and 10 nM), and then dialyzed at 37 °C using a 50 kDa molecular weight cutoff dialysis membrane at a 1:1000 sample-to-dialysis buffer volume ratio. After 48 h, the dialyzed toxin was evaluated for holotoxin complex retention using immunoblot analysis, by employing an antibody specific for *Cj*-CdtB. The ratios of the input mixtures and corresponding recovered retentates of the same concentration were independently compared for each concentration using densitometric analyses, indicated above the blot. (*i.e.*, for the 10 μM *Cj*-CdtB concentration we compared non-dialyzed input to dialysis retentate). For the 5 μM *Cj*-CdtA/B/C sample, the variance (between the 3 independent biological replicates) of the ratio between non-dialyzed sample to dialysis retentate was calculated as **(A)** ± 0.06 and **(B)** ± 0.09. For the 10 μM *Cj*-CdtA/B/C sample, the variance of the ratio between non-dialyzed sample to dialysis retentate was calculated as **(A)** ± 0.05 and **(B)** ± 0.14. **(C)** Dialysis of *Cj*-CdtA, *Cj*-CdtB, and *Cj*-CdtC subunits that were refolded concurrently together (denatured subunits refolded concurrently) was compared to mixed *Cj*-CDT subunits (denatured subunits refolded individually). Data shown are representative of 3 independent biological replicates (n =3).

Table 3.1

MST-derived *Cj*-CDT subunit binding parameters[a]				
subunit combinations[b]	**binding affinity[c]**	**first concentration of titrant yielding detectable signal above background[d]**	**saturable binding[e]**	**R^{2f}**
A + B*	>20 μM	2.0 μM	no	0.95
A* + C	0.65 (+/- 0.1) μM	0.31 μM	yes	0.95
B* + C	0.48 (+/- 0.1) μM	0.15 μM	yes	0.93

[a] NTA fluorescent dye labeled *Cj*-CdtA or *Cj*-CdtB were incubated with unlabeled *Cj*-CDT subunits (no *, 0.02 – 20 μM) and evaluated for binding using MST

[b] A = *Cj*-CdtA, B = *Cj*-CdtB, C = *Cj*-CdtC, * = NTA labeled subunit

[c] binding affinity derived from a nonlinear regression model fitted to an equation, describing dose (log (*Cj*-CDT)) vs response (fraction bound)

[d] concentrations of titrant at which MST signals above background were first observed

[e] observation of a clear saturated binding curve for the indicated subunit interaction combination

[f] R^2 values indicate fit of the data to the regression model

Figure 3.5

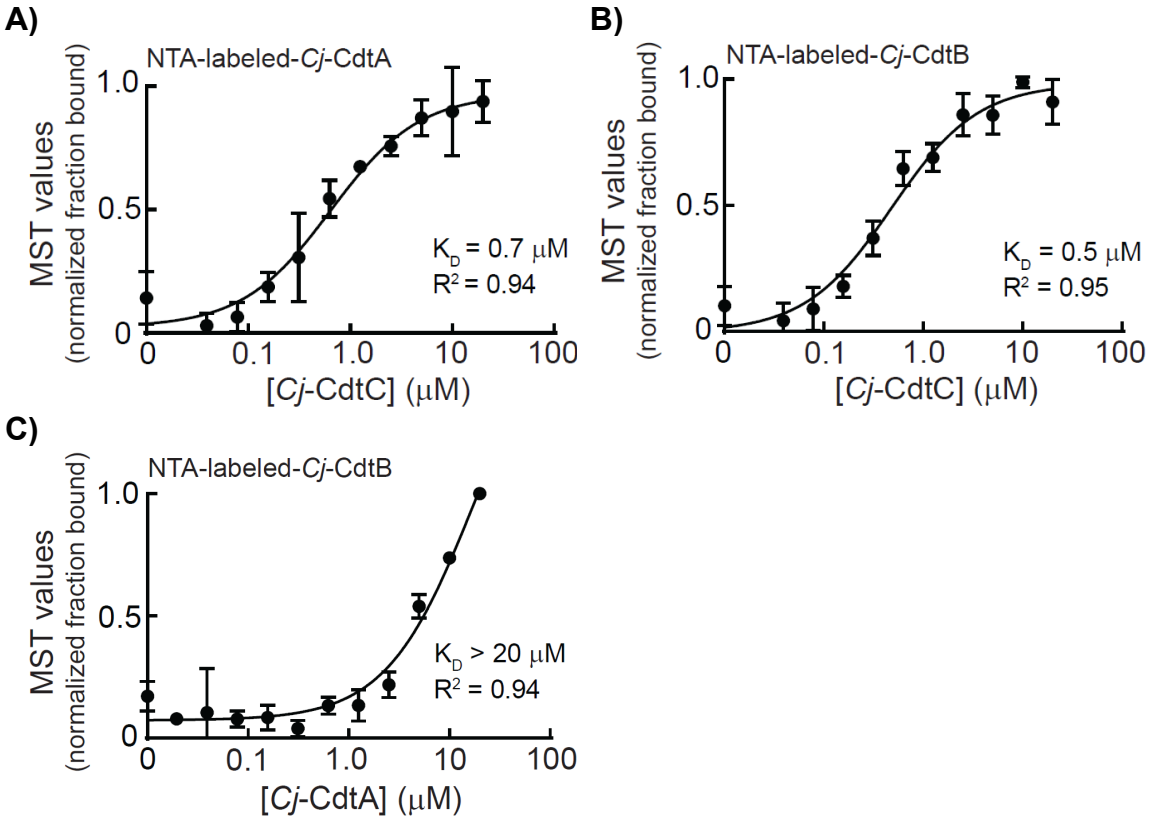

Figure 3.5: Microscale thermophoresis analysis of *Cj*-CdtA, *Cj*-CdtB, and *Cj*-CdtC subunit interactions. NTA fluorescent labeled *Cj*-CdtA or *Cj*-CdtB subunits were incubated at 37 °C with the indicated unlabeled *Cj*-CDT subunit(s) (with polyhistidine tags removed) as follows: **(A)** NTA-labeled-*Cj*-CdtA (0.1 μM) + unlabeled-*Cj*-CdtC (0.04 – 20 μM), **(B)** NTA-labeled-*Cj*-CdtB (0.1 μM) + unlabeled-*Cj*-CdtC (0.04 – 20 μM), and **(C)** NTA-labeled-*Cj*-CdtB (0.1 μM) + unlabeled-*Cj*-CdtA (0.02 – 20 μM), as indicated on the graphs. After 1 h, subunits were evaluated for binding at 37 °C using microscale thermophoresis. The data on the graph were combined from 3 independent biological replicates (n = 3). The data were fit to a log[*Cj*-CDT] vs response equation on GraphPad Prism 8.1.2. The K_D was derived from each binding curve. R^2 values indicate fit of the data to the regression model.

Figure 3.6

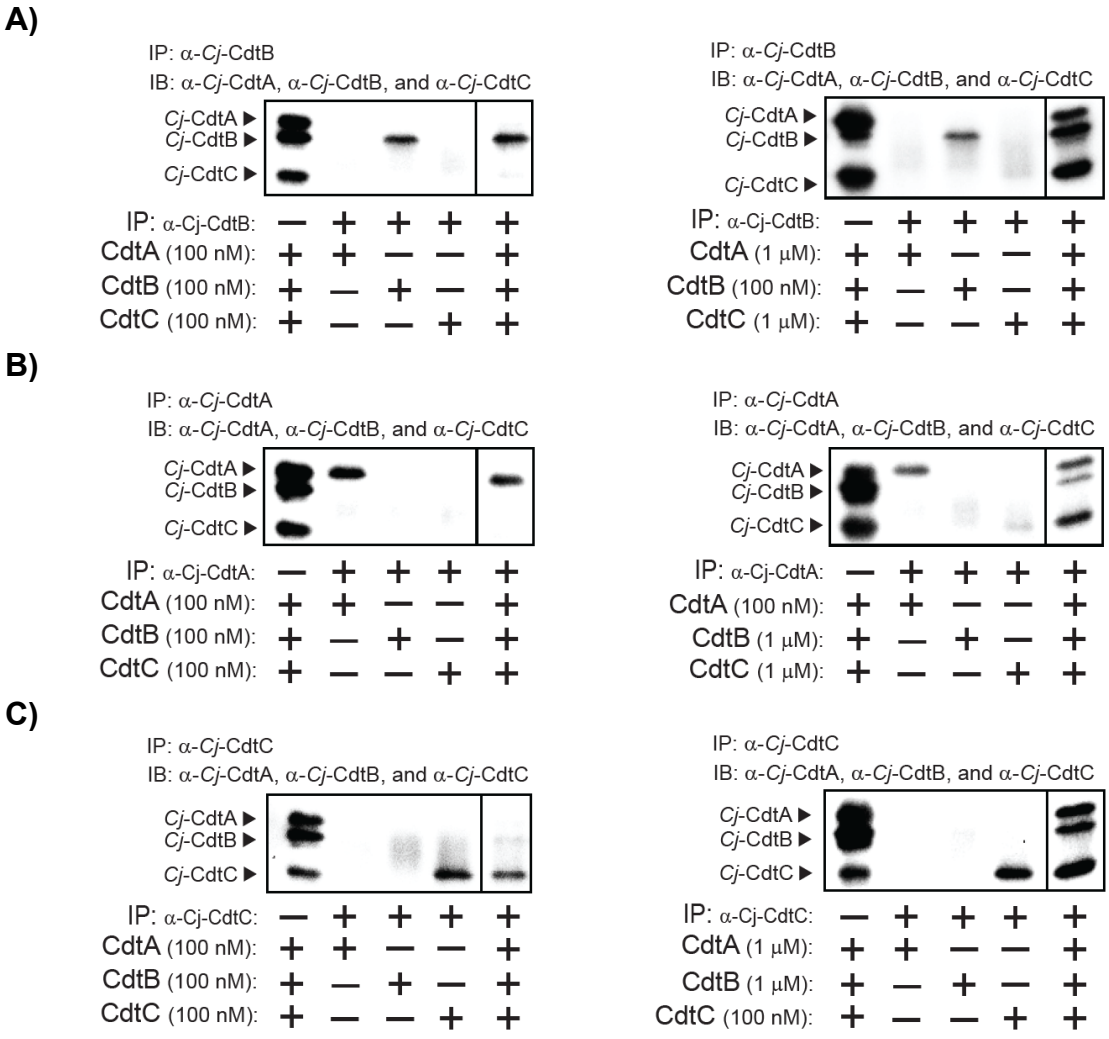
A)
IP: α-Cj-CdtB
IB: α-Cj-CdtA, α-Cj-CdtB, and α-Cj-CdtC
Cj-CdtA ▶
Cj-CdtB ▶
Cj-CdtC ▶
IP: α-Cj-CdtB: — + + + +
CdtA (100 nM): + + — — +
CdtB (100 nM): + — + — +
CdtC (100 nM): + — — + +
IP: α-Cj-CdtB
IB: α-Cj-CdtA, α-Cj-CdtB, and α-Cj-CdtC
Cj-CdtA ▶
Cj-CdtB ▶
Cj-CdtC ▶
IP: α-Cj-CdtB: — + + + +
CdtA (1 μM): + + — — +
CdtB (100 nM): + — + — +
CdtC (1 μM): + — — + +
B)
IP: α-Cj-CdtA
IB: α-Cj-CdtA, α-Cj-CdtB, and α-Cj-CdtC
Cj-CdtA ▶
Cj-CdtB ▶
Cj-CdtC ▶
IP: α-Cj-CdtA: — + + + +
CdtA (100 nM): + + — — +
CdtB (100 nM): + — + — +
CdtC (100 nM): + — — + +
IP: α-Cj-CdtA
IB: α-Cj-CdtA, α-Cj-CdtB, and α-Cj-CdtC
Cj-CdtA ▶
Cj-CdtB ▶
Cj-CdtC ▶
IP: α-Cj-CdtA: — + + + +
CdtA (100 nM): + + — — +
CdtB (1 μM): + — + — +
CdtC (1 μM): + — — + +
C)
IP: α-Cj-CdtC
IB: α-Cj-CdtA, α-Cj-CdtB, and α-Cj-CdtC
Cj-CdtA ▶
Cj-CdtB ▶
Cj-CdtC ▶
IP: α-Cj-CdtC: — + + + +
CdtA (100 nM): + + — — +
CdtB (100 nM): + — + — +
CdtC (100 nM): + — — + +
IP: α-Cj-CdtC
IB: α-Cj-CdtA, α-Cj-CdtB, and α-Cj-CdtC
Cj-CdtA ▶
Cj-CdtB ▶
Cj-CdtC ▶
IP: α-Cj-CdtC: — + + + +
CdtA (1 μM): + + — — +
CdtB (1 μM): + — + — +
CdtC (100 nM): + — — + +

Figure 3.6 (cont.)

Figure 3.6: Co-immunoprecipitation of *Cj*-CdtA, *Cj*-CdtB, and *Cj*-CdtC. Immunoprecipitation (IP) was conducted as follows: **(A)** Mixtures of purified *Cj*-CdtA, *Cj*-CdtB, and *Cj*-CdtC (at 100 nM) (panel on the left), or, mixtures of purified *Cj*-CdtB and *Cj*-CdtC (at 1 μM) and *Cj*-CdtA (at 100 nM) were incubated together on ice (panel on the right). After 1h, the mixtures were incubated with α-*Cj*-CdtA antibody bound protein A Dynabeads at 4 °C. The next day, the beads were washed, and the bound subunit(s) was/were then eluted and evaluated using immunoblot (IB) analysis, probing with antibodies specific for *Cj*-CdtA, *Cj*-CdtB, or *Cj*-CdtC subunit. This process was repeated using **(B)** purified *Cj*-CdtA, *Cj*-CdtB, and *Cj*-CdtC (at 100 nM) or, mixtures of purified *Cj*-CdtA and *Cj*-CdtC (at 1 μM) and *Cj*-CdtB (at 100 nM), incubated with α-*Cj*-CdtB antibody bound protein A Dynabeads at 4 °C. Finally, **(C)** purified *Cj*-CdtA, *Cj*-CdtB, and *Cj*-CdtC (at 100 nM) or, mixtures of purified *Cj*-CdtA and *Cj*-CdtB (at 1 μM) and *Cj*-CdtC (at 100 nM), incubated with α-*Cj*-CdtC antibody bound to protein A Dynabeads at 4 °C. Each immunoblot presents data, at identical exposure times, from a single experiment representative of results collected from 3 independent biological replicates (n = 3). The dividing line in each image indicates data that were not directly relevant to the figure and were therefore spliced out.

CHAPTER 4: UNDERSTANDING CDT ACTIVITY AS A WEAKLY ASSOCIATED HETEROTRIMERIC COMPLEX

4.1 INTRODUCTION

In this chapter, we delve into further preliminary work related to our studies on subunit interaction and toxin activity. This encompasses experiments that were excluded from our publications, along with endeavors aimed at addressing new gaps in knowledge. Our exploration into understanding the significance of subunit interactions for toxin activity suggests a need to reevaluate the existing model of *Cj*-CDT subunits interacting with the host as a preassembled, heterotrimeric complex. A significant gap in knowledge identified in the previous chapter is how the *Cj*-CDT subunits could operate independently of a holotoxin complex in solution. Drawing from our understanding of bacterial toxins, we propose two potential models to explain this phenomenon.

First of all, the *Cj*-CDT subunits might assemble into a functional heterotrimeric complex at the host cell surface. This model suggests that subunits bypass the weak assembly nature of the holotoxin in solution by binding to a host cell receptor, utilizing receptor subunit interactions to drive complex formation, potentially with higher affinity akin to many pore-forming toxins (85). Within this chapter, we detail studies evaluating the ability of *Cj*-CDT to assemble into an active toxin complex at the host cell surface. Our findings indicate that the *Cj*-CDT subunit could indeed have the potential to form an active complex at the host cell surface.

In the second model, we propose that the toxin interacts with cells as an assembled heterotrimeric complex, albeit at concentrations so low they are undetectable by experimental approaches used in this study. This suggests that assembled *Cj*-CDT may possess a much higher specific activity than previously determined experimentally, challenging earlier perceptions. Notably, much of the previous work done on *Cj*-Cdts has demonstrated cellular activity in the mid nanomolar range. An important point is that it is difficult to compare specific activities between different species of CDTs as cell types have a strong impact on activities. However the general observation is that compared to other species of CDT, the specific activity of *Cj*-Cdts are much higher than *Ec* and *Aa*-CDTs, but lower than that of *Hd*-Cdts (50). To address this model, we conducted several experiments following up on important results observed in the previous chapter, assessing the relationship between subunit complex formation and toxin activity. In addition to the higher specific activity model, we propose that the *Cj*-CDT toxin still behaves as a weakly assembled holotoxin complex. While initially seeming counterintuitive from the pathogen's perspective, this strategy may allow the pathogen to limit toxin activity on host cells. Though not directly addressed, we discuss the plausibility of this idea.

Regarding additional incomplete and future work, we include preliminary but relevant findings that could not be incorporated into the paper but contribute to understanding cytolethal distending toxin intracellular trafficking, structure-function relationships, and host cell interaction.

4.2 MATERIALS AND METHODS

Mammalian Cell Culture. HCT116 (Human colon cancer epithelial cell line, male) cells were maintained in McCoy's 5A (modified) medium supplemented with a 10% final concentration of fetal bovine serum (FBS). HeLa (Human adenocarcinoma epithelial cell line) cells were maintained in DMEM supplemented with a 10% final concentration of FBS. Cell lines were tested for mycoplasma contamination using MycoAlert Mycoplasma Detection Kit. All cells were maintained at 37°C in a humidified atmosphere under CO_2 (5%).

Bacterial strains. Escherichia coli BL21 used for protein expression and purification were grown as previously described. *Campylobacter jejuni* strains containing *cdt* genes (81-176), cytolethal distending toxin mutants (DS104), and DS104 mutants complemented with *cdt* genes in trans (DS104(pRAM33), were given to us by the Guerry lab (68). *Campylobacter jejuni* strains were streaked on Mueller Hinton plates supplemented with Iron(II) Sulfate Heptahydrate, Sodium Bisulfite, and Sodium Pyruvate (0.25 mg/mL final concentration) and grown in a tri-gas incubator at 42 °C, with 10% CO_2 and 5% O_2. After 2 days, plates containing *C. jejuni* were then used for further experiments.

Cj-CDT expression and purification. Recombinant forms of *Cj*-CdtA, *Cj*-CdtB, *Cj*-CdtC were generated and purified as previously described (50). Subunit purity was evaluated using sodium dodecyl sulfate polyacrylamide gel electrophoresis (SDS-PAGE) (Biorad, Hercules, CA) followed by Coomassie Brilliant Blue staining (Sigma, St. Louis, MO), and quantified using the Pierce BCA protein assay (Thermo, Rockford, IL).

Removal of polyhistidine fusion peptides. His-tagged recombinant subunits were incubated at 21 ˚C with biotinylated thrombin (Novagen, Billerica, MA). After 20–24 h, biotinylated thrombin and cleaved polyhistidine peptides were removed using Pierce streptavidin agarose beads (ThermoFisher, Waltham, MA) and TALON Metal Affinity Resin (TaKaRa, Mountain View, CA), respectively. The beads and resin were removed using Spin-X centrifuge tube filters (pore size, 0.22 μm; Corning Costar, NY). *Cj*-CDT subunits free of polyhistidine fusion peptides were quantified using the Pierce BCA assay. Polyhistidine removal was confirmed using SDS-PAGE and Coomassie Brilliant Blue staining.

Cell cycle phase determination of recombinant Cj, Ec, and Hd-CDTs. Cj-CDT-dependent arrest of cell cycle progression at the G2/M interface was assessed using flow cytometry (FACSymphony A1, BD Biosciences, Franklin Lakes, NJ) as previously described (50, 62). Briefly, the indicated cell lines were seeded (approximately 0.04-0.05 X 10^6 cells per well) on 24-well culture plates and incubated at 37 °C and under 5% CO_2. For *Cj*-CDT warm or cold pulse intoxications, after 24-36 h the cells were incubated on ice and under atmospheric conditions (cold pulse) or kept at 37 °C and under 5% (warm pulse). After 30 mins, media was removed and cells were incubated with cold PBS (cold pulse) or warm PBS (warm pulse) containing CDT or in the absence of CDT at the combinations and concentrations as indicated in the figures, on ice and under atmospheric conditions. After 1 h, PBS with or without toxin was removed and replaced with complete medium and incubated at 37 °C and under 5% CO_2. After

24, cell culture medium was removed and cells were washed twice with PBS. After 24 h, cell culture medium containing CDT or PBS, as the carrier control, was removed and cells were washed twice with PBS. Cells were then detached from the cell culture plate by trypsinization at 37 °C. After detachment of cells was observed, 10% final concentration of FBS in PBS was added to inhibit trypsin activity. Cells were then pelleted (500 × g, 5 min) and resuspended by adding ice cold 70% ethanol dropwise with constant vortexing. Cells were incubated at -20 °C in the presence of 70% ethanol. After a minimum of 1 h, cells were pelleted (800 × g, 5 min) and resuspended in PBS pH. After 30 min at room temperature, cells were pelleted and resuspended in staining solution (300 μL per sample; containing 0.1% Triton X-100, 1 mg/mL RNase A, and 10 μg/mL propidium iodide in PBS). After 1 h at room temperature, cells were analyzed using a BD FACS Canto II flow cytometry analyzer. Flow cytometry data were processed using FCS Express software (De Novo Software) and statistics performed using GraphPad Prism 7 (GraphPad Software). For *Ec*-CDT and *Hd*-CDT intoxication conditions, after 24-36 h the cells were incubated at 37 °C and under 5% CO_2 in complete medium containing CDT at the indicated concentrations, or were incubated with PBS in place of CDT, as indicated in the figure legends. All individually refolded *Ec* and *Hd*-CDT subunit combinations were mixed together at a final concentration of 10 μM and incubated on ice for 1 h prior to dilution and subsequent intoxication. After 48 h, cell culture medium containing CDT or PBS, as the carrier control, was removed and cells were

washed twice with. Cells were then detached and analyzed for cell cycle arrest as previously mentioned.

Krypton staining and immunoblotting. Following SDS-PAGE, resolved proteins were either stained with Krypton Protein Stain or transferred to PVDF membranes (Millipore Sigma, Burlington, MA) using a wet/tank blotting system (Bio-Rad). Membranes were blocked with 5% bovine serum albumin (Sigma-Aldrich, St. Louis, MO) in TBS-T (0.1% Tween-20 in TBS pH 7.4, Fisher, Fair Lawn, NJ) and incubated with primary antibodies. Primary antibodies specific for each *Cj*-CDT subunit were generated commercially against peptide sequences unique to *Cj*-CdtA, *Cj*-CdtB, and *Cj*-CdtC (YenZme, San Francisco, CA) as follows: antibodies specifically targeting the *Cj*-CdtA-specific sequence 255-CPFTAKPLYRQGEVR-268, the *Cj*-CdtB-specific sequence 185-CDFNRDPSTITSTVDRELANR-204, and the *Cj*-CdtC-specific sequence 44-CFRDTSKDPIDQNWNIK-59. Membranes were then incubated with anti-rabbit IgG biotinylated antibodies (Cell Signaling, Danvers, MA), and subsequently with anti-biotin HRP-linked antibodies (Cell Signaling, Danvers, MA). Immunoblots were imaged using the ChemiDoc system (XRS+, Bio-Rad, Hercules, CA) following exposure to a 1:5 mixture of SuperSignal West Femto Maximum Sensitivity: Pico Plus Chemiluminescent Substrates (Thermo, Rockford, IL). Immunoblot densitometry analyses were performed using Image Lab software (Bio-Rad, Version 6.0).

Microscale thermophoresis analysis (MST). Polyhistidine-tagged *Cj*-CDT, *Ec*-CDT, and *Hd*-CDT subunits, which had been labeled with NTA – Atto 647 N

dye (NanoTemper, München, Germany), were incubated at 37 °C and with non-polyhistidine-tagged, non-labeled, non-cognate subunits. After 1 h, samples were loaded into capillary tubes (Monolith NT .115 Series capillaries, NanoTemper, München, Germany) and placed into the microscale thermophoresis instrument (Monolith NT .115, software version 1.2.1, NanoTemper, München, Germany). Samples were allowed to equilibrate, in the instrument, for an additional 15 min at 37 °C before collecting data. All readings were taken using the MO.Control program (version 1.6.1, NanoTemper, München, Germany) using red excitation (650 nm, 30-100% power), and medium MST power (40%). MST values were determined, at the 3 second temperature jump. Data were normalized to the fraction of complexed molecules (FB) as previously described (173). MST values were fit to a log [*Cj*-CDT subunit] vs response equation to generate binding curves (GraphPad Prism version 8.1.2).

Alphafold modeling of Cj-CDT subunit interactions. Alphafold models for all the *Cj*-CDT subunit combinations included in this thesis were generated using ChimeraX version 1.4 using the command Alphafold function. Briefly, amino acid sequences for the different CDT subunits that we wanted to model were imputed into the ChimeraX program in a fasta format under the tools:Alphafold function and run through the prediction program to generate our predicted models (102).

Cj-CDT size exclusion chromatography. Concurrently refolded Cj-CDT subunits or *Cj*-CdtB subunit alone was loaded onto a Bio-Gel P-60 gel filtration column (Bio-rad, Hercules, CA) that was previously equilibrated in PBS pH 7.4. Fractions (1 mL) were collected and protein content of each fraction was

analyzed by running on an SDS-PAGE gel followed immunoblot analysis probing for each subunit as previously described.

Paraformaldehyde crosslinking evaluation of Cj-CDT subunit interactions. *Cj*-CDT subunits were incubated at the indicated subunit concentrations and combinations on ice. After 1 h, samples were crosslinked at 37 °C with 1% paraformaldehyde. After 10 mins, samples with quenched with 500 mM glycine. After 5 mins, quenched, crosslinked *Cj*-CDT subunits were either boiled or un-boiled at 100 °C for 10 mins. Samples were then run on a 12% SDS-PAGE gel and toxin subunits were evaluated either using Krypton Protein Stain or immunoblotting with the indicated primary antibodies as previously described.

Cj-CDT subunit sequential exposure intoxication experiments. *Cj*-CDT-dependent arrest of cell cycle progression at the G_2/M interface was assessed using flow cytometry (FACSymphony A1, BD Biosciences, Franklin Lakes, NJ) as previously described (50, 62). For all sequential exposure experiments, treatments were performed with Cj-CDT subunits that had the polyhistidine tag removed. To evaluate *Cj*-CDT subunit sequential exposure activity, HCT116 cells lines were seeded (approximately 0.04-0.05 X 10^6 cells per well) on 24-well culture plates and incubated at 37 °C and under 5% CO_2. After 24-48 h, cells were chilled on ice at atmospheric conditions. After 30 mins, cells were exposed to the indicated *Cj*-CDT toxin combinations, as indicated in the figures, in cold PBS pH 7.4 or cold media, on ice, and under atmospheric conditions. After 30 mins, as indicated in the figures, toxin containing PBS or media was removed and cells were either washed twice with cold PBS or media, or unwashed. Cells

were then exposed to the second set of Cj-CDT toxin combinations, as indicated in the figures, in cold PBS or cold media, on ice, and under atmospheric conditions. After another 30 mins, as indicated in the figures, toxin containing PBS was washed once with cold PBS or for the media condition was unwashed. For cells that were subjected to a third set of exposures, cells were exposed to the third set of Cj-CDT subunits in cold media, on ice, and under atmospheric conditions for 30 mins before the cells were washed with media. After the final wash step or incubation step, cells were incubated with complete medium at 37 °C and under 5% CO_2. After 24, cell culture medium was removed, and cells were washed twice with PBS. Cells were then detached from the cell culture plate by trypsinization at 37 ° C, harvested, and analyzed in the same manner as previous cell cycle experiments described above.

Cj-CDT subunit dialysis activity experiments. Purified *Cj*-CDT subunits, individually refolded and concurrently refolded, were incubated together on ice at a final concentration of 10 μM. After 1 h, the mixtures were diluted to a final concentration of 1 μM and either incubated at 37 °C or dialyzed at 37 °C against PBS pH 7.4 (1:1000 sample to buffer ratio), using Micro Float-A-Lyzer Dialysis Devices with a Molecular weight cutoff (MWCO) of 50 kDa (Spectrum Labs, CA). After 48 h, samples were harvested and evaluated for retention of *Cj*-CdtB using immunoblot analyses (normalized to 10 nM) and cellular activity under warm pulse conditions. Briefly, HCT116 cells were seeded (approximately 0.04-0.05 X 10^6 cells per well) on 24-well culture plates and incubated at 37 °C and under 5% CO_2. After 24-36 h, media was removed and cells were incubated with PBS

containing recombinant CDT, either dialyzed or un-dialyzed, or in the absence of CDT at the dilution factors indicated in the figures, under atmospheric conditions. After 1 h, PBS with or without toxin was removed and replaced with complete medium and incubated at 37 °C and under 5% CO_2. After 24, cell culture medium was removed, and cells were washed twice with PBS. Cells were then detached from the cell culture plate by trypsinization at 37 ° C, harvested, and analyzed in the same manner as previous cell cycle experiments described above.

Campylobacter jejuni native toxin expression quantification and biological activity assays. C. jejuni (81-176), (DS104), and (DS104(pRAM33)) strains were streaked onto MH plates as previously described. After the formation of colonies, an individual colony was selected and incubated in 10 mL of Mueller Hinton broth in a tri-gas incubator at 42 °C, with 10% CO_2 and 5% O_2, shaking at 120 rpm. After an overnight incubation, the cultures were allowed to reach an OD ~ 0.6, culture optical density was measured at 600 nm (Genesis 20 Spectrophotometer, Thermo, Rockford, IL), and then was spun at 8,000 x g for 10 mins to pellet the bacteria. Culture supernatant, devoid of bacteria, was collected and filtered through a 0.22 μm filter (Millex-MP, Millipore, Carrigtwohill. IRL). Culture filtrate was then immunoblotted with antibodies specific to all three *Cj*-CDT subunits, as previously described. Alternatively, culture filtrate was used to intoxicate host cells to evaluate cellular activity. *Cj*-CDT-dependent and *C. jejuni* culture filtrate arrest of cell cycle progression at the G_2/M interface was assessed using flow cytometry (FACSymphony A1, BD Biosciences, Franklin Lakes, NJ) as previously described (50, 62). To evaluate *C. jejuni* culture filtrate activity,

HCT116 cells were seeded (approximately 0.04-0.05 X 10^6 cells per well) on 24-well culture plates and incubated at 37 °C and under 5% CO_2. After 24-36 h, media was removed and cells were incubated with PBS pH 7.4 containing recombinant CDT, *C. jejuni* culture filtrate, or in the absence of CDT at the concentrations or dilutions indicated in the figures, at 37 °C under atmospheric conditions. After 1 h, PBS with or without toxin was removed and replaced with complete medium and incubated at 37 °C and under 5% CO_2. After 24, cell culture medium was removed, and cells were washed twice with PBS. Cells were then detached from the cell culture plate by trypsinization at 37 ° C, harvested, and analyzed in the same manner as previous cell cycle experiments described above.

Campylobacter jejuni infection studies. C. jejuni (81-176), (DS104), and (DS104(pRAM33)) strains were streaked onto MH plates as previously described. After the formation of colonies, an individual colony was selected and incubated in 10 mL of Mueller Hinton broth in a tri-gas incubator at 42 °C, with 10% CO_2 and 5% O_2, shaking at 120 rpm. After an overnight incubation, the cultures were allowed to reach an OD ~ 0.6, culture optical density was measured at 600 nm (Genesis 20 Spectrophotometer, Thermo, Rockford, IL). *C. jejuni* density was calculated previously at 1 x 10^{10} CFU/mL per 1 OD. HCT116 that were seeded (approximately 0.04-0.05 X 10^6 cells per well) on 24-well culture plates and incubated at 37 °C and under 5% CO_2 for 24-48 h, were then counted using a hemocytometer and infected with the indicated multiplicity of infection (MOI) of *C. jejuni* or not infected, in complete medium at 37 °C and

under 5% CO_2. After 24, cell culture medium was removed, and cells were washed twice with PBS pH 7.4. Cells were then detached from the cell culture plate by trypsinization at 37 ° C, harvested, and analyzed in the same manner as previous cell cycle experiments described above.

Cj-CDT receptor crosslinking and identification. Epitope tagged *Cj*-CdtC-HA subunit were treated with SATA reagent (Thermo, Rockford, IL) to add protected sulfhydryl groups onto the subunit at a 10 x molar access of SATA to *Cj*-CDT. SATA modified proteins were deacetylated using 0.5 M hydroxylamine and desalted to purify the sulfhydryl-modified protein from the hydroxylamine. Immediately after desalting, our bifunctional crosslinker KMUH (Thermo, Rockford, IL) was added at a 10 x molar excess to our sulfhydryl modified protein. *Cj*-CdtC-HA subunits conjugated to our KMUH crosslinker was then dialyzed to remove un-bound crosslinker, quantified using Coomassie Plus (Bradford) assay (Thermo, Rockford, IL), and analyzed by running the protein-crosslinker on a 12% SDS-PAGE gel followed by Coomassie staining. In order to prepare cells for *Cj*-CdtC-HA subunit-receptor crosslinking, HCT116 cells were treated with 15 mM sodium periodate on ice, in the dark. After 30 mins of sodium periodate treatment, cells were incubated with 10 μM *Cj*-CdtC-HA-KMUH on ice. After 2 h, unbound *Cj*-CDT was removed and cells detached using an enzyme-free, PBS-based, cell dissociation buffer (Gibco, Grand Island, NY) incubated at 37 °C. Membrane proteins containing crosslinked *Cj*-CdtC-HA subunits were isolated from detached cells using the Mem-PER Plus membrane protein extraction kit (Thermo, Rockford, IL). *Cj*-CdtC-HA subunits crosslinked to

membrane proteins were separated from un-crosslinked membrane proteins using immunoprecipitation with an HA-tag rabbit monoclonal antibody conjugated to magnetic beads (Cell Signaling, Danvers, MA). Purified *Cj*-CdtC-HA crosslinked to host cell receptor proteins were then submitted to mass spectrometry (Mass Spectrometry Lab, Univ. Illinois, Urbana, IL) for receptor identification.

Statistical Analyses. Each experiment was performed at least three independent times, signified as n = 3, unless otherwise indicated. Error bars represent standard deviations. Statistical analyses were performed using GraphPad Prism 8.1.2. Dose response curves were fit to a log (agonist) vs response (three parameters) equation. R2 values indicate fit of the data to the regression model. Analysis of statistical differences was performed using one-way ANOVA followed by the Tukey's post-hoc test. Statistical significance ($P < 0.05$) was determined at $\alpha = 0.05$.

4.3 RESULTS

4.3.1 *Cj*-CDT subunit interaction evaluation through Alphafold, size exclusion chromatography, and paraformaldehyde crosslinking

Our previous findings suggest that the Cj-CDT subunits might not assemble into a functional heterotrimeric complex before interacting with host cells, challenging the previous assumption that Cj-CDT complex formation is crucial for toxin activity. To investigate this further, we conducted additional studies including Alphafold modeling, gel filtration, and paraformaldehyde complex crosslinking. First, to better understand how the *Cj*-CDT subunits might

be interacting with one another to form a heterotrimeric complex, we use Alphafold to predict the protein structures of the different *Cj*-CDT subunit interactions. We confirmed the accuracy of Alphafold in predicting CDT structures by comparing an Alphafold prediction of the *Hd*-CDT heterotrimeric complex to that of the known crystal structure of *Hd*-CDT, yielding a root-mean-square-deviation, a measure of the average distance between the atoms of the superimposed molecules, of 0.21 angstroms (Figure 4.1A). Using Alphafold we modeled the Cj-CDT heterotrimer (*Cj*-CdtA + *Cj*-CdtB + *Cj*-CdtC) (Figure 4.1B), heterodimer (*Cj*-CdtA + *Cj*-CdtB, *Cj*-CdtA + *Cj*-CdtC, and *Cj*-CdtB + *Cj*-CdtC) (Figure 4.2A-C), and homodimers (*Cj*-CdtA + *Cj*-CdtA, *Cj*-CdtB + *Cj*-CdtB, and *Cj*-CdtC + *Cj*-CdtC) (Figure 4.3A-C). The Alphafold predictions suggested that the *Cj*-Cdt subunits were able to interact with each other to form heterodimer and heterotrimer complexes, with high confidence. In addition, only the *Cj*-CdtC subunit was predicted to interact with itself to form a homodimer complex with high confidence (Figure 4.3C), implying that Alphafold did not predict interactions between the *Cj*-CdtA or *Cj*-CdtB homodimers. The *Cj*-CdtC homodimer structural prediction is interesting because it suggests the possibility that *Cj*-CdtC homodimers may facilitate the association of *Cj*-CdtA or *Cj*-CdtB subunits, possibly by providing a stable intermediate complex preceding heterotrimer formation. To test this idea, we used Alphafold to model *Cj*-CdtC homodimer interactions with either *Cj*-CdtA (*Cj*-CdtC + *Cj*-CdtC + *Cj*-CdtA) (Figure 4.4A) or *Cj*-CdtB (*Cj*-CdtC + *Cj*-CdtC + *Cj*-CdtB) (Figure 4.4B). Interestingly, Alphafold predicted that the *Cj*-CdtC homodimer could interact with the *Cj*-CdtB subunit,

suggesting that *Cj*-CdtC + *Cj*-CdtC + *Cj*-CdtB complex, involving the *Cj*-CdtC homodimer could form during subunit interaction and complex assembly.

It has been previously shown that higher molecular weight *Cj*-CDT complexes could be isolated using size exclusion chromatography (81). To verify that our toxin behaved similarly to previous findings, we conducted size exclusion chromatography on assembled *Cj*-CDT holotoxin and observed the formation of higher molecular weight complexes (Figure 4.5). While other groups have seen the capacity of the CDTs to form a higher molecular weight complex, there is a lack of association between complex formation and toxin activity. Therefore, to further assess the significance of the predicted tripartite *Cj*-CDT structure for toxin activity, we determined the concentrations at which mixtures of *Cj*-CdtA, *Cj*-CdtB, and *Cj*-CdtC could be crosslinked using paraformaldehyde. In experiments using 0.5 μM of *Cj*-CdtA and increasing concentrations of equimolar *Cj*-CdtB and *Cj*-CdtC, we saw formation of high molecular weight complexes (~100 kDa) only when incubated with 5 and 10 μM of *Cj*-CdtB and *Cj*-CdtC (Figure 4.6A,B). In addition, we only detected the formation of heterodimeric complexes at subunit concentrations above 1 μM (Figure 4.7A) and only the formation of a *Cj*-CdtC homodimer complex at concentrations above 1 μM (Figure 4.7B). When taken together with our dialysis retention, MST, and co-immunoprecipitation results as described earlier, our findings further support the idea that, at the lowest concentrations of toxin sufficient to induce arrest of cell cycle progression, mixtures of *Cj*-CdtA, *Cj*-CdtB, and *Cj*-CdtC primarily consist of noninteracting subunit monomers.

4.3.2 MST reveals low affinity interactions in different species of CDTs

In the previous chapter, microscale thermophoresis (MST) studies revealed low binding affinities for the individual *Cj*-CDT subunits in the formation of heterodimer, notably contrasting with the concentrations requisite for cellular toxin activity. Furthermore, the retrieval of the heterotrimer complex via dialysis retention and immunoprecipitation exhibited similarly low affinities. To provide a more quantitative assessment of Cj-CDT heterotrimeric complex formation, we utilized MST to probe heterotrimer formation. Similar to the binary *Cj*-CDT subunit interactions, *Cj*-CdtA + *Cj*-CdtB + *Cj*-CdtC subunit interaction occurred with a very low affinity, as evidenced by MST measurements yielding a non-saturable, non-sigmoidal binding curve with an apparent KD of >20 μM (Figure 4.8). Notably, the first concentration of titrate yielding detectable signal above background in our MST binding curve was 10 μM, implying even lower affinity of *Cj*-CDT heterotrimer formation compared to heterodimer pairs. These data are consistent with the idea that *Cj*-CDT heterotrimer complex formation occurs with low affinity. However, given that MST gauges the change in movement of a labeled subunit to determine binding, a notable limitation arises regarding its use in assessing heterotrimeric complexes, as it cannot distinguish between heterodimeric and heterotrimeric interactions. Given the propensity of *Cj*-CDT subunits to form dimeric complexes, we believe that the formation of various subunit complexes may impede our measurement of heterotrimeric complex formation via MST.

All preceding data collectively suggest a need to reassess the model of *Cj*-CdtA, Cj-CdtB, and Cj-CdtC interacting functionally with host cells as a preassembled, heterotrimeric complex. However, it remains uncertain whether this behavior is unique to *Cj*-CDT or if other CDTs exhibit similar characteristics. To address this gap, we conducted MST measurements with *Ec*-CDT and *Hd*-CDT subunits. Consistent with prior findings (62), our studies revealed that both *Ec*-CDT and *Hd*-CDT-dependent arrest of cell cycle progression occurs in a dose-dependent manner (Figure 4.9A,B), with *Ec*-CDT having a lower specific activity compared to *Hd*-CDT (CCA_{50} = 150 (± 13.0) nM and 14 (± 3.0) pM, respectively). Overall, these studies indicated that *Hd*-CDT subunit interactions (*i.e.*, *Hd*-CdtA + *Hd*-CdtB, *Hd*-CdtA + *Hd*-CdtC, *Hd*-CdtB + *Hd*-CdtC, and *Hd*-CdtA + *Hd*-CdtB + *Hd*-CdtC) occurred with relatively low affinity and were not detectable by MST at concentrations which the toxin induces arrest of cell cycle progression (*i.e.*, 10-100 pM) (Figure 4.9B). Sigmoidal, saturable binding curves were obtained for mixtures of *Hd*-CdtA and *Hd*-CdtB as well as mixtures of *Hd*-CdtA and *Hd*-CdtC, with dissociation constants (KD) of approximately 0.16 μM and 0.31 μM respectively (Figure 4.10A,B). *Hd*-CdtB interactions with *Hd*-CdtC occurred with even lower affinity, as MST measurements yielded non-saturable, non-sigmoidal binding curve with an apparent KD of >5 μM (Figure 4.10C), as well as the trimer combination which yielded a non-saturable, non-sigmoidal binding curve with an apparent KD of >10 μM (Figure 4.10D). On the other hand, for the *Ec*-CDT subunit interactions we obtained non-saturable, non-sigmoidal binding curves for all subunit combinations at the concentrations tested (Figure

4.11A-D), suggesting that the *Ec*-CDT subunits were not interacting with each other under the MST conditions used. These data suggest that similar to *Cj*-CDTs, the *Ec* and *Hd*-CDT subunits consist of primarily non-interacting subunits at the lowest concentrations of toxin found to be sufficient to induce arrest of cell cycle progression.

4.3.3 *Cj*-CDT subunits holotoxin complex formation could be occurring at the host cell surface

Previous experiments evaluating subunit interactions suggest that *Cj*-CDT may not require heterotrimer complex formation prior to interacting with host cells. Given the requirement of all three *Cj*-CDT subunits for maximum cellular activity and the incongruence between *Cj*-CDT heterotrimeric complex formation prior to interacting with host cells and toxin biological activity, we suggest the possibility that the *Cj*-CDT subunits might be overcoming the weak affinity for complex formation in solution by forming an active complex at the host cell surface. To evaluate the possibility of active complex formation at the host cell surface we performed several *Cj*-CDT subunit sequential exposure experiments, where cells were exposed to different combinations of subunits under non-internalizing conditions, to limit subunit interaction and the formation of an active holotoxin complex to that of only membrane associated *Cj*-CDT subunits. We utilized different conditions such as toxin subunit combinations, washing conditions, and buffers. HCT116 were chilled on ice to block subunit endocytosis (37, 78). After 30 mins, cells were incubated with the first set of indicated subunit

combinations in cold complete media. After 30 additional minutes, cells were washed twice with cold complete media to remove any unbound subunits and then incubated with the second set of indicated subunit combinations in warm complete media at 37 °C and under 5% CO_2. After 24 h, cells were then harvested and evaluated for cell cycle arrest. This sequential exposure condition revealed that HCT116 cells were insensitive to media washed sequential exposure to 10 nM of *Cj*-CDT subunits (Figure 4.12A). However, the media washed sequential exposure to 100 nM of *Cj*-CDT subunits resulted in toxin activity (Figure 4.12B), specifically the A+BC and AC+BC sequence of *Cj*-CDT subunit exposures. For both the 10 nM and 100 nM concentrations, toxin that was concurrently premixed and exposed to cells had greater biological activity (Figure 4.12A,B).

We also evaluated the effects of exposing cells to sequential exposures of toxin in PBS instead of media, which yielded no activity with 100 nM of *Cj*-CDT subunits (Figure 4.13). Under these conditions cells were washed once more with ice cold PBS after the final incubation step, which led to a loss in toxin activity in the sequential exposure conditions compared to concurrently exposed Cj-CDT subunits. Notably, toxin activity was slightly lower for conditions where toxin subunits were concurrently mixed during the second exposure compared to toxin that was premixed and added to cell (Figure 4.13), which suggests the possibility that toxin subunits that is in complex prior to contact with host cells, preassembled toxin, is more active than toxin subunits that are assembling

concurrently at the host cell surface, mixed toxin subunits at the second exposure step.

A concern raised with the previous experiments was that the washing conditions during sequential exposure might impact toxin complex formation at the host cell surface. To address this, we evaluated another condition wherein cells were exposed to sequential Cj-CDT subunit exposures in media without washing steps. After cells were incubated in cold complete media with the first set of subunit combinations, we removed media containing toxin subunits and added in the second set of subunit combinations, without washing, in warm complete media at 37 °C and under 5% CO_2, as indicated in the figures. After 24 h, cells were then harvested and evaluated for cell cycle arrest. Under this no wash sequential exposure condition, we saw activity even at the 10 nM subunit concentration (Figure 4.14A), as well as full activity compared to concurrent toxin exposure for the 100 nM subunit concentration (Figure 4.14B).

Finally, we performed a three-step sequential exposure experiment, where a single subunit was added to host cells under chilled media conditions and washed between each sequential exposure. Under these conditions, we observed no activity when toxin subunits were individually and sequentially exposed at 100 nM (Figure 4.15). The loss of toxin activity in this experiment could be due to several factors, we think the primary reason was due to the extensive washing steps after each exposure. HeLa cells were also tested under the PBS pulse conditions and did not exhibit activity similar to that of HCT116 cells (data not shown). While we cannot distinguish whether the *Cj*-CDT toxin

subunits are forming a complex at the host cell surface or in solution under these experimental conditions, we believe that it is possible that the assembly of active *Cj*-CDT holotoxin could be occurring at the cell surface level.

4.3.4 Specific activity of *Cj*-CDT could be much higher than previously observed

Sequential exposure experiments described immediately above suggest the possibility of complex formation on the host cell surface as an alternative mechanism for holotoxin complex assembly despite the low subunit affinities observed in solution. However, biological activity was observed under sequential exposure conditions where either cells were exposed to high concentrations of toxin (100 nM) (Figure 4.12B) or under conditions where cells were not washed prior to sequential exposure steps (Figure 4.14A,B). Under these conditions, we cannot rule out the possibility of the *Cj*-CDT subunits forming heterotrimeric complex, albeit at levels much lower than used to treat cells. It is plausible that *Cj*-CDT heterotrimeric complex formation prior to encountering the host cell is required for toxin activity, but the toxin might be in complex at concentrations undetectable by the experimental approaches used in our studies. An alternative model to the relationship between *Cj*-CDT heterotrimer complex formation and biological activity is that *Cj*-CDT specific activity is much higher than previously observed. Based on our subunit interaction studies, if the affinity for *Cj*-CDT heterotrimeric complex formation seems to exceed 1 μM, then that suggests that at our determined CCA_{50} concentrations for *Cj*-CDT G_2/M arrest activities (~1 nM) only 0.1% of our toxin would be in complex. This would imply that the CCA_{50}

of active toxin in complex is in the low pM range. To evaluate the activity of *Cj*-CDT toxin that's in complex, we compared the biological activities of our dialyzed toxin to that of un-dialyzed toxin. Toxin activity was evaluated by treating cells with *Cj*-CDT under a warm pulse 1 h PBS pulse, which we observed to have slightly higher biological activities compared to toxin that was cold pulsed in PBS (Figure 4.16). *Cj*-CDT holotoxin where the subunits were refolded together or where the subunits were refolded individually was diluted to 1 μM and dialyzed for 48 h at a 1:1000 (sample:buffer ratio) at 37 °C, resulting in a loss of subunit in complex (Figure 4.17A), as previously shown (samples were normalized to 10 nM for immunoblot analysis), indicating that retentates had toxin in complex well below 10 nM in concentration. Post dialysis retentates and un-dialyzed toxin, incubated at 37 °C (1 μM), were then sequentially diluted and used to intoxicate HCT116 cells. While immunoblot analysis revealed that less than 10 nM of toxin was retained post dialysis (Figure 4.17A), toxin activity was measurable up to 3 log fold dilutions of what was contained in the post dialysis retentates (Figure 4.17B,C). These data demonstrate that the dialysis retentates, which should consist of toxin in its heterotrimeric form, had toxin activity in the low pM concentration ranges, supporting the idea that the *Cj*-CDT holotoxin might have a much higher specific activity that previously observed.

A significant gap in knowledge regarding the structure-function relationships of the *Cj*-CDT toxin lies in understanding its behavior during infection. To address this relationship, we measured the specific activity of *Cj*-CDT expressed in cultures of *C. jejuni.* It's worth noting that little is known about

the *Cj*-CDT complex during infection, and a major challenge in studying CDT during infection is the low levels of toxin produced by the pathogen. *Campylobacter jejuni* strains containing *cdt* genes (81-176), cytolethal distending toxin mutants (DS104), and DS104 mutants complemented with *cdt* genes in trans (DS104(pRAM33), were grown overnight to an OD ~ 0.6 (600 nm). Filtrate from all three Cj-CDT strains were then evaluated for the presence of Cj-CDT toxin using immunoblot analysis and G_2/M arrest activity under a warm pulse treatment. Interestingly, our immunoblot measurements of *Cj*-CDT subunit content failed to detect any of the *Cj*-CDT subunits in the culture filtrate from *C. jejuni* (81-176) (Figure 4.18), *C. ejuni* (DS104), or *C. jejuni* (DS104(pRAM33)) (Data not shown). Our limit for subunit detection using immunoblot analysis was 10 nM, suggesting that less than that amount of *Cj*-CDT, if any, was present in the culture filtrate of our *C. jejuni* strains. Additionally, we could not quantify toxin concentration through mass spectrometry (data not shown). However, when we evaluated culture filtrate activity, G2/M arrest was measurable up to 2 log fold dilutions from *C. jejuni* (81-176) and *C. jejuni* (DS104(pRAM33)) culture filtrates (Figure 4.19A,C). *C. jejuni* (DS104) a mutant strain that has been shown to not express *Cj*-CDT (68), had no biological activity, suggesting that G2/M arrest response from culture filtrate treatment was caused by *Cj*-CDT in the culture filtrate. As a control, we intoxicated HCT116 cells with recombinant *Cj*-CDT under the same conditions as the culture filtrates (Figure 4.19D). These data suggest that CDT produced by *C. jejuni* were biologically active and has an activity in the sub nM concentration ranges, supporting the idea that that the *Cj*-

CDT holotoxin might have a much higher specific activity. Furthermore, when comparing the activity to our previous subunit interaction studies, the data suggests that the majority of toxin produced by the pathogen would not be in a complex.

Finally, to better understand how toxin levels produced by *C. jejuni* during infection translates to toxin activity from culture filtrates and recombinant *Cj*-CDT studies, we perform multiplicity of infection studies to evaluate cellular G_2/M response to *C. jejuni* as a surrogate for measuring toxin concentration. Our infection experiments revealed a significant increase in G2/M arrest in host cells infected with 1 – 10 MOI of *C. jejuni* (81-176) (Figure 4.20A) but not in cells infected with *C. jejuni* (DS104) or (DS104(pRAM33)) (Figure 4.20B,C). In addition, G_2/M arrest never exceeded 50% and was similar to cellular response to the lower range of recombinant toxin concentrations (< 1 nM). These data suggest that either *Cj*-CDT is being produced at low concentrations during infection or other factors from the pathogen are limiting *Cj*-CDT mediated G_2/M arrest activities.

4.4 DISCUSSION

The studies described in this chapter provide additional work to better understand *Cj*-CDT subunit interactions and how *Cj*-CDTs might be functioning independently of a holotoxin complex in solution. Previous work conducted using CDT from different mucocutaneous human pathogens have contributed to the widely accepted model that CDT binds to and intoxicates sensitive host cells as

an assembled tripartite toxin (40, 81, 141). However, our work has demonstrated that *Cj*-CDT exists predominantly as monomers in solution at concentrations shown to have cellular activity (24). In addition, interaction studies with both *Ec*-CDTs and *Hd*-CDT suggest that the weakly associated heterotrimeric nature of CDTs might extend beyond just *Cj*-CDTs. Regarding these results, we conducted additional experiments to evaluate *Cj*-CDT holotoxin assembly and to further demonstrate that higher molecular weight complexes were forming at lower affinities than previously realized. Our studies revealed that *Cj*-CDT complex formation might not be as straightforward as we previously believed. For instance, Alphafold modeling of *Cj*-CDT subunit interactions and paraformaldehyde crosslinking experiments revealed that the *Cj*-CdtC subunit could potentially interact with itself to form homodimer complexes. Evidence for *Cj*-CdtC subunit interaction with itself to form a homodimer complex has been seen but not discussed in previous studies (81). The possibility that the *Cj*-CdtC subunit can form different heterotrimeric complexes with itself and the other *Cj*-CdtA and *Cj*-CdtB subunits might also explain why in our MST studies we are unable to measure sigmoidal binding curves with NTA-565-dye-labeled *Cj*-CdtC subunits, as the termini used to label the *Cj*-CdtC subunit could be important for subunit interactions. It is unclear as to the significance or relevance of the formation of these homodimeric *Cj*-CdtC complexes, but it could possibility play a role in toxin assembly and function. Since all three *Cj*-CDT subunits have been shown to interact with each other, homodimeric *Cj*-CdtC subunits could be important for the assembly of the heterotrimeric complex, which we have shown

to have a rather weak affinity (24). Alphafold predictions of the *Cj*-CdtC homodimer suggest that the complex has a pocket where the *Cj*-CdtB subunit can interact within (Figure 4.4B). This homodimer pre-complex could be important in recruiting the *Cj*-CdtA and *Cj*-CdtB subunits together. In addition, the ability of the *Cj*-CdtC subunit to interact at different sites and configurations shown in the Alphafold models perhaps suggests that the *Cj*-CdtC subunit plays an important role in holding the heterotrimeric complex together. This idea is also supported by our MST data which demonstrated that the *Cj*-CdtA + *Cj*-CdtC and *Cj*-CdtB + *Cj*-CdtC subunit combinations have significantly higher affinity than the *Cj*-CdtA + *Cj*-CdtB subunit combination.

One major takeaway from our subunit interaction studies is the puzzling notion of how *Cj*-CDTs could function independently of a holotoxin complex in solution. We believe it's unlikely that the subunits can function in isolation without interacting with each other, as there's no precedent among AB toxins or other bacterial toxins where protein subunits independently interact in a manner resulting in site-specific intracellular trafficking. However, it's conceivable that CDTs could be secreted as individual subunits and only assemble into a functional complex after secretion. This strategy for toxin assembly is seen in other multi-component toxins such as anthrax toxins (26) and Iota toxin from *Clostridium perfringens* (128), which assemble at the host cell surface. We hypothesize that the *Cj*-CDT subunits may interact with a host factor, specifically the host cell surface receptor, to facilitate the assembly of the heterotrimeric complex. Previous studies have demonstrated that the *Cj*-CDT subunits (84), as

well as the subunits from other species of CDTs (19, 71, 98), can bind independently to the plasma membrane of sensitive cells, suggesting that *Cj*-CDT subunits could associate at the host cell plasma membrane as a precursor to complex assembly. In addition, considering the known role of the CdtC subunits in binding to host cells (39, 103, 107), it's possible that the previously observed homodimeric *Cj*-CdtC complexes could further enhance host receptor recognition and surface assembly. Studies conducted to assess the involvement of surface assembly in toxin activity, employing sequential exposure experiments, suggest the plausibility of this model. Based on our current understanding of the roles of the three *Cj*-CDT subunits, particularly the notion that *Cj*-CdtA and *Cj*-CdtC serve as the canonical binding and transport subunits, one would anticipate toxin surface assembly to occur sequentially, with the initial binding of *Cj*-CdtA and/or *Cj*-CdtC preceding *Cj*-CdtB binding as a necessary step. However, our findings indicate that cellular activity could still be measured when cells were sequentially exposed to the *Cj*-CdtB subunit before the *Cj*-CdtA and *Cj*-CdtC subunits. This observation contradicts the notion that *Cj*-CDT assembles at the host cell surface, as the *Cj*-CdtB subunit is believed to be unable to bind to host cells independently (84). In addition, it has been previously shown that precomplexed subunit combinations, specifically the *Hd*-CdtA and *Hd*-CdtC subunits, could block the cell killing activities of *Hd*-CDTs expressed in culture filtrates (37). This study supports the model that *Hd*-CDTs are functioning as a preassembled complex prior to reaching the host cell surface rather than assembling into an active holotoxin complex at the host cell surface. In order to

better understand how *Cj*-CDTs are interacting at the host cell surface, we believe it's important to identify the specific host receptor. Currently we are working to identify potential *Cj*-CDT host cell receptors using cross-linking mass spectrometry.

Another possible explanation to the disparity between the structure function relationships of *Cj*-CDT is that the toxin does interact with cells as an assembled heterotrimeric complex, albeit at extremely low concentrations that were previously undetectable by experimental methods used in earlier studies. Our data indicate that even at toxin concentrations well below the limit of detection, we are able to observe toxin activity. These findings suggest that the specific activity of *Cj*-CDT is significantly higher than previously recognized, possibly with CC_{50} values in the pM or even fM concentration ranges.

One of the major gaps in knowledge concerning host-pathogen interactions involves understanding the role of toxins, particularly CDTs, in bacterial infections. This poses a major challenge because replicating similar infection conditions in laboratory settings is nearly impossible. To gain a better understanding of these roles, it's crucial to study toxin functions under physiological conditions, such as concentrations relevant to infection conditions. Unfortunately, many studies on CDTs overlook evaluating the dose-response to the toxin and often use concentrations much higher than those likely to be physiologically relevant. While numerous studies have reported the cytolethal/cell-killing effects of CDT, our infection studies have not observed cell death (data not shown). Although the role of CDTs during infection remains

poorly understood, it's highly unlikely that *C. jejuni* produces CDT with the intention of killing host cells; rather, it may disrupt cellular homeostasis in a manner advantageous to the pathogen. We speculate that the amounts of toxin produced and secreted during infection are critical and likely well controlled by the pathogen. Hence, we propose that *Cj*-CDT might have evolved to possess low subunit affinity as a post-translational strategy to limit toxin activity to local environments (Figure 4.21). We envision this as the toxin having a built-in "kill switch" mechanism, where if the toxin disperses too far from the site of infection, it is turned off due to disassembly. This hypothesis aligns with our model of how *C. jejuni* colonizes and modulates its surrounding environment, particularly the crypt region of the intestines. During infection, *Cj*-CDT is secreted as a holotoxin complex, targeting and damaging crypt cells at the infection site. These cells are in close proximity or even in direct contact with the pathogen, resulting in the effective presence of toxin at extremely high concentrations. However, as the toxin diffuses away from the infection site, the complex begins to disassemble and deactivate due to the weak subunit affinities for complex formation and the significant change in the concentration gradient, from close cell contact to the open villus space. This concept of a "kill switch" feature in toxins is novel and warrants further exploration. It sheds light on new potential mechanisms by which pathogens could regulate toxin activity and adapt to their host environments.

4.5 FIGURES

Figure 4.1

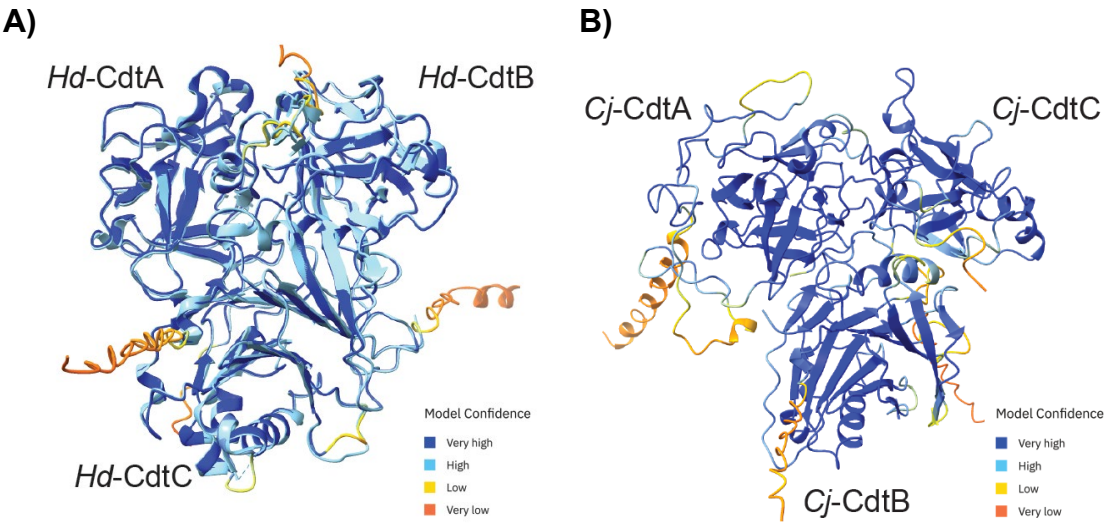

Figure 4.1: Alphafold models of *Hd*-CDT and *Cj*-CDT heterotrimeric complexes. (A) *Hd*-CDT crystal structure (teal) was superimposed onto the Alphafold generated *Hd*-CDT heterotrimeric complex shown with high confidence residues colored blue, and lower confidence in yellow, orange and red. **(B)** The Alphafold generated *Cj*-CDT heterotrimeric complex prediction shown with high confidence residues colored blue, and lower confidence in yellow, orange and red.

Figure 4.2

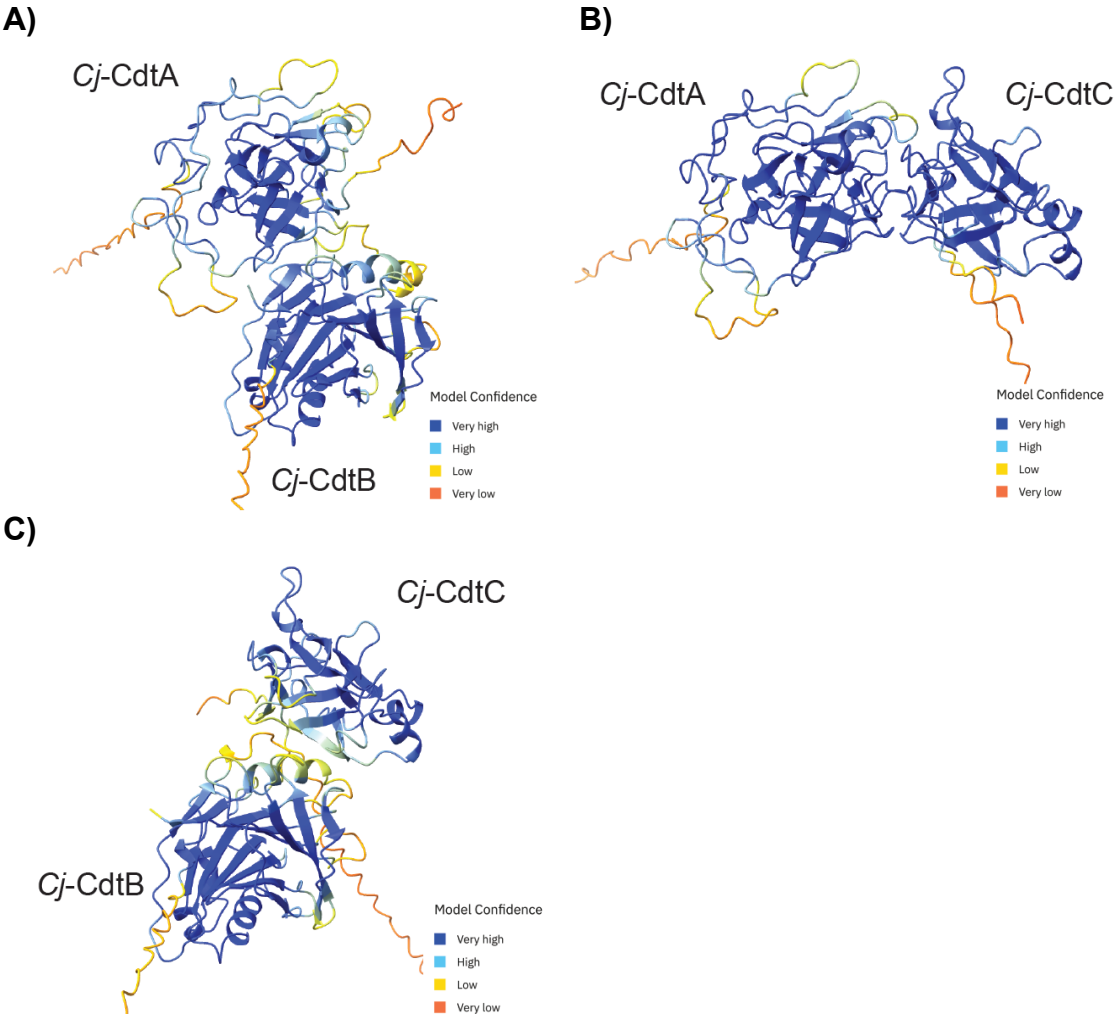

Figure 4.2: Alphafold models of *Cj*-CDT heterodimer combinations. (A) Alphafold generated *Cj*-CdtA + *Cj*-CdtB, **(B)** *Cj*-CdtA + *Cj*-CdtC, **(C)** *Cj*-CdtB + *Cj*-CdtC subunit heterodimer complex predictions shown with high confidence residues colored blue, and lower confidence in yellow, orange and red.

Figure 4.3

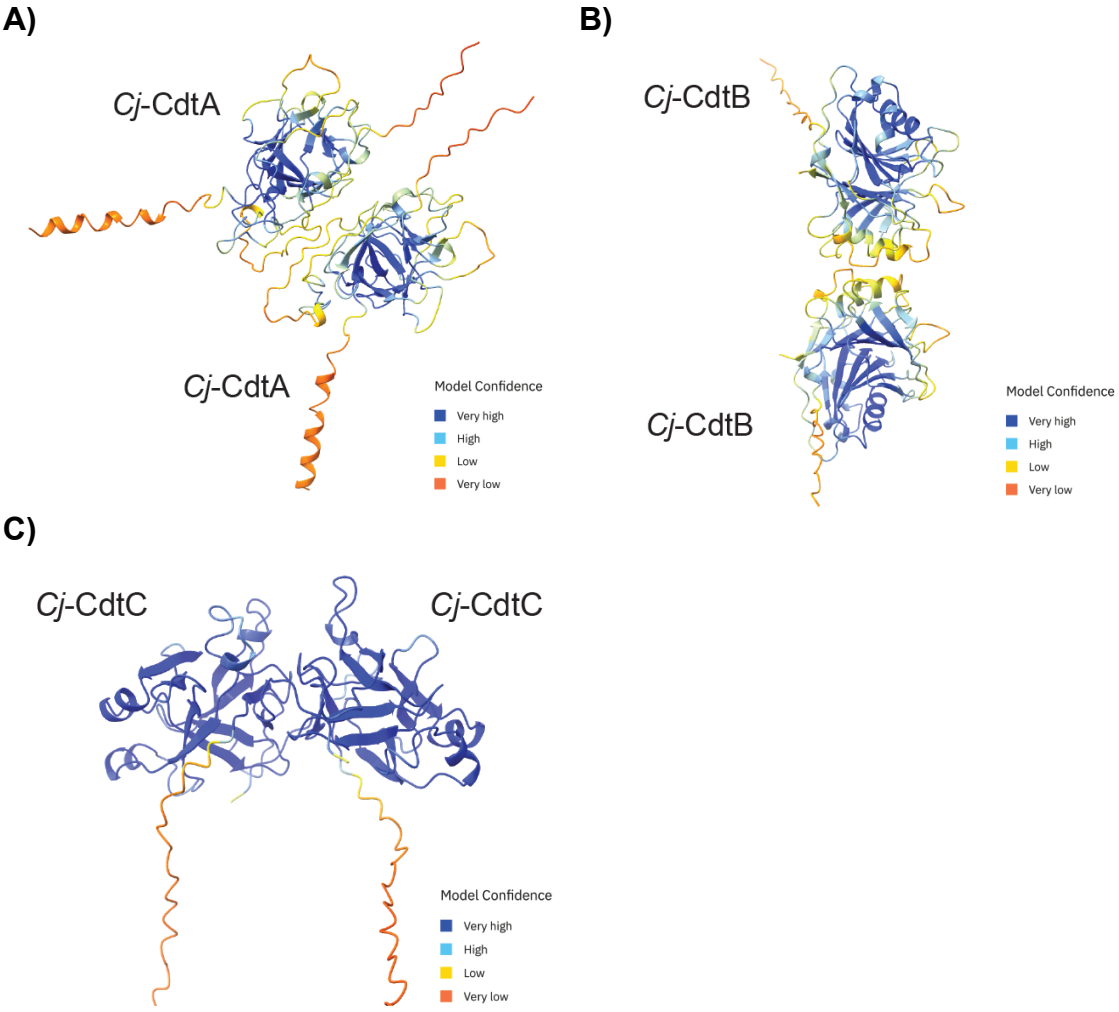

Figure 4.3: Alphafold models of *Cj*-CDT homodimer combinations. (A) Alphafold generated *Cj*-CdtA + *Cj*-CdtA, **(B)** *Cj*-CdtB + *Cj*-CdtB, **(C)** *Cj*-CdtC + *Cj*-CdtC subunit homodimer complex predictions shown with high confidence residues colored blue, and lower confidence in yellow, orange and red.

Figure 4.4

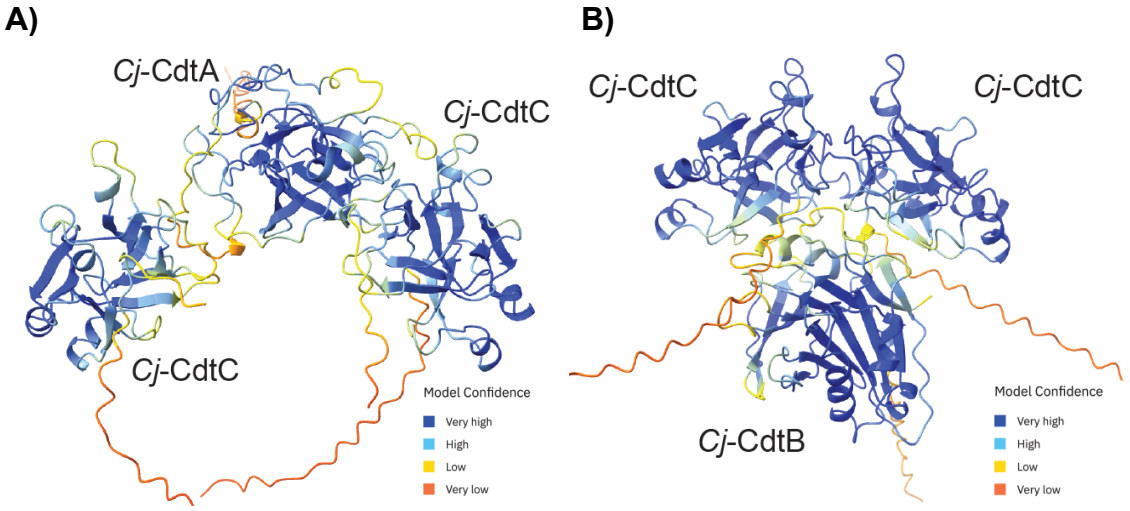

Figure 4.4: Alphafold models of Cj-CdtC homodimer binding with the Cj-CdtA and Cj-CdtB subunits. (A) Alphafold generated *Cj*-CdtA + *Cj*-CdtC + *Cj*-CdtC, **(B)** *Cj*-CdtB + *Cj*-CdtC + *Cj*-CdtC subunit heterotrimer complex predictions shown with high confidence residues colored blue, and lower confidence in yellow, orange and red.

Figure 4.5

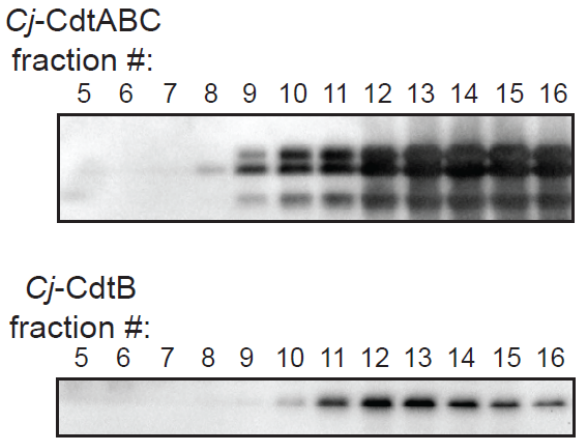

Figure 4.5: *Cj*-CDT heterotrimer size exclusion chromatography. Purified *Cj*-CDT subunits, refolded concurrently (*Cj*-CdtABC) or the individual *Cj*-CdtB subunit, were loaded onto a Bio-Gel P-60 gel filtration column. Fractions (1 mL) were collected and analysis by immunoblot analysis probed with primary antibodies specific to each individual *Cj*-Cdt subunit. Data shown are representative of 2 independent biological replicates (n =2).

Figure 4.6

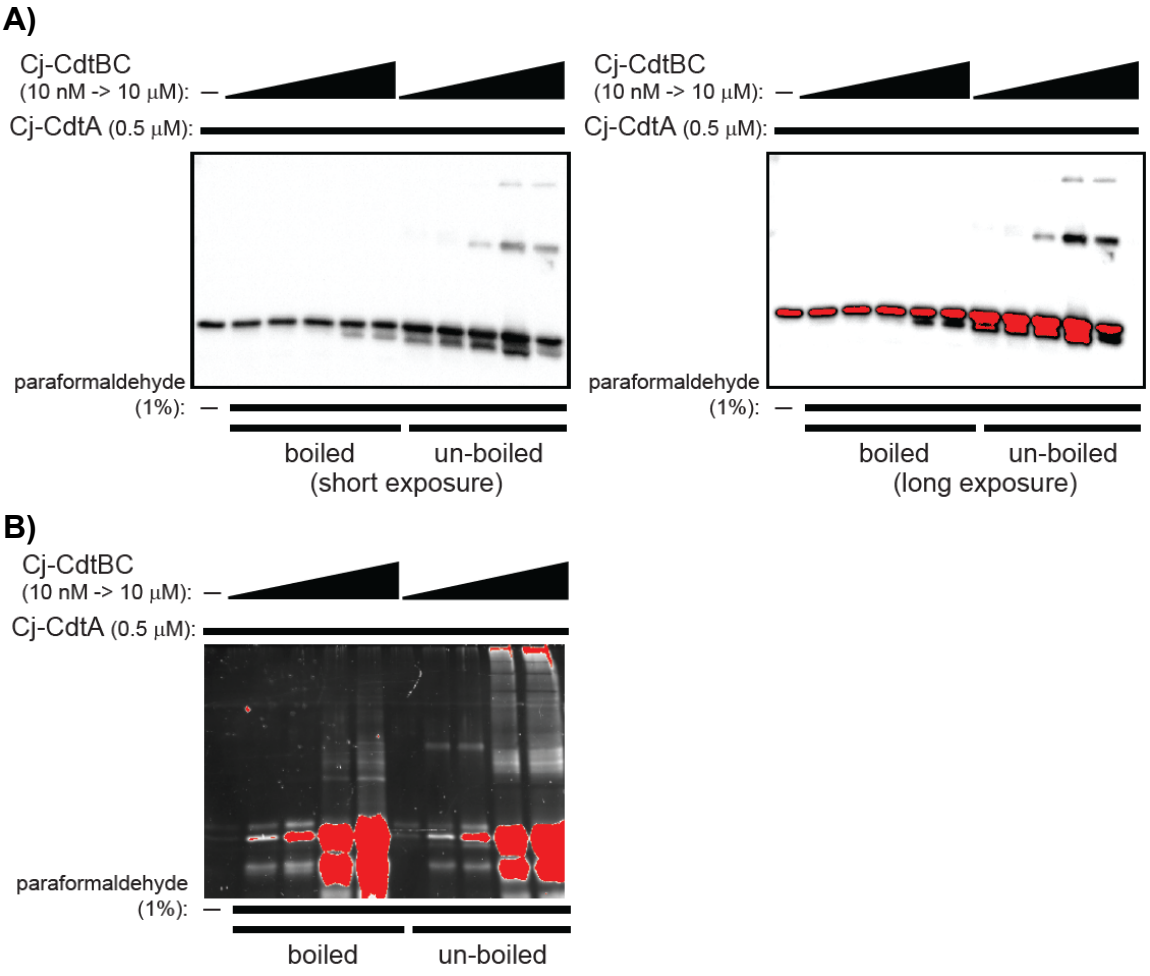

Figure 4.6: *Cj*-CDT heterotrimer paraformaldehyde crosslinking. Purified *Cj*-CdtA (0.5 mM) was incubated with equimolar concentrations of both *Cj*-CdtB and *Cj*-CdtC (10 nM – 10 μM) on ice. After 1 h, 1% paraformaldehyde was added to the subunit mixtures at 37 °C. After 10 mins, samples with quenched with 500 mM glycine. After 5 mins of quenching, crosslinked *Cj*-CDT subunits were either boiled or un-boiled at 100 °C for 10 mins. Samples were then run on a 12% SDS-PAGE gel and toxin subunits were evaluated either using Krypton Protein Stain or immunoblotting with anti-*Cj*-CdtA primary antibodies. Data shown are representative of 3 independent biological replicates (n =3).

Figure 4.7

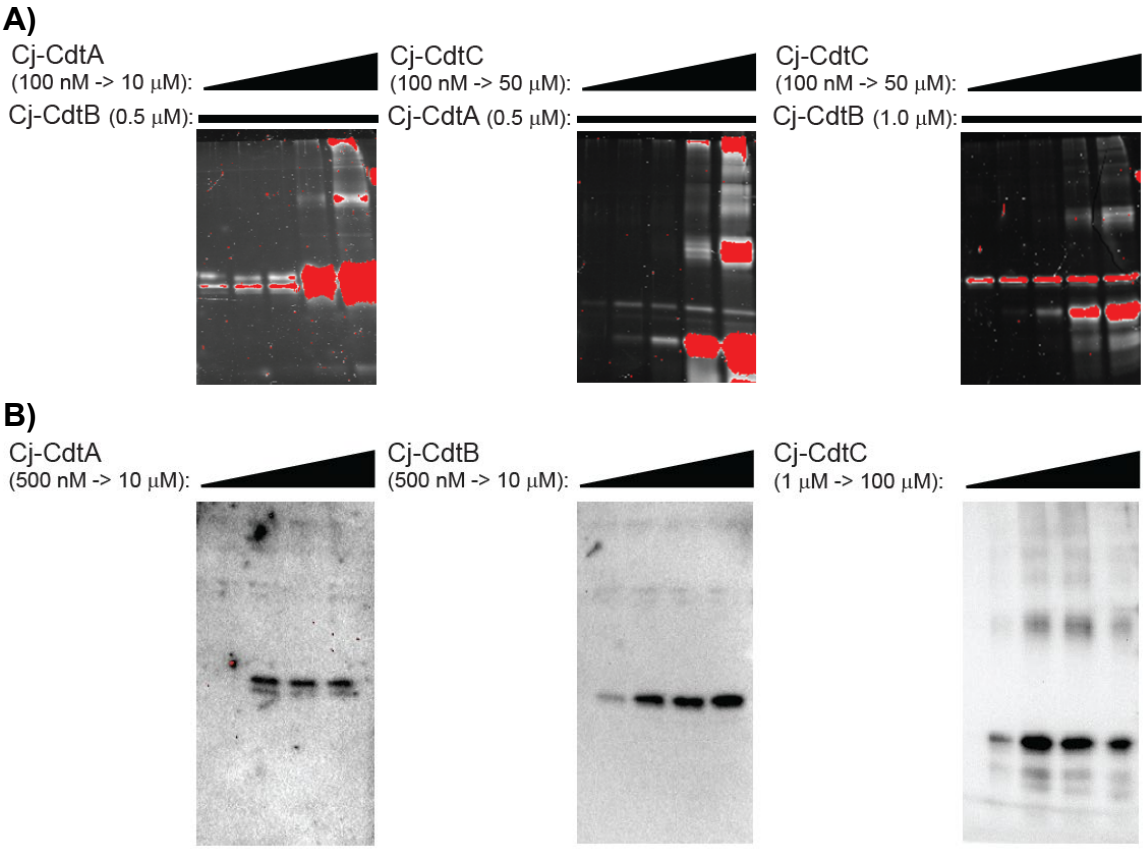

Figure 4.7: *Cj*-CDT heterodimer and homodimer paraformaldehyde crosslinking. (A) Purified *Cj*-CdtB (0.5 μM) + *Cj*-CdtA (100 nM – 10 μM), *Cj*-CdtA + *Cj*-CdtC (10 nM – 50 μM), and *Cj*-CdtB + *Cj*-CdtC (10 nM – 50 μM) were incubated on ice. After 1 h, 1% paraformaldehyde was added to the subunit mixtures at 37 °C. After 10 mins, samples with quenched with 500 mM glycine. After 5 mins of quenching, crosslinked *Cj*-CDT subunits were boiled or un-boiled (data not shown) at 100 °C for 10 mins. Samples were then run on a 12% SDS-PAGE gel and evaluated using Krypton Protein Stain. **(B)** Purified *Cj*-CdtA (500 nM – 10 μM), *Cj*-CdtB (500 nM – 10 μM), and *Cj*-CdtC (1 μM – 100 μM) were incubated on ice. After 1 h, 1% paraformaldehyde was added to the subunit mixtures at 37 °C. After 10 mins, samples with quenched with 500 mM glycine. After 5 mins of quenching, crosslinked *Cj*-CDT subunits were boiled or un-boiled (data not shown) at 100 °C for 10 mins. Samples were then run on a 12% SDS-PAGE gel and evaluated using immunoblotting with anti-*Cj*-CdtA, anti-*Cj*-CdtB, or anti-*Cj*-CdtC primary antibodies. Data shown are representative of 2 independent biological replicates (n =2).

Figure 4.8

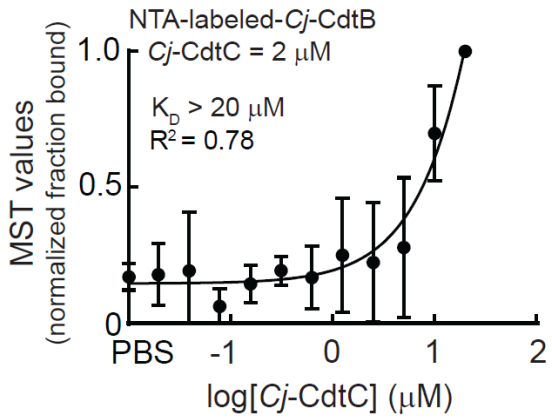

Figure 4.8: Microscale thermophoresis analysis of Cj-CdtA, Cj-CdtB, and Cj-CdtC subunit heterotrimer interaction. NTA fluorescent labeled *Cj*-CdtB subunits were incubated at 37 °C with, polyhistidine tags deficient, unlabeled-*Cj*-CdtC (2 μM) + unlabeled-*Cj*-CdtA (0.02 – 20 μM) subunits, as indicated on the graph. After 1 h, subunits were evaluated for binding at 37 °C using microscale thermophoresis. The data on the graph were combined from 3 independent biological replicates (n = 3). The data were fit to a log[*Cj*-CDT] vs response equation on GraphPad Prism 8.1.2. The K_D was derived from the binding curve. R^2 values indicate fit of the data to the regression model.

Figure 4.9

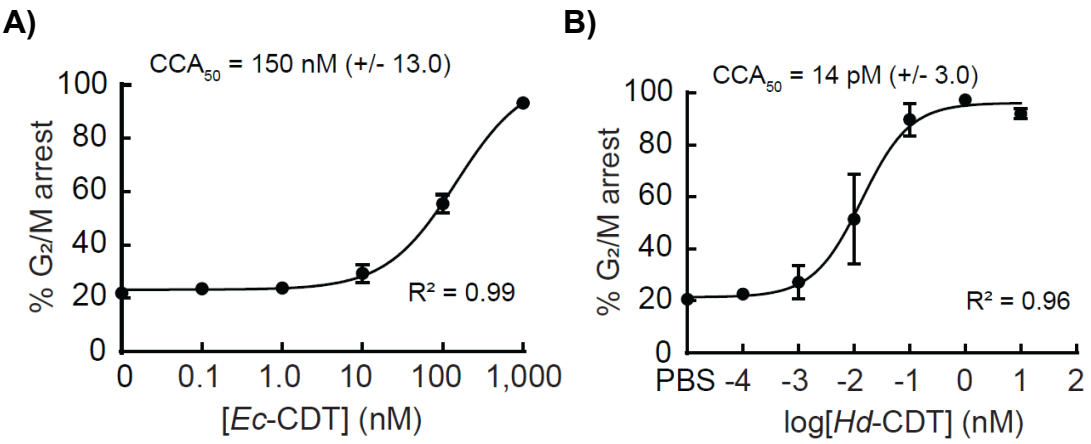

Figure 4.9: Biological activities of *Hd*-CDT and *Ec*-CDT. HeLa cells were incubated in DMEM medium + 10% FBS, at 37 °C, and under 5% CO2, in the absence or presence of **(A)** *Ec*-CDT containing all three individually refolded *Ec*-CdtA, *Ec*-CdtB, and *Ec*-CdtC subunits (100 pM – 1 μM) or **(B)** *Hd*-CDT subunits containing all three individually refolded *Hd*-CdtA, *Hd*-CdtB, and *Hd*-CdtC subunits (100 fM – 10 nM). 48 h after the initial intoxication, cells were harvested and evaluated for cell cycle arrest progression. The data were combined from 3 independent biological replicates (n = 3) and represent the percentage of cells within the monolayer arrested at the G_2/M interface. Error bars represent standard deviations. The data were fit to a log[CDT] vs response equation on GraphPad Prism (version 8.1.2). The CCA_{50} (i.e., EC_{50}) value was determined for each condition. R^2 values indicate fit of the data to the regression model.

Figure 4.10

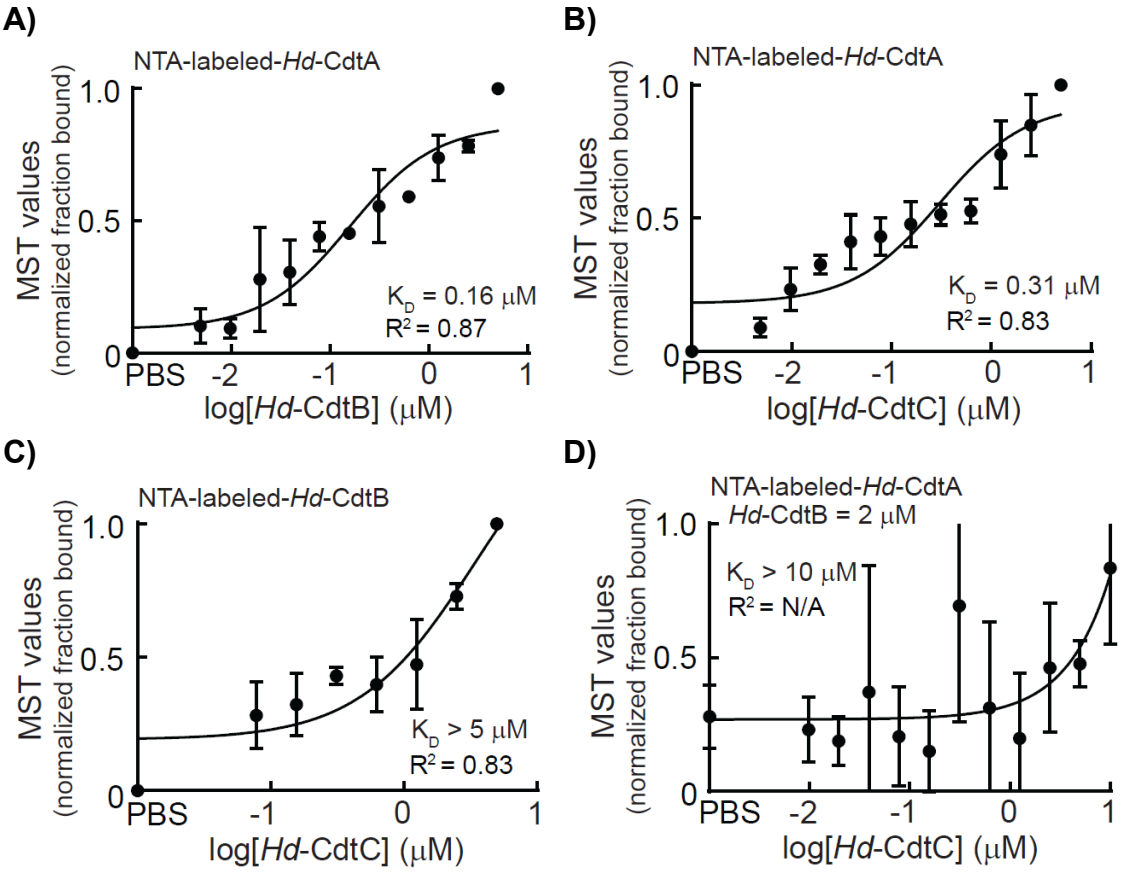

Figure 4.10: Microscale thermophoresis analysis of *Hd*-CdtA, *Hd*-CdtB, and *Hd*-CdtC subunit interactions. NTA fluorescent labeled *Hd*-CdtA or *Hd*-CdtB subunits were incubated at 37 °C with the indicated unlabeled *Hd*-CDT subunit(s) (without polyhistidine tags) as follows: **(A)** NTA-labeled-*Hd*-CdtA (0.1 μM) + unlabeled-*Hd*-CdtB (0.005 – 5 μM), **(B)** NTA-labeled-*Hd*-CdtA (0.1 μM) + unlabeled-*Hd*-CdtC (0.005 – 5 μM), **(C)** NTA-labeled-*Hd*-CdtB (0.1 μM) + unlabeled-*Hd*-CdtC (0.08 – 5 μM) and **(D)** NTA-labeled-*Hd*-CdtA (0.1 μM) + unlabeled-*Hd*-CdtB (2 μM) + unlabeled-*Hd*-CdtC (0.005 – 5 μM), as indicated on the graphs. After 1 h, subunits were evaluated for binding at 37 °C using microscale thermophoresis. The data on the graph were combined from 3 independent biological replicates (n = 3). The data were fit to a log[*Hd*-CDT] vs response equation on GraphPad Prism 8.1.2. The K_D was derived from each binding curve. R^2 values indicate fit of the data to the regression model.

Figure 4.11

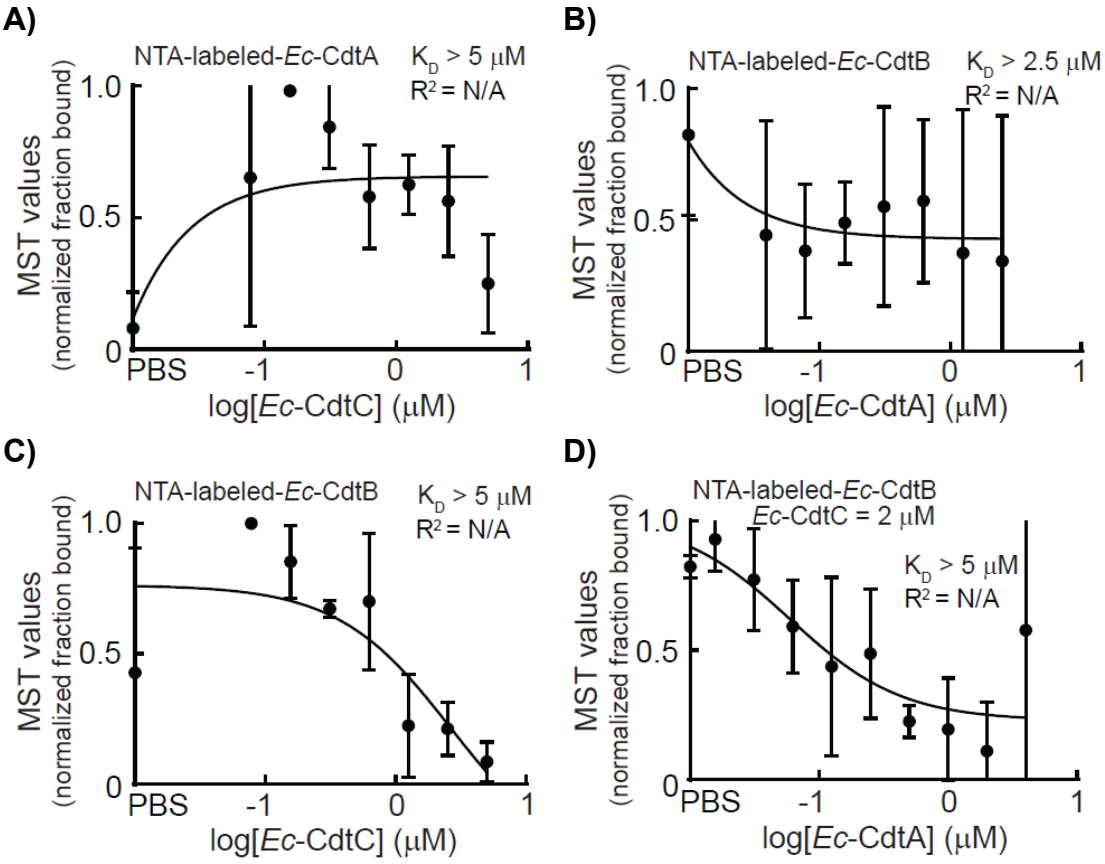

Figure 4.11: Microscale thermophoresis analysis of *Ec*-CdtA, *Ec*-CdtB, and *Ec*-CdtC subunit interactions. NTA fluorescent labeled *Ec*-CdtA or *Ec*-CdtB subunits were incubated at 37 °C with the indicated unlabeled *Ec*-CDT subunit(s) (without polyhistidine tags) as follows: **(A)** NTA-labeled-*Ec*-CdtA (0.1 μM) + unlabeled-*Ec*-CdtC (0.08 – 5 μM), **(B)** NTA-labeled-*Ec*-CdtB (0.1 μM) + unlabeled-*Ec*-CdtA (0.004 – 2.5 μM), **(C)** NTA-labeled-*Ec*-CdtB (0.1 μM) + unlabeled-*Ec*-CdtC (0.08 – 5 μM) and **(D)** NTA-labeled-*Ec*-CdtB (0.1 μM) + unlabeled-*Ec*-CdtC (2 μM) + unlabeled-*Ec*-CdtA (0.002 – 4 μM), as indicated on the graphs. After 1 h, subunits were evaluated for binding at 37 °C using microscale thermophoresis. The data on the graph were combined from 3 independent biological replicates (n = 3). The data were fit to a log [*Ec*-CDT] vs response equation on GraphPad Prism 8.1.2. The K_D was derived from each binding curve. R^2 values indicate fit of the data to the regression model.

Figure 4.12

A)

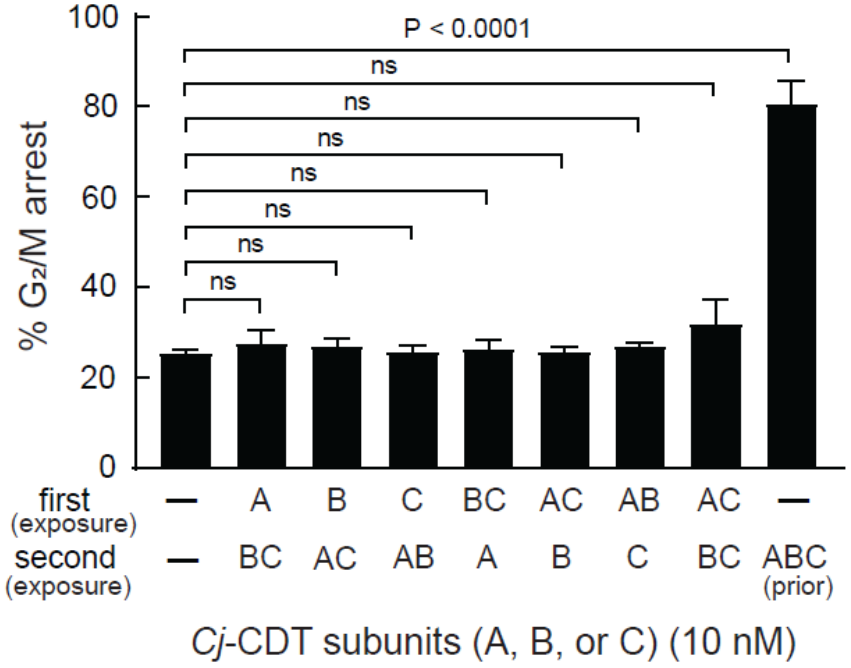

B)

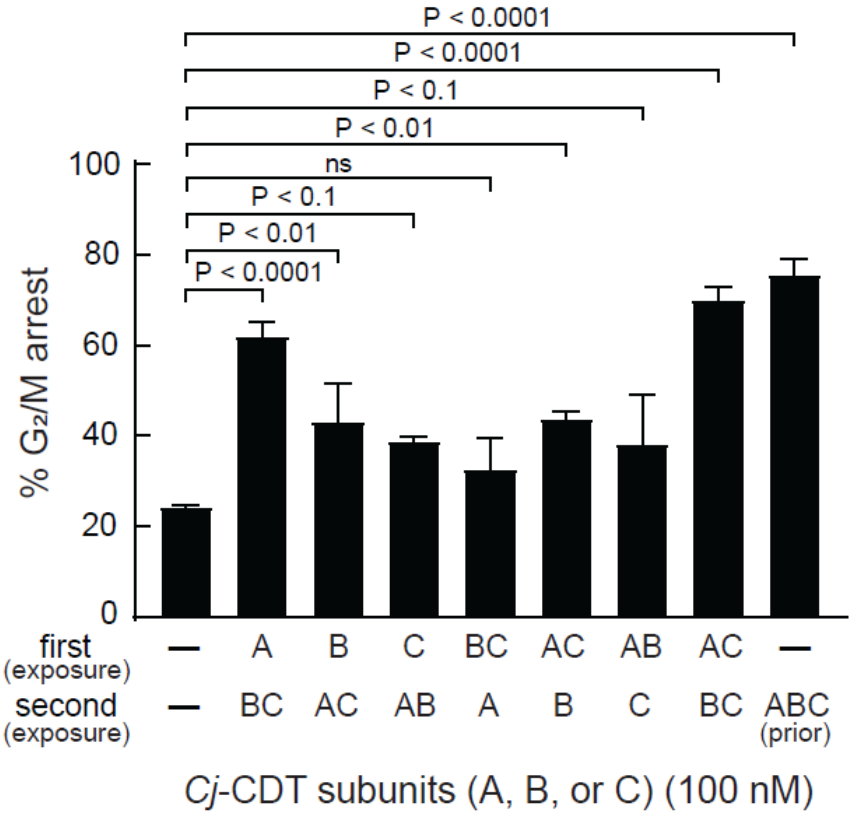

Figure 4.12 (cont.)

Figure 4.12: G_2/M cell cycle arrest activities of *Cj*-CDT subunit sequential exposures with media washing. HCT116 cells were chilled on ice. After 30 mins, cells were incubated in cold McCoy's 5A medium + 10% FBS, on ice, and at atmospheric conditions, in the absence or presence of the first combination of indicated *Cj*-CDT subunit(s) (first exposure). After 30 mins, cells were washed twice with cold media and incubated in warm medium, at 37 °C, and under 5% CO_2, in the absence or presence of the second combination of the indicated *C*j-Cdt subunit(s) (second exposure). After 24 h, cells were harvested and evaluated for cell cycle arrest progression. Toxin exposures were performed with either **(A)** 10 nM or **(B)** 100 nM of *Cj*-CDT subunits (without polyhistidine tags). "ABC (prior)" indicates *Cj*-CDT subunits that were mixed in equimolar concentrations prior to second exposure step. The data were combined from 3 independent biological replicates (n = 3) and represent the percentage of cells within the monolayer arrested at the G_2/M interface. Error bars represent standard deviations. Statistical analyses of the data were conducted using one-way Anova, followed by Tukey's multiple comparisons test. $P < 0.05$ indicates statistical significance ($\alpha = 0.05$), "ns" indicates differences were not statistically significant.

Figure 4.13

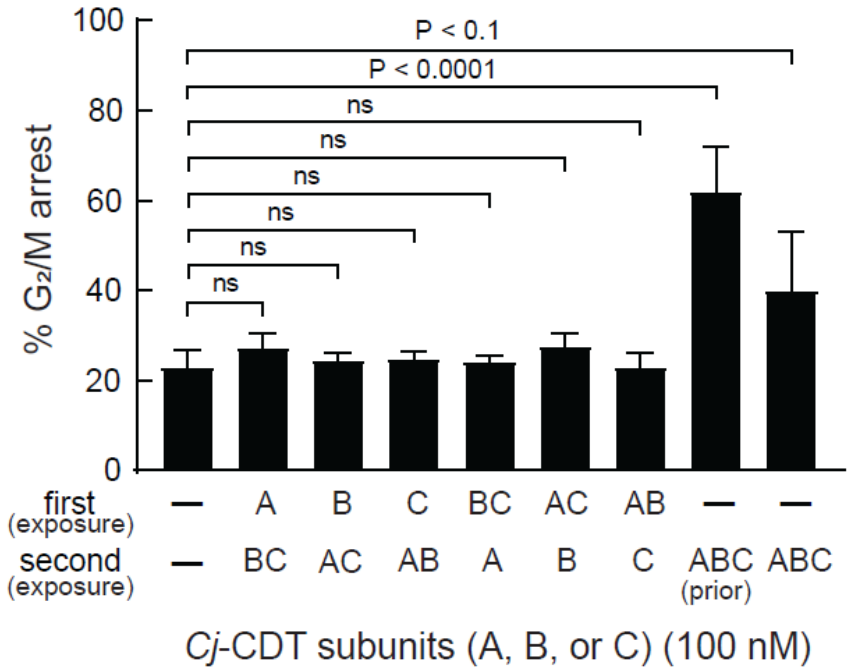

Figure 4.13: G_2/M cell cycle arrest activities of *Cj*-CDT sequential exposures with PBS washing. HCT116 cells were chilled on ice. After 30 mins, cells were incubated in cold PBS, on ice and at atmospheric conditions, in the absence or presence of the first combination of indicated *Cj*-CDT subunit(s) (first exposure). After 30 mins, cells were washed twice with cold PBS and were incubated in cold PBS, on ice, and under atmospheric conditions, in the absence or presence of the second combination of the indicated *C*j-Cdt subunit(s) (second exposure). After 30 mins, cells were washed once with cold media and incubated in warm medium, at 37 °C, and under 5% CO_2. After 24 h, cells were harvested and evaluated for cell cycle arrest progression. Toxin exposures were performed with 100 nM of *Cj*-CDT subunits (without polyhistidine tags). "ABC (prior)" indicates *Cj*-CDT subunits that were mixed in equimolar concentrations prior to second exposure step. "ABC" indicates *Cj*-CDT subunits that were mixed on the cells during the second exposure step. The data were combined from 3 independent biological replicates (n = 3) and represent the percentage of cells within the monolayer arrested at the G_2/M interface. Error bars represent standard deviations. Statistical analyses of the data were conducted using one-way Anova, followed by Tukey's multiple comparisons test. $P < 0.05$ indicates statistical significance ($\alpha = 0.05$), "ns" indicates differences were not statistically significant.

Figure 4.14

A)

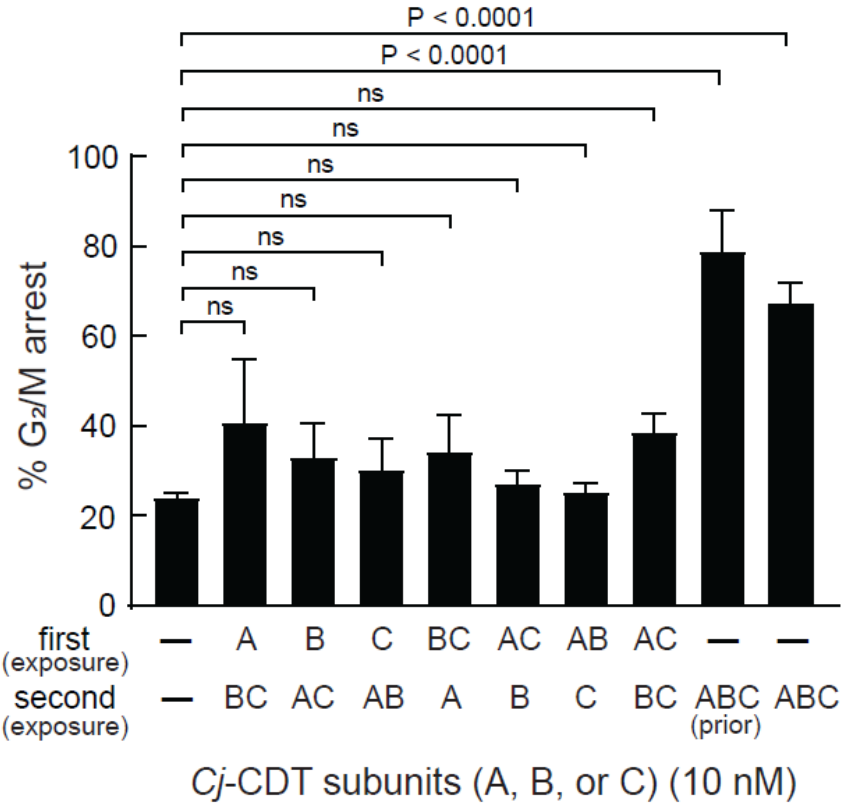
P < 0.0001
P < 0.0001
ns
ns
ns
ns
ns
ns
ns
100
80
60
40
20
0
% G2/M arrest
first (exposure) — A B C BC AC AB AC — —
second (exposure) — BC AC AB A B C BC ABC (prior) ABC
Cj-CDT subunits (A, B, or C) (10 nM)

Figure 4.14 (cont.)

B)

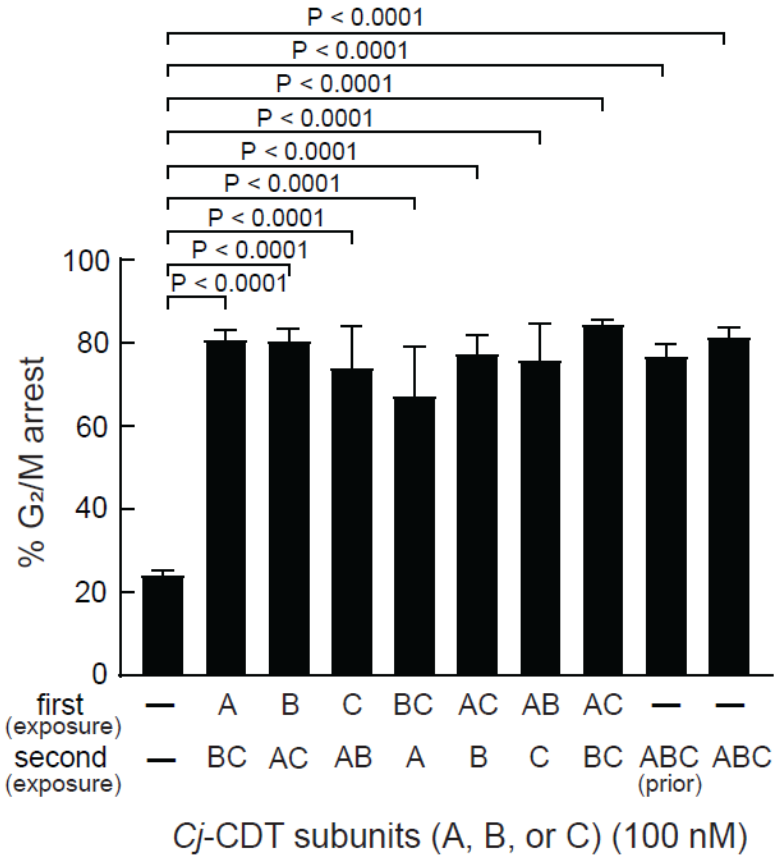

Figure 4.14: G_2/M cell cycle arrest activities of Cj-CDT sequential exposures in media without washing. HCT116 cells were chilled on ice. After 30 mins, cells were incubated in cold McCoy's 5A medium + 10% FBS, on ice, and at atmospheric conditions, in the absence or presence of the first combination of the indicated *Cj*-CDT subunit(s) (first exposure). After 30 mins, media with/without toxin was removed and cells were incubated in warm medium, at 37 °C, and under 5% CO_2, in the absence or presence of the second combination of the indicated *C*j-Cdt subunit(s) (second exposure). After 24 h, cells were harvested and evaluated for cell cycle arrest progression. Toxin exposures were performed with either **(A)** 10 nM or **(B)** 100 nM of *Cj*-CDT subunits (without polyhistidine tags). "ABC (prior)" indicates *Cj*-CDT subunits that were mixed in equimolar concentrations prior to second exposure step. "ABC" indicates *Cj*-CDT subunits that were mixed on the cells during the second exposure step. The data were combined from 3 independent biological replicates (n = 3) and represent the percentage of cells within the monolayer arrested at the G_2/M interface. Error bars represent standard deviations. Statistical analyses of the data were conducted using one-way Anova, followed by Tukey's multiple comparisons test. $P < 0.05$ indicates statistical significance ($\alpha = 0.05$), "ns" indicates differences were not statistically significant.

Figure 4.15

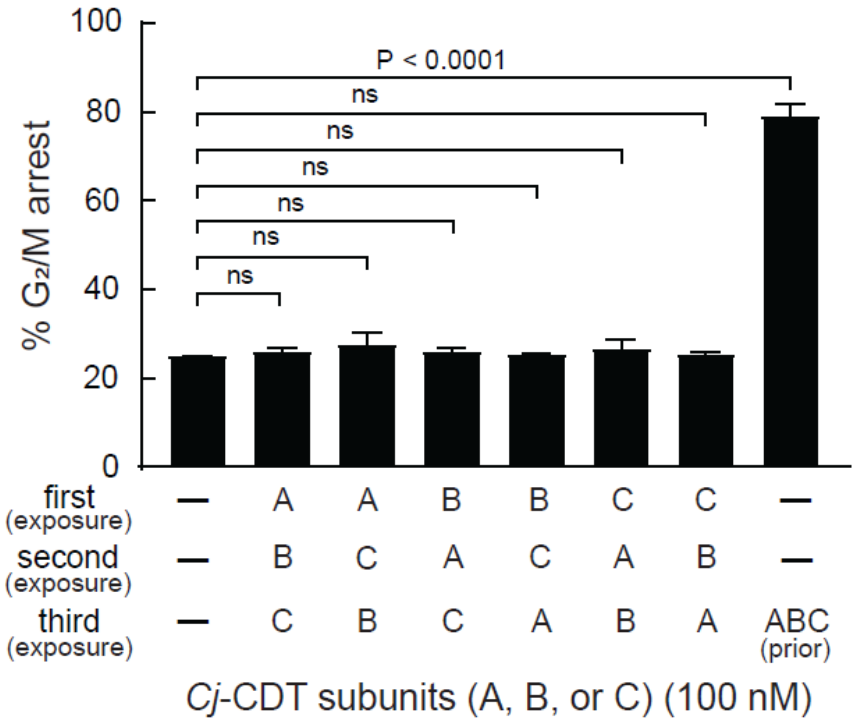

Figure 4.15: G_2/M cell cycle arrest activities of *Cj*-CDT sequential exposure in media with washing after each individual subunit. HCT116 cells were chilled on ice. After 30 mins, cells were incubated in cold McCoy's 5A medium + 10% FBS, on ice, and at atmospheric conditions, in the absence or presence of the first combination of the indicated *Cj*-CDT subunit (first exposure). After 30 mins, cells were washed twice with cold media and incubated in cold medium, on ice, and at atmospheric conditions, in the absence or presence of the second combination of the indicated *C*j-Cdt subunit (second exposure). After 30 mins, cells were washed twice with cold media and incubated in warm medium, at 37 °C, and under 5% CO_2, in the absence or presence of the third combination of the indicated *C*j-Cdt subunit (third exposure). After 24 h, cells were harvested and evaluated for cell cycle arrest progression. Toxin exposures were performed with 100 nM of *Cj*-CDT subunits (with polyhistidine tags removed). "ABC (prior)" indicates *Cj*-CDT subunits that were mixed in equimolar concentrations prior to second exposure step. The data were combined from 3 independent biological replicates (n = 3) and represent the percentage of cells within the monolayer arrested at the G_2/M interface. Error bars represent standard deviations. Statistical analyses of the data were conducted using one-way Anova, followed by Tukey's multiple comparisons test. $P < 0.05$ indicates statistical significance ($\alpha = 0.05$), "ns" indicates differences were not statistically significant.

Figure 4.16

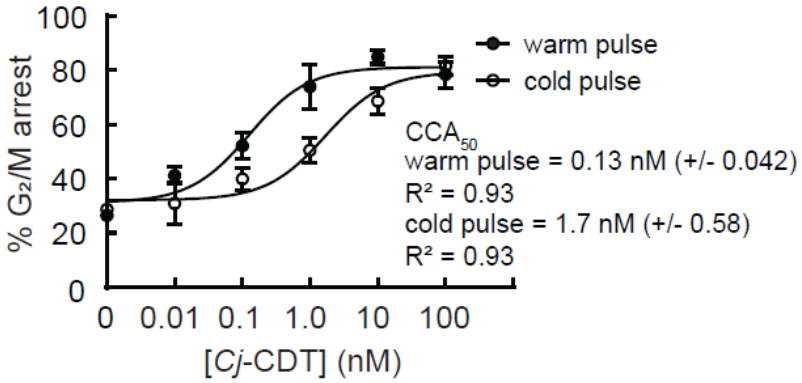

Figure 4.16: *Cj*-CDT warm vs cold pulse intoxication G_2/M cell cycle arrest activities. HCT116 cells were either incubated at 37 °C (warm pulse) or chilled on ice (cold pulse). After 30 mins, cells were incubated in PBS, at 37 °C (warm pulse) or on ice (cold pulse), and under 5% CO_2 (warm pulse) or atmospheric conditions (cold pulse), in the absence or presence of *Cj*-CDT containing all three individually refolded *Cj*-CdtA, *Cj*-CdtB, and *Cj*-CdtC subunits (10 pM – 100 nM). After an additional 30 mins, toxin was removed and cells were incubated with culture medium + 10% FBS, at 37 °C, and under 5% CO_2. After 24 h, cells were harvested and evaluated for cell cycle arrest progression. The data were combined from 3 independent biological replicates (n = 3) and represent the percentage of cells within the monolayer arrested at the G_2/M interface. Error bars represent standard deviations. The data were fit to a log[*Cj*-CDT] vs response equation on GraphPad Prism (version 8.1.2). The CCA_{50} (i.e., EC_{50}) value was determined for each condition. R^2 values indicate fit of the data to the regression model.

Figure 4.17

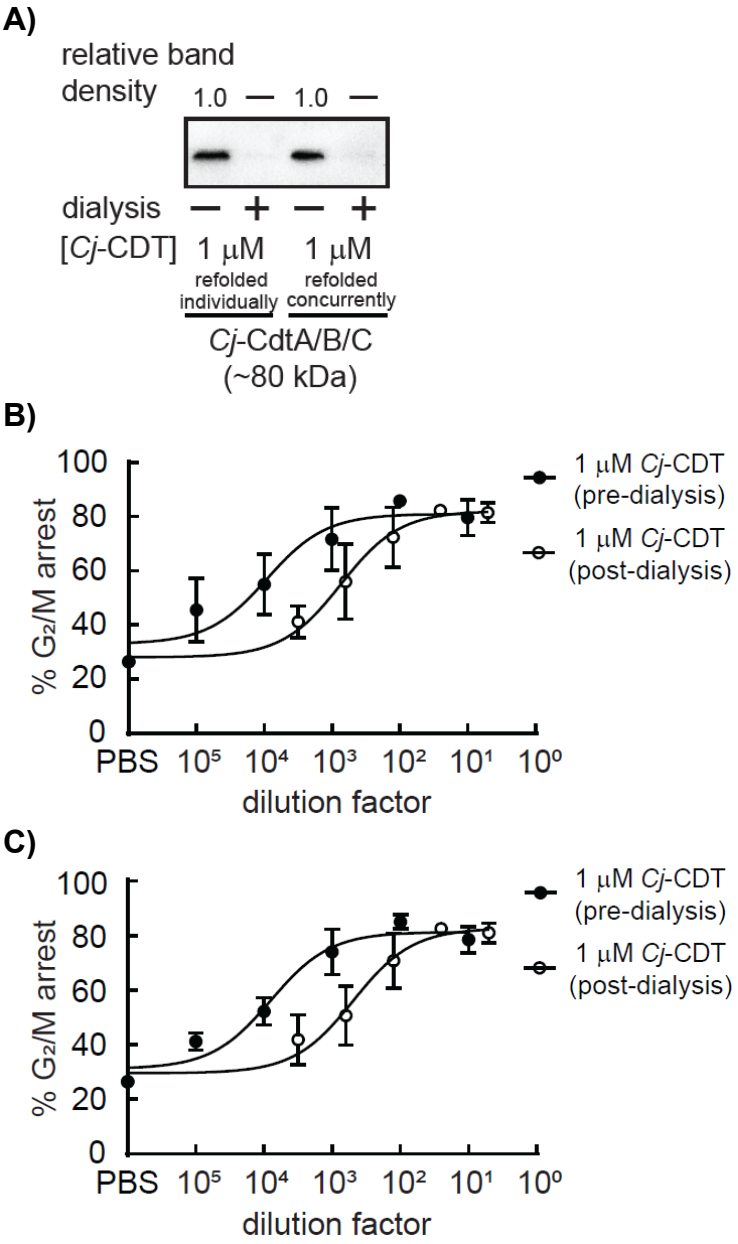
A)
relative band density
1.0
1.0
dialysis
[Cj-CDT]
1 μM
1 μM
refolded individually
refolded concurrently
Cj-CdtA/B/C
(~80 kDa)
B)
% G2/M arrest
100
80
60
40
20
0
PBS
10⁵
10⁴
10³
10²
10¹
10⁰
dilution factor
1 μM Cj-CDT (pre-dialysis)
1 μM Cj-CDT (post-dialysis)
C)
% G2/M arrest
dilution factor
1 μM Cj-CDT (pre-dialysis)
1 μM Cj-CDT (post-dialysis)

Figure 4.17 (cont.)

Figure 4.17: *Cj*-CDT pre- and post-dialysis G_2/M cell cycle arrest activities. (A) Dialysis of *Cj*-CdtA, *Cj*-CdtB, and *Cj*-CdtC subunits that were mixed (denatured subunits refolded individually) was compared to refolded concurrently together (denatured subunits refolded concurrently) *Cj*-CDT subunits before (pre-dialysis) and after dialysis (post-dialysis) of the toxin, as previously shown. HCT116 cells were incubated in PBS, at 37 °C, and under 5% CO_2, in the absence or presence of 1 μM Cj-CDT subunits that were **(B)** mixed or **(C)** refolded concurrently together, pre-dialysis or post-dialysis at the dilutions indicated, (10 – 100,000 fold for pre-dialysis) and (5 – 3125 fold for post dialysis). After an additional 30 mins, toxin was removed and cells were incubated with culture medium + 10% FBS, at 37 °C, and under 5% CO_2. After 24 h, cells were harvested and evaluated for cell cycle arrest progression. The data were combined from 3 independent biological replicates (n = 3) and represent the percentage of cells within the monolayer arrested at the G_2/M interface. Error bars represent standard deviations.

Figure 4.18

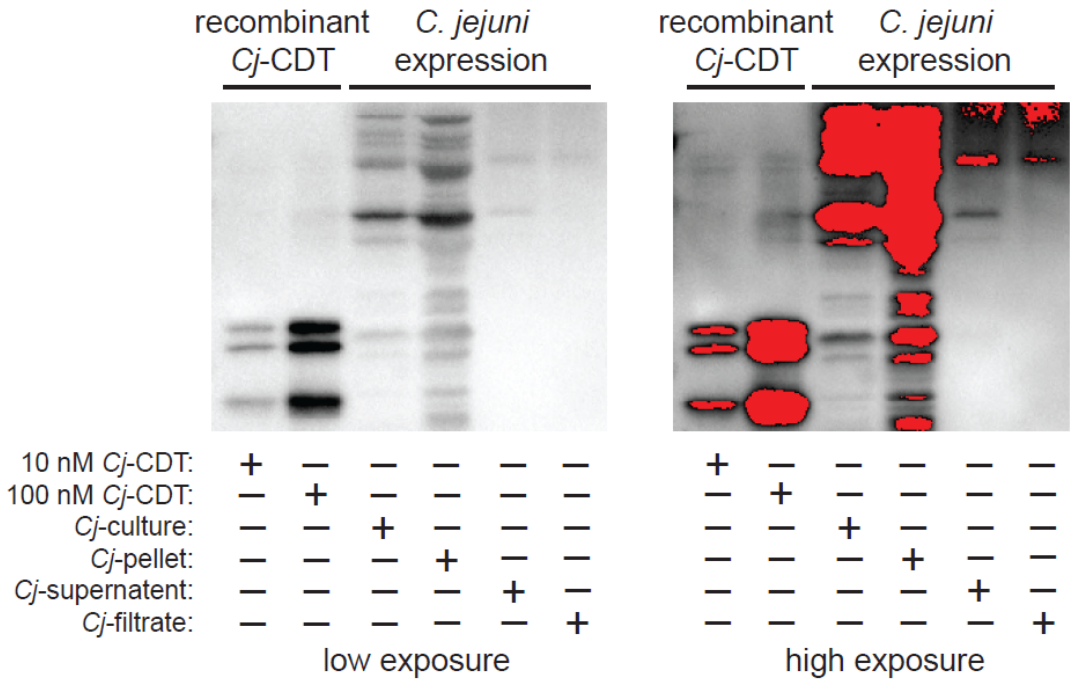

Figure 4.18: *C. jejuni* native CDT culture expression. *C. jejuni* (81-176) was grown to an OD ~ 0.6, pelleted, and culture supernatant filtered. Samples collected from the culture, pellet, supernatant, and culture filtrate, along with 10 and 100 nM of purified recombinant *Cj*-CDT, was ran on a 12% SDS-PAGE gel and immunoblotted with primary antibodies specific to each *Cj*-CdtA, *Cj*-CdtB, and *Cj*-CdtC subunit. Data shown are representative of 3 independent biological replicates (n = 3).

Figure 4.19

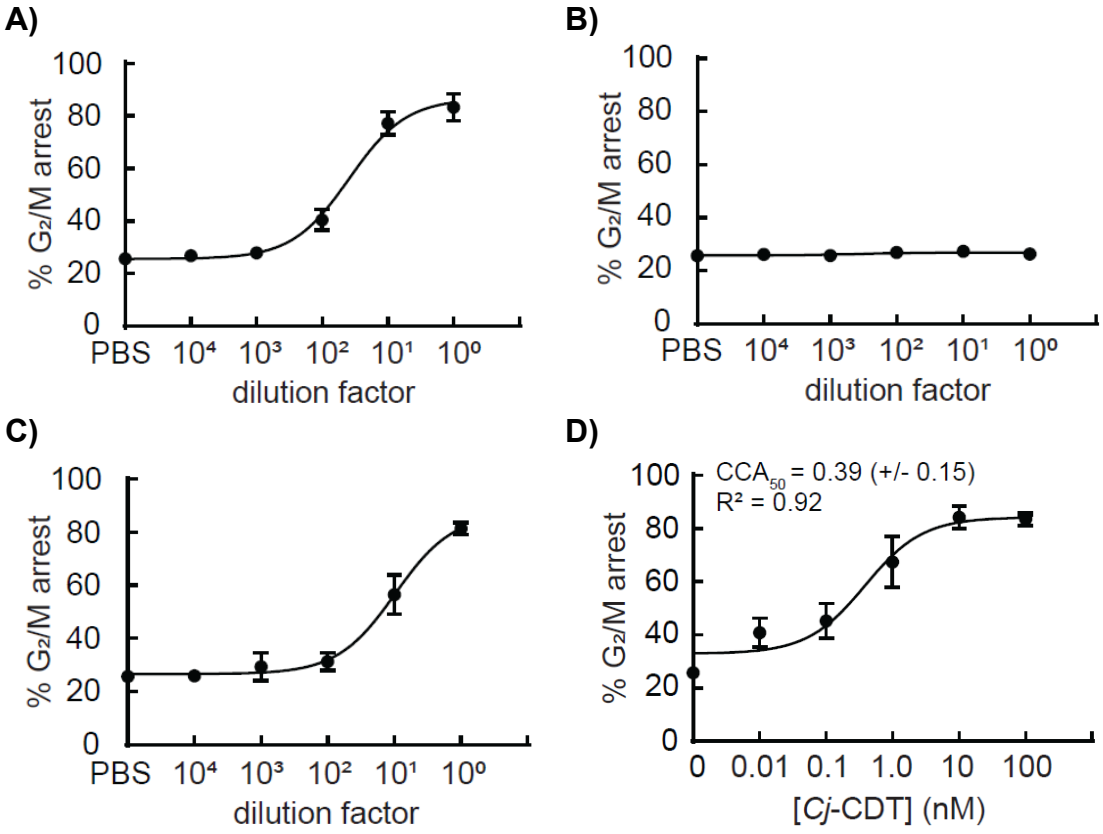

Figure 4.19: *C. jejuni* culture filtrate G_2/M cell cycle arrest activities. *C. jejuni* (81-176), (DS104), and (DS104(pRAM33)) were grown to an OD ~ 0.6, pelleted, and culture supernatant filtered. HCT116 cells were incubated in PBS, at 37 °C, and under 5% CO_2, in the absence or presence of different dilutions of **(A)** *C. jejuni* (81-176), **(B)** (DS104), and **(C)** (DS104(pRAM33)) culture filtrate (1 – 10,000 fold). After 30 mins, culture filtrates were removed and cells were incubated with culture medium + 10% FBS at 37 °C and under 5% CO_2. After 24 h, cells were harvested and evaluated for cell cycle arrest progression. **(D)** HCT116 cells were incubated in PBS, at 37 °C, and under 5% CO_2, in the absence or presence of *Cj*-CDT containing all three individually refolded *Cj*-CdtA, *Cj*-CdtB, and *Cj*-CdtC subunits (10 pM – 100 nM). After an additional 30 mins, toxin was removed and cells were incubated with culture medium + 10% FBS at 37 °C and under 5% CO_2. After 24 h, cells were harvested and evaluated for cell cycle arrest progression. The data were combined from 3 independent biological replicates (n = 3) and represent the percentage of cells within the monolayer arrested at the G_2/M interface. Error bars represent standard deviations. **(D)** The data were fit to a log[*Cj*-CDT] vs response equation on GraphPad Prism (version 8.1.2). The CCA_{50} (i.e., EC_{50}) value was determined from the dose response curve. R^2 values indicate fit of the data to the regression model.

Figure 4.20

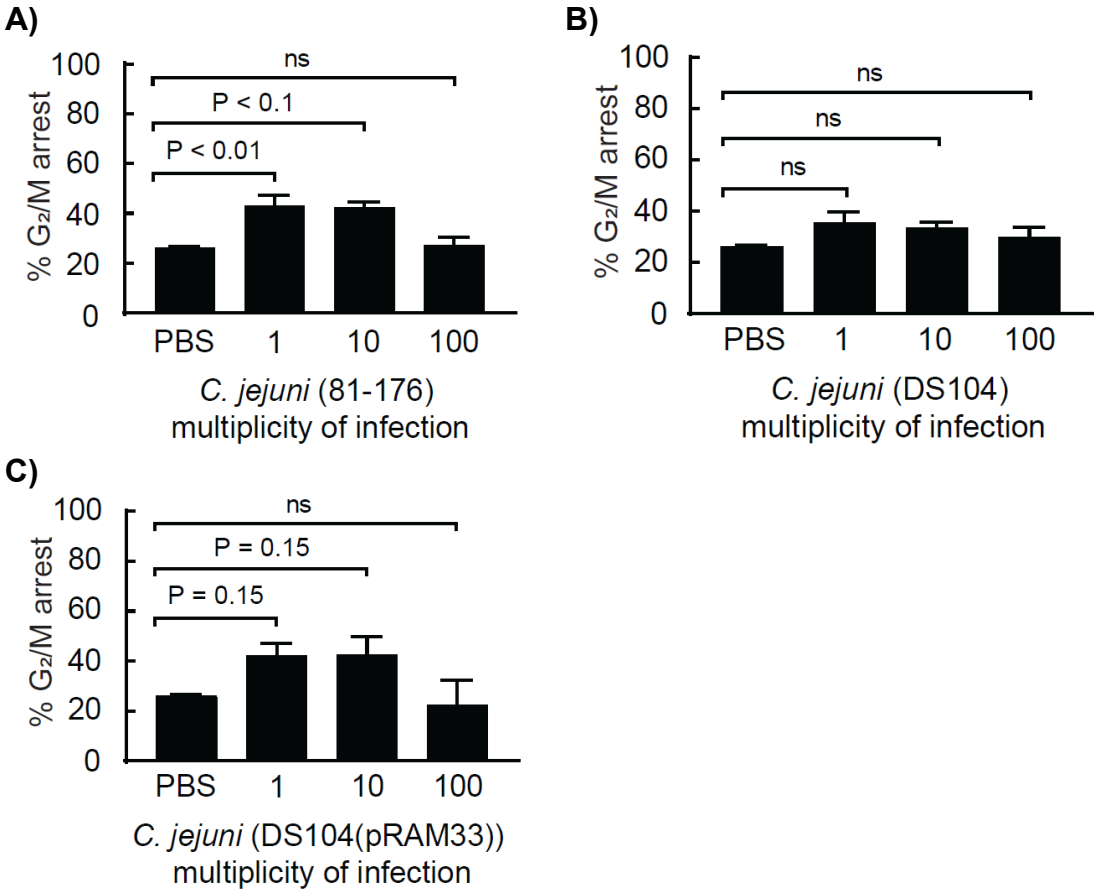

Figure 4.20: *C. jejuni* infection activities. *C. jejuni* (81-176), (DS104), and (DS104(pRAM33)) were grown to an OD ~ 0.6. HCT116 cells were incubated in McCoy's 5A medium + 10% FBS, at 37 °C, and under 5% CO_2, with uninfected or 1, 10, or 100 multiplicities of infection of **(A)** *C. jejuni* (81-176), **(B)** (DS104), and **(C)** (DS104(pRAM33)). After 24 h, cells were harvested and evaluated for cell cycle arrest progression. The data were combined from 2 independent biological replicates (n = 2) and represent the percentage of cells within the monolayer arrested at the G_2/M interface. Error bars represent standard deviations. Statistical analyses of the data were conducted using one-way Anova, followed by Tukey's multiple comparisons test. $P < 0.05$ indicates statistical significance ($\alpha = 0.05$). "ns" indicates differences were not statistically significant.

Figure 4.21

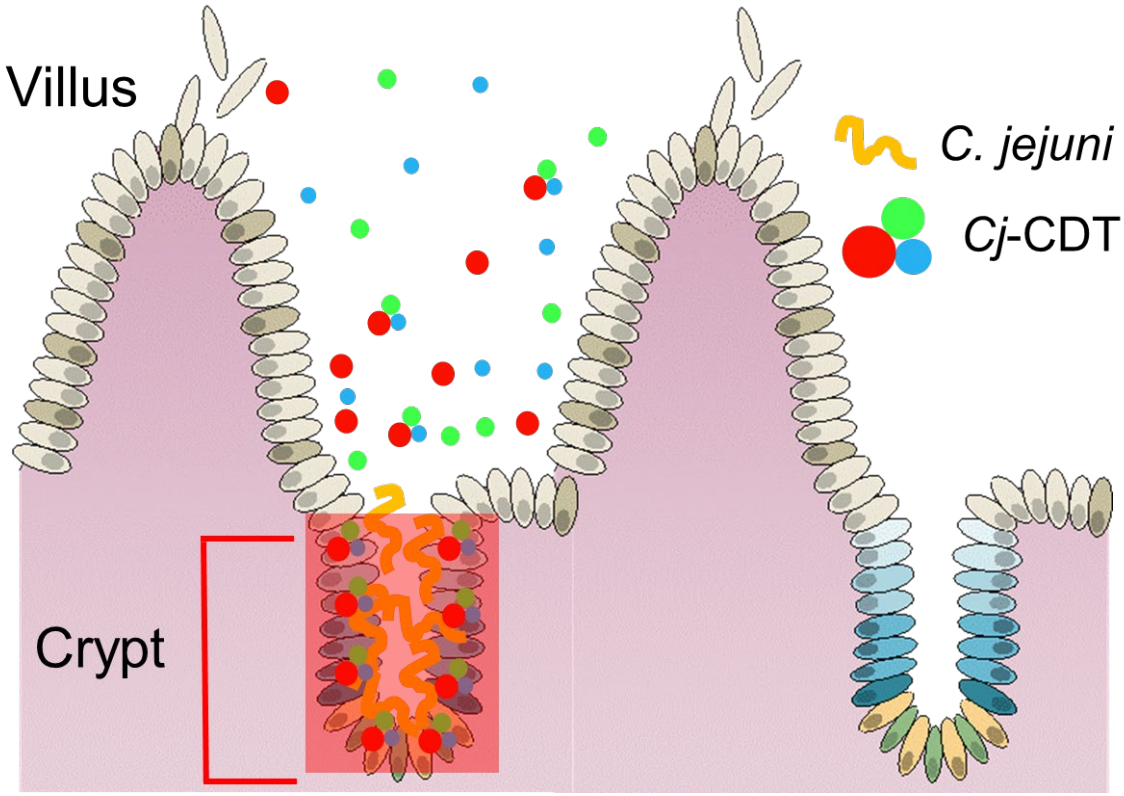

Figure 4.21: Model of low toxin affinity post translational limitation of *Cj*-CDT toxin activity. *C. jejuni* colonizes the intestinal crypts, a small space compared to the rest of the intestine. When *Cj*-CDT is secreted by the pathogen, which is in close contact to host cells, they are released into a very confined space and are theoretically at a high enough concentration to maintain a heterotrimeric complex and be biologically active. However, as the toxin diffuses away into the larger villus space, the toxin is essentially being diluted, resulting in the toxin being at lower concentrations that do not support complex formation and activity.

CHAPTER 5: CONCLUSION AND FUTURE DIRECTIONS

5.1 CONCLUSIONS

Bacteria protein toxins, specifically CDTs, are worthy of attention because they “are proteins capable of achieving multiple remarkable tasks. They function as autonomous molecular devices, targeting specific cells in an organism, punching holes in their membranes, or modifying intracellular components. Intoxication processes involve highly specialized steps of great complexity. It is thus tempting for the biochemist, the protein engineer, the biotechnologist, or the medical scientist to exploit the sophisticated properties of bacterial toxins to design new toxin-derived molecules for research, biotechnology, or medical treatments” (10). Bacterial toxins can also be powerful tools for the researcher to better understand host cellular processes and strategies used by pathogens during infections. Our understanding of bacterial toxins has advanced considerably over the years, but there's still much to learn. Despite significant progress, there are still challenges in understanding the full scope of bacterial toxin function, particularly regarding less-studied toxins and their interactions with host cells. To do this we need a good grasp on their mechanisms of action, contribution to pathogenesis, response to toxins, and even evolution. Only then can we elucidate their roles in disease and develop effective strategies for prevention and treatment.

This thesis addresses several poorly understood concepts regarding Cj-CDT biology, including subunit intracellular trafficking, subunit function

relationships, and subunit host cell interaction. CDTs, functioning as multimeric toxins, are typically categorized as AB-type toxins, with the CdtB subunit as the active component (A) and the CdtA and CdtC subunits as the binding component (B). However, the precise role of CdtA and CdtC in toxin function remains a significant gap in knowledge. Little is known about the structural interaction between CdtA, CdtC, and CdtB during cellular intoxication, their interactions with host cells at the surface level, or their involvement in the intracellular trafficking of the toxin to the nucleus, where toxin activity occurs. This summary highlights our major findings and briefly discusses their implications for understanding the functions of CDTs.

It is widely acknowledged that the CDT subunits interact to form a heterotrimeric complex comprising CdtA, CdtB, and CdtC subunits, which is crucial for toxin function. However, exceptions to this model exist. For instance the *Ec*-CDTs and *Hd*-CDTs have been shown to have activity with only binary combinations of the subunits, CdtA + CdtB or CdtB + CdtC (40). In addition, with high enough concentrations of *Cj*-CDTs, toxin activity can also be observed in binary combinations of toxin (84). While these studies challenge the idea that a heterotrimeric complex is necessary for toxin function, our studies strongly support the model that all three *Cj*-CDT subunits are required for maximum cellular activity. Additionally, our findings underscore the significance of experimental conditions in evaluating toxin activities. We demonstrated that toxin activity could be measured with as little as 10 nM of toxin exposure for as short as 10 minutes, contrasting with many studies involving CDTs that employ

extended incubation times (> 1 - 2 days) and high concentrations of the toxin (> 100 nM). These previously reported conditions may lack physiological relevance, given the dynamic nature of the infection microenvironment and the limited production of toxin by the pathogen. Therefore, we emphasize the importance of thoroughly testing the effects of different experimental conditions and being mindful when comparing how these conditions may reflect the host cellular response.

That being said, our studies demonstrate that *Cj*-CDT, and possibility *Ec*-CDT and *Hd*-CDT, required high concentrations (>100 nM) to form heterotrimeric complexes. Contrary to our activity studies, binding data suggest that at the lower concentrations of toxin sufficient to induce a cellular response, the majority of the *Cj*-CDT toxin exists as non-assembled monomers. This discovery is significant as it fundamentally alters our understanding of *Cj*-CDT and possibly other CDTs' behavior. The challenge lies in comprehending how the toxin functions without being in a complex. For most AB-type toxins, a key obstacle is delivering the catalytically active subunit to the intracellular destination where it can elicit its activities. In the case of CDT, not only does the toxin need attach itself to the host cell, but it must also utilize preexisting host mechanisms to traffic the active CdtB subunit into the nucleus, where it induces DNA damage. A portion of our work aimed to better understand the trafficking mechanisms of Cj-CDT, particularly how the Cj-CdtA and Cj-CdtC subunits are involved in transporting the Cj-CdtB subunit intracellularly to the nucleus. Similar to previous work, our studies supported the idea that *Cj*-CDT intracellular trafficking was dependent on

functional endosomes, Golgi apparatus, and endoplasmic reticulum. However, in our trafficking studies, we encountered challenges in reliably measuring the intracellular trafficking of the *Cj*-CdtA, *Cj*-CdtC, and even the *Cj*-CdtB subunits to these organellar compartments. These incomplete experiments suggest that the intracellular trafficking *Cj*-Cdt is very dynamic and difficult to capture, as we can only see strong localization of the *Cj*-CdtB subunit at the end point of the trafficking pathway, the nucleus. It's possible that only a small fraction of the toxin is active under our experimental conditions, leaving a limited amount of toxin available for capture in our trafficking studies. Additionally, we lack a comprehensive understanding of the receptors involved in CDT host cell recognition; perhaps the toxin targets a receptor that is not abundant, resulting in only a fraction of the toxin binding and entering the cell. Alternatively, it's conceivable that the *Cj*-CdtA and *Cj*-CdtC subunits are not trafficked intracellularly with the *Cj*-CdtB subunit.

Without being in a complex, it appears unlikely that the CdtB subunit alone possesses the capability to execute all the necessary trafficking functions while inducing DNA damage. Therefore, our data suggests two models considering our current understanding of the structure function relationships to Cj-CDT. In our first proposed model, the active toxin may not function as an assembled entity in solution before reaching host cells. Instead, it might adopt a post-secretion assembly approach, where individual non-associated subunits utilize host factors, such as a cell surface receptor, to facilitate assembly on the host plasma membrane. Our data suggest this scenario as a possibility, but further

experiments are necessary to validate this model. The second proposed model is that the toxin has a much higher specific activity than previously observed. Specifically, the concentrations at which we observe biological activity may not reflect the true concentration of active toxin, but rather only a very small fraction of the toxin might be active at those concentrations. This could explain our inability to detect toxin trafficking and why we observe toxin activity at concentrations much lower than previously documented. Moreover, this disparity between toxin complex formation and activity could be deliberate. The toxin may have evolved to be most effective in the local infection microenvironment, where the concentration of toxin is much higher than sites more distal to the infection. Cells are highly intolerant to DNA damage, and numerous cellular mechanisms exist to respond to it. Thus, from the pathogen's perspective, it's crucial to finely tune and control the amount of DNA damage inflicted on host cells, regardless of the role that damage might play during infection.

5.2 ADDITIONAL QUESTIONS AND FUTURE WORK

In this final section of the thesis, we aim to delve into the remaining questions concerning our work and the CDT field. We will discuss current and future studies, along with highlighting some of the major outstanding questions related to the research presented.

What is the host cell receptor for Cj-CDT? To address a significant portion of the questions raised in this thesis, a better understanding of the host cell receptor targeted by *Cj*-CDT is imperative. Currently, neither the host cell

receptor for CDT nor the mechanisms involved in toxin internalization are fully understood. Many AB-type toxins target host membrane glycoproteins and glycolipids. Our ongoing research endeavors in the laboratory are focused on utilizing cross-linking mass spectrometry to identify potential host membrane glycoproteins and glycolipids that could serve as the receptor for *Cj*-CDT. By resolving the receptor question, we aim to design experiments that will enhance our comprehension of how the toxin gains entry into cells, which subunits mediate this entry, and whether *Cj*-CDTs assemble into a heterotrimeric complex at the cell surface rather than in solution.

What is the quaternary structure and mechanism of assembly of Cj-CDT? Our knowledge of the quaternary structure of *Cj*-CDT remains limited, and recent data challenge the necessity of a heterotrimeric complex for toxin activity. The advent of artificial intelligence, exemplified by programs like Alphafold, offers promising avenues for predicting *Cj*-CDT's structure. However, a deeper understanding of subunit interactions is essential for elucidating toxin function. This understanding could unveil critical subunit residues relevant for host cell recognition and intracellular trafficking, akin to findings in *Aa*-CDT and *Hd*-Cdt. Furthermore, the mechanism of toxin assembly remains enigmatic. While some studies propose assembly in the bacterial periplasm followed by secretion as a holotoxin complex, our research indicates potential assembly of individually refolded subunits in solution or at the host cell surface. Additionally, other studies suggest association of CDTs with outer membrane vesicles, potentially influencing toxin delivery and function. A better understanding of toxin assembly

would offer insights into its behavior during infection and cellular intoxication, informing strategies to combat toxin activity and potentially facilitating the development of protein molecules we could use for research and medicine that mimic CDT functions, such as nuclear delivery.

What are the roles of the CdtA and CdtC subunits and how does the CdtB subunit traffic to the nucleus? The role of the CdtA and CdtC subunit remains a major gap in knowledge in the CDT field. While it's apparent that one or both subunits are crucial for binding to host cells, their potential additional functions beyond host cell recognition remain unclear. In our investigations, we encountered challenges in evaluating the trafficking behavior of these subunits. To reach the nucleus, the active CdtB subunit must hijack existing host trafficking mechanisms, moving against the typical direction of cellular proteins. This process involves signal sequences directing the protein to specific organelles. However, little is known about the signal sequences involved in CDT-mediated nuclear transport, including which subunits participate in transporting CdtB to the Golgi apparatus and endoplasmic reticulum. Furthermore, the specific mechanisms of CDT intracellular transport involving the CdtA, CdtB, and CdtC subunits remain poorly understood. Despite previous pathways for protein retrograde transport and nuclear localization, discovered mechanisms do not seem to apply to CDTs. Unraveling these mysteries of CDT transport will enhance our comprehension of host protein retrograde transport mechanisms and could lead to the design of molecules utilizing host mechanisms for various applications, including the development of improved research tools and drugs.

What is the role of CDTs in pathogenesis? Understanding the role of bacterial toxins in pathogenesis poses one of the most challenging questions in this field. CDTs are the only known bacterial protein toxins to cause DNA damage. Targeting host DNA offers an appealing strategy for manipulating cellular homeostasis, given DNA's fundamental role in many cellular processes. However, the precise benefit to the pathogen conferred by DNA damage remains elusive. Many researchers speculate that bacterial effectors causing DNA damage primarily act to subtly modulate the host immune response, thereby promoting colonization and subsequent bacterial spread to new hosts, rather than directly enhancing the virulence traits of the infection process. Currently, our laboratory is exploring the potential role for *Cj*-CDT-mediated DNA damage, which we believe is to alter intestinal barrier function in a manner that facilitates invasion by *C. jejuni*. Ultimately, deciphering the role of CDTs in pathogenesis holds promise for the development of effective strategies to combat infections.

REFERENCES

1. Abrami, L., Bischofberger, M., Kunz, B., Groux, R., & van der Goot, F. G. (2010). Endocytosis of the anthrax toxin is mediated by clathrin, actin and unconventional adaptors. *PLOS Pathogens, 6*(3), e1000792. doi:10.1371/journal.ppat.1000792.

2. Abrami, L., Kunz, B., & van der Goot, F. G. (2010). Anthrax toxin triggers the activation of src-like kinases to mediate its own uptake. *Proc Natl Acad Sci USA, 107*(4), 1420-1424. doi:10.1073/pnas.0910782107.

3. Abrami, L., Liu, S., Cosson, P., Leppla, S. H., & van der Goot, F. G. (2003). Anthrax toxin triggers endocytosis of its receptor via a lipid raft-mediated clathrin-dependent process. *J Cell Biol, 160*(3), 321-328. doi:10.1083/jcb.200211018.

4. Akifusa, S., Heywood, W., Nair, S. P., Stenbeck, G., & Henderson, B. (2005). Mechanism of internalization of the cytolethal distending toxin of Actinobacillus actinomycetemcomitans. *Microbiology, 151*(Pt 5), 1395-1402. doi:10.1099/mic.0.27671-0.

5. Akifusa, S., Poole, S., Lewthwaite, J., Henderson, B., & Nair, S. P. (2001). Recombinant Actinobacillus actinomycetemcomitans cytolethal distending toxin proteins are required to interact to inhibit human cell cycle progression and to stimulate human leukocyte cytokine synthesis. *Infect Immun, 69*(9), 5925-5930. doi:10.1128/IAI.69.9.5925-5930.2001.

6. Alby, F., Mazars, R., de Rycke, J., Guillou, E., Baldin, V., Darbon, J. M., & Ducommun, B. (2001). Study of the cytolethal distending toxin (CDT)-activated cell cycle checkpoint. Involvement of the CHK2 kinase. *FEBS Letters, 491*(3), 261-265. doi:10.1016/s0014-5793(01)02205-0.

7. Alone, P. V., Malik, G., Krishnan, A., & Garg, L. C. (2007). Deletion mutations in N-terminal alpha1 helix render heat labile enterotoxin B subunit susceptible to degradation. *PNAS, 104*(41), 16056-16061. doi:10.1073/pnas.0707897104.

8. Ando-Suguimoto, E. S., da Silva, M. P., Kawamoto, D., Chen, C., DiRienzo, J. M., & Mayer, M. P. (2014). The cytolethal distending toxin of Aggregatibacter actinomycetemcomitans inhibits macrophage phagocytosis and subverts cytokine production. *Cytokine, 66*(1), 46-53. doi:10.1016/j.cyto.2013.12.014.

9. Bagley, K. C., Abdelwahab, S. F., Tuskan, R. G., Fouts, T. R., & Lewis, G. K. (2002). Pertussis toxin and the adenylate cyclase toxin from Bordetella pertussis activate human monocyte-derived dendritic cells and dominantly inhibit cytokine production through a cAMP-dependent pathway. *Journal of Leukocyte Biology, 72*(5), 962-969. doi:10.1189/jlb.72.5.962.

10. Barbier, J., & Gillet, D. (2015). 35 - Engineering of bacterial toxins for research and medicine. In J. Alouf, D. Ladant, & M. R. Popoff (Eds.), *The Comprehensive Sourcebook of Bacterial Protein Toxins (Fourth Edition)* (pp. 1016-1044). Boston: Academic Press.

11. Basilio, D., Juris, S. J., Collier, R. J., & Finkelstein, A. (2009). Evidence for a proton-protein symport mechanism in the anthrax toxin channel. *J Gen Physiol, 133*(3), 307-314. doi:10.1085/jgp.200810170.

12. Belibasakis, G. N., Johansson, A., Wang, Y., Chen, C., Lagergard, T., Kalfas, S., & Lerner, U. H. (2005). Cytokine responses of human gingival fibroblasts to Actinobacillus actinomycetemcomitans cytolethal distending toxin. *Cytokine, 30*(2), 56-63. doi:10.1016/j.cyto.2004.11.008.

13. Belibasakis, G. N., Mattsson, A., Wang, Y., Chen, C., & Johansson, A. (2004). Cell cycle arrest of human gingival fibroblasts and periodontal ligament cells by Actinobacillus actinomycetemcomitans: involvement of the cytolethal distending toxin. *APMIS, 112*(10), 674-685. doi:10.1111/j.1600-0463.2004.apm1121006.x.

14. Bellisola, G., Fracasso, G., Ippoliti, R., Menestrina, G., Rosen, A., Solda, S., . . . Colombatti, M. (2004). Reductive activation of ricin and ricin A-chain immunotoxins by protein disulfide isomerase and thioredoxin reductase. *Biochem Pharmacol, 67*(9), 1721-1731. doi:10.1016/j.bcp.2004.01.013.

15. Bezine, E., Vignard, J., & Mirey, G. (2014). The cytolethal distending toxin effects on Mammalian cells: a DNA damage perspective. *Cells, 3*(2), 592-615. doi:10.3390/cells3020592.

16. Bielaszewska, M., Sinha, B., Kuczius, T., & Karch, H. (2005). Cytolethal distending toxin from Shiga toxin-producing Escherichia coli O157 causes irreversible G2/M arrest, inhibition of proliferation, and death of human endothelial cells. *Infect Immun, 73*(1), 552-562. doi:10.1128/IAI.73.1.552-562.2005.

17. Blanke, S. R. (2006). Portals and Pathways: Principles of Bacterial Toxin Entry into Host Cells. *Microbe, 1*(1), 26-32.

18. Blazkova, H., Krejcikova, K., Moudry, P., Frisan, T., Hodny, Z., & Bartek, J. (2010). Bacterial intoxication evokes cellular senescence with persistent DNA damage and cytokine signalling. *J Cell Mol Med, 14*(1-2), 357-367. doi:10.1111/j.1582-4934.2009.00862.x.

19. Boesze-Battaglia, K., Besack, D., McKay, T., Zekavat, A., Otis, L., Jordan-Sciutto, K., & Shenker, B. J. (2006). Cholesterol-rich membrane microdomains mediate cell cycle arrest induced by *Actinobacillus actinomycetemcomitans* cytolethal-distending toxin. *Cell Microbiol, 8*(5), 823-836. doi:10.1111/j.1462-5822.2005.00669.x.

20. Boesze-Battaglia, K., Brown, A., Walker, L., Besack, D., Zekavat, A., Wrenn, S., . . . Shenker, B. J. (2009). Cytolethal distending toxin-induced cell cycle arrest of lymphocytes is dependent upon recognition and binding to cholesterol. *J Biol Chem, 284*(16), 10650-10658. doi:10.1074/jbc.M809094200.

21. Burns, D. L. (2021). Secretion of Pertussis Toxin from Bordetella pertussis. *Toxins, 13*(8). doi:10.3390/toxins13080574.

22. Cao, L., Volgina, A., Huang, C. M., Korostoff, J., & DiRienzo, J. M. (2005). Characterization of point mutations in the cdtA gene of the cytolethal distending toxin of Actinobacillus actinomycetemcomitans. *Mol Microbiol, 58*(5), 1303-1321. doi:10.1111/j.1365-2958.2005.04905.x.

23. Carette, J. E., Guimaraes, C. P., Wuethrich, I., Blomen, V. A., Varadarajan, M., Sun, C., . . . Brummelkamp, T. R. (2011). Global gene disruption in human cells to assign genes to phenotypes by deep sequencing. *Nat Biotechnol, 29*(6), 542-546. doi:10.1038/nbt.1857.

24. Chen, H., Ang, C. J., Crowder, M. K., Brieher, W. M., & Blanke, S. R. (2023). Revisiting bacterial cytolethal distending toxin structure and function. *Front Cell Infect Microbiol, 13*, 1289359. doi:10.3389/fcimb.2023.1289359.

25. Chinnapen, D. J., Chinnapen, H., Saslowsky, D., & Lencer, W. I. (2007). Rafting with cholera toxin: endocytosis and trafficking from plasma membrane to ER. *FEMS Microbiol Lett, 266*(2), 129-137. doi:10.1111/j.1574-6968.2006.00545.x.

26. Collier, R. J., & Young, J. A. (2003). Anthrax toxin. *Annu Rev Cell Dev Biol, 19*, 45-70. doi:10.1146/annurev.cellbio.19.111301.140655.

27. Comayras, C., Tasca, C., Pérès, S. Y., Ducommun, B., Oswald, E., & De Rycke, J. (1997). Escherichia coli cytolethal distending toxin blocks the HeLa cell cycle at the G2M transition by preventing cdc2 protein kinase dephosphorylation and activation. *Infection and Immunity, 65*(12), 5088-5095.

28. Cope, L. D., Lumbley, S., Latimer, J. L., Klesney-Tait, J., Stevens, M. K., Johnson, L. S., . . . Hansen, E. J. (1997). A diffusible cytotoxin of *Haemophilus ducreyi*. *PNAS, 94*(8), 4056–4061. doi:10.1073/pnas.94.8.4056.

29. Cortes-Bratti, X., Chaves-Olarte, E., Lagergård, T., & Thelestam, M. (1999). The cytolethal distending toxin from the chancroid bacterium Haemophilus ducreyi induces cell-cycle arrest in the G2 phase. *The Journal of Clinical Investigation, 103*, 107-115. doi:10.1172/JCI3831.

30. Cortes-Bratti, X., Chaves-Olarte, E., Lagergård, T., & Thelestam, M. (2000). Cellular Internalization of Cytolethal Distending Toxin from Haemophilus ducreyi. *Infection and Immunity, 68*(12), 6903–6911. doi:10.1128/iai.68.12.6903-6911.2000.

31. Critchley, D. R., Magnani, J. L., & Fishman, P. H. (1981). Interaction of cholera toxin with rat intestinal brush border membranes. Relative roles of gangliosides and galactoproteins as toxin receptors. *Journal of Biological Chemistry, 256*(16), 8724-8731. doi:10.1016/s0021-9258(19)68904-0.

32. Damek-Poprawa, M., Haris, M., Volgina, A., Korostoff, J., & DiRienzo, J. M. (2011). Cytolethal distending toxin damages the oral epithelium of gingival explants. *J Dent Res, 90*(7), 874-879. doi:10.1177/0022034511403743.

33. Damek-Poprawa, M., Jang, J. Y., Volgina, A., Korostoff, J., & DiRienzo, J. M. (2012). Localization of Aggregatibacter actinomycetemcomitans cytolethal distending toxin subunits during intoxication of live cells. *Infect Immun, 80*(8), 2761-2770. doi:10.1128/IAI.00385-12.

34. Damek-Poprawa, M., Korostoff, J., Gill, R., & DiRienzo, J. M. (2013). Cell junction remodeling in gingival tissue exposed to a microbial toxin. *J Dent Res, 92*(6), 518-523. doi:10.1177/0022034513486807.

35. Daniel A Scott, J. B. K. (1994). Cloning and sequencing of the genes encoding *Escherichia coli* cytolethal distending toxin. *Infection and Immunity, 62*(1), 44-251. doi:10.1128/iai.62.1.244-251.1994.

36. Day, P. J., Owens, S. R., Wesche, J., Olsnes, S., Roberts, L. M., & Lord, J. M. (2001). An interaction between ricin and calreticulin that may have implications for toxin trafficking. *J Biol Chem, 276*(10), 7202-7208. doi:10.1074/jbc.M009499200.

37. Deng, K., & Hansen, E. J. (2003). A CdtA-CdtC complex can block killing of HeLa cells by Haemophilus ducreyi cytolethal distending toxin. *Infect Immun, 71*(11), 6633-6640. doi:10.1128/IAI.71.11.6633-6640.2003.

38. Deng, K., Latimer, J. L., Lewis, D. A., & Hansen, E. J. (2001). Investigation of the interaction among the components of the cytolethal distending toxin of Haemophilus ducreyi. *Biochem Biophys Res Commun, 285*(3), 609-615. doi:10.1006/bbrc.2001.5223.

39. DiRienzo, J. M. (2014). Uptake and processing of the cytolethal distending toxin by mammalian cells. *Toxins, 6*(11), 3098-3116. doi:10.3390/toxins6113098.

40. Dixon, S. D., Huynh, M. M., Tamilselvam, B., Spiegelman, L. M., Son, S. B., Eshraghi, A., . . . Bradley, K. A. (2015). Distinct Roles for CdtA and CdtC during Intoxication by Cytolethal Distending Toxins. *PLoS One, 10*(11), e0143977. doi:10.1371/journal.pone.0143977.

41. Duesbery, N. S., Webb, C. P., Leppla, S. H., Gordon, V. M., Klimpel, K. R., Copeland, T. D., . . . Vande Woude, G. F. (1998). Proteolytic Inactivation of MAP-Kinase-Kinase by Anthrax Lethal Factor. *Science, 280*(5364), 734-737. doi:10.1126/science.280.5364.734.

42. el Bayâ, A., Linnemann, R., von Olleschik-Elbheim, L., Robenek, H., & Schmidt, M. A. (1997). Endocytosis and retrograde transport of pertussis toxin to the Golgi complex as a prerequisite for cellular intoxication. *European Journal of Cell Biology, 73*(1), 40-48.

43. Elmi, A., Watson, E., Sandu, P., Gundogdu, O., Mills, D. C., Inglis, N. F., . . . Dorrell, N. (2012). Campylobacter jejuni outer membrane vesicles play an important role in bacterial interactions with human intestinal epithelial cells. *Infect Immun, 80*(12), 4089-4098. doi:10.1128/IAI.00161-12.

44. Elwell, C. A., Chao, K., Patel, K., & Dreyfus, L. A. (2001). *Escherichia coli* CdtB mediates cytolethal distending toxin cell cycle arrest. *Infect Immun, 69*(5), 3418-3422. doi:10.1128/IAI.69.5.3418-3422.2001.

45. Elwell, C. A., & Dreyfus, L. A. (2000). DNase I homologous residues in CdtB are critical for cytolethal distending toxin-mediated cell cycle arrest. *Molecular Microbiology, 37*(4), 952-963. doi:10.1046/j.1365-2958.2000.02070.x.

46. Endo, Y., Mitsui, K., Motizuki, M., & Tsurugi, K. (1987). The mechanism of action of ricin and related toxic lectins on eukaryotic ribosomes. The site and the characteristics of the modification in 28 S ribosomal RNA caused by the toxins. *Journal of Biological Chemistry, 262*(12), 5908-5912. doi:10.1016/s0021-9258(18)45660-8.

47. Endo, Y., & Tsurugi, K. (1988). The RNA N-glycosidase activity of ricin A-chain. The characteristics of the enzymatic activity of ricin A-chain with ribosomes and with rRNA. *Journal of Biological Chemistry, 263*(18), 8735-8739. doi:10.1016/s0021-9258(18)68367-x.

48. Escalas, N., Davezac, N., De Rycke, J., Baldin, V., Mazars, R., & Ducommun, B. (2000). Study of the cytolethal distending toxin-induced cell cycle arrest in HeLa cells: involvement of the CDC25 phosphatase. *Exp Cell Res, 257*(1), 206-212. doi:10.1006/excr.2000.4878.

49. Eshraghi, A., Dixon, S. D., Tamilselvam, B., Kim, E. J., Gargi, A., Kulik, J. C., . . . Bradley, K. A. (2014). Cytolethal distending toxins require components of the ER-associated degradation pathway for host cell entry. *PLoS Pathog, 10*(7), e1004295. doi:10.1371/journal.ppat.1004295.

50. Eshraghi, A., Maldonado-Arocho, F. J., Gargi, A., Cardwell, M. M., Prouty, M. G., Blanke, S. R., & Bradley, K. A. (2010). Cytolethal distending toxin family members are differentially affected by alterations in host glycans and membrane cholesterol. *J Biol Chem, 285*(24), 18199-18207. doi:10.1074/jbc.M110.112912.

51. Fabbri, A., Travaglione, S., Falzano, L., & Fiorentini, C. (2008). Bacterial Protein Toxins: Current and Potential Clinical Use. *Current Medicinal Chemistry, 15*(11), 1116-1125. doi:10.2174/092986708784221430.

52. Fahrer, J., Huelsenbeck, J., Jaurich, H., Dorsam, B., Frisan, T., Eich, M., . . . Fritz, G. (2014). Cytolethal distending toxin (CDT) is a radiomimetic agent and induces persistent levels of DNA double-strand breaks in human fibroblasts. *DNA Repair (Amst), 18*, 31-43. doi:10.1016/j.dnarep.2014.03.002.

53. Fedor, Y., Vignard, J., Nicolau-Travers, M. L., Boutet-Robinet, E., Watrin, C., Salles, B., & Mirey, G. (2013). From single-strand breaks to double-strand breaks during S-phase: a new mode of action of the Escherichia coli Cytolethal Distending Toxin. *Cell Microbiol, 15*(1), 1-15. doi:10.1111/cmi.12028.

54. Fox, J. G., Rogers, A. B., Whary, M. T., Ge, Z., Taylor, N. S., Xu, S., . . . Erdman, S. E. (2004). Gastroenteritis in NF- B-Deficient Mice Is Produced with Wild-Type *Camplyobacter jejuni* but Not with *C. jejuni* Lacking Cytolethal Distending Toxin despite Persistent Colonization with Both Strains. *Infection and Immunity, 72*(2), 1116-1125. doi:10.1128/iai.72.2.1116-1125.2004.

55. Fraser, M. E., Chernaia, M. M., Kozlov, Y. V., & James, M. N. (1994). Crystal structure of the holotoxin from Shigella dysenteriae at 2.5 A resolution. *Nature Structural Biology, 1*(1), 59-64. doi:10.1038/nsb0194-59.

56. Frisan, T., Cortes-Bratti, X., Chaves-Olarte, E., Stenerlow, B., & Thelestam, M. (2003). The Haemophilus ducreyi cytolethal distending toxin induces DNA double-strand breaks and promotes ATM-dependent activation of RhoA. *Cellular Microbiology, 5*(10), 695-707. doi:10.1046/j.1462-5822.2003.00311.x.

57. Frisk, A., Lebens, M., Johansson, C., Ahmed, H., Svensson, L., Ahlman, K., & Lagergård, T. (2001). The role of different protein components from the Haemophilus ducreyi cytolethal distending toxin in the generation of cell toxicity. *Microbial Pathogenesis, 30*, 313-324. doi:10.1006/mpat.2001.0436.

58. Furstenberg, C. (2008). Computer genereated model of Ricin toxin.

59. Gabbert, A. D., Mydosh, J. L., Talukdar, P. K., Gloss, L. M., McDermott, J. E., Cooper, K. K., . . . Konkel, M. E. (2023). The Missing Pieces: The Role of Secretion Systems in Campylobacter jejuni Virulence. *Biomolecules, 13*(1). doi:10.3390/biom13010135.

60. Gao, M., & Schulten, K. (2006). Onset of anthrax toxin pore formation. *Biophys J, 90*(9), 3267-3279. doi:10.1529/biophysj.105.079376.

61. Gargi, A., Reno, M., & Blanke, S. R. (2012). Bacterial toxin modulation of the eukaryotic cell cycle: are all cytolethal distending toxins created equally? *Front Cell Infect Microbiol, 2*, 124. doi:10.3389/fcimb.2012.00124.

62. Gargi, A., Tamilselvam, B., Powers, B., Prouty, M. G., Lincecum, T., Eshraghi, A., . . . Blanke, S. R. (2013). Cellular interactions of the cytolethal distending toxins from *Escherichia coli* and *Haemophilus ducreyi*. *J Biol Chem, 288*(11), 7492-7505. doi:10.1074/jbc.M112.448118.

63. Gelfanova, V., Hansen, E. J., & Spinola, S. M. (1999). Cytolethal distending toxin of Haemophilus ducreyi induces apoptotic death of Jurkat T cells. *Infection and Immunity, 67*(12), 6394-6402. doi:10.1128/IAI.67.12.6394-6402.1999.

64. Guerra, L., Cortes-Bratti, X., Guidi, R., & Frisan, T. (2011). The biology of the cytolethal distending toxins. *Toxins (Basel), 3*(3), 172-190. doi:10.3390/toxins3030172.

65. Guerra, L., Teter, K., Lilley, B. N., Stenerlow, B., Holmes, R. K., Ploegh, H. L., . . . Frisan, T. (2005). Cellular internalization of cytolethal distending toxin: a new end to a known pathway. *Cell Microbiol, 7*(7), 921-934. doi:10.1111/j.1462-5822.2005.00520.x.

66. Hassane, D. C., Lee, R. B., & Pickett, C. L. (2003). *Campylobacter jejuni* Cytolethal Distending Toxin Promotes DNA Repair Responses in Normal Human Cells. *Infection and Immunity, 71*(1), 541-545. doi:10.1128/iai.71.1.541-545.2003.

67. Hausman, S. Z., & Burns, D. L. (1993). Binding of pertussis toxin to lipid vesicles containing glycolipids. *Infection and Immunity, 61*(1), 335-337. doi:10.1128/iai.61.1.335-337.1993.

68. Hickey, T. E., McVeigh, A. L., Scott, D. A., Michielutti, R. E., Bixby, A., Carroll, S. A., . . . Guerry, P. (2000). Campylobacter jejuni cytolethal distending toxin mediates release of interleukin-8 from intestinal epithelial cells. *Infection and Immunity, 68*(12), 6535-6541. doi:10.1128/iai.68.12.6535-6541.2000.

69. Hochegger, H., Takeda, S., & Hunt, T. (2008). Cyclin-dependent kinases and cell-cycle transitions: does one fit all? *Nature Reviews. Molecular cell biology, 9*(11), 910-916. doi:10.1038/nrm2510.

70. Huang, G., Boesze-Battaglia, K., Walker, L. P., Zekavat, A., Schaefer, Z. P., Blanke, S. R., & Shenker, B. J. (2021). The Active Subunit of the Cytolethal Distending Toxin, CdtB, Derived From Both *Haemophilus ducreyi* and *Campylobacter jejuni* Exhibits Potent Phosphatidylinositol-3,4,5-Triphosphate Phosphatase Activity. *Front Cell Infect Microbiol, 11*, 664221. doi:10.3389/fcimb.2021.664221.

71. Huhn, R. G., Torres-Mangual, N., Clore, J., Cilenti, L., Frisan, T., & Teter, K. (2021). Endocytosis of the CdtA subunit from the *Haemophilus ducreyi* cytolethal distending toxin. *Cell Microbiol, 23*(11), e13380. doi:10.1111/cmi.13380.

72. Jackson, S. P., & Bartek, J. (2009). The DNA-damage response in human biology and disease. *Nature, 461*(7267), 1071-1078. doi:10.1038/nature08467.

73. Jain, D., Prasad, K. N., Sinha, S., & Husain, N. (2008). Differences in virulence attributes between cytolethal distending toxin positive and negative *Campylobacter jejuni* strains. *J Med Microbiol, 57*(Pt 3), 267-272. doi:10.1099/jmm.0.47317-0.

74. Johannes, L., & Romer, W. (2010). Shiga toxins--from cell biology to biomedical applications. *Nat Rev Microbiol, 8*(2), 105-116. doi:10.1038/nrmicro2279.

75. Johnson, W. M., & Lior, H. (1988). A new heat-labile cytolethal distending toxin (CLDT) produced by Escherichia coli isolates from clinical material. *Microbial Pathogenesis, 4*, 103-113. doi:10.1016/0882-4010(88)90052-6.

76. Juodeikis, R., & Carding, S. R. (2022). Outer Membrane Vesicles: Biogenesis, Functions, and Issues. *Microbiology and molecular biology reviews, 86*(4). doi:10.1128/mmbr.00032-22.

77. Karlsson, K. A., Teneberg, S., Angström, J., Kjellberg, A., Hirst, T. R., Berström, J., & Miller-Podraza, H. (1996). Unexpected carbohydrate cross-binding by Escherichia coli heat-labile enterotoxin. Recognition of human and rabbit target cell glycoconjugates in comparison with cholera toxin. *Bioorganic and Medicinal Chemistry, 4*(11), 1919-1928. doi:10.1016/s0968-0896(96)00174-5.

78. Kohlhaas, S. L., Craxton, A., Sun, X. M., Pinkoski, M. J., & Cohen, G. M. (2007). Receptor-mediated endocytosis is not required for tumor necrosis factor-related apoptosis-inducing ligand (TRAIL)-induced apoptosis. *J Biol Chem, 282*(17), 12831-12841. doi:10.1074/jbc.M700438200.

79. Lai, Y. R., Chang, Y. F., Ma, J., Chiu, C. H., Kuo, M. L., & Lai, C. H. (2021). From DNA Damage to Cancer Progression: Potential Effects of Cytolethal Distending Toxin. *Front Immunol, 12*, 760451. doi:10.3389/fimmu.2021.760451.

80. Langerak, P., & Russell, P. (2011). Regulatory networks integrating cell cycle control with DNA damage checkpoints and double-strand break repair. *Philos Trans R Soc Lond B Biol Sci, 366*(1584), 3562-3571. doi:10.1098/rstb.2011.0070.

81. Lara-Tejero, M., & Galan, J. E. (2001). CdtA, CdtB, and CdtC form a tripartite complex that is required for cytolethal distending toxin activity. *Infect Immun, 69*(7), 4358-4365. doi:10.1128/IAI.69.7.4358-4365.2001.

82. Lara-Tejero, M., & Galán, J. E. (2000). A bacterial toxin that controls cell cycle progression as a deoxyribonuclease I-like protein. *Science, 290*, 354-357. doi:10.1126/science.290.5490.354.

83. Lee, J., & Tanya, T. P. (2005). ATM activation by DNA double-strand breaks through the Mre11-Rad50-Nbs1 complex. *Science, 308*(5721), 551-554. doi:10.1126/science.1108297.

84. Lee, R. B., Hassane, D. C., Cottle, D. L., & Pickett, C. L. (2003). Interactions of *Campylobacter jejuni* cytolethal distending toxin subunits CdtA and CdtC with HeLa cells. *Infect Immun, 71*(9), 4883-4890. doi:10.1128/IAI.71.9.4883-4890.2003.

85. Lemichez, E., & Barbieri, J. T. (2013). General aspects and recent advances on bacterial protein toxins. *Cold Spring Harb Perspect Med, 3*(2), a013573. doi:10.1101/cshperspect.a013573.

86. Leppla, S. H. (1982). Anthrax toxin edema factor: a bacterial adenylate cyclase that increases cyclic AMP concentrations of eukaryotic cells. *PNAS, 79*(10), 3162-3166. doi:10.1073/pnas.79.10.3162.

87. Lewis, D. A., Stevens, M. K., Latimer, J. L., Ward, C. K., Deng, K., Blick, R., . . . Hansen, E. J. (2001). Characterization of Haemophilus ducreyi cdtA, cdtB, and cdtC mutants in in vitro and in vivo systems. *Infect Immun, 69*(9), 5626-5634. doi:10.1128/IAI.69.9.5626-5634.2001.

88. Li, L., Sharipo, A., Chaves-Olarte, E., Masucci, M. G., Levitsky, V., Thelestam, M., & Frisan, T. (2002). The Haemophilus ducreyi cytolethal distending toxin activates sensors of DNA damage and repair complexes in proliferating and non-proliferating cells. *Cell Microbiol, 4*(2), 87-99. doi:10.1046/j.1462-5822.2002.00174.x.

89. Lin, C. D., Lai, C. K., Lin, Y. H., Hsieh, J. T., Sing, Y. T., Chang, Y. C., . . . Lai, C. H. (2011). Cholesterol depletion reduces entry of Campylobacter jejuni cytolethal distending toxin and attenuates intoxication of host cells. *Infect Immun, 79*(9), 3563-3575. doi:10.1128/IAI.05175-11.

90. Lindmark, B., Rompikuntal, P. K., Vaitkevicius, K., Song, T., Mizunoe, Y., Uhlin, B. E., . . . Wai, S. N. (2009). Outer membrane vesicle-mediated release of cytolethal distending toxin (CDT) from Campylobacter jejuni. *BMC Microbiol, 9*, 220. doi:10.1186/1471-2180-9-220.

91. Liyanage, N. P., Manthey, K. C., Dassanayake, R. P., Kuszynski, C. A., Oakley, G. G., & Duhamel, G. E. (2010). Helicobacter hepaticus cytolethal distending toxin causes cell death in intestinal epithelial cells via mitochondrial apoptotic pathway. *Helicobacter, 15*(2), 98-107. doi:10.1111/j.1523-5378.2010.00749.x.

92. Lönnroth, I., & Holmgren, J. (1973). Subunit Structure of Cholera Toxin. *Microbiology, 76*(2). doi:10.1099/00221287-76-2-417.

93. Massol, R. H., Larsen, J. E., Fujinaga, Y., Lencer, W. I., & Kirchhausen, T. (2004). Cholera toxin toxicity does not require functional Arf6- and dynamin-dependent endocytic pathways. *Mol Biol Cell, 15*(8), 3631-3641. doi:10.1091/mbc.e04-04-0283.

94. Matsuoka, S., Ballif, B. A., Smogorzewska, A., McDonald 3rd, E. R., Hurov, K. E., Luo, J., . . . Elledge, S. J. (2007). ATM and ATR substrate analysis reveals extensive protein networks responsive to DNA damage. *Science, 316*(5828), 1160-1166. doi:10.1126/science.1140321.

95. Mayer, M. P., Bueno, L. C., Hansen, E. J., & DiRienzo, J. M. (1999). Identification of a Cytolethal Distending Toxin Gene Locus and Features of a Virulence-Associated Region in *Actinobacillus actinomycetemcomitans*. *Infection and Immunity, 67*(3), 1227-1237. doi:10.1128/IAI.67.3.1227-1237.1999.

96. McAuley, J. L., Linden, S. K., Png, C. W., King, R. M., Pennington, H. L., Gendler, S. J., . . . McGuckin, M. A. (2007). MUC1 cell surface mucin is a critical element of the mucosal barrier to infection. *J Clin Invest, 117*(8), 2313-2324. doi:10.1172/JCI26705.

97. McSweeney, L. A., & Dreyfus, L. A. (2004). Nuclear localization of the *Escherichia coli* cytolethal distending toxin CdtB subunit. *Cell Microbiol, 6*(5), 447-458. doi:10.1111/j.1462-5822.2004.00373.x.

98. McSweeney, L. A., & Dreyfus, L. A. (2005). Carbohydrate-binding specificity of the *Escherichia coli* cytolethal distending toxin CdtA-II and CdtC-II subunits. *Infect Immun, 73*(4), 2051-2060. doi:10.1128/IAI.73.4.2051-2060.2005.

99. Merritt, E. A., & Hol, W. G. (1995). AB5 toxins. *Current Opinion in Structural Biology, 5*(2), 165-171. doi:10.1016/0959-440X(95)80071-9.

100. Merritt, E. A., Sarfaty, A., Chang, T., Palmer, L. M., Jobling, M. G., Holmes, R. K., & Hol, W. G. (1995). Surprising leads for a cholera toxin receptor-binding antagonist: crystallographic studies of CTB mutants. *Structure, 3*(6), 561-570. doi:10.1016/s0969-2126(01)00190-3.

101. Miller, S. I., & Salama, N. R. (2018). The gram-negative bacterial periplasm: Size matters. *PLoS Biol, 16*(1), e2004935. doi:10.1371/journal.pbio.2004935.

102. Mirdita, M., Schutze, K., Moriwaki, Y., Heo, L., Ovchinnikov, S., & Steinegger, M. (2022). ColabFold: making protein folding accessible to all. *Nat Methods, 19*(6), 679-682. doi:10.1038/s41592-022-01488-1.

103. Mise, K., Akifusa, S., Watarai, S., Ansai, T., Nishihara, T., & Takehara, T. (2005). Involvement of ganglioside GM3 in G(2)/M cell cycle arrest of human monocytic cells induced by Actinobacillus actinomycetemcomitans cytolethal distending toxin. *Infect Immun, 73*(8), 4846-4852. doi:10.1128/IAI.73.8.4846-4852.2005.

104. Mogridge, J., Cunningham, K., Lacy, D. B., Mourez, M., & Collier, R. J. (2002). The lethal and edema factors of anthrax toxin bind only to oligomeric forms of the protective antigen. *Proc Natl Acad Sci U S A, 99*(10), 7045-7048. doi:10.1073/pnas.052160199.

105. Moisenovich, M., Tonevitsky, A., Maljuchenko, N., Kozlovskaya, N., Agapov, I., Volknandt, W., & Bereiter-Hahn, J. (2004). Endosomal ricin transport: involvement of Rab4- and Rab5-positive compartments. *Histochem Cell Biol, 121*(6), 429-439. doi:10.1007/s00418-004-0652-6.

106. Montfort, W., Villafrancas, J. E., Monzingo, A. F., Ernst, S. R., Katzin, B., Rutenber, E., . . . Robertus, J. D. (1987). The Three-dimensional Structure of Ricin at 2.8 A. *The Journal of Biological Chemistry, 262*(11), 5398-5403. doi:10.1016/S0021-9258(18)61201-3.

107. Nesic, D., Hsu, Y., & Stebbins, E. (2004). Assembly and function of a bacterial genotoxin. *Nature, 429*. doi:10.1038/nature02532.

108. Nesic, D., & Stebbins, C. E. (2005). Mechanisms of assembly and cellular interactions for the bacterial genotoxin CDT. *PLoS Pathog, 1*(3), e28. doi:10.1371/journal.ppat.0010028.

109. Nishikubo, S., Ohara, M., Ueno, Y., Ikura, M., Kurihara, H., Komatsuzawa, H., . . . Sugai, M. (2003). An N-terminal segment of the active component of the bacterial genotoxin cytolethal distending toxin B (CDTB) directs CDTB into the nucleus. *J Biol Chem, 278*(50), 50671-50681. doi:10.1074/jbc.M305062200.

110. O'Neal, C. J., Jobling, M. G., Holmes, R. K., & Hol, W. G. (2005). Structural basis for the activation of cholera toxin by human ARF6-GTP. *Science, 309*, 1093-1096. doi:10.1126/science.1113398.

111. Odumosu, O., Nicholas, D., Yano, H., & Langridge, W. (2010). AB toxins: a paradigm switch from deadly to desirable. *Toxins (Basel), 2*(7), 1612-1645. doi:10.3390/toxins2071612.

112. Ohara, M., Hayashi, T., Kusunoki, Y., Miyauchi, M., Takata, T., & Sugai, M. (2004). Caspase-2 and caspase-7 are involved in cytolethal distending toxin-induced apoptosis in Jurkat and MOLT-4 T-cell lines. *Infect Immun, 72*(2), 871-879. doi:10.1128/IAI.72.2.871-879.2004.

113. Ohara, M., Hayashi, T., Kusunoki, Y., Nakachi, K., Fujiwara, T., Komatsuzawa, H., & Sugai, M. (2008). Cytolethal distending toxin induces caspase-dependent and -independent cell death in MOLT-4 cells. *Infect Immun, 76*(10), 4783-4791. doi:10.1128/IAI.01612-07.

114. Ohara, M., Miyauchi, M., Tsuruda, K., Takata, T., & Sugai, M. (2011). Topical application of Aggregatibacter actinomycetemcomitans cytolethal distending toxin induces cell cycle arrest in the rat gingival epithelium in vivo. *J Periodontal Res, 46*(3), 389-395. doi:10.1111/j.1600-0765.2011.01348.x.

115. Orlandi, P. A., Critchley, D. R., & Fishman, P. H. (1994). The heat-labile enterotoxin of Escherichia coli binds to polylactosaminoglycan-containing receptors in CaCo-2 human intestinal epithelial cells. *Biochemistry, 33*(43), 12886-12895. doi:10.1021/bi00209a021.

116. Paton, J. C., & Paton, A. W. (1998). Pathogenesis and Diagnosis of Shiga Toxin-Producing Escherichia coli Infections. *Clinical Microbiology Reviews, 11*(3), 450-479. doi:10.1128/cmr.11.3.450.

117. Pere-Vedrenne, C., Prochazkova-Carlotti, M., Rousseau, B., He, W., Chambonnier, L., Sifre, E., . . . Menard, A. (2017). The Cytolethal Distending Toxin Subunit CdtB of Helicobacter hepaticus Promotes Senescence and Endoreplication in Xenograft Mouse Models of Hepatic and Intestinal Cell Lines. *Front Cell Infect Microbiol, 7*, 268. doi:10.3389/fcimb.2017.00268.

118. Peres, S. Y., Marches, O., Daigle, F., Nougayrede, J. P., Herault, F., Tasca, C., . . . Oswald, E. (1997). A new cytolethal distending toxin (CDT) from Escherichia coli producing CNF2 blocks HeLa cell division in G2/M phase. *Mol Microbiol, 24*(5), 1095-1107. doi:10.1046/j.1365-2958.1997.4181785.x.

119. Pickett, C., Pesci, E. C., Cottle, D. L., Russell, G., Erdem, A. N., & Zeytin, H. (1996). Prevalence of cytolethal distending toxin production in Campylobacter jejuni and relatedness of Campylobacter sp. cdtB gene. *Infection and Immunity, 64*(6), 2070–2078. doi:10.1128/iai.64.6.2070-2078.1996.

120. Pickett, C. L., & Whitehouse, C. A. (1999). The cytolethal distending toxin family. *Trends in microbiology, 7*(7). doi:10.1016/s0966-842x(99)01537-1.

121. Pokkunuri, V., Pimentel, M., Morales, W., Jee, S. R., Alpern, J., Weitsman, S., . . . Chang, C. (2012). Role of Cytolethal Distending Toxin in Altered Stool Form and Bowel Phenotypes in a Rat Model of Post-infectious Irritable Bowel Syndrome. *J Neurogastroenterol Motil, 18*(4), 434-442. doi:10.5056/jnm.2012.18.4.434.

122. Purdy, D., Buswell, C., Hodgson, A. E., McAlpine, K., Henderson, I., & Leach, S. A. (2000). Characterisation of cytolethal distending toxin (CDT) mutants of Campylobacter jejuni. *Journal Medical Microbiology, 49*, 473-479. doi:10.1099/0022-1317-49-5-473.

123. Purven, M., & Lagergard, T. (1992). Haemophilus ducreyi, a Cytotoxin-Producing Bacterium. *Infection and Immunity, 60*(3), 1156-1162. doi:10.1128/iai.60.3.1156-1162.1992.

124. Remacle, A. G., Gawlik, K., Golubkov, V. S., Cadwell, G. W., Liddington, R. C., Cieplak, P., . . . Strongin, A. Y. (2010). Selective and potent furin inhibitors protect cells from anthrax without significant toxicity. *Int J Biochem Cell Biol, 42*(6), 987-995. doi:10.1016/j.biocel.2010.02.013.

125. Rogakou, E. P., Boon, C., Redon, C., & Bonner, W. M. (1999). Megabase chromatin domains involved in DNA double-strand breaks in vivo. *The journal of Cell Biology, 146*(5), 905-916. doi:10.1083/jcb.146.5.905.

126. Rompikuntal, P. K., Thay, B., Khan, M. K., Alanko, J., Penttinen, A. M., Asikainen, S., . . . Oscarsson, J. (2012). Perinuclear localization of internalized outer membrane vesicles carrying active cytolethal distending toxin from Aggregatibacter actinomycetemcomitans. *Infect Immun, 80*(1), 31-42. doi:10.1128/IAI.06069-11.

127. Saiki, K., Konishi, K., Gomi, T., Nishihara, T., & Yoshikawa, M. (2001). Reconstitution and Purification of Cytolethal Distending Toxin of Actinobacillus actinomycetemcomitans. *Microbiology and Immunology, 45*, 497-506. doi:10.1111/j.1348-0421.2001.tb02650.x.

128. Sakurai, J., Nagahama, M., Oda, M., Tsuge, H., & Kobayashi, K. (2009). Clostridium perfringens iota-toxin: structure and function. *Toxins, 1*(2), 208-228. doi:10.3390/toxins1020208.

129. Sanchez, J., & Holmgren, J. (2008). Cholera toxin structure, gene regulation and pathophysiological and immunological aspects. *Cell Mol Life Sci, 65*(9), 1347-1360. doi:10.1007/s00018-008-7496-5.

130. Sandkvist, M., Bagdasarian, M., & Howard, S. P. (2000). Characterization of the multimeric Eps complex required for cholera toxin secretion. *Int J Med Microbiol, 290*(4-5), 345-350. doi:10.1016/S1438-4221(00)80038-7.

131. Sandvig, K. (2001). Shiga toxins. *Toxicon, 39*(11), 1629-1635. doi:10.1016/s0041-0101(01)00150-7.

132. Sandvig, K., Bergan, J., Dyve, A. B., Skotland, T., & Torgersen, M. L. (2010). Endocytosis and retrograde transport of Shiga toxin. *Toxicon, 56*(7), 1181-1185. doi:10.1016/j.toxicon.2009.11.021.

133. Sandvig, K., Garred, O., Prydz, K., Kozlov, J. V., Hansen, S. H., & van Deurs, B. (1992). Retrograde transport of endocytosed Shiga toxin to the endoplasmic reticulum. *Nature, 358*, 510-512. doi:10.1038/358510a0.

134. Sandvig, K., Ryd, M., Garred, O., Schweda, E., Holm, P. K., & van Deurs, B. (1994). Retrograde transport from the Golgi complex to the ER of both Shiga toxin and the nontoxic Shiga B-fragment is regulated by butyric acid and cAMP. *The journal of Cell Biology, 126*(1), 53-64. doi:10.1083/jcb.126.1.53.

135. Sandvig, K., & van Deurs, B. (1996). Endocytosis, intracellular transport, and cytotoxic action of Shiga toxin and ricin. *Physiological Reviews, 76*(4), 949-966. doi:10.1152/physrev.1996.76.4.949.

136. Sandvig, K., & van Deurs, B. (2000). Entry of ricin and Shiga toxin into cells: molecular mechanisms and medical perspectives. *EMBO J, 19*(22), 5943-5950. doi:10.1093/emboj/19.22.5943.

137. Sandvig, K., & van Deurs, B. (2002). Transport of protein toxins into cells: pathways used by ricin, cholera toxin and Shiga toxin. *FEBS Lett, 529*(1), 49-53. doi:10.1016/s0014-5793(02)03182-4.

138. Sattler, J., & Wiegandt, H. (1975). Studies of the subunit structure of choleragen. *Eur J Biochem, 57*(1), 309-316. doi:10.1111/j.1432-1033.1975.tb02302.x.

139. Schengrund, C. L., & Ringler, N. J. (1989). Binding of Vibrio cholera Toxin and the Heat-labile Enterotoxin of Escherichia coli to GM1, Derivatives of GM1, and Nonlipid Oligosaccharide Polyvalent Ligands. *Journal of Biological Chemistry, 264*(22), 13233-13237. doi:10.1016/s0021-9258(18)51619-7.

140. Schreiner, H., Li, Y., Cline, J., Tsiagbe, V. K., & Fine, D. H. (2013). A comparison of Aggregatibacter actinomycetemcomitans (Aa) virulence traits in a rat model for periodontal disease. *PLoS One, 8*(7), e69382. doi:10.1371/journal.pone.0069382.

141. Shenker, B. J., Besack, D., McKay, T., Pankoski, L., Zekavat, A., & Demuth, D. R. (2004). *Actinobacillus actinomycetemcomitans* Cytolethal Distending Toxin (Cdt): Evidence That the Holotoxin Is Composed of Three Subunits: CdtA, CdtB, and CdtC. *The Journal of Immunology, 172*(1), 410-417. doi:10.4049/jimmunol.172.1.410.

142. Shenker, B. J., Hoffmaster, R. H., Zekavat, A., Yamaguchi, N., Lally, E. T., & Demuth, D. R. (2001). Induction of apoptosis in human T cells by Actinobacillus actinomycetemcomitans cytolethal distending toxin is a consequence of G2 arrest of the cell cycle. *J Immunol, 167*(1), 435-441. doi:10.4049/jimmunol.167.1.435.

143. Shenker, B. J., McKay, T., Datar, S., Miller, M., Chowhan, R., & Demuth, D. (1999). *Actinobacillus actinomycetemcomitans* Immunosuppressive Protein Is a Member of the Family of Cytolethal Distending Toxins Capable of Causing a G2 Arrest in Human T Cells. *Journal of Immunology, 162*, 4773-4780.

144. Shenker, B. J., Ojcius, D. M., Walker, L. P., Zekavat, A., Scuron, M. D., & Boesze-Battaglia, K. (2015). Aggregatibacter actinomycetemcomitans cytolethal distending toxin activates the NLRP3 inflammasome in human macrophages, leading to the release of proinflammatory cytokines. *Infect Immun, 83*(4), 1487-1496. doi:10.1128/IAI.03132-14.

145. Shenker, B. J., Walker, L. P., Zekavat, A., Dlakic, M., & Boesze-Battaglia, K. (2014). Blockade of the PI-3K signalling pathway by the Aggregatibacter actinomycetemcomitans cytolethal distending toxin induces macrophages to synthesize and secrete pro-inflammatory cytokines. *Cell Microbiol, 16*(9), 1391-1404. doi:10.1111/cmi.12299.

146. Sixma, T. K., Kalk, K. H., van Zanten, B. A., Dauter, Z., Kigma, J., Witholt, B., & Hol, W. G. (1992). Refined Structure of Escherichia coli Heat-labile Enterotoxin, a Close Relative of Cholera Toxin. *Molecular Biology, 1*(230), 890-918. doi:10.1006/jmbi.1993.1209.

147. Sixma, T. K., Pronk, S. E., Kalk, K. H., van Zanten, B. A., Berghuis, A. M., & Hol, W. G. (1992). Lactose binding to heat-labile enterotoxin revealed by X-ray crystallography. *Nature, 355*, 561-564. doi:10.1038/355561a0.

148. Sixma, T. K., Pronk, S. E., Kalk, K. H., Wartna, E. S., van Zanten, B. A., Witholt, B., & Hol, W. G. (1991). Crystal structure of a cholera toxin-related heat-labile enterotoxin from E. coli. *Nature, 351*, 371-377. doi:10.1038/351371a0.

149. Spangler, B. D. (1992). Structure and function of cholera toxin and the related Escherichia coli heat-labile enterotoxin. *Microbiological Reviews, 54*(4), 622-647. doi:10.1128/mr.56.4.622-647.1992.

150. Spilsberg, B., Van Meer, G., & Sandvig, K. (2003). Role of lipids in the retrograde pathway of ricin intoxication. *Traffic, 4*(8), 544-552. doi:10.1034/j.1600-0854.2003.00111.x.

151. Spooner, R. A., Smith, D. C., Easton, A. J., Roberts, L. M., & Lord, J. M. (2006). Retrograde transport pathways utilised by viruses and protein toxins. *Virol J, 3*, 26. doi:10.1186/1743-422X-3-26.

152. Stein, P. E., Boodhoo, A., Armstrong, G. D., Cockle, S. A., Klein, M. H., & Read, R. J. (1994). The crystal structure of pertussis toxin. *Structure, 2*(1), 45-57. doi:10.1016/s0969-2126(00)00007-1.

153. Stevens, M. K., Latimer, J. L., Lumbley, S. R., Ward, C. K., Cope, L. D., Lagergard, T., & Hansen, E. J. (1999). Characterization of a Haemophilus ducreyi mutant deficient in expression of cytolethal distending toxin. *Infection and Immunity, 67*(8), 3900-3908. doi:10.1128/IAI.67.8.3900-3908.1999.

154. Sugai, M., Kawamoto, T., Pérès, S. Y., Ueno, Y., Komatsuzawa, H., Fujiwara, T., . . . Oswald, E. (1998). The cell cycle-specific growth-inhibitory factor produced by Actinobacillus actinomycetemcomitans is a cytolethal distending toxin. *Infection and Immunity, 66*(10), 5008-5019. doi:10.1128/IAI.66.10.5008-5019.1998.

155. Svensson, L. A., Tarkowski, A., Thelestam, M., & Lagergard, T. (2001). The impact of Haemophilus ducreyi cytolethal distending toxin on cells involved in immune response. *Microb Pathog, 30*(3), 157-166. doi:10.1006/mpat.2000.0422.

156. Teter, K. (2019). Intracellular Trafficking and Translocation of Pertussis Toxin. *Toxins (Basel), 11*(8). doi:10.3390/toxins11080437.

157. Trofa, A. F., Ueno-Olsen, H., Oiwa, R., & Yoshikawa, M. (1999). Dr. Kiyoshi Shiga: discoverer of the dysentery bacillus. *Clinical Infectious Diseases, 29*(5), 1303-1306.

158. Tsuruda, K., Matangkasombut, O., Ohara, M., & Sugai, M. (2018). CdtC-Induced Processing of Membrane-Bound CdtA Is a Crucial Step in Aggregatibacter actinomycetemcomitans Cytolethal Distending Toxin Holotoxin Formation. *Infect Immun, 86*(3). doi:10.1128/IAI.00731-17.

159. Ueno, Y., Ohara, M., Kawamoto, T., Fujiwara, T., Komatsuzawa, H., Oswald, E., & Sugai, M. (2006). Biogenesis of the Actinobacillus actinomycetemcomitans cytolethal distending toxin holotoxin. *Infect Immun, 74*(6), 3480-3487. doi:10.1128/IAI.00739-05.

160. van den Akker, F., Sarfaty, S., Twiddy, E. M., Connell, T. D., Holmes, R. K., & Hol, W. G. (1996). Crystal structure of a new heat-labile enterotoxin, LT-IIb. *Structure, 4*(6), 665-678. doi:10.1016/S0969-2126(96)00073-1.

161. van der Goot, G., & Young, J. A. (2009). Receptors of anthrax toxin and cell entry. *Mol Aspects Med, 30*(6), 406-412. doi:10.1016/j.mam.2009.08.007.

162. Vitale, G., Pellizzari, R., Recchi, C., Napolitani, G., Mock, M., & Montecucco, C. (1998). Anthrax lethal factor cleaves the N-terminus of MAPKKs and induces tyrosine/threonine phosphorylation of MAPKs in cultured macrophages. *Biochem Biophys Res Commun, 248*(3), 706-711. doi:10.1006/bbrc.1998.9040.

163. Ward, I. M., & Chen, J. (2001). Histone H2AX is phosphorylated in an ATR-dependent manner in response to replicational stress. *J Biol Chem, 276*(51), 47759-47762. doi:10.1074/jbc.C100569200.

164. Wernick, N. L., Chinnapen, D. J., Cho, J. A., & Lencer, W. I. (2010). Cholera toxin: an intracellular journey into the cytosol by way of the endoplasmic reticulum. *Toxins (Basel), 2*(3), 310-325. doi:10.3390/toxins2030310.

165. Whitehouse, C. A., Balbo, P. B., Pesci, E. C., Cottle, D. L., Mirabito, P. M., & Pickett, C. L. (1998). *Campylobacter jejuni* Cytolethal Distending Toxin Causes a G2-Phase Cell Cycle Block. *Infection and Immunity, 66*(5), 1934-1940. doi:10.1128/IAI.66.5.1934-1940.1998.

166. Wienken, C. J., Baaske, P., Rothbauer, U., Braun, D., & Duhr, S. (2010). Protein-binding assays in biological liquids using microscale thermophoresis. *Nat Commun, 1*, 100. doi:10.1038/ncomms1093.

167. Wising, C., Azem, J., Zetterberg, M., Svensson, L. A., Ahlman, K., & Lagergard, T. (2005). Induction of apoptosis/necrosis in various human cell lineages by Haemophilus ducreyi cytolethal distending toxin. *Toxicon, 45*(6), 767-776. doi:10.1016/j.toxicon.2005.01.016.

168. Worthington, Z. E., & Carbonetti, N. H. (2007). Evading the proteasome: absence of lysine residues contributes to pertussis toxin activity by evasion of proteasome degradation. *Infect Immun, 75*(6), 2946-2953. doi:10.1128/IAI.02011-06.

169. Yamada, T., Komoto, J., Saiki, K., Konishi, K., & Takusagawa, F. (2006). Variation of loop sequence alters stability of cytolethal distending toxin (CDT): crystal structure of CDT from *Actinobacillus actinomycetemcomitans*. *Protein Sci, 15*(2), 362-372. doi:10.1110/ps.051790506.

170. Yu, M., & Haslam, D. B. (2005). Shiga toxin is transported from the endoplasmic reticulum following interaction with the luminal chaperone HEDJ/ERdj3. *Infect Immun, 73*(4), 2524-2532. doi:10.1128/IAI.73.4.2524-2532.2005.

171. Zhao, H., & Piwnica-Worms, H. (2001). ATR-mediated checkpoint pathways regulate phosphorylation and activation of human Chk1. *Mol Cell Biol, 21*(13), 4129-4139. doi:10.1128/MCB.21.13.4129-4139.2001.

172. Zheng, J., Meng, J., Zhao, S., Singh, R., & Song, W. (2008). Campylobacter-induced interleukin-8 secretion in polarized human intestinal epithelial cells requires Campylobacter-secreted cytolethal distending toxin- and Toll-like receptor-mediated activation of NF-kappaB. *Infect Immun, 76*(10), 4498-4508. doi:10.1128/IAI.01317-07.

173. Zillner, K., Jerabek-Willemsen, M., Duhr, S., Braun, D., Längst, G., & Baaske, P. (2012). Microscale Thermophoresis as a Sensitive Method to Quantify Protein: Nucleic Acid Interactions in Solution. *815*, 241-252. doi:10.1007/978-1-61779-424-7_18.

174. Zou, L., & Elledge, S. J. (2003). Sensing DNA damage through ATRIP recognition of RPA-ssDNA complexes. *Science, 300*(5625), 1542-1548. doi:10.1126/science.1083430.